Characterization and modelling of cellulose and hemicellulose interactions in microfibrillated cellulose (MFC)

Léa Falcoz-Vigne

Communauté
UNIVERSITÉ Grenoble Alpes

THÈSE

Pour obtenir le grade de

DOCTEUR DE LA COMMUNAUTE UNIVERSITE GRENOBLE ALPES

Spécialité: Chimie Physique Moléculaire et Structurale

Arrêté ministériel: 7 août 2006

Présentée par

Léa FALCOZ-VIGNE

Thèse dirigée par **Laurent HEUX** et codirigée par **Valérie MEYER, Yoshiharu NISHIYAMA et Karim MAZEAU**

préparée au sein du **Centre de Recherches sur les Macromolécules Végétales (CERMAV)**
dans **l'École Doctorale Chimie Science du Vivant**

Caractérisation et modélisation des interactions cellulose - hémicelluloses au sein des microfibrilles de cellulose (MFC)

Characterization and modelling of cellulose and hemicellulose interactions in microfibrillated cellulose (MFC)

Thèse soutenue publiquement le **30/11/2016**,
devant le jury composé de:

Monsieur Naceur BELGACEM
Professeur, LGP2-Grenoble (Président)
Monsieur Johnny BEAUGRAND
Chargé de Recherche, INRA-Reims (Rapporteur)
Monsieur Bernard CATHALA
Directeur de Recherche, INRA-Nantes (Rapporteur)
Madame Monika ÖSTERBERG
Professeur, AALTO-Finland (Examinateur)
Monsieur Laurent HEUX
Directeur de Recherche, CERMAV-Grenoble (Membre)
Madame Valérie MEYER
Ingénieur Recherche, CTP-Grenoble (Membre)

Remerciements

J'adresse tout d'abord mes remerciements à Madame et Messieurs les membres du jury : Madame Monika Österberg, Monsieur Johnny Beaugrand, Monsieur Bernard Cathala et Monsieur Naceur Belgacem pour avoir accepté de juger ces travaux de thèse.

Je voudrais ensuite exprimer mes remerciements à Monsieur Gilles Lenon, directeur du Centre Technique du Papier (CTP), Monsieur Redouane Borsali, directeur (2008-2016) du CEntre de Recherche sur les MAcromolécules Végétales (CERMAV) et Madame Christelle Breton, directrice de l'Ecole Doctorale de Chimie et Sciences du Vivant (EDSCV) pour m'avoir permis de réaliser cette thèse au sein de leur établissement.

Je souhaite également remercier Madame Corinne Bardou, Responsable des Ressources Humaines au CTP et Monsieur Michel Petit-Conil, Manager de l'équipe Chimie des Lignocelluloses - InTechFibres, pour leur accueil respectif au Centre Technique du Papier et au sein de l'équipe A.

Cette thèse a également bénéficié du support de l'Agence Nationale de la Recherche et la Technologie (ANRT), de l'Institut Carnot Polynat, ainsi que des clients CTPi par le biais du projet NaMiMod du CTP.

Je souhaite ensuite adresser mes remerciements à mes différents encadrants : Madame Valérie Meyer (CTP) et Messieurs Laurent Heux, Karim Mazeau et Yoshiharu Nishiyama (CERMAV) qui m'ont suivi tout au long de ces trois années et m'ont fait découvrir le monde de la cellulose : des polymères jusqu'aux applications papetières.

Ensuite ma thèse n'aurait sans doute pas été la même sans l'aide précieuse de toutes les personnes que j'ai pu côtoyer pendant ces trois années que ce soit au CTP ou au CERMAV.

Je voudrai plus particulièrement remercier pour leurs disponibilités, leurs conseils et surtout leur sympathie l'ensemble des personnes des équipes SPG, Intechfibres mais aussi David Guérin et son équipe que j'ai souvent sollicitée.

Je voudrai aussi remercier les deux étudiants : Nayara Campos-Barbosa et Louis Gbodossou qui ont fait preuve d'une grande motivation, de beaucoup d'engagement et de de persévérance au cours de leur stage.

Pendant ces trois ans, j'ai aussi eu la chance de pourvoir travaillé sur la modélisation atomistique avec l'aide de Yu Ogawa que je remercie pour ses conseils, son aide et sa patience. En effet, me faire entrer des lignes de commande sous linux n'était pas gagné d'avance et pourtant j'ai même réussi à y prendre goût !

Je souhaite remercier Henri Chanzy : pour toutes ses petites et discrètes intentions : à commencer par la relecture de mon manuscrit de thèse mais aussi pour les publications sélectionnées et déposées sur le bureau, les discussions scientifiques, les discussions sur la montagne…

Enfin je souhaite remercier ma voisine de bureau, ma voisine de labo, Marie-France Métral qui m'a accompagnée depuis mon arrivée, qui m'a intégrée à l'équipe et au labo et qui a été d'une aide précieuse tout au long de ces trois ans. Toujours de bonne humeur et passionnée, beaucoup de manips n'auraient pas fonctionné si « super Marie- France » n'avait pas été là avec ses trucs et astuces ! A commencer par les petits sandwiches de cellulose qui n'auraient sans doute pas vu le jour !!!

Je vais aussi remercier pour leur aide, leur disponibilité et leur bonne humeur Pierre Saillier et Eric Bayma. Ils vont me manquer les petits « coucou » et les « hééééééééééé » au détour des couloirs !

Parce que la thèse est aussi une question d'humain, je tiens à remercier toutes les personnes qui m'ont soutenue dans les moments les plus pénibles, et il y en eu, professionnellement mais aussi personnellement.

Aussi, Marie-France, Valérie, Harisoa, Marlène et Clélia, je ne vous remercierais jamais assez pour tout ce que vous avez fait pour moi : les soirées filles, les pauses thé, les discussions à bâtons rompus …

Je voudrai remercier aussi toutes les personnes qui, peut-être sans s'en rendre compte, ont égayé mon quotidien et m'ont ainsi aidée à surmonter les difficultés. Donc un grand MERCI pour les midis courses à pied, les pauses café de 10h, les repas d'équipes, le pré-apéro repas d'équipe, les barbecues, les soirées etc…

Même si pendant ces trois ans, je pense être passé par tout le champ d'émotion disponible dans le genre humain, je vais essayer de garder que le bon. Je garde donc en mémoire que des visages souriants et des personnes toujours disposées à aider.

Je vais terminer par remercier mes proches et en particulier mon frère et mes parents.

List of abbreviations **1**

General Introduction **3**

Economic Context **5**

1. Potential markets for nanocelluloses 6
2. Nanocellulose production 7
3. Zoom on potential markets for MFC in papers and boards 8
   - 3.1 General definition of paper and challenges 8
   - 3.2 MFC use at the wet-end 9
   - 3.3 MFC coating layer 9
   - 3.4 Active packaging 10
   - 3.5 Intelligent paper 10
4. Challenges for the MFC markets 11

General Bibliography

Structure and composition of wood fibers **14**

1. Wood chemical composition 14
   - 1.1 Wood polysaccharides 14
   - 1.2 Lignin 17
   - 1.3 Extractible compounds and minerals 17
2. Association between wood constituents 18
3. Fiber cell wall structure 19
4. Secondary cell wall biosynthesis 21
   - 4.1 Biosynthesis of cellulose 21
   - 4.2 Cellulose crystallinity and microfibrils structure 23

Pulping process **25**

1. Sulfite cooking pulp 25
2. Kraft cooking pulp 26
   - 2.1 Carbohydrates degradation 26
   - 2.2 Hexenuronic acid formation 27
   - 2.3 Xylans adsorption on cellulose fibers 28
3. Bleaching 29
4. Final remarks on sulfite pulp (specialty cellulose) and kraft pulp 31

MFC production **32**
1. Difference between microfibrils and microfibrillated cellulose (MFC) 32
2. Pre-treatment before MFC production 33
   2.1 Mechanical pretreatment 33
   2.2 Chemical pretreatment 34
   2.3 Enzymatic pretreatment 34
   2.4 Conclusion on the pretreatment 35
3. MFC production process 35

Cellulose - xylan interaction **37**
1. Spectroscopy techniques 38
2. Microscopy or piezoelectric techniques 39
3. Biosynthesis models 40
4. Improvement in mechanical properties 40

Materials and Methods

Materials **44**
1. MFC suspensions 44
   1.1 Pre-treatment of the pulp 44
   1.2 Homogenization of the pre-treated pulp 45
2. Pulp samples from CTP 46
3. Xylans samples 46
4. Solvents and materials 46

Methods **47**
1. Samples characterization 47
   1.1 Chemical composition with sugar analysis 47
   1.2 Morphological analysis of residual coarse elements 47
   1.3 MFC dispersion with UV visible spectroscopy 47
   1.4 Samples freeze- drying 47
   1.5 Samples composition and structure by ^{13}C solid state NMR 48
2. MFC and pulp components isolation 48
   2.1 Solvent exchange (tert-butyl alcohol =TBA) and aerogel formation 48
   2.2 MFC specific surface measured with BET 48
   2.3 Optimized protocol of xylan extraction 49
   2.4 Xylan composition and structure with liquid state NMR 49

3. Xylan DP characterization 49
3.1 Liquid NMR 49
3.2 Viscosimetry 50
3.3 SEC- MALS 50
4. MFC films production 51
4.1 MFC films by casting 51
4.2 Deionized MFC films by casting 51
4.3 MFC films by handsheet method 51
5. MFC film examinations with SEM-FEG 54
6. Three layers systems of MFC films and xylan 54
6.1 Xylan gel formation 54
6.2 Optimized protocol of three layers system formation System 1 (for peeling test) 55
6.3 Optimized protocol of three layers system formation System 2 (for shearing test) 56
6.4 Three layers system formation System 2 (for shearing test) with hot melt glue 56
6.5 Adhesion on the three layer model 57

Chapter 1

MFC components isolation and characterization 60

1. Initial composition of MFC 61
1.1 MFC characterization by solid state NMR of dry sample 61
1.2 Influence of drying history and the presence of salts on the solid state NMR spectra 63
1.3 Solid state NMR spectra of wet MFC: effect of the cooking process 64
2. Xylan extraction from birch kraft MFC 65
2.1 Protocol description 65
2.2 Optimization of the extraction protocol 66
2.3 Extracted MFC characterization 69
2.4 Determination of extraction yield 71
3. Extension of the extraction protocol 72
4. Characterization of the extracted xylans 74
4.1 Chemical composition of the extracted xylans 74
4.2 Solid state NMR characterization of the extracted xylan 75
4.3 Liquid state NMR characterization of the extracted xylan 77
4.4 Conclusion on the xylan extracted from birch kraft samples 80

5. Characterization of the xylose homopolymer 81
5.1 Crystallinity 81
5.2 Degree of Polymerization 82
Annex 1: MFC chemical composition by sugar analysis 87
Annex 2: MFC chemical composition by sugar analysis for xylan extraction protocol optimization 88
Annex 3: Characterization of xylan mineral impurity 89
1. Ash content of extracted xylan 90
2. Energy Dispersive X-Ray Analysis of xylan ash 91
Annex 4: Chemical composition of MFC before and after xylan extraction 92
Annex 5: Extracted xylan chemical composition by sugar analysis 93
Annex 6: Xylan peaks attribution on NMR liquid spectra 94
1. Xylan extracted from MFC from birch kra-nd 95
2. Xylan extracted from birch wood chips 96
3. Commercial xylan extracted from oat 98

Chapter 2

Characterization of MFC dispersion in suspension and dried forms 104
1. Light scattering of fibrillar objects 105
2. Wave-length dependence of the turbidity with the size of the objects 106
2.1 Very thin fibrils 106
2.2 Thin fibrils 107
2.3 Thick fibrils 107
3. MFC suspension analysis with turbidity measurements 107
4. Specific surface area and dispersion of MFC 110
5. Correlation of MFC dispersion with reinforcement capacity 112
6. Conclusion 114
Annex 7: Influence of solvent exchange by turbidimetry 115
Annex 8: Influence of xylan extraction 117

Chapter 3

Conformational adaptation of β-(1→4) Xylan at the Cellulose Surface in Nature and Biomimetic Reconstruction 122

Abstract 123

Introduction 124

Experimental section 125

Results and discussion 128

1. Solid-State ^{13}C NMR Spectral Analysis of Xylan onto Cellulose Surface 128
   - 1.1 Conformational Diversity of Xylan 128
   - 1.2 Conformational Adaptation of Xylan upon re-adsorption MFC 130
2. Estimation of the Surface Area of MFC Samples Accessible to Xylan 132
3. Molecular Dynamics (MD) Simulation of Adsorption of Xylan on Cellulose 133
   - 3.1 Molecular Conformation of Xylan in Water without Cellulose 133
   - 3.2 Adsorption Simulation of Xylan on the Cellulose Surfaces 134

Conclusion 138

References 139

Supporting Information 141

Annex 9: Xylan - Cellulose adsorption energy 149

Annex 10: Re-adsorption after TBA freeze-drying 150

Annex 11: Arabino-xylan re-adorsption 151

Chapter 4

Adhesion between cellulose and xylan 156

1. Adhesion mechanisms 156
2. Three layer system formation 157
   - 2.1 MFC films 158
   - 2.2 Xylan deposition 159
3. Peeling test results 160
   - 3.1 Peeling test principle 160
   - 3.2 Preliminary study 161
   - 3.3 Peeling test on three layer system 162
   - 3.4 Conclusion on peeling test 163
4. Shear test 164

4.1 Shear test principle 164
4.2 Shear test results 166
5. Conclusion on peeling and shear tests 167
Annex 12: Energy dispersive X-ray analysis (EDXA) on MFC film casting 168
Annex 13: Xylan non penetration control 169
1. Xylan grafting with fluorescein isothiocyanate isomer I 169
2. Xylan substitution degree measurement with UV-vis spectroscopy 169
2.1 Calibration curve 169
2.2 Xylan substitution degree 170
3. Fluorescence microscopy observation of three layers structure 171
Annex 14: Technical informations on Tape AT-206 172
Annex 15: DSC measurement on xylan 173
Annex 16: Composite films and tensile test 174

General Conclusion and Perspectives 177

Conclusion Chapter
Xylanase pre-treatment before MFC production 184
1. MFC production 184
2. Chemical composition of MFC 185
2.1 Sugar analysis 185
2.2 Solid State NMR analysis 186
3. Energy consumption 187
4. MorFi analysis and optical microscopy 188
5. Turbidity analysis 190
6. Conclusion 191

References 193

Résumé Etendu 206

List of abbreviations

CP-MAS NMR: Cross Polarization Magic Angle Spinning, solid state Nuclear Magnetic Resonance

DMAC: Dimethylacetamide

DMF: Dimethylformamide

DMSO: Dimethylsulfoxide

DMSO-D_6: Deuterated dimethylsulfoxide

D_2O: Deuterated oxide

DP: Degree of Polymerization

EDXA: Energy Dispersive X-Ray Analysis

Et_3N: triethylamine

EtOH: Ethanol

FITC: Fluorescein isothiocyanate isomer 1

LiCl: Lithium chloride salt

LS: Light Scaterring

MFC: Microfibrillated cellulose

MorFi: Morphological Analysis

NaOD: Sodium deuteroxide

NaOH: Sodium hydroxide

RI: Refractive Index

SEC-MALS: Size Exclusion Chromatography with Multi-Angle-Light-Scattering

SEM: Scanning Electron Microscope

TBA: tert-butyl alcohol

TGA: Thermogravimetric analysis

THF: Tetrahydrofuran

Tg: glass transition temperature

XRD: X-ray Diffraction

General Introduction

MFCs have gained a great importance as a nanostructured material thanks to their property to be natural, renewable, biodegradable, sustainable and biocompatible. In addition, they have a high strength and Young modulus and due to their functionality, they can be easily chemically modified.

For the past years, techniques to deconstruct the walls of cellulosic fibers and liberate the microfibrils have been improved to reduce the energy consumption from 27 MWh/t down to 0.5-2.3 MWh/t (Ankerfors 2015) and thus are able to produce nano-objects at a competitive price. Until 2013, MFC had been mainly manufactured at lab scale, in kilogram batches. Nowadays, several production facilities are being built worldwide with up to 3 tons per day capacities. This recent development of large pilot/industrial facilities (Future markets 2015) open the way for the use of these materials in the manufacture of industrial products.

CTP recently carried out a study on eight different commercial pulps as raw materials for MFC production. MFC were manufactured by intensive mechanical treatment including refining with enzymatic pretreatment to weaken the structure, followed by a homogenization with a GEA Niro Soavi homogenizer. The results highlighted a “pulp origin” effect, mainly due to the pulping process and also to the pulp drying. The presence of hemicelluloses seems to have a major influence on the pulp behaviour during homogenization. Pulps with higher hemicelluloses content led to more homogeneous MFC suspensions and higher strength were observed when MFC were added to the fiber matrix. These previous results led to the goal of this PhD project, which is to study the influence of the interactions between the structural components of the fibers, on the cellulose microfibril (MFC) production process.

In this framework, the main objective has been to develop a fundamental knowledge about the interactions between the principal components of the secondary wall fibers i.e. the cellulose – hemicellulose interaction in the MFC. Solving this would help to better select fibers pretreatment to reduce the energy consumption for the MFC production.

The main steps of this project will be (Figure 1)

- The identification and characterization of the different constituents of the MFC
- The development of a test and a model structure to understand and measure the adhesion between the main constituents of the MFC
- The modeling of the interactions between the MFC constituents

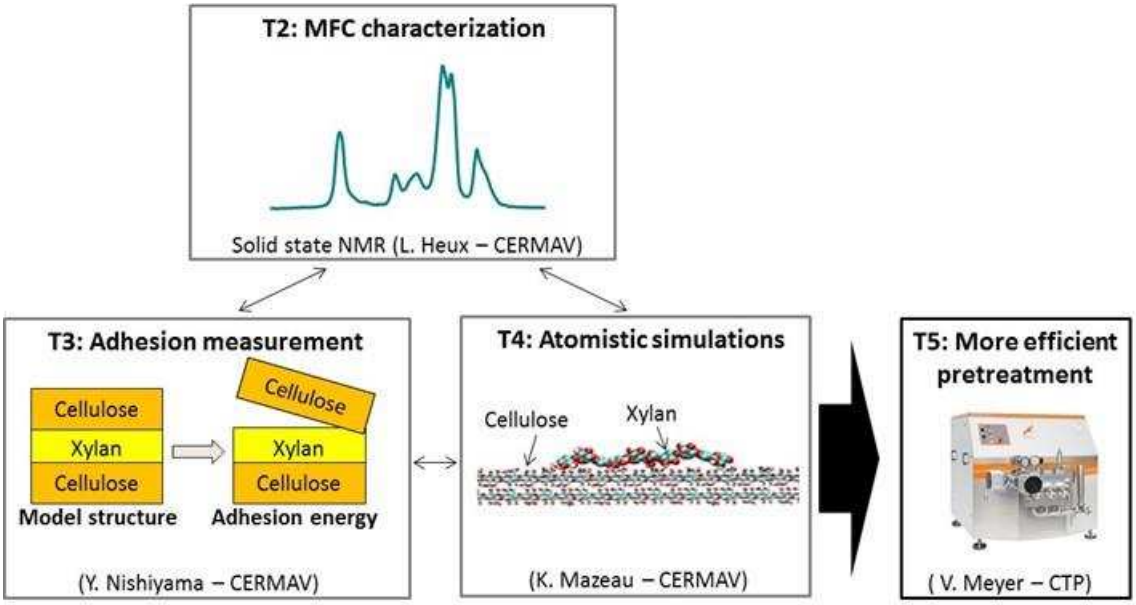

Figure 1: Illustration of the main steps of the project.

In the present manuscript, the first chapter corresponds to a general introduction and a bibliographic survey.
The second chapter describes the isolation and characterization of the different MFC constituents.
The dispersion of the MFC in relation with the hemicelluloses content and the pulp drying history are analyzed by UV spectroscopy in the third chapter.
The interaction between the cellulose and one of the main hemicelluloses content in MFC, the xylan is studied by ^{13}C solid state NMR and atomistic simulation in the fourth chapter.
In the fifth chapter, a model with films made of pure cellulose MFC and xylan layers was built and some peeling tests on this layered structure were performed to directly measure the interactions between cellulose and xylan.
As a manuscript conclusion, a production of MFC with a combination of xylanase and cellulase as a pulp pretreatment will be proposed.

Economic Context

In view of their outstanding physical properties, the interest for biosourced nanomaterials is growing as they are frequently proposed as an alternative to petroleum products. In this context, nanocelluloses, composed of NanoCrystalline Cellulose (NCC), MicroFibrillated Cellulose (MFC) and Bacterial Cellulose (BC) appear very promising. They have a high strength, high Young modulus, high-aspect ratio, together with dimensional and thermal stability, interesting optical and surface area properties. In addition, they can be chemically functionalized and used as moisture absorbent material.

In 2008, the main actors in the nanocellulose production were located in North America, Europe, East Asia and South America (Figure 2).

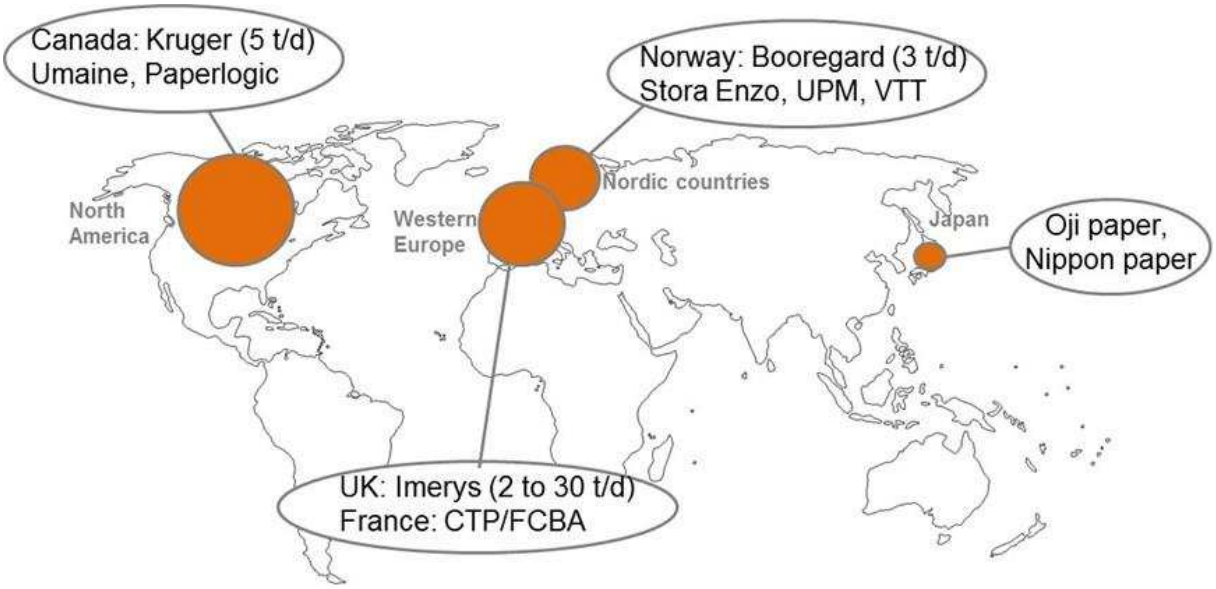

Figure 2: Centers for microfibrillated production and development (adapted from Future Market 2015).

In 2015, the current nanocellulose production was estimated to be 25-80 tons per annum and in this, MFC accounted for approximately 45-50 tons of this estimate (Future Markets Inc. 2015). For the next coming year, the company FP Innovations estimates the market to be worth $250 million in North America by 2020 and the USDA (United State Department of Agriculture) has forecasted that the global nanocellulose market could amount to over 35 million tons per annum by 2040 (Future Markets Inc 2015).

1. Potential markets for nanocelluloses

The nanocellulose applications are divided into three domains: high-volume applications, low-volume applications and novel applications. For each of these, the progression is mentioned from "Research basic concept" to "Commercial in operation" (Table 1). In the high-volume applications, nanocelluloses are already at the commercialization step: as cement additives, pharmaceutical and self-cleaning coating. They are also used as prototype in anti-static coating, transparent barrier films in food packaging, paper composites and filtration. In low-volume application, they are found as insulation and medical implants, but they are still at research and development stage. In novel applications, we find them in electronics and drug delivery.

Table 1: Nanocellulose applications: Stage of commercialization (Adapted from Future Markets 2015).

Applications	**Research**	**Applied research and development**	**Demonstration**	**Commercial**
Progression	Basic concept	Proof of concept	Basic prototype	Fully tested
High Volume Applications				
Cement additives				
Anti-static coatings				
Transparent barrier films in food packaging				
Polymer composites				
Printing paper				
Pharmaceutical (filler)				
Paper composites				
Self cleaning coatings				
Filtration				
Low Volume Applications				
Insulation				
Medical implants				
Flexible circuits, printable electronics, conductive substrates				
Drug delivery				

Developed In progress Future

Nanocellulose potential applications can be summarized in 6 main areas ranging from pulp and paper to electronics and additives (Figure 3).

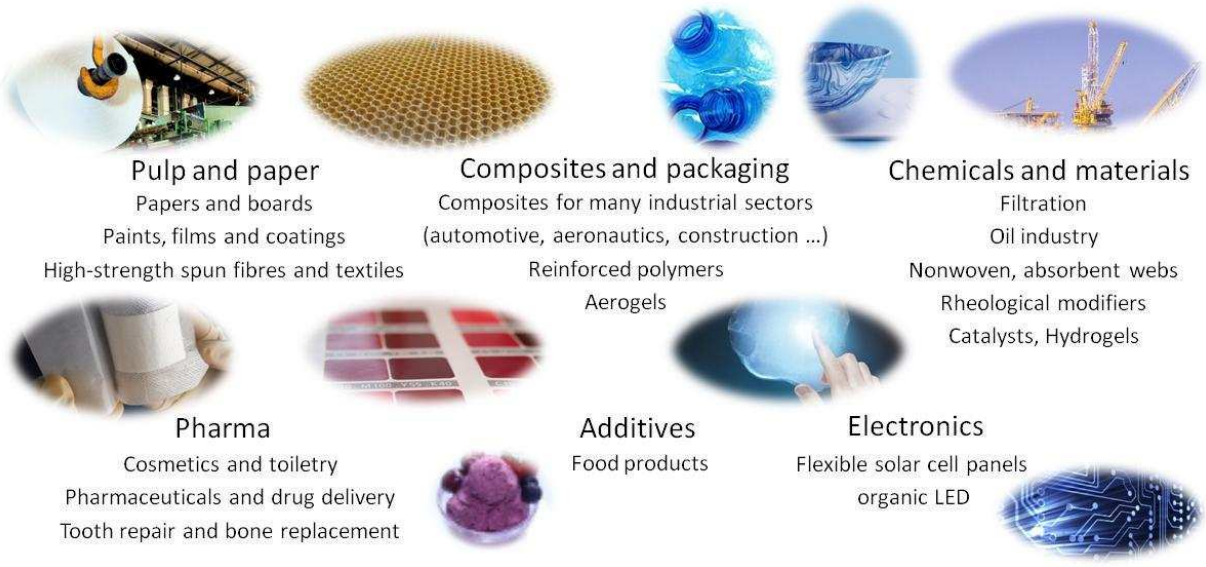

Figure 3: Potential markets for MFC applications (adapted from Future Markets 2015).

2. Nanocellulose production

In 2015, the worldwide nanocellulose production was estimated to be between 400 and 1700 tons, depending on optimistic or conservative point of views. In the next ten years, it is supposed to reach between 2 200 and 10 500 tons, which means a 5-fold increase in production (Figure 4).

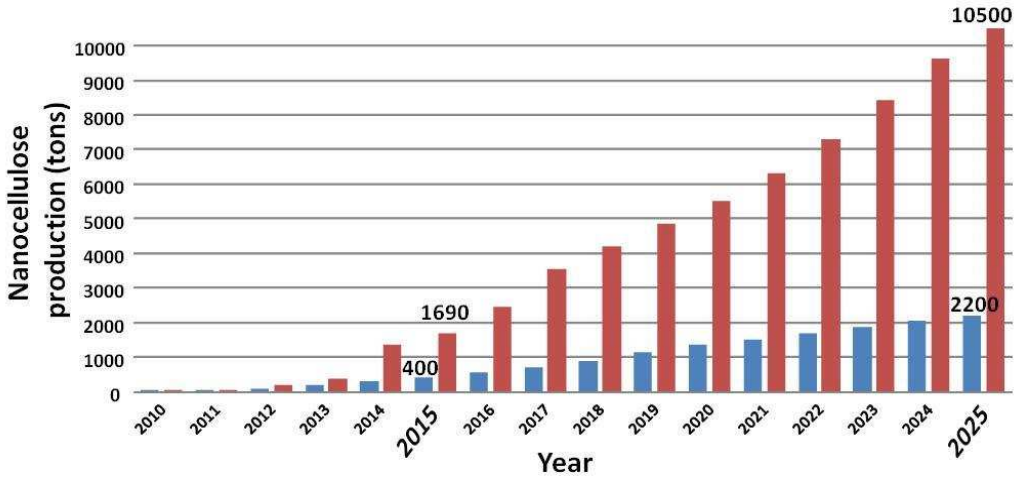

Figure 4: Global nanocellulose production in tons/year, 2010-2025. Conservative estimate (blue), optimistic (red) (adapted from Future Markets 2015).

In 2015, the prices for MFC were approximately 4 - 40 $/kg (Future Markets Inc 2015).

3. Zoom on potential markets for MFC in papers and boards

3.1 General definition of paper and challenges

Paper is formed on a fine screen –the wire- from an aqueous suspension of wood pulp and mineral pigments (fillers). The mineral pigments are usually made from high-brightness calcite (ground marble or limestone), of china clay (kaolin), which has undergone various grinding and separation processes, precipitated calcium carbonate or titanium dioxide. To improve gloss, shade, opacity, and printing properties, paper is often coated with a coating layer, consisting of an aqueous dispersion of mineral pigments with a finer particle size distribution than those used as filler. To increase the gloss and/or paper opacity, around 10% by weight of adhesive (binder) are added in form of synthetic latex particles or synthetic plastic pigment (polystyrene spheres). Additives may also be present to enhance the binding and/or provide flocculation, which affects the paper structure on drying (Gane *et al.* 1996).

Major development trends for the principal paper sectors, namely the "Packaging" and "Printing and writing paper", are to increase the materials performance itself and to decrease the production cost by reducing the basis weight of the product (Table 2). Since paper is not considered only as a support, new functionalities are now promoted, such as active packaging and intelligent papers, which generate new challenges.

Table 2: Major development trends for principal paper's sectors.

Sectors	Major development trends
Packaging	➢ higher performance materials: better mechanical and barrier properties ➢ lower basis weight ➢ bio-sourced raw materials products
Printing and writing paper	➢ lower production cost: cheaper materials, higher filler content ➢ lower basis weight ➢ multi-printability products
Active packaging	➢ extended protection for food product with active substances included in the packaging (Lavoine *et al.* 2014; Lavoine and Desloges 2014)
Intelligent paper	➢ cheaper electronic devices: paper cost 10 times less per square meter than PET (polyethylene terephthalate) commonly used in electronic (Pereira *et al.* 2014) ➢ electronics devices with light weight, flexibility and ability to be recyclable

In this context, the use of MFC is one of the most appropriate solutions to improve the papermaking process. MFCs can be added either at the wet-end or at the coating step, which means that they can be directly added into the paper matrix (as additives) or coated at the paper surface as a supplementary layer (Beneventi *et al.* 2014).

3.2 MFC use at the wet-end

In papermaking, it is a very demanding task to enhance the physical properties of paper without simultaneously deteriorating the drainage characteristics: indeed it is this drainage that limits the production efficiency of a paper machine (Norell, Johansson, and Persson 2009). Non-chemically modified MFCs have a negatively charged surface (zeta potential about - 25mV) and can be used as carrier of cationic products (Ahola, Österberg and Laine 2008). This could greatly improve the retention and location of the product in the paper sheet, leading to a more efficient use of conventional paper additives and a decrease in the basis weight (Esser 2012). For the reinforcement of mechanical properties of paper, MFCs can be added to the pulp slurry, together with cationic polyelectrolytes, used in papermaking process, such as cationic starch (Taipale *et al*. 2010) and polyamideamine epichhlohydrin (PAE).

In literature, it has been reported that 1% to 6% of MFC with 0.5% of PAE, improved the dry and wet tensile strength from 2.5 to 3 times but these results are sensitive to the formulation preparation (Ahola, Österberg and Laine 2008). The improvements of the mechanical properties have been only observed, when PAE and MFC were added one by one to the pulp slurry, allowing a stirring time between each product addition, and not when they were first mixed together. These conditions, observed at lab-scale, could potentially induce a flocculation on the paper machine at pilot and industrial scales. Finally, the use of MFC could dramatically decrease the dewatering of the fibrous mat (drainage). Taipale *et al.* (2010) has demonstrated a severe loss in drainage rate but a 1.4 time increase in the mechanical properties of paper, with a mixture of 3% MFC and 1.5% starch. But this performance is very sensitive to the MFC grades. So the use of MFC, at the wet-end, is in competition with the use of other cationic polyelectrolytes. It will increase only if the cost/performance chart is proven to be substantially profitable.

3.3 MFC coating layer

3.3.a Barrier coating material and reinforcement layer

Cellulosic fibers have traditionally been used in packaging for a wide range of food categories such as dry, frozen, or liquid foods and beverages. For example, cellophane, which is regenerated cellulose obtained from wood pulp, is extensively used as a material for food packaging (Del Nobile, Fava, and Piergiovanni 2002), as it presents a low water vapor permeability of $1.25.10^{-9}$ mol.cm/(cm^2.s.atm). Similarly, parchment paper is also known for its low water permeability.

Many publications present the interest of using MFCs as a barrier material thanks to their film forming behaviour (Syverud and Stenius 2009). Indeed, they display excellent barrier properties towards grease and oxygen (Aulin, Gällstedt, and Lindström 2010). Typically, a MFC film with a basis weight of 35 g/m^2 had tensile index of 146 ± 18 Nm/g and elongation of 8.6 ± 1.6%. The E modulus (17.5 ± 1.0 GPa) of a film composed of randomly oriented fibrils was comparable to the values obtained with those of cellulose fibers with a fibril angle of 50°. The oxygen transmission rates (OTR) as low as 17 ml/m^2.day were obtained for films prepared from pure MFC (Syverud and Stenius 2009). This value was comparable to those observed for synthetic packagings based on oriented polyester coated with polyvinylidene chloride. Despite all this, the use of MFC as barrier is limited due to their poor water and water vapor resistance: indeed at 30°C and 90% RH, the equilibrium moisture content is around 15% (Henriksson and Berglund 2007). This is too high for packaging but could be improved by treating the MFC film surface with hexamethyldisilazane (HDMS). Thanks to the silylation process, the sylilated surface of the treated MFC films becomes hydrophobic and thus its water wettability is reduced (Chinga-Carrasco *et al.* 2012).

However the most common way to use MFC as reinforcement layer is to coat them at the paper surface with a dynamic sheet former (Syverud and Stenius 2009) at lab scale or with a spray coating (Beneventi *et al.* 2014) at pilot scale. MFC can be used alone (Beneventi *et al.* 2014) but fillers, such as kaolin, will increase the film density, while decreasing the water vapor sensitivity (Spence *et al.* 2011). It is also possible to replace the filler with some natural polysaccharide-based hydrocolloids such as starch (Ankerfors *et al.* 2009).

3.3.b Receiving ink

One of the difficulties during paper printing is the occurrence of lint and dust, which result from the tendency of a paper surface to loose weakly bonded particles, which will accumulate on the blanket during offset printing. Ideal printing paper must absorb ink very quickly, without a high penetration. The ink absorption action is generally controlled by a latex layer, which is a common adhesive used in coating at the ink interface (Gane and Koivunen 2010). In literature, coated MFC or coated cationic starch are compared in their propensity to adsorb selectively different pigment sizes (Ridgway and Gane 2013). It is reported that MFC tend to stay on top of the pigment layer, whereas cationic starch is completely adsorbed. It was found that papers coated with polysaccharides hydrocolloid (starch), then coated with MFC improve their surface dry-pick resistance and thus reduce the linting and dusting phenomena (Ankerfors *et al.* 2009).

3.4 Active packaging

The idea of active packaging is to add an active substance into the packaging material itself instead of incorporating an active compound into the food formulation and promote a longer protected food product. Recent studies have reported the development of antibacterial packaging using MFC coatings as delivery system, which provide a slow and continuous release of active substance thanks to their nanometric dimension and porous system and their ability to form strong films (Lavoine *et al.* 2014). It was shown that a MFC-coated packaging is able to release antimicrobial molecules over 1 month compared to 18 days without MFC *(*Lavoine *et al*. 2014). These results are promising for future food-packaging applications.

3.5 Intelligent paper

The paper applications in electronics described in literature are: dielectrics for super capacitors (Pushparaj *et al.* 2007), permeable membranes in liquid electrolyte batteries (Nyström *et al.* 2009), microfluid channels (Carrilho, Martinez, and Whitesides 2009), organic thin film transistors and printed sensors (Yang *et al.* 2007), batteries (Hilder, Winther-Jensen, and Clark 2009) and foldable circuit boards (Siegel *et al.* 2010).

A recent study has shown that paper can not only be used as a substrate but also as the dielectric for devices based on semiconductor oxides (Pereira *et al.* 2014). This semiconductor performance has been improved by using MFC sheet. Thanks to their homogenous surfaces and dense structures, the highest resistivity was obtained with MFC due to the low mobility of H^+ and OH^-, as these ions make an important contribution to the electrical conductivity. This field of application is promising but still limited by the rather slow switching time (time for the command execution) of the MFCs.

4. Challenges for the MFC markets

MFC is a promising material for many applications but its development is limited by the lack of characterization and standardization. The first point of improvement is thus to establish global standard and characterization methods for MFC (structure, surface properties, performance) to enable reproducibility and comparative analysis.

The second point is to improve the MFC production and quality along different axes devoted to:

- The decrease in the damages in MFC due to the extraction process
- The control of the dispersions and the quality of MFC: particle size, aspect ratio, rheology, which directly influence the MFC properties
- The reducing of the cost of extraction process and the energy consumption
- The scale-up of the production to industrial scale

Despite these priorities materials based on MFC will have to deal with some limits:

- The hydrophilic and polar nature limit their exploitation (too low solids content in MFC and too high moisture sensitivity)
- The new regulations about the use of nanoparticles

General Bibliography

Structure and composition of wood fibers

1. Wood chemical composition

Wood is mainly composed of polysaccharides (cellulose, hemicelluloses and pectins) and lignin, which represent more than 90% of the wood dry mass. It also contains a low percentage of extractible compounds and minerals. Their proportions vary as a function of the wood species: hardwood or softwood (Table 3).

Table 3: Wood composition in percentage of dried mass adapted from Thomas 1977.

Chemical composition	Hardwood	Softwood
Cellulose	43 - 47%	40 - 44%
Hemicelluloses	28 - 32%	25 - 29%
Lignin	17 - 23%	25 - 31%
Extractible compounds	2 - 8%	1 - 5%

1.1 Wood polysaccharides

1.1.a Cellulose

Cellulose is the main constituent of the plant cell wall. It is a linear homopolymer (Figure 5) consisting of glucosyl unit connected through a β-(1,4) type of linkage (Timell 1967). The cellulose chemical formula corresponds to $(C_6H_{10}O_5)_n$ where n is the number of glucosidic units corresponding to the degree of polymerization (DP). The cellulose DP is strongly dependent on the cellulose origin. In wood, the cellulose native chains have a DP estimated between 2500 and 4500 while the DP may increase to 20 000 in cotton and even more in some seaweed cellulose.

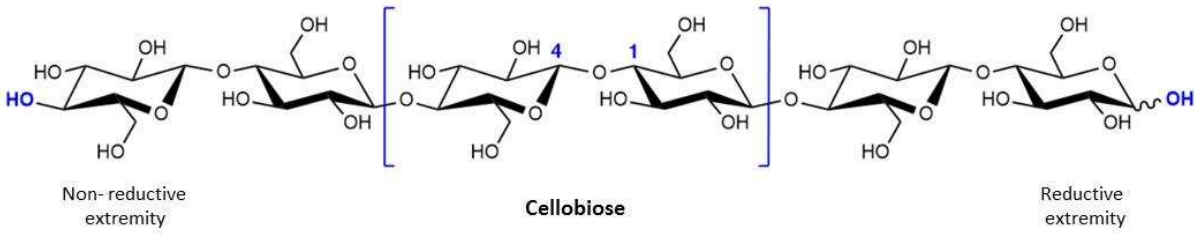

Figure 5: The cellulose chain structure.

The cellulose chains are oriented with two non-equivalent extremities. One extremity is called reductive and is terminated by a hemiacetal group at C1, whereas in the other extremity, called non-reductive, the C4 is part of a secondary alcohol moiety (Figure 5).

1.1.b Hemicelluloses

Hemicelluloses are the second polysaccharides present in the wood after the cellulose. They represent a large group of heteropolymers, which differs from each other with their sugar backbones and their branches.

The different sugar constituents of hemicelluloses (Figure 6) have been classified in four general groups (Timell 1967):

- hexose (D-glucose, D-mannose and D-galactose)
- pentose (D-xylose, L-arabinose and D-arabinose)
- deoxyhexose (L-rhamnose and L-fucose)
- hexenuronic acids (D-glucuronic acid, 4-O-methyl-D-glucuronic acid and D-galacturonic acid) .

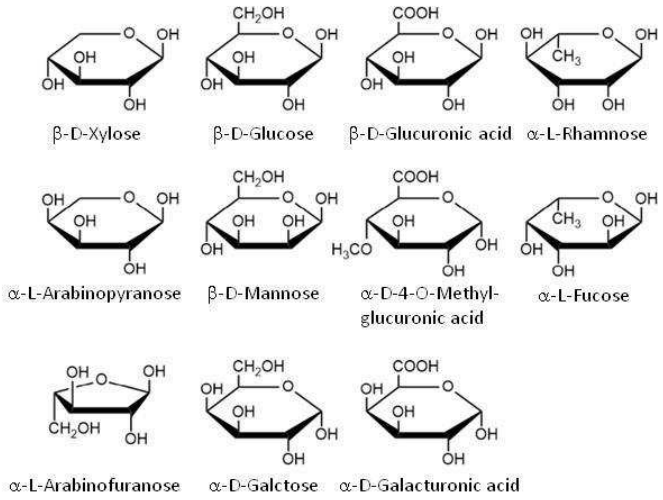

Figure 6: Sugar constituent of the hemicelluloses.

The hemicellulose chains are shorter compared to those of cellulose and their DP in native wood is estimated between 100 and 200 (Timell 1967). According to the different cell walls, hemicelluloses can be divided into four general classes of polysaccharide types: xylans, mannans, β-glucans with mixed linkages, and xyloglucans (Ebringerová, Hromádková, and Heinze 2005). In the case of secondary cell wall, the main hemicelluloses are the O-acetyl galacto-glucomannan and the arabino-4-O-methylglucuronoxylan in softwood, while the O-acetyl-4-O-methylglucuronoxylan and glucomannan without substitution are dominating in hardwood.

The O-acetyl-4-O-methyl-glucuronoxylan (Figure 7 A) contains a backbone of β-D xylosyl residues linked in β-(1,4) and substituted with α–D-4-O-methylglucuronic acid and acetate groups. Glucuronic acid is only branched in O2 of xylosyl for steric reasons, while the acetates are linked without preference to O2 and O3 (Ebringerová, Hromádková, and Heinze 2005).
By comparison, in softwoods, the arabino-4-O-methyl-glucuronoxylan (Figure 7 B) consists of a similar β-(1,4)-xylan backbone but α-L-arabinofuranosyl residues present in hardwood xylan mainly replace the acetate substitutions. Softwood xylan can also be acetylated but in lower proportion than the hardwood xylan counterpart (Ebringerová, Hromádková, and Heinze 2005).

In contrast with β-1,4-xylan, glucomanans (Figure 7 C) have a backbone of glucosyl and mannosyl linked in β-1,4. The distribution of glucosyl and mannosyl is not regular and the ratio of mannosyl/glucosyl is generally of the order of 1:2 (Timell 1967). In the case of softwoods, galacto-glucomanans are slightly branched with α-D-galactosyl in O6 of the mannosyl residues only. Some acetyl substitutions are also found in O2 or O3 while no branching is observed for hardwood glucomannans (Ebringerová, Hromádková, and Heinze 2005).

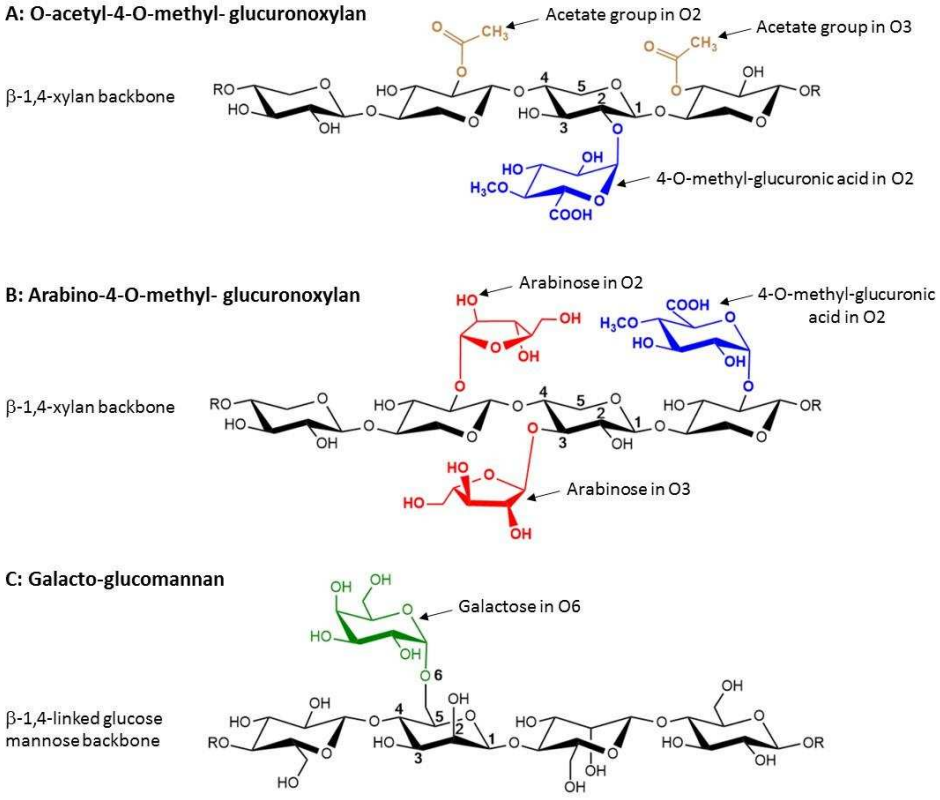

Figure 7: Softwood and hardwood hemicelluloses structures (Ebringerová and Heinze 2000).

1.1.c Pectins

The last group of wood polysaccharides is pectins, which represent only 1 to 2% of the wood dry-mass. Pectins mainly consist of α-D-galacturonic acids linked in α-(1,4) and branched with acetyl and methyl groups. It is also possible to find in their backbone, α-L-rhamnosyl residues bound in α-(1,2) to the galacturonic acids moieties. The rhamnose may be sometimes substituted with lateral chain made of arabinose and galactose.

1.2 Lignin

Lignin confers to the plants their rigidity, reduces the water permeability of the plant tissues and renders the wood more resistant to microorganisms attack and oxidative phenomena. The lignification of the cell wall is one of the last steps of the wood cell construction, which happens after the polysaccharides depositions in the cell wall. The lignin is a complex non-polysaccharidic polymer (Lewis and Yamamoto 1990). It is based on three units of hydrophenylpropane (Figure 8):

- the p-coumarylic alcohol (4-hydroxycinnamique alcohol), also called p-hydroxyphenyl (H)
- the coniferylic alcohol (4-hydroxy-3-methoxycinnamic alcohol), also called gaïacyl (G)
- the sinapylic alcohol (4-hydroxy-3,5, dimethoxycinnamic), also called syringyl (S)

The softwood lignin is characterized with more than 90% of G units while the hardwood lignin contains a mixture of G and S. For both hardwoods and softwoods, the H units have the lowest proportion (Thomas 1976).

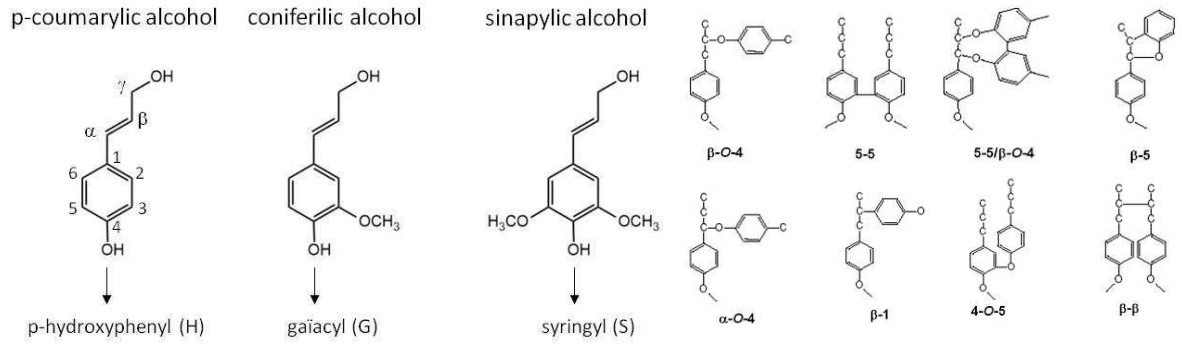

Figure 8: Hydrophenylpropane units of lignin and main linkages.

The lignin structure is still not fully understood and its final composition may result from the condensation of three hydrophenylpropane units hooked together by ether (C-O-C) and carbon-carbon (C-C) bonds. Different possible linkages between the three units are considered and presented in Figure 8. The linkages β-O-4 and α-O-4 are dominant in hardwoods and softwoods respectively. They are labile because they are non-condensed and may be cleaved more easily than the other condensed linkages (Lewis and Yamamoto 1990).

1.3 Extractible compounds and minerals

The extractible compounds or extractives represent a large group of low molecular material, which vary as a function of the wood species, the age of wood and of the wood constituting parts. Even if they are in minor quantity in wood, they can induce an increase in chemical consumption during the pulping process. They are most often removed from wood by water or organic solvents (Thomas 1976). Minerals are normally characterized as ash content. There is less than 1% of mineral in wood but they are essential for the wood structure. The main components are calcium, potassium, magnesium, manganese and sodium ions, but some traces of other constituents such as aluminum or copper may be also found.

2. Association between wood constituents

This exact organization of the plant cell wall is not fully understood but it is admitted that it is made of a network of cellulose microfibrils included in a matrix of pectin, hemicelluloses and lignin. The cohesion of this network results from a series of rather weak bonds, namely Van der Waals interactions, hydrogen bonds and a few covalent bonds.

The cellulose chains are organized into microfibrils. Within a given microfibril, the cellulose chains are hooked to one another by hydrogen bonds to form layers, which themselves are stabilized on top of one another by Van der Waals interactions. This organization confers to the microfibrils hydrophobic and hydrophilic surfaces. Thanks to the combination of this duality, the cellulose microfibrils are able to interact with hemicelluloses by interactions of either Van der Waals or hydrogen bonding types.

Regarding the lignin, it is susceptible to interact with the hemicelluloses through covalent linkages, commonly named Lignin-Carbohydrate-Complexes (LCC). In these, three linkages have been identified between the hemicellulose branches or their reductive extremity and the lignin (Figure 9). In softwoods, benzylic ether linkages have been characterized between the carbon Cα of the lignin and the arabinosyl or galactosyl units of the arabino-xylan and of the galactoglucomannan. The carbon Cα of the lignin may also interact with the glucuronic acid branches of xylan in hardwoods and softwoods through a benzylic ester linkage (Joseleau and Gancet 1981). Phenol glycosidic ether linkage may be also formed between the hydroxyl phenol group of the lignin and the reductive extremity of hemicelluloses (Merewether, Samsuzzaman, and Cooke 1972; Joseleau and Kesraoui 1986).

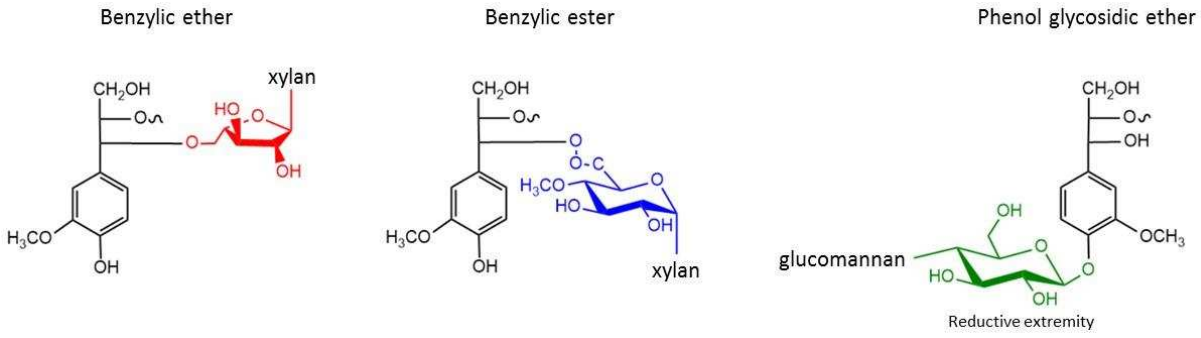

Figure 9: Main LCC linkages between lignin and polysaccharides.

With similar linkages, the lignin may also be associated with pectins, containing arabinan or galactan backbones (Meshitsuka *et al.* 1982) and possibly cellulose (Jin *et al.* 2006).

3. Fiber cell wall structure

Fiber cell walls have multi-scale dimensions with length of 1 to 3 mm, width of 10 to 50 µm and wall thickness of 1 to 5 µm (Figure 10 A). They are composed of a cell lumen (L), a middle lamella also called intercellular material, a primary wall, and a secondary wall, which is subdivided into three secondary layers S1, S2 and S3 (Figure 10 B).

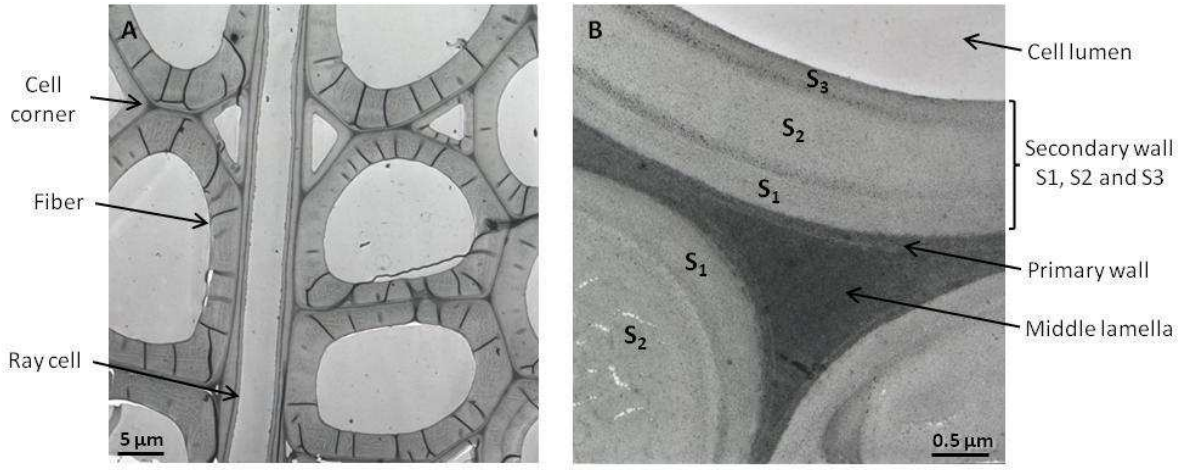

Figure 10: Fibers and cell wall structure, (A): Fibers cross section (B): Zoom on the cell corner (Adapted from Meyer-Pinson 2001).

The intercellular cohesion is given by the middle lamella, which is a very thin layer from 0.5 to 1.5 µm (Plomion, Leprovost, and Stokes 2001). The primary wall, which consist also of a very thin layer (0.3 to 1 µm), promotes the cellular growth. The thick secondary wall represents 75 to 85% of the whole cell wall volume and is the most important part for the mechanical support of the tree. In the secondary wall, the S2 layer is the thickest layer (1 to 10 µm) than S1 and S3 from 0.1 to 0.35 µm and 0.5 to 1.1 µm respectively (Plomion, Leprovost, and Stokes 2001).

The major component of the S1, S2 and S3 layers, consist of cellulose microfibrils. In the opposite of the primary wall where they are disordered, cellulose microfibrils are in parallel arrangement in the secondary wall but with different orientation angles from one layer to another. Indeed the microfibrils in S1 and S3 layers are oriented from 60° to 80° and from 60° to 90° (with respect to the cell axis) while in S2 layer, the microfibrils are oriented from 5° to 30° (Plomion, Leprovost, and Stokes 2001). The microfibrils orientation in the S2 layer has a strong influence on the wood mechanical properties, as the wood becomes less rigid (e.g. in juvenile wood) as the microfibrils angle increases.

The repartition of lignin, cellulose and hemicelluloses varies according to their localization in the cell wall. The lignin content is maximal in the middle lamellae, which also contains pectins. The primary wall is made of lignin, cellulose microfibrils, hemicelluloses and pectins, with xyloglucan being the main hemicellulose, representing 20 to 25% of the primary wall dry mass (Hayashi 1989). The maximum of cellulose content is found in the S2 layer. Because it is also the thicker layer of the cell wall, it contains most of the lignin, cellulose and hemicelluloses of the wood. On the other hand, even if the lignin content in the middle lamellae is estimated to be 70% in softwoods, it only represents 10% of the whole wood lignin because of the low thickness of the lamellae. In the S2 layer, only xylans and mannans are represented as hemicelluloses (Table 4) and their proportions vary with wood species (Meier 1985).

Table 4: Polysaccharides composition of the S2 layer of hardwoods and softwoods (adapted from Meier 1985).

	Hardwood		**Softwood**
Polysaccharides	*Birch*	*Pine*	*Spruce*
Cellulose	48.0%	64.3%	66.5%
Glucurono-xylan (gluc)	47.7% (O-acetyl-4-O-methyl-gluc)	10.7% (Arabino-4-O-methyl-gluc)	15.7% (Arabino-4-O-methyl-gluc)
Glucomannan	2.1%	24.4%	24.6%
Arabinan	1.5%	0.8%	0.0%
Galactan	0.7%	0.0%	1.6%

The softwood hemicelluloses are characterized by a high proportion of glucomannans (24.5%), slightly branched with galactose (in spruce) and a smaller proportion of arabino-4-O-methyl- glucuronoxylan (11 to 16%), while in hardwoods, they are mainly composed of O-acetyl-4-O-methyl- glucuronoxylan (48%).

4. Secondary cell wall biosynthesis

The organization of the different constituents of the secondary cell wall (cellulose microfibrils embedded in a matrix of hemicelluloses, pectins and lignin) is directly related to the biogenesis of the wall.

4.1 Biosynthesis of cellulose

In the case of wood, the only known component identified in the cellulose biosynthesis is the Cellulose Synthase Catalytic (CESA) protein (Pear *et al.* 1996) but mutations in genes indicate that several other proteins are also involved in the overall process of cellulose synthesis (Somerville 2006). The cellulose chains are synthesis at the plasma membrane, using uridine diphosphate activated glucose (UDP-Glc) as a monomer. As soon as the monomer is present, the CESA units secrete the cellulose chains, which collapse into microfibrils under Van der Waals forces.

In the case of higher plants (such as wood or cotton, Figure 11 A), the CESA subunits are believed to be organized in hexametric rosettes containing 36 CESA subunits according to cryo-fracture TEM observations performed on the plasma membrane (Saxena and Brown 2005; Herth 1983). Larger structures of rosette, with more than 1000 CESA, have been also observed in the case of the alga *Valonia ventricosa* synthases (Itoh and Brown 1984). The formation of the rosette is supposed to originate from the Golgi apparatus, from where they migrate toward the plasma membrane along cortical microtubules (Figure 11 B). It is only in the plasma membrane that the rosette becomes active and synthesizes cellulose chains (Somerville 2006).

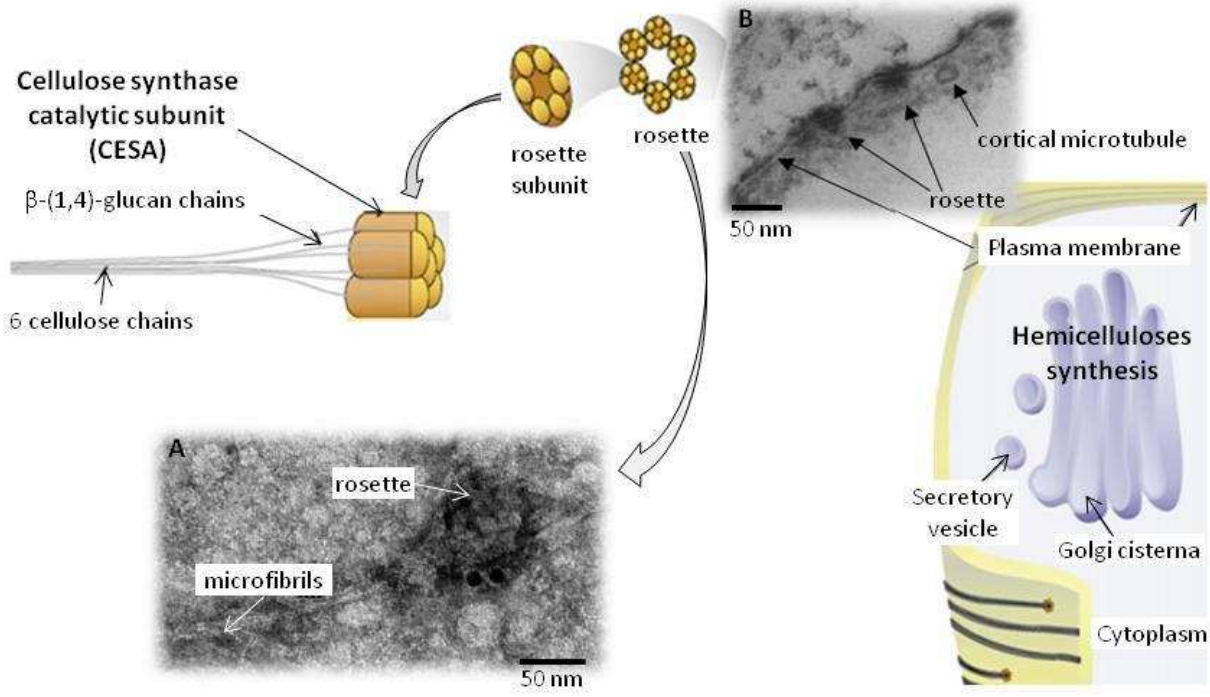

Figure 11: Schematic representation of wall polysaccharides biosynthesis (adapted from Saxena and Brown 2005; Lerouxel *et al.* 2006), A: In vitro synthesis of cellulose microfibrils of cotton, B: Ultrathin section through the plasma membrane of an alga (*Boergesenia forbesi*).

The orientation and the position of the cellulose chain in the microfibrils are determined by the CESA subunit (Figure 12). The β-1,4-glucan chains are formed by adding one by one the glucosyl units from the non-reductive end of the emerging chain.

In the case of wood, it is admitted that 30 to 40 cellulose chains are assembled into one elementary microfibril. Two types of CESA subunits, α and β, would be required to allow such a structure to spontaneously assemble in microfibrils. Each β subunit needs to interact with two others and two different α isoforms can be distinguished: α_1 which interacts with two β isoforms and α_2 which interacts with three isoforms, another α_2 and two β isoforms (Scheible et al. 2001).

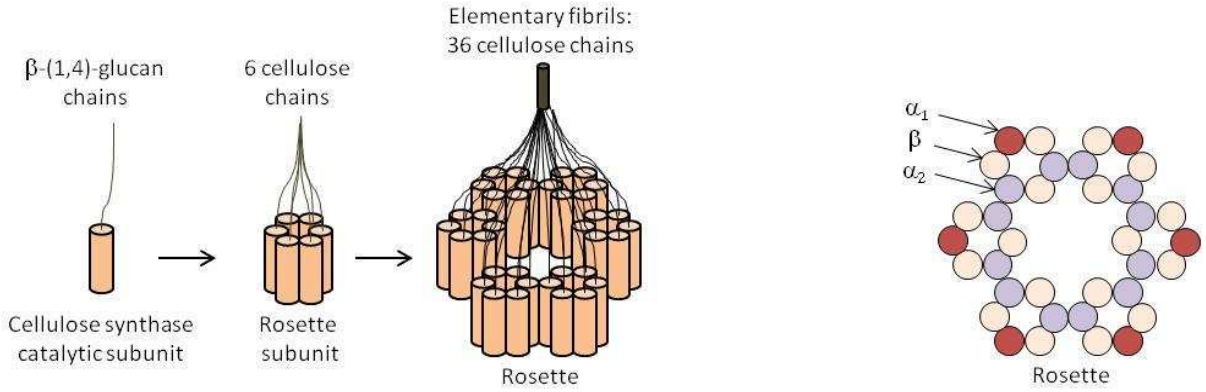

Figure 12: A model for the structure of the rosette. A CESA is believed to contain 8 helices defining a pore through which the nascent cellulose chain is spun. 6 CESA subunits are assembled to form a rosette subunit. These subunits are themselves assembled to form the rosette containing 36 CESA from where emerges the cellulose elementary microfibril, (adapted from Doblin *et al.* 2002).

At present, the molecular description of the functioning of CESA is not known. However, the functioning CESA is believed to be quite similar to that of the cellulose synthase system in cellulose producing bacteria, namely the BcsA/BscB. A recent spectacular crystallographic study describes the molecular mechanism that converts the UDP-glucose into a cellulose chain emerging from a tunnel located at the center of the BcsA/BscB. Structural snapshots of the biosynthesis process indicate that cellulose is translocated one monomer at a time, via a ratcheting mechanism involving a proteinaceous "finger helix" that contacts the polymer terminal glucosyl and pushes the nascent chain toward the exit of the tunnel. (Morgan *et al.* 2016).

To the opposite of the cellulose chain, the hemicelluloses are synthesized in the Golgi apparatus and delivered to the wall by secretory vesicles (Figure 11). With hemicelluloses, the biosynthesis may start with the backbone synthesis and then the branches such as acetates and glucuronic acids are added by glucuronyltransferase catalyzed reactions. The main constituents of the lignin (three hydrophenylpropanes) are synthesized inside the cell and thus the lignin polymerization appears outside the plasma membrane, following a mechanism, which is still unknown.

4.2 Cellulose crystallinity and microfibrils structure

One of the first cellulose crystalline characterizations was done on cotton, due to the lack of lignin and of the high cellulose content. Solid state ^{13}C NMR spectra (Teeäär, Serimaa, and Paakkari 1987) have revealed the presence of amorphous and crystalline parts with a ratio determined by peak integration of the NMR resonances. For cotton, this gave an amorphous/crystalline ratio of 3.1/6.9, which was confirmed by X-ray measurements: 3.3/6.7.

Two different crystalline phases of cellulose, namely Iα and Iβ, were revealed by ^{13}C NMR spectroscopy, X-ray, neutron and electron diffraction, together with FTIR. From electron micro diffraction diagrams obtained on individual cellulose microfibrils of disencrusted *Microdictyon tenuis* cell wall, the unit-cell parameters and symmetry elements of both cellulose Iα and Iβ could be resolved (Sugiyama, Vuong, and Chanzy 1991) . Iα has a P1 triclinic structure with one cellulose chain per unit cell whereas Iβ has a $P2_1$ monoclinic structure with two chains per cell and the axis of the cellulose chain located on the 2_1 screw axes. The unit cell and symmetry elements of both crystalline structures are given in Table 5 (Sugiyama, Vuong, and Chanzy 1991) and represented in Figure 13. Both structures share the same fiber axis parameter *c* of 1.036 nm, corresponding to a cellobiosyl unit. Remarkably, the crystalline density of cellulose Iβ is of 1.63 and that of cellulose Iα is only of 1.61. This difference clearly indicates that cellulose Iβ is more stable than Iα. In fact, cellulose Iα can be converted into Iβ by a hydrothermal treatment, but the reverse is not possible.

Table 5: Iα and Iβ unit-cell parameters (adapted from Sugiyama, Vuong, and Chanzy 1991).

	Unit cell parameters					
	Lengths (nm)			Angles (degree)		
Crystalline forms	***a***	***b***	***c***	**α**	**β**	**γ**
Iβ monoclinic structure	0.801	0.817	1.036	90	90	97.3
Iα triclinic structure	0.674	0.593	1.036	117	113	81

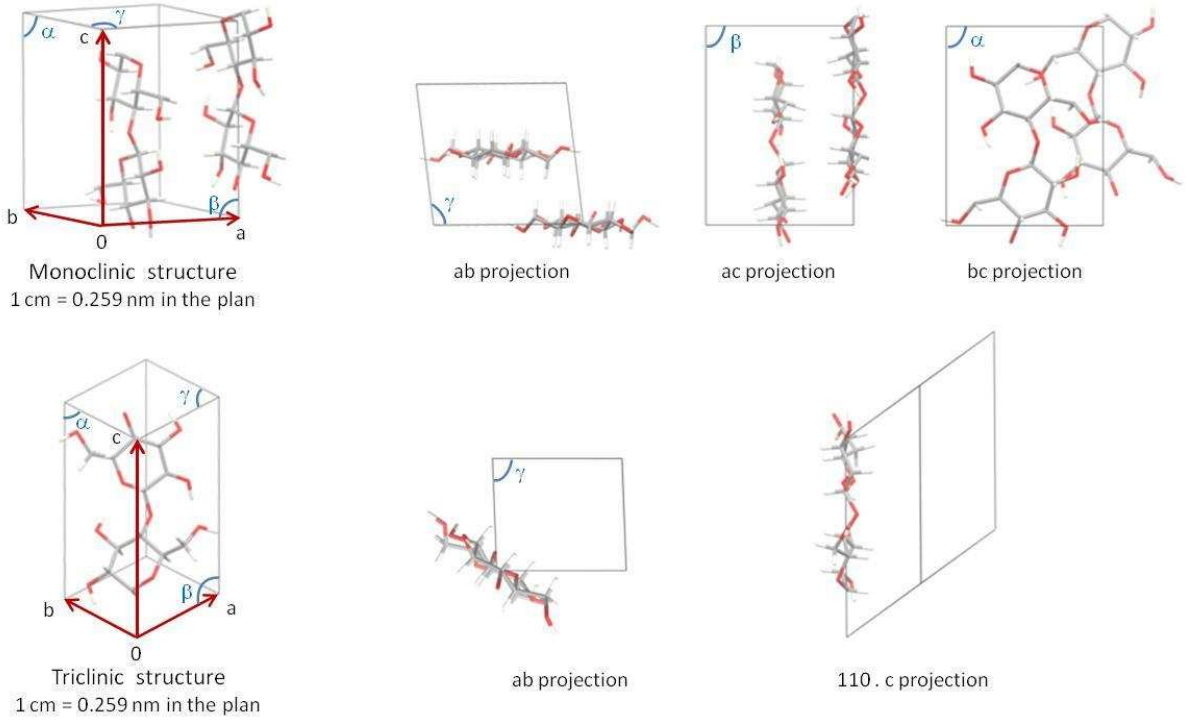

Figure 13: Cellulose unit cells: Iα and Iβ forms (Nishiyama *et al.* 2002,Nishiyama *et al.* 2003).

The ratio of the cellulose crystalline forms Iα and Iβ varies with the cellulose origin according to solid state NMR (Lennholm, Larsson, and Iversen 1994), X-ray measurements (Wada, Okano, and Sugiyama 2001) and FTIR data (Sugiyama, Persson and Chanzy 1991). Cellulose samples can be then sorted in two groups: the algae and bacterial types, where the Iα crystalline form is predominant (around 90%) and the cotton/ramie types with the Iβ form predominant. Tunicin, the animal cellulose, is considered as the model of cellulose Iβ since it is not only of high crystallinity, but contains more than 90% of this allomorph (Nishiyama *et al.* 2002). For cellulose Iα, samples extracted from the highly crystalline cell wall of the alga *Glaucocystis nostochinearum* are considered as model of this allomorph (Nishiyama *et al.* 2003).
However, it is more difficult to evaluate the Iα/Iβ ratio in the case of wood because of the presence of other components like lignin and hemicelluloses but it has been estimated to be Iβ predominant by X-ray measurements (Wada, Okano, and Sugiyama 2001).

Cellulose microfibrils from wood can be modeled as a semi-crystalline system possessing a crystalline core and amorphous surface due to the organization of the cellulose chains (Figure 14).

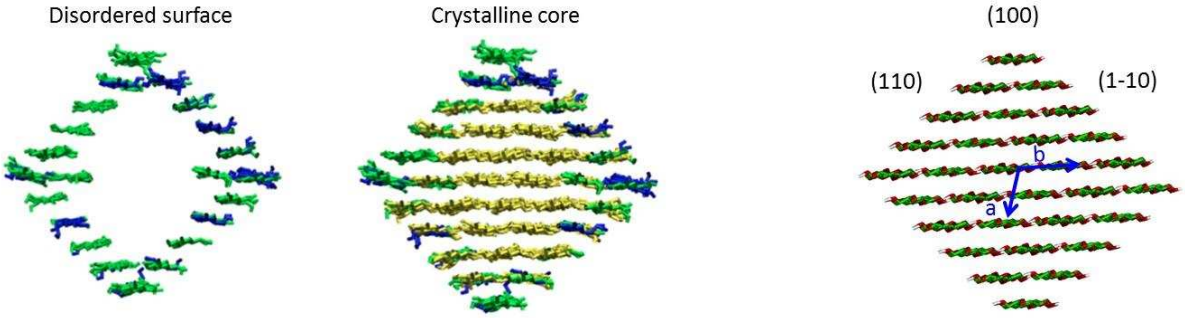

Figure 14: Microfibril model with 36 cellulose chains. Cross-section view along c axis right: Disordered surface and crystalline core (adapted from Chen 2013); left: Hydrophilic (110) and (1-10) surfaces and hydrophobic (100) surfaces (Mazeau 2011).

The squarish representation of the wood microfibril section is hypothetical since it is too small to be directly confirmed by diffraction contrast TEM images, as in the case of algal cellulose (squarish) or that of tunicin (lozenge-like). The representation, shown in Figure 14, limits the percentage of hydrophobic surface, which is only found at the corner of the section. Other authors favor a hexagonal section, which gives much more ground for the (100) hydrophobic surface. At present, it is not clear whether the squarish or the hexagonal model is the most realistic for wood cellulose.

Pulping process

The word "pulping" refers to the process of fiber liberation from the wood structure. It can be carried out mechanically, thermally, chemically or by combination of these treatments. The resulting product of pulping process is called "pulp", which corresponds to a fibrous raw material. In this study, we will focus only on "wood pulp" produced by chemical pulping.

The chemical pulping consists in lignin removal to facilitate the wood fiber separation. To attack the lignin structure and solubilize it, the wood chips are cooked in aqueous solution with chemicals at elevated temperature (100 to 175°C) under pressure for several hours. The cooking can be achieved under alkaline or acidic conditions, using respectively, sodium hydroxide and sodium sulfide (kraft cooking) or aqueous sulfur dioxide (SO_2) and a base such as calcium, sodium, magnesium or ammonium (sulfite cooking).

None of the cooking process is completely selective to the lignin structure and both of them also attack the hemicelluloses and decrease the cellulose DP. Nevertheless the alkaline conditions are anyway milder than the acidic ones. The kraft cooking is the predominant chemical pulping process for paper industry (around 90% in the world) principally because it better maintains the mechanical pulp properties than the sulfite counterpart.

1. Sulfite cooking pulp

The pH requested during the sulfite cooking is between 1.5 to 4.0, which induces the hydrolysis of the β 1-4 glucosidic linkages and decreases strongly the cellulose DP. The hemicelluloses are also degraded and about 70% of the glucomannans and 50% of the xylans can be lost in a spruce sulfite pulp (Gellerstedt 2007b). In the case of dissolving pulp production, the sulfite cooking is usually followed by alkali treatments to remove the residual hemicelluloses and obtain a pulp suitable for the production of viscose or cellulose derivative products such as carboxymethylcellulose and cellulose acetate. For these, obtaining high mechanical properties is not the interest, but the goal is to obtain pure cellulose, also called "specialty cellulose" devoided of hemicelluloses, which disturb the dissolution during the derivatization processes. In some cases, the hemicelluloses are recovered from the cooking liquor and effluents from alkaline treatments and are commercialized as high added value specialty products (e. g. xylitol).

2. Kraft cooking pulp

During the kraft cooking, the lignin is not the only wood component to be degraded. Even if it is not desired, a part of hemicelluloses and low molecular polysaccharides, such as pectins, are also removed during the cooking. The chemical pulping yield is around 40% to 50% of the initial raw material (Smook 2002), whereas lignin represents only 20 to 30% of wood component.

2.1 Carbohydrates degradation

Under alkaline conditions, the pectins are easily dissolved in the cooking liquor and the acetyl groups are also removed quite instantly from the hemicelluloses backbone (Aurell and Hartler 1965). The cellulose and hemicelluloses are also degraded because of a peeling reaction at the beginning of the cooking, then with alkaline hydrolysis at higher temperature (Aurell and Hartler 1965).

2.1.a Peeling reaction

The peeling reaction starts from the reducing end groups of the hemicelluloses chain and cleave them one monomer at a time (Aurell and Hartler 1965). The reaction is initiated by a keto-enol tautomerization (Figure 15), which opens the pyranose ring into aldehyde and alcohol (***a***). In the case of no branches in O2 and O3, the chain ends are reorganized with a benzylic rearrangement (***b***) and the β-H elimination in C4 take place (***c***). One free monomer is generated (***d***) and reorganized into isosaccharinic acid (***e***), while the rest of the chain (**R-OH**) turns back to the first step of reaction.

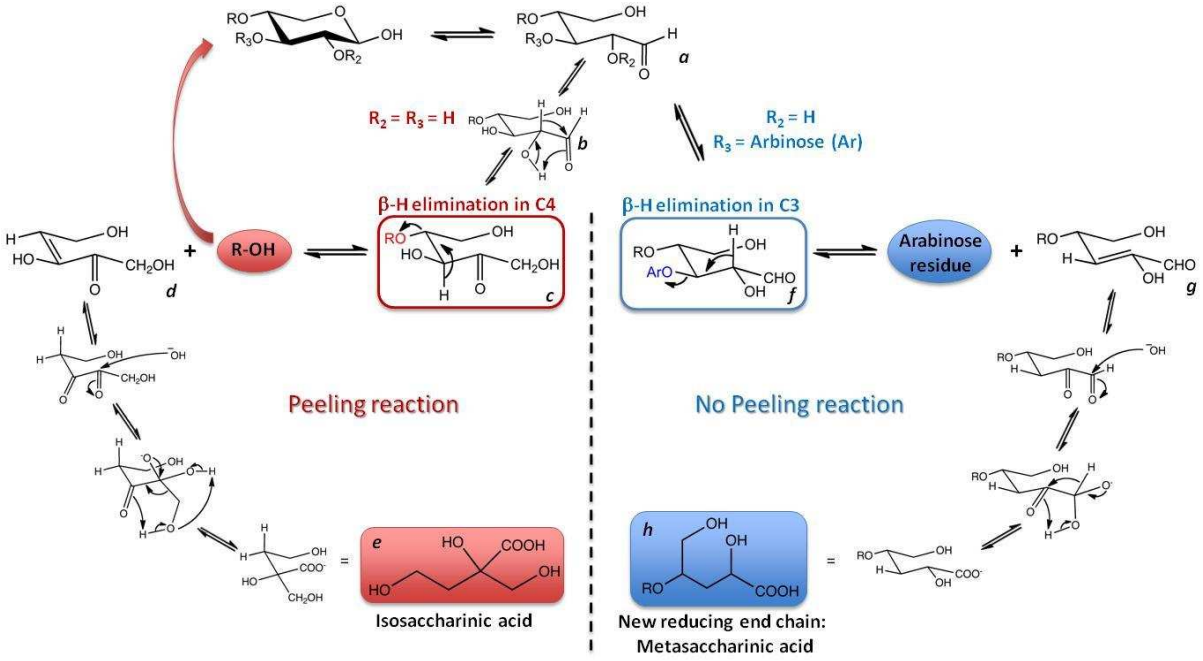

Figure 15: Peeling reaction (adapted from Gellerstedt 2007b).

The hemicellulose chains can be cleaved monomer by monomer until the β-H elimination in C3 (***f***) became more favored than in C4 (***c***) and this induces the end of the peeling reaction. Elimination in C3 (***f***) happens when O3 is branched with an arabinosyl residue (Aurell and Hartler 1965). In this case, arabinose is a better leaving group. Its elimination is favored in comparison with the hemicellulose depolymerization. Then the resulting chain end (***g***) is reorganized into metasaccharinic acid as a new reducing end group (***h***). The peeling reaction is prevented when O2 is branched with 4-O methyl-glucuronic acid (Aurell and Hartler 1965) because the keto-enol tautomerization equilibrium is no more possible (Figure 14 ***a***).

The glucomannans, which have no branches in O2 and O3, are the most sensitive to the peeling reaction and are eliminated at the beginning of the kraft cooking while xylans are protected thanks to their arabinosyl and glucuronic acid substitutions (Aurell and Hartler 1965 ; Wigell, Brelid, and Theliander 2007). However, the arabinosyl residues are removed when the temperature increases during the cooking process and xylans are exposed to alkaline hydrolysis, also called secondary peeling (Aurell and Hartler 1965; Hansson and Hartler 1968).

2.1.b Alkaline hydrolysis

The alkaline hydrolysis affects the DP of both xylan and cellulose (Hansson and Hartler 1968) by cutting the chain (Figure 16). The hydrolysis is initiated by a nucleophilic attack of the hydroxide ion O2 on C1 position (***a***) and an epoxy linkage (***b***) is formed by the chain elimination (**R-OH**). The epoxy is opened with sodium hydroxide ion and forms a new reducing end group (***c***).

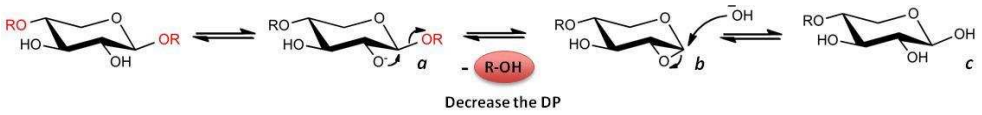

Figure 16: Alkaline hydrolysis or secondary peeling (adapted from Gellerstedt 2007b).

The cellulose DP, estimated between 7 000 to 10 000 in wood (Thomas 1976), is reduced from 2 000 to 800 in kraft pulp because of the combination of alkaline hydrolysis and peeling reaction on the new reducing end group (Figure 16 ***c***). The residual xylan, which stays in the pulp at the end of the cooking, seems to be less impacted than cellulose and its DP is reduced from 200 to 140-160 (Hansson and Hartler 1968).

2.2 Hexenuronic acid formation

Under alkaline condition, the 4-O-methyl-glucuronic acids branched on xylans (Figure 17 ***a***), are converted into hexenuronic acids (Johansson and Samuelson 1977; Buchert *et al.* 1995) by methanol elimination (***b***) even if at first it was believed that it were removed during cooking (Hansson and Hartler 1968). This confusion is explained by the degradation of hexenuronic acid (Figure 17) into 5-formylfuronic acid (***c***) and furanic acid (***d***) under acidic conditions used in conventional glucuronic acid analyses (Li and Gellerstedt 1996).

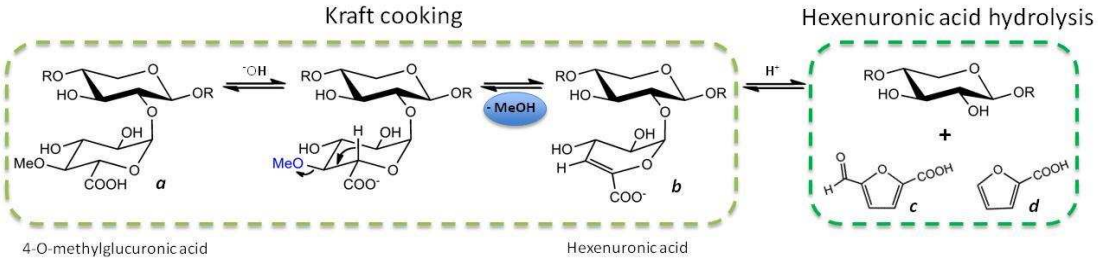

Figure 17: Hexenuronic acid formation in xylan and degradation (adapted from Johansson and Samuelson 1977; Li and Gellerstedt 1996).

More recently, hexenuronic acids have been characterized both in the pulp after kraft cooking (Buchert *et al.* 1995) and in the cooking liquor (Teleman *et al.* 1995). The presence of hexenuronic acids in the pulp is not suitable because of their unsaturation. Indeed they have similar reactive unsaturation properties than in the lignin.

Consequently, the determination of the residual lignin (Kappa number) can be overestimated and the demand in bleaching chemicals is increased because the hexenuronic acids consume a part of chemicals instead of lignin (Li and Gellerstedt 1996). Some studies highlighted that it is possible to remove them before bleaching or at the beginning of the bleaching sequence with mild acidic treatment, especially for hardwoods pulps (Bergnor-Gidnert, Tomani, and Dahlman 1998).

2.3 Xylans adsorption on cellulose fibers

During the kraft cooking, a part of the hemicelluloses is dissolved in the cooking liquor. A part is degraded because of the peeling reaction and the alkaline hydrolysis but another may also be redeposited at the fiber surfaces. Indeed, it is believed that the arabinose and acetyl removal, decreases the xylan solubility in the cooking liquor and thus favors its recrystallization and precipitation onto cellulosic fibers (Yllner and Enström 1957). The xylan re-adsorption on the fibers during kraft cooking has been extensively studied before the discovery of the glucuronic acids conversion into hexenuronic acids. At that time, the glucuronic acids were considered to be removed from the xylans under alkaline condition (Hansson and Hartler 1968) and it was difficult to investigate the role of the hexenuronic acids in the xylans redeposition. More recently, the xylans re-adsorption scheme gains a new interest because it improves the yield of chemical pulping by increasing the final pulp weight at the end of the cooking (Danielsson and Lindström 2005). This new study observes similar conditions for the xylans re-adsorption.

As previously described, the xylans are better redeposited onto the cellulose fibers at 140°C to 160°C under low alkaline concentration (Aurell 1965; Hansson and Hartler 1969). However the xylans re-adsorption only occurs in the first hour of cooking (Danielsson and Lindström 2005) and then the degradation reactions, such as alkaline hydrolysis, in the black liquor,are found to be dominant (Figure 18). After 3h at 165°C, the xylan DP in the cooking liquor is determined to be around 45 by Size Exclusion Chromatography (SEC) which is 3 to 5 times smaller than the xylan DP in wood (Danielsson and Lindström 2005; Jacobs and Dahlman 2001).

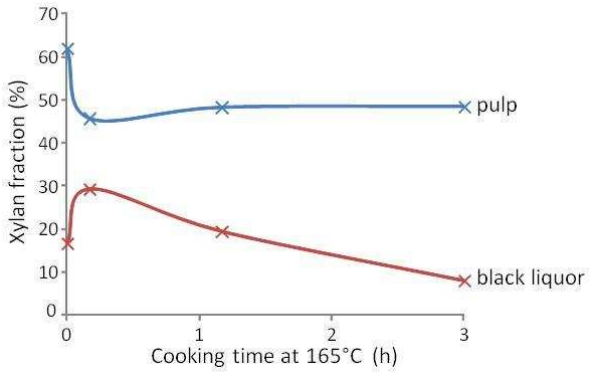

Figure 18: Xylan concentration evolution: in pulp and black liquor during kraft cooking at 165°C (adapted from Danielsson and Lindström 2005).

.

3. Bleaching

At the end of the cooking process, most of the lignin is degraded but some residual groups, also called chromophore groups, stay into the pulp and color it. To remove the residual lignin groups and provide a colorless pulp, the cooking process is always followed by a bleaching step including oxidative and extraction treatments (Gellerstedt 2007a).

The lignin content in the pulp after cooking (unbleached pulp) and after bleaching (bleached pulp) is determined with the Kappa number. The pulp brightness is also used to determine the pulp ability to reflect monochromatic light compared to a standard. Because the sulfite cooking is more efficient to remove the lignin than the kraft process the sulfite pulps before bleaching are lighter in color, compared to the unbleached kraft pulps (Figure 19).

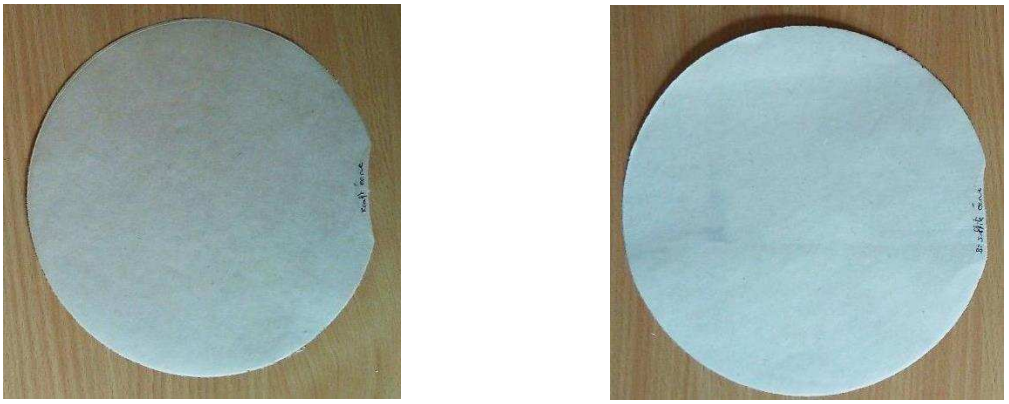

Unbleached kraft pulp (Brightness, 30% ISO) Unbleached Sulfite pulp (Brightness, 46% ISO)

Figure 19: Images of unbleached kraft and sulfite pulp (CTP).

The bleaching sequences are proper to each mill. In principal, the bleaching process is common with kraft and sulfite pulp regardless of the wood species and the sequence is modulated to achieve the pulp properties and the targeted applications. Common bleaching sequences start with a complementary delignification stage, called also O-stage (O for oxygen), which oxidizes the residual lignin unsaturations using dioxygen. Then chlorine dioxide stage (D-stage) and alkaline extraction sequences (E-stage) are repeated to solubilize and dissolve the oxidized lignin residues. One example of a bleaching sequence can be ODED. In some cases, the first oxidation stage, the O-stage, can be replaced by chlorine dioxide and alkaline extraction steps like DEDED.

But nowadays, all the modern chemical pulp mills possess an O stage at the beginning of the bleaching sequence. In some companies, a mild acid treatment may be also added after the delignification stage (O stage) to remove the hexenuronic acids formed during the kraft cooking (Buchert *et al.* 1995; Dahlman *et al.* 2003).

Today, the common bleaching ECF (elemental chlorine free), using chlorine dioxide (D) and alkaline treatments (E) is still the most used. It is called "elemental chlorine free", because it was initially developed to replace the first bleaching step, which uses chlorine gas to solubilize the lignin and thus emits more toxic byproducts such as dioxin.
Totally chlorine free bleaching (TCF) is proposed to avoid the chlorine emission by replacing chlorine dioxide treatment (D) with ozone (Z) and peroxide (P) stages. An example of bleaching TCF sequence could be OZP. However, the applications of TCF bleaching sequences are still limited because ozone and peroxide treatments decrease the cellulose DP (and the pulp viscosity) and limit the final brightness of the pulp. As in the cooking process, the bleaching ECF modifies the cellulose and the residual hemicelluloses contents in the pulp (Gellerstedt 2007a). If they have not been removed with mild acid treatment at the beginning of the bleaching sequence, the hexenuronic acid groups, branched on xylans, are most often degraded during the oxidation (O-stage).

The cellulose DP is reduced during the oxidation (O-stage) and the alkaline extraction (E-stage) because of oxidative cleavages (Figure 20 A). Indeed, hydroxyl groups along the cellulose chain are oxidized during the O-stage (***a***), then the alkaline conditions of the E-stage favored the β-H elimination in C4 and the chain is cut (***b***). The new reducing end is reorganized into pentose ring (***c***).

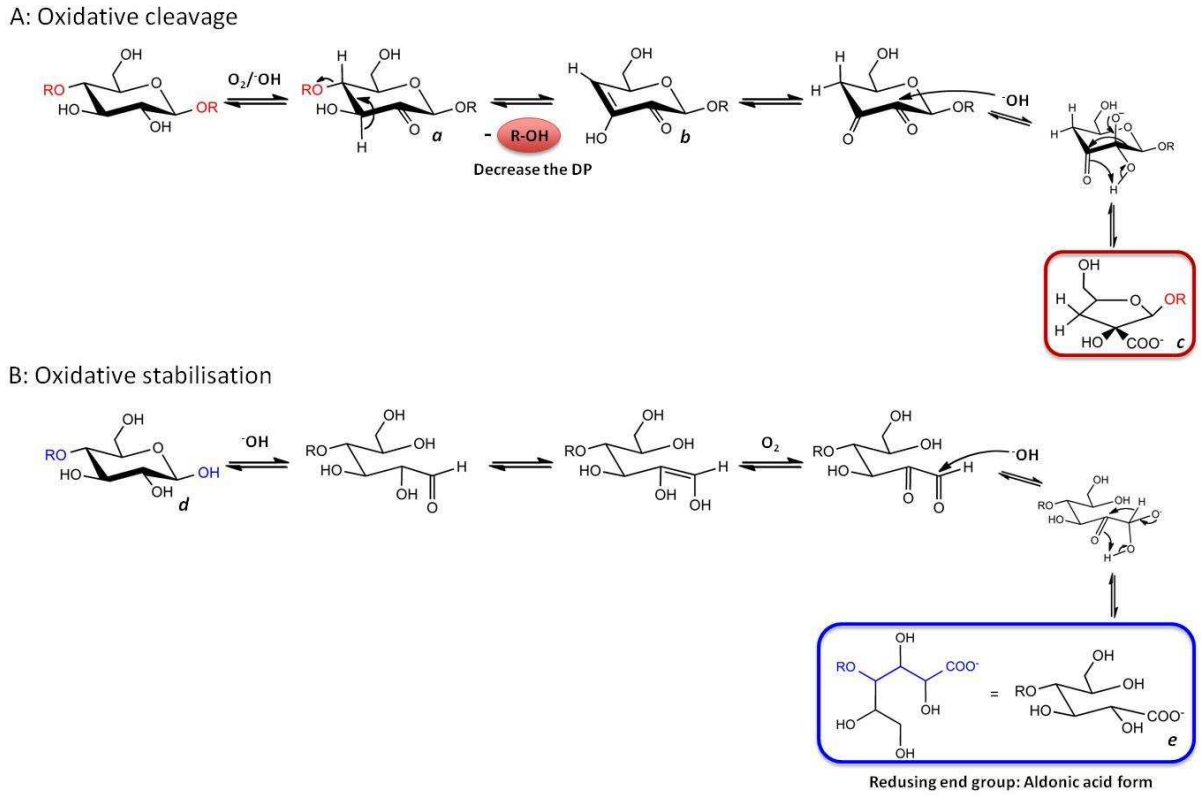

Figure 20 : Oxidative cleavage of a polysaccharide chain and oxidative stabilization of reducing end group (adapted from Gellerstedt 2007b)

During the bleaching, the oxidative stabilization (Figure 20 B) protects the cellulose chain from the peeling reaction (Gellerstedt 2007a). In the O-stage, the reducing end groups of the cellulose chain (***d***) are oxidized and rearranged in the aldonic acid form (***e***), which avoids the chain degradation monomer by monomer as at is the case during the cooking.

4. Final remarks on sulfite pulp (specialty cellulose) and kraft pulp

The fiber are longer in the kraft pulp than in the sulfite one (Figure 21) because the cooking conditions are less destructive in the case of the kraft process. In both cases, the lignin is fully removed after the bleaching and the bleached pulps may be considered as consisting of cellulose and hemicelluloses.

Kraft pulp Sulfite pulp

Figure 21: Optical microscopic examinations of kraft and sulfite pulp (CTP).

The drastic conditions applied in the case of the sulfite pulp for specialty cellulose production are responsible of the very low hemicelluloses content to the opposite of the kraft pulp where the hemicelluloses are less degraded even if a part of them are eliminated during the cooking (Table 6). The cellulose DP is also more damaged in the sulfite cooking due to the acid hydrolysis and the fibers are more deconstructed.

Table 6: Sulfite and kraft pulps characteristics.

Pulp grade	**Hemicellulose Content (%)**	**Cellulose DP**	**Fiber length (µm)**
Softwood sulfite pulp	4	760	1900
Softwood kraft pulp	16	1100	2400

To sum up the kraft and sulfite pulps have different advantages and defects, which make them suitable for different applications (Table 7).

Table 7: Kraft or sulfite process.

	Kraft process	**Sulfite process**
Chemicals	• alkaline cooking: NaOH and Na_2S	• acidic cooking: $H_2SO_3^-$ and counter ion • (Na^+, Ca^+, Mg^+, or NH_4^+), pH 3-5
Advantages	• produces highest strength pulp • keeps hemicelluloses	• produces brighter unbleached pulp • removes hemicelluloses and cut cellulose chain (decreases mechanical paper properties)
Applications	• strongest paper	• specialty cellulose

MFC production

1. Difference between microfibrils and microfibrillated cellulose (MFC)

The term "microfibril" designs one of the main components of the cell wall. In the case of wood, the microfibrils correspond to an assembly of elementary fibrils, each of them constituted of 30 to 40 cellulose chains as a result of the biosynthesis by the rosette complex (Saxena and Brown 2005; Herth 1983). The wood microfibrils size has been first estimated to 3.5 nm (Meier 1962) and since the diameter of one cellulose chain is around 0.1 nm, the number of cellulose in the elementary is around 35, in agreement with the biosynthesis model of the rosette. A recent study (Chinga-Carrasco 2011) has provided size estimation with TEM images of 28 nm for the microfibril and 3.5 nm for the elementary fibrils (Figure 22 left) which is in good correlation with previous values.

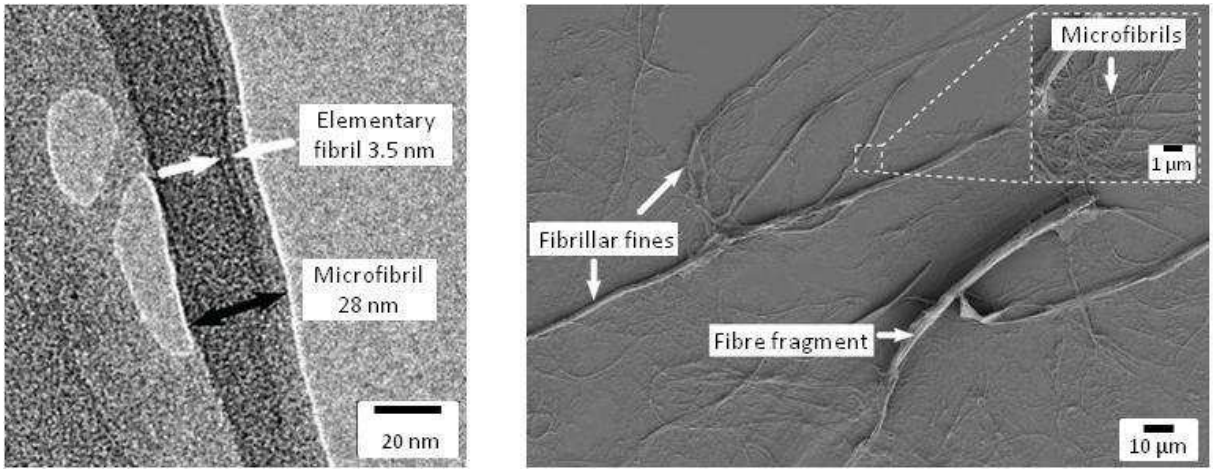

Figure 22: Difference between microfibrils and microfibrillated cellulose (MFC); left :*Pinus radiata* microfibril image (TEM); right: microfibrillated cellulose suspensions, dried on glass slides (homogenization 5 passes at 1000 bar), (Adapted Chinga-Carrasco 2011).

The first MFC suspensions were produced in 1977 at the ITT Rayonier Eastern Research laboratory in Whippany, USA by Turbak and his team (Turbak, Snyder, and Sandberg 1983; Herrick *et al.* 1983). Their elegant method consisted in running a 3% slurry of chopped pulp fibers through a high pressure Manton Gaulin milk homogenizer where a large pressure drop facilitated the microfibrillation. As the slurry reached 80°C at 8,000 psi, the fibers started to undergo a total phase change and turned into a translucent firm “gel” that they called microfibrillated cellulose (MFC). An example of MFC is shown in Figure 22 right. It is a non-homogeneous system mainly composed of microfibrils but also containing some residual larger structures such as fibers, fiber fragments and fibrillar fines. The microfibrils present in the MFC have diameters less than 100 nm, which explains why they are sometimes called nanofibrils, where “nano” refers to sizes between 0.001 and 0.1 µm (Chinga-Carrasco 2011).

Even if wood was the principal source of cellulosic materials, MFC can also be produced from a large panel of non-woody sources (Lavoine *et al.* 2012) such as sugar beet pulp (Dinand, Chanzy, and Vignon 1999), straw (Alemdar and Sain 2008), bagasse (Bhattacharya, Germinario, and Winter 2008), palm tree rachis (Bendahou, Kaddami, and Dufresne 2010) or even banana tree fibers (Deepa *et al.* 2011).

To avoid confusion between microfibrils, as a cell wall component, and microfibrils as a part of the microfibrillated cellulose (MFC), a list of terminology has been established with size correlation (Chinga-Carrasco 2011) and will be used in the rest of the manuscript (Table 8).

Table 8: Sizes according to terminology and morphology (adapted from Chinga-Carrasco 2011).

Diameter (µm)	Biological structures	Technological terms
10 to 50	Tracheid	Cellulose fiber
< 1	Macrofibrils	Fibrillar fines, fibrils
< 0.1	**/**	**Microfibrilated cellulose (MFC), microfibrils, nanofibril, nanofibers**
< 0.035	**Microfibrils**	**/**
$3.5 . 10^{-3}$	Elementary fibril	Elementary fibril , 36 to 40 cellulose chains
$0.1 . 10^{-3}$	β-1,4-glucan	Cellulose chain

2. Pre-treatment before MFC production

Because any process of MFC production has never succeeded in a perfect fiber deconstruction, it is generally needed to repeat the mechanical shearing several times to promote a good microfibrillation. This mechanical treatment consumes a large amount of energy: about 27 000 kWh per ton of MFC were necessary to produce a suspension from a sulfite pulp (Klemm *et al.* 2011).

To reduce the energy need, three categories of pretreatments were developed in order to facilitate the fiber deconstruction (Nechyporchuk, Naceur, and Bras 2016).

- Mechanical treatment with a mechanical cutting (Nakagaito and Yano 2004)
- Chemical treatment with carboxymethylation (Wågberg *et al.* 2008) or TEMPO-mediated oxidation (Saito *et al.* 2006)
- Enzymatic pre-treatment with cellulases (Pääkko *et al.* 2007)

2.1 Mechanical pretreatment

The microfibrillation may be improved by reducing the fiber length by mechanical cutting prior to the homogenization (Herrick *et al.* 1983). A combination of repeated mechanical forces was developed to promote the fibrillation of cellulose fibers with 30 passes through a refiner and then 14 passes in a homogenizer (Nakagaito and Yano 2004). More recently, a general mechanical method was developed and scaled-up industrially (Zimmermann, Bordeanu, and Strub 2010). First, the pulp was milled in a preliminary step to reduce the fiber dimensions and improve the swelling capacity in water, and then a mechanical pre-treatment was conducted in a thermostatic reactor with on-line dispersing system. After cooling to 15°C and dispersion at 20.000 rpm, cellulose fibril bundles were obtained. Then, these suspensions were introduced in a microfluidizer high shear processor.

The mechanical technique has its limits and the energy consumption is always high.

2.2 Chemical pretreatment

The fibers' deconstruction can be facilitated by chemical modification of cellulose before the homogenization. The TEMPO oxidation and carboxymethylation pretreatments both generate charges at the fibers surface, which improve the microfibrillation. The carboxymethylation consists in the substitution of the hydroxyl groups by carboxymethyl groups (CH_2COOH) while the TEMPO oxidizes selectively the primary alcohol groups of cellulose into carboxylic acids. Indeed, the introduction of charged groups into the fiber pulp has long been known to enhance delamination of the fiber walls. With the carboxymethylation pretreatment, the liberated fibrils had diameters of 5-15 nm and a length of more than 1 μm with a charge density about 0.5 meq/g.

The TEMPO oxidation presents the advantage of disintegrating fibers into microfibrils with width of 10-20 nm, using a much lower energy input. The dispersion of the fibers into microfibrils are facilitated by electrostatic repulsions caused by the anionic carboxylic groups between the TEMPO-oxidized cellulose microfibrils and the consequent decreases of the number of hydrogen bonds present in the wood cell walls (Saito and Isogai 2006). It is today a very common technique for producing well-dispersed MFC.

2.3 Enzymatic pretreatment

The combination of enzymatic hydrolysis and mechanical shearing has been developed for the MFC production (Pääkko *et al.* 2007; Henriksson *et al.* 2007) and patented (Lindström, Ankerfors, and Henriksson 2007). Pääkko *et al.* proposed a method to produce MFC with refining, enzymatic hydrolysis, second refining then homogenization of 2 wt.% aqueous suspension by 8 passes through a microfluidizer, while Henriksson *et al.* (2007) applied different enzyme concentrations, and use a homogenizer for 20 passes.

Commonly the enzymatic pretreatment performed are using celllulases which can be divided into three groups:

- the β-(1,4)-endoglucanases
- the exoglucanases
- the β-glucosidases.

The endoglucanase hydrolyzes randomly, the accessible intramolecular β-(1,4)-glucosidic bond of the cellulose chain and generates oligosaccharides. In the opposite of the “endo”, the exoglucanase is acting processively from the chain extremity and releases cellobiose (two units of glucose bond with β-(1,4) or glucose units in function if the enzyme is a cellobiohydrolase or a glucanohydrolase respectively. The β-glucosidases hydrolyze each β-(1,4)-glucosidic bond into glucose: it is particularly effective to break the cellobiose released by the other enzymes when multi-enzymatic cellulases are used. Comparative studies have shown that the endoglucanase had better effect on the microfibril separation (Nechyporchuk and Belgacem 2015).

2.4 Conclusion on the pretreatment

The use of pretreatment decreases the energy consumption of the MFC production (Table 9). The lowest energy requirement for the MFC production is obtained with chemical modification such as TEMPO and carboxymethylation. However, the TEMPO- MFC are the most expensive to produce because of the chemistry cost.

To produce MFCs with enzymatic pretreatment requires three times more energy than that of a chemical pretreatment. Nevertheless the cost for the enzymatic treatment is lower than that for the TEMPO chemistry. At least, the use of an enzymatic pretreatment shows advantages from the environmental point of view, compared to chemical methods

Table 9: Influence of pre-treatment on the energy consumption and the cost.

Pretreatment	Bleached Pulp type	MFC diameter (d) and length (l)	Energy requirement (kWht)
None	Kraft/Sulfite		Plugging problems
Carboxymethylation (DS=0.1)	Kraft/Sulfite	d = 5-15 nm l > 1 µm	-
TEMPO		d = 10-20 nm	4 000
Enzymatic	Sulfite	d = 20-50 nm	10 000

3. MFC production process

Different processes to generate MFC have been developed with the same idea of microfibril individualization.
Steam explosion, ball milling and blending have been used to deconstruct the fibers under the mechanism of pressurized steam then rapid release of pressure (Deepa *et al.* 2011). Mechanical crushing, with balls collision in a rotating cylinder (Zhang, Tsuzuki, and Wang 2015) and speed blender are also applied (Shahril *et al.* 2015). However, these processes are still limited by the MFC quality and homogeneity and the most common ways to produce MFC are the homogenization and grinding process (Figure 23).

The grinding system consists in a strong and ultra-fine refining system where the wood pulp is passed through static and rotating disks (Nechyporchuk and Belgacem 2015) whereas the pulp is injected through a small gap at high pressure (1500 bar) in the homogenization process. Two types of homogenization process have been developed, using homogenizers or microfluidizers. In the homogenizer, the pulp fibers are delaminated in the contact of the impact ring, while in the microfluidizer the pulp is circulating in the thin chamber, with specific geometry (Z or Y).

Both homogenization and grinding processes are available at pilot and industrial scale even if the microfluidizer is more dedicated to lab scale.

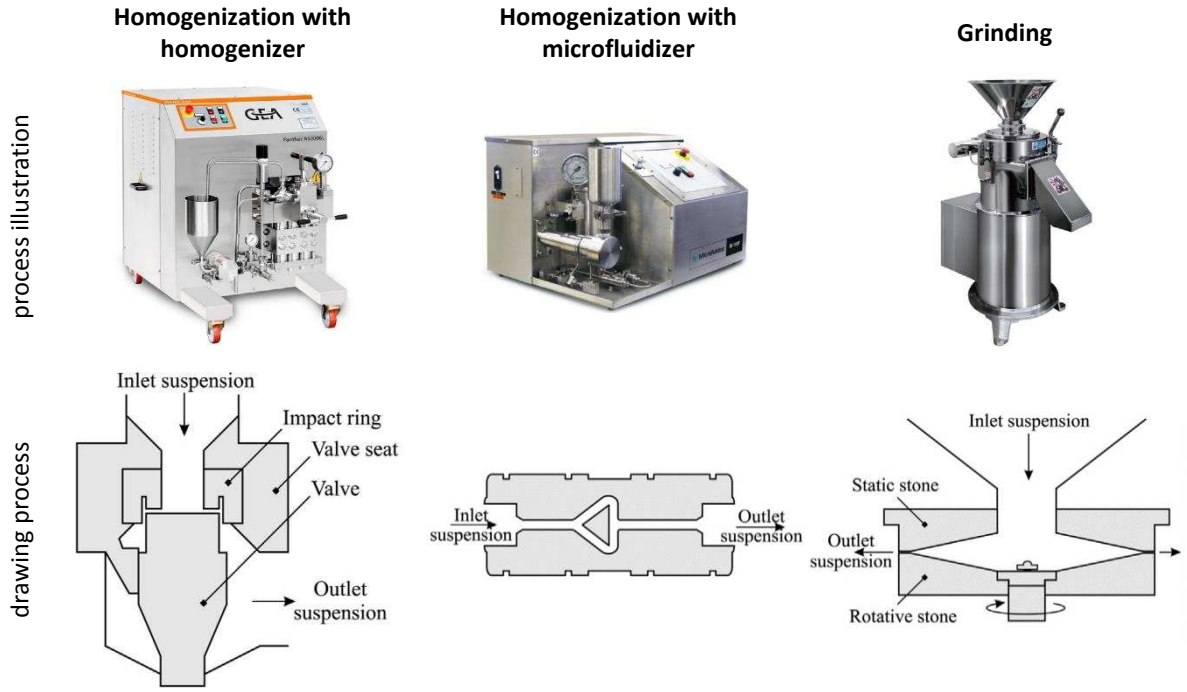

Figure 23: Process of MFC production (adapted from Nechyporchuk, Naceur, and Bras 2016).

More recently, new processes to produce MFC have been proposed, namely an extrusion process where the pulp is injected into a twin screw (Ho *et al.* 2015) or ultrasonication (Saito *et al.* 2013; Kaboorani, Riedl, and Blanchet 2013), which delaminates the fibers thanks to small vacuum bubbles created by the ultrasonic waves. The extrusion process is interesting because it allows working at 25 to 40% consistency whereas the pulp in the homogenizers needs to be injected at only 2-3%. Another industrial process has also been developed by FP Innovation, which produces "cellulose filaments" thanks to a long high consistency refining. The final product differs from MFC by their micro length size.

Each aforementioned process of MFC production and pre-treatment provides different types of MFC with different quality and properties. In this study, we will focus only on MFC produced by the homogenization process with homogenizer and refining as pretreatment, together with enzymatic step. The wood pulps used for the MFC production result from chemical pulping, (kraft or sulfite cooking) and bleaching.

Cellulose - xylan interaction

The interactions between the cellulose and hemicelluloses are of main interest due to their application for the paper industry as well as for cellulose-based materials. Indeed, this interaction may enhance the paper strength properties but negatively leads to increases in (i) the energy consumption for the fiber liberation and (ii) the chemical consumption.

Xylans were first supposed to induce the microfibrils helicoidal rotation as twisting agent and to maintain spaces between the microfibrils thanks to the glucuronic acid branches (Reis and Vian 2004). It is now admitted that xylan helps for the microfibrillar cohesion by bonding cellulose microfibrils together, but the role of the xylan branches in the interaction with cellulose is still under discussion. Some recent investigations performed with simplified model, e.g. *Arabidopsis thaliana*, highlight the fact that two kinds of glucuronic acid situation can be defined regarding the regularity of their arrangement along the xylose backbone (Bromley *et al.* 2013). It is then proposed to divide the xylan chain in different zones, with minor or major glucuronic acid content. Even it was first believed that the glucuronic acids favor the xylan interaction with cellulose, thanks to its negative charges, it is more admitted today that xylans interact better with cellulose when they are branch-free or with a minor amount residues. It was recently proposed that a xylan chain might be bonded on two cellulose microfibrils. In that case, the xylan part in interaction with the cellulose corresponds to that with the minor glucuronic content while the part between the microfibrils are those, which are branched in majority (Busse-Wicher *et al.* 2016).
The tridimensional conformation of xylan is not fully elucidated when it is in interaction with cellulose. Indeed, crystalline xylan has been described to be in a left-handed 3 fold helical system (3_1) (Nieduszynski and Marchessault 1972), which corresponds to its most stable conformation in water (Figure 24 A) while cellulose is in a 2 fold helical screw conformation (2_1).

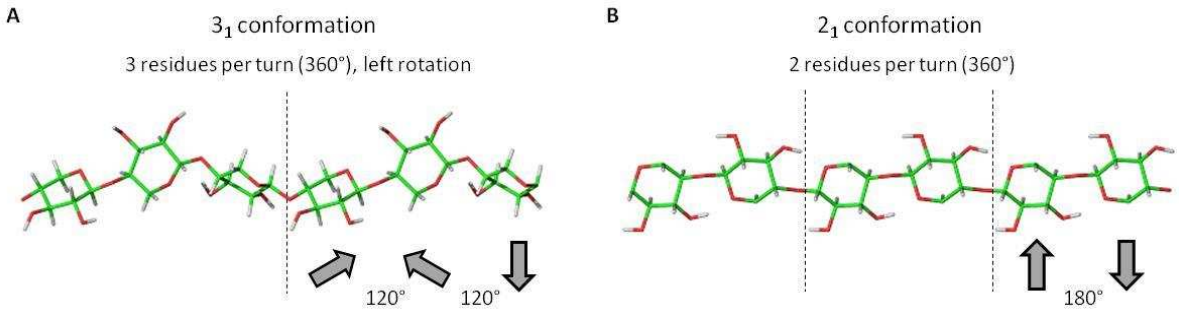

Figure 24: Two fold (2_1) and three fold (3_1) conformations of a homoxylan (with 6 residues).

By atomistic simulation, it was found that xylan was able to modify its conformation in some specific cases, e.g. when it is branched, and to adopt the 2_1 conformation (Figure 24 B) (Mazeau *et al.* 2005). Recent studies on *Arabidopsis thaliana*, have also suggested that xylan was preferentially in the 2_1 conformation in the presence of cellulose (Dupree *et al.* 2015; Busse-Wicher *et al.* 2016). Different techniques have been used to better understand the interactions between cellulose and hemicelluloses.

1. Spectroscopy techniques

The solid state NMR interaction was used to understand the cellulose structure and its interaction with the other components of the wood pulp. The solid-state ^{13}C NMR signal of cellulose is made of six signals related to the 6 carbons of the anhydroglucose unit. The signal at carbon C4 presents sharp resonances at 86 - 92 ppm, attributed to crystalline cellulose together with broad resonances attributed to amorphous domains (80 - 86 ppm). The C4 resonances may be subdivided into signals with the contribution of the cellulose crystalline forms Iα and Iβ, the paracrystalline cellulose, and the cellulose accessible and inaccessible surfaces (Larsson *et al.* 1999). Larsson's study revealed that hemicelluloses contribute to the amorphous cellulose signal, with a specific signal at 82 ppm and 84 ppm, by comparing the spectra of wood pulp spectrum with that of pure cellulose taken from cotton linters. A new signal appears at 82 ppm when xylan, isolated from wood pulp is adsorbed on cotton linters (Larsson *et al.* 1999). A diminution of the peak intensity at 82 ppm is observed on NMR pulp signal after xylan removal by alkali treatment (Teleman, Larsson, and Iversen 2001). Compared to the first study, the contribution of xylan in the pulp spectrum is better noticed because the NMR analysis was performed on never dried samples.

More recently, 2D solid state NMR with ^{13}C labeling was used to characterize the organization of the primary cell wall of *Brachypodium* grass (Wang *et al.* 2014) and the secondary wall of *Arabidopsis thaliana* (Wang *et al.* 2014; Dupree *et al.* 2015). In the first study, the *Brachypodium* was prefered to the *Arabidopsis thaliana* because of the highest concentration in glucuroarabinoxylan and the lowest content in pectins and proteins. It was reported that the 2D NMR ^{13}C -^{13}C correlation showed unambiguous interactions between cellulose and xylan and cellulose and arabinose branches.

Dupree *et al.* (2015) performed similar 2D NMR ^{13}C -^{13}C correlation experiment on *Arabidopsis thaliana* but only on dry samples. They reported that the two cellulose domains with the interior crystalline chains and the amorphous surface chains could by identified with 2D NMR. The cellulose was found to be spatially close to pectins and lignin and different conformations of xylan were observed but among these, very few were in the 3_1 conformation. However the effect of drying on the results and especially on the spatial proximity of the different constituents of secondary wall was not detailed.
The hemicelluloses and cellulose interactions were also studied with dynamic Fourier Transformed Infrared (FTIR) spectroscopy. Åkerholm *et al.* (2001) compared the glucomannan and xylan interaction with cellulose thanks to their specific wavenumber on FTIR signal: cellulose (1300 cm^{-1}), glucomannan (870 and 810 cm^{-1}) and xylan (1735, 1600 and 1245 cm^{-1}). Xylan and glucomannan appeared to be organized differently with the IR polarization (parallel or perpendicular). Glucomannan was found to be in closer association with cellulose than xylan as it was moving synchronously with the cellulose fibers while the xylan interaction seemed to be more indirect.

2. Microscopy or piezoelectric techniques

Models were built to study the interaction between cellulose and xylan with atomic force microscopy (AFM) or quartz crystal microbalance with dissipation (QCM-D) where the change in frequency is proportional to the adsorbed mass. Xylan coated on mica surfaces, which were studied by surface force apparatus (SFA) (Österberg *et al.* 2001), showed that xylan adsorption was minor and mainly controlled by the low xylan solubility (Tammelin, Paananen, and Österberg 2009).

Xylan adsorption on cellulose-coated surface was also observed with AFM and QCM-D techniques (Paananen *et al.* 2003). Xylan was adsorbed at the cellulose surface even when it was negatively charged. However, the swelling of cellulose in water and the problem of xylan solubility seemed to be limited factors. More recently, QCM-D techniques were used to characterize the adsorption of various hemicelluloses isolated from spruce pulp, on cellulose spun-coated film and compared with the adsorption of commercial galacto-glucomannan and xylan on cellulose film (Tammelin, Paananen, and Österberg 2009 ; Eronen *et al.* 2011). Cellulose film models were obtained by MFC spin coating then characterized by AFM visualization (Ahola *et al.* 2008). These model surfaces were found to be stable in QCM-D swelling experiments at different electrolyte concentration and pH.
Adsorption at the cellulose surface was observed with hemicelluloses extracted from spruce pulp and compared with the adsorption of commercial xylan and glucomannan. The extracted hemicelluloses were found to be strongly adsorbed onto cellulose, even it was noticed that the pulp treatment (peroxide) prior to the extraction may have an influence on their adsorption. It seems that the hemicellulose adsorption driving force is not electrostatic. However the xylan adsorption at the cellulose surface seems to be due to the lack of solubility of xylan into water, which favored its deposition on cellulose.

The influence of xylan branches on its adsorption at the cellulose surface has been also evaluated by QCM-D. It was found that debranched xylan is better adsorbed than arabinose-xylan on the cellulose coated surface (Bosmans *et al.* 2014). However this debranched xylan was deposited at the cellulose as aggregated particles. The influence of branches on the xylan adsorption was also studied with various commercial xylans (from corn cob, oat, spelt, wheat birch wood and beech wood) grafted with model branches to simulate the glucuronic acid and arabinose substitution (Littunen *et al.* 2015). All the xylans were grafted successfully, but only the wheat xylan was water dispersible. In this case the grafting may decrease the adsorption of xylan at the cellulose surface.

3. Biosynthesis models

Some studies have proposed to add hemicelluloses, such as xyloglucan, arabinoxylan and glucomannan to the cultivating medium of bacterial cellulose and to observe the influence of these additives on the cellulose microfibril organization, the cellulose crystallinity and the mechanical resistance of cellulose films made from these microfibrils (Tokoh *et al.* 2002; Martinez-Sanz *et al.* 2015; Mikkelsen *et al.* 2015). Microscopy examinations of the hemicelluloses deposition along the cellulose microfibrils with gold labelling led to similar conclusions: the xylan and xyloglucan were deposited as nodules along the cellulose microfibrils and are believed to bridge adjacent cellulose microfibrils (Martinez-Sanz *et al.* 2015; Mikkelsen *et al.* 2015), while glucomannan was more distributed all along of the fibers (Tokoh *et al.* 2002).
Tokoh's study demonstrated by XRD that xylan and mannan affected the cellulose crystallinity. Martinez-Sanz's study relying on SANS and SAXS measurement indicated that only xyloglucan altered the lateral crystallite dimension of cellulose and that there was no clear evidence of the crystallinity modification with arabinoxylan. It was concluded that during the biosynthesis, the arabinoxylan-cellulose interactions were developed after the cellulose microfibrils assembly while the xyloglucan incorporation was helpful for the inter microfibrillar cohesion.

The points of view are also divergent regarding the hemicelluloses influence on the solid state NMR signal of cellulose. In Tokoh's study (Tokoh *et al.* 2002), signal modification was observed at 82 ppm with additional xylan in the cultivated medium while Mikkelsen *et al.* (2015) did not observe it but detected xylan or xyloglucan in the mobile phase. Furthermore, in Mikkelsen's study, no improvement in mechanical test performed on film was noticed in presence of hemicelluloses and the best properties were obtained with pure cellulose without any addition of xylan and xyloglucan. The limit of this system may be explained by the repartition of the xylan as nodules in the cellulose matrix, which induce heterogeneity in the composites. A better dispersion of hemicelluloses in the cellulose, as it is the case for initial MFC produced from kraft pulp (high hemicelluloses content) improves the mechanical resistance compare to the MFC produced from sulfite pulp (low hemicelluloses content).

4. Improvement in mechanical properties

Another way to characterize the cellulose/xylan interactions is to study the influence of hemicelluloses content on the pulp mechanical properties. The influence of xylan content on the water stability of MFC film was studied by removing xylan from the initial pulp with enzymatic treatment prior the MFC production (Tenhunen *et al.* 2014). It was found that xylan prevents the MFC aggregation but the water permeability and oxygen barrier were only slightly impacted by the decrease in xylan content. AFM was used to characterize the cellulose fibers modification after xylan precipitation at the surface of wood pulp and viscose (Miletzky, Punz, *et al.* 2015). The xylan adsorption only occurs in the case of wood pulp but no improvement in tensile index was observed. As previously described with hemicelluloses addition in cultivated medium of bacterial cellulose, a heterogeneous dispersion of xylan particles, with diameter from 10 to 15 nm, is observed at the cellulose surface, which may limit the mechanical properties. The measurement of the tensile strength of single fibers or fiber-fiber joint resistance was measured with micro-bond tester (Miletzky, Fischer, *et al.* 2015). The hemicelluloses content in the initial pulp was varied with alkali extraction or xylan precipitation at the fibers surface and their influence on the mechanical resistance of the fibers was observed. The modulus of elasticity of individual fibers was not affected by the extraction or precipitation of xylan, however the additional xylan improved the resistance of the fiber-fiber joints.

Materials and Methods

Materials

1. MFC suspensions

From the market bleached pulp, MFC were prepared according to the STFI/Innventia patent (Lindström, Ankerfors, and Henriksson 2007) based on a mechano-enzymatic pre-treatment, optimized at CTP and followed by homogenization at high pressure, thanks to A. Janodet and F. Cottin (CTP).

1.1 Pre-treatment of the pulp

After pulp rehydration in a conventional pulper, the suspension at 4.5% consistency was pre-refined with a 12" single disc (30 cm) refiner at a speed of 1500 rpm (Figure 25).

This pre-treatment was dedicated to open the fiber structure in order to facilitate the penetration of the enzymes into the fiber wall and to improve the efficiency of this enzyme treatment.

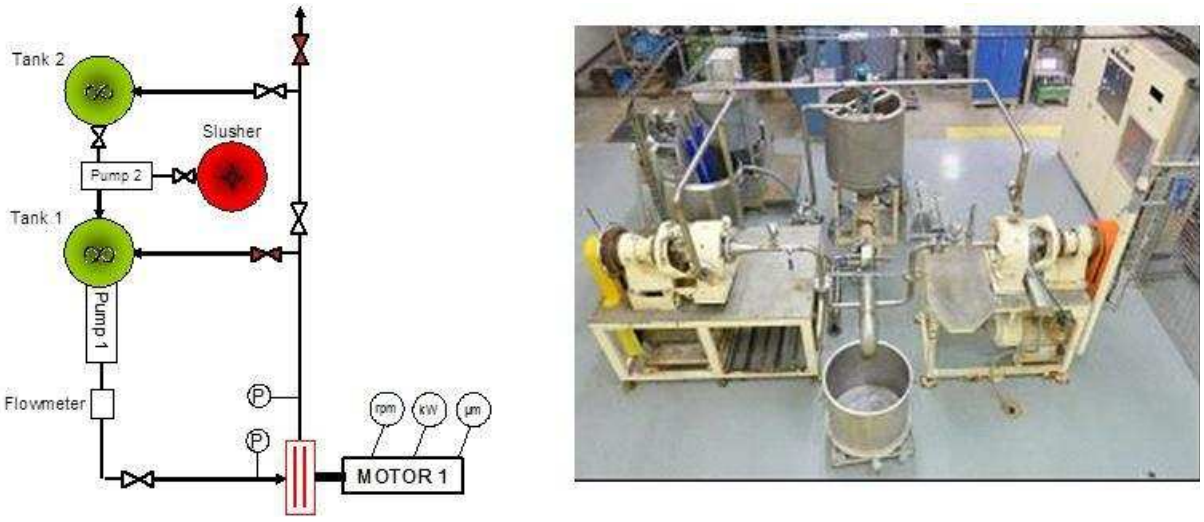

Figure 25: Lay-out and picture of the refining pilot plant (CTP)

The pre-refined pulp, in one of the tank of the refining pilot was treated with a commercial solution of endoglucanases (FibreCare R from Novozyme) at pH 5.0 at 50°C for one hour.

A final post-refining was carried out in the 12" single disc refiner at a speed of 1500 rpm to reach the highest possible drainage index.

The pulp was pre-treated with this mechano-enzymatic protocol in order to obtain a suspension of fibers with a mean fiber length lower than 300 µm.

1.2 Homogenization of the pre-treated pulp

The pre-treated pulp was transferred from the refining pilot to one of the tanks of the NaMiCell pilot. The suspension was adjusted at 2% consistency before starting the homogenization.

The production of MFCs was obtained by submitting the fiber fragments to high pressure in a specific chamber. An industrial homogenizer, supplied by GEA Niro Soavi, with a capacity of 1000 L/h, equipped with a 55 kW motor, was used for this production (Figure 26). Different passes were done to reach the MFC level: one pass at 1000 bar and then four passes at 1500 bar.

At the output of the homogenizing zone, the suspension was cooled with cold water in order to limit an important increase in temperature.

Figure 26: GEA Ariete homogenizer and picture of the NaMiCell pilot plant (CTP)

In this study, eight MFC suspensions with four different wood species were produced under the conditions described below (Table 10) from sulfite/kraft pulp and dried/never dried pulps.

Table 10: Panel of produced MFC

MFC from	Wood species	Pulping process	Pulp drying history
birch-kra-nd	birch	kraft	never dried pulp
birch-kra	birch	kraft	dried pulp
spruce-kra	spruce	kraft	dried pulp
pine96-sul-nd	pine (96% of cellulose)	sulfite	never dried pulp
pine96-sul	pine (96% of cellulose)	sulfite	dried pulp
pine92-sul-nd	pine (92% of cellulose)	sulfite	never dried pulp
pine92-sul	pine (92% of cellulose)	sulfite	dried pulp
euc-sul	eucalyptus	sulfite	dried pulp

2. Pulp samples from CTP

Three different market wood pulps were selected to perform xylan extraction. They correspond to those used to produce MFC (Table 11).

Table 11: Panel of pulp

Pulp from	Wood species	Pulping process	Pulp drying history	Pulp refining history
birch-kra-nd	birch	kraft	never dried	refined pulp
birch-kra	birch	kraft	dried	refined pulp
birch-kra-nd-nr	birch	kraft	never dried	non refined pulp

Samples were taken at different steps during the pulps pre-treatment prior to the MFC production (conditions described above in Figure 25). The initial never dried non refined pulp, the never dried pulp after refining and the dried pulp after pulping and refining were selected to evaluate the impact of each steps on the xylan extraction yield and on xylan structure.

3. Xylans samples

Xylans extracted from the birch kraft samples (pulp and MFC) were compared with a commercial arabino-xylan extracted from an oat species (*Avena*) from Janssen Chemica and an arabino-xylan extracted at CTP from birch wood chips.

The xylan extraction from birch wood chips was performed with optimized conventional procedure. The wood chips were cooked with 5% of sodium hydroxide then the xylan dissolved in the sodium hydroxide solution was separated from the insoluble wood chips by centrifugation. The pH of the xylan solution was neutralized with hydrochloric acid then the xylan was precipitated for one night with ethanol/water mixture at 5°C. The xylan precipitate was isolated and washed by repeated centrifugation and redispersion of the pellet in ethanol. The recovered solid xylan was dried in the oven at 55°C.

4. Solvents and materials

Dimethylsulfoxide (DMSO - analytical grade), tert-buthyl alcohol (TBA - 99.5%) and lithium chloride salt (LiCl - 99%) were purchase at Fisher Chemical, Acros-organics and Sigma Aldrich respectively. After opening the flask, the DMSO was kept with molecular sieves from Aldrich (4 Å).

Deionized water was produced by water circulation on column aquadem-E300 from Véolia. Dialysis membranes cellulose, with cut-off of 12000 Da were purchased from Roth.

The centrifugations were performed on Sigma Laboratory Centrifuges 6K15 (rotor 12256, 11 200 rpm tube polypropylene copolymer 250 mL), 3K30 (rotor 12158, 23793 rpm, tube polypropylene copolymer 30 mL) and 2-16P (rotor 12139, 15000 rpm, tube polypropylene copolymer 30 mL).

Methods

1. Samples characterization

1.1 Chemical composition with sugar analysis

The chemical composition of pulp, MFC and xylan was analyzed using high-pressure liquid chromatography (HPLC) Dionex DX500, column Carbopac PA10 with water/NaOH 150 mM gradient thanks to the kind helps of Dr M. Schelcher and A. Janodet (CTP). Prior to the analysis, the MFC samples were freeze-dried, dissolved and hydrolyzed by sulfuric acid. Fucose (Sigma Aldrich) was used as internal standard.

1.2 Morphological analysis of residual coarse elements

The MorFi laboratory version analyzer was designed and developed for the morphological characterization of fibers and fines. The analysis is done on a fiber network (precisely 0.4 g of dry matter is diluted in about 700 mL of water), so that the measurement occurs in the fibers' natural unrestrained environment. This approach allows reliable statistical measurement of thousands of fibers at high speed and accurate determination of important characteristics such as curl and kinks. The optical system is composed of a high-resolution CCD camera, a measurement cell avoiding cell plugging and a light source. Images acquired by the camera are immediately treated by a computer. The measurement is a statistically accurate view of the fiber characteristics: fiber content (length > 80 µm), fines content (length < 80µm) and mean area-weighted length, among others, are the three characteristics studied in this report (each sample measured twice).

1.3 MFC dispersion with UV visible spectroscopy

The MFC suspensions were diluted at 1% and introduced into a UV quartz cell with cover (dimension of 44.5 x 12.5 x 3.5 mm and layer thickness of 1 mm). A concentration below 0.5% resulted in sedimentation, and higher concentration suffered from too strong attenuation resulting in non-linearity with respect to the concentration. The optical density of each sample was measured at wavelength of 200 to 800 nm using a UV - visible spectrometer (Varian Carry-50 Bio). The data were collected at the scan speed of 600 nm/min and a resolution of 1 nm.

1.4 Samples freeze- drying

The samples were placed in round bottom flask. In the case of pulp or MFC, the initial suspension at 2%, was diluted to 1% with deionized water to facilitate its manipulation.
The suspension was frozen in liquid nitrogen then freeze-dried at 100 mili-torr for two days.

1.5 Samples composition and structure by ^{13}C solid state NMR

NMR experiments were performed on a Bruker Avance spectrometer (^{13}C frequency of 100 MHz), using magic angle spinning (MAS) and cross-polarization (CP). The spinning speed was set at 12 kHz, sweep width 29761 Hz, and recycle delay 2s. Each sample was analyzed under dry and wet conditions. The MFC spectra were averaged over 24 kscans and 5 kscans for wet and dry samples respectively. The xylan spectra were averaged over 2 kscans. The ^{13}C chemical shifts were calibrated with the glycine carboxyl group (176.03 ppm).
The spectra were normalized with respect to the integrated intensity between 50 and 120 ppm.
The dried samples of pulp, MFC and xylan were prepared by freeze-drying the initial suspension in water. The wet samples of pulp, MFC and binary system of MFC samples with re-adsorbed xylan were obtained as centrifugation pellet (13 500 rpm 2 h) of the suspension and the water excess was blotted with filter paper. Xylan wet samples were prepared by rehydrating the freeze-dried samples at 97% relative humidity in a desiccator using saturated potassium sulphate aqueous solution.

2. MFC and pulp components isolation

2.1 Solvent exchange (tert-butyl alcohol =TBA) and aerogel formation

- Harsh exchange:

Water contain in the MFC suspensions (2% solid content) was replaced with tert-butyl alcohol (TBA) by repeated centrifugation (11 200 rpm, 2 h, 25°C) and redispersion of the pellet in TBA using a double cylinder type disperser, Ultra-turrax.
After the third centrifugation, the MFC were suspended in TBA at 1.25wt% (Fumagalli *et al.* 2013) and frozen with liquid nitrogen and freeze-dried at 100 mili-torr for two days.

- Soft exchange:

To avoid interface tension between water and TBA which might induce irreversible aggregation among cellulose fibrils, the water of the MFC suspensions (2% solid content) was replaced with ethanol (3 times) prior to TBA (3 times) and the centrifugation speed was decreased to 2000 tr/min. The rest of the procedure is identical of the harsh exchange.

2.2 MFC specific surface measured with BET

Specific surface area of freeze-dried samples (MFC or pulp) were measured using adsorption-desorption isotherms of nitrogen with the kind help of Dr. Sonia Molina-Boisseau (CERMAV). The freeze dried samples (0.07 – 0.15 g) was first degassed in the Nova 1200e surface area analyzer (Quantachrome instruments) at 105°C for 15 h and the adsorption-desorption isotherms were measured at 77 K in the pressure range of 0.01-0.3 bar. The specific surface area was calculated using BET equation (Braunauer, Emmett, and Teller 1938) as described by Fumagalli *et al.* 2013.

2.3 Optimized protocol of xylan extraction

The freeze-dried MFC or pulp samples were subjected to the extraction of residual xylan. They were first suspended in DMSO-5% LiCl at the concentration of 8 g/L (i.e. 0.7 wt%), then the suspensions were stirred at room temperature for 20 h.
Then the xylan extracted in DMSO was separated from the MFC and pulp samples by centrifugation (20000 g, 15 h, 25°C). The extracted xylan and the MFC after extraction were regenerated separately by dialysis against water using dialysis membrane with cut off of 12000 Da, which excluded DMSO and LiCl from the specimen.
After dialysis for 7 days, the MFC suspension was kept at the wet state and the xylan suspension was concentrated by rotary evaporator (30°C, 7 mbar) and then freeze-dried.

2.4 Xylan composition and structure with liquid state NMR

The freeze-dried xylan samples (10 to 15 mg) were dissolved in 0.75 mL of deuterated solvent under agitation at room temperature for 12 h. Then the spectra of proton (^{1}H) and carbon (^{13}C) NMR were recorded at 353 K with a Bruker Advance spectrometer at 400 MHz and 100 MHz respectively.

Proton-carbon correlation (HSQC) NMR was also performed with proton probe at 400MHz at 353 K with a Bruker Advance spectrometer. Because of solubility, the xylan extracted from pulp or MFC samples and the commercial xylan extracted from oat were dissolved in deuterated-dimethylsulfoxide (DMSO-d_6- 99.9% deuterium- Aldrich) while the xylan extracted from birch wood chips was dissolved in deuterated water (D_2O - 99.96% deuterium - Euriso-top).

3. Xylan DP characterization

3.1 Liquid NMR

The freeze-dried xylan extracted from MFC from birch kraft never dried pulp (10 to 15 mg) is dissolved in 1 mL of deuterated water (D_2O - 99.96% deuterium - Euriso-top) and 9% of sodium deuteroxide (NaOD - 40% wt solution in D_2O - <99% deuterium - Aldrich) under agitation at room temperature.
Then the proton (^{1}H) liquid NMR was directly recorded after the xylan dissolution at 25°C because the xylan solubility in deuterated water and sodium deuteroxide mixture was very low. A xylan precipitate was formed when the temperature was increased from 298 K to 353 K or if too much time (< 1h) was left between the disolution and the measurement.

The degree of polymerization was determined from the relative intensities of the signals from the anomeric protons. Spectral deconvolution was performed with the"peak fitting" Mestrenova tool.

3.2 Viscosimetry

Viscosimetry measurements were performed in the laboratory of rheology and process (LRP), thanks to Dr. Denis Roux on the Microviscosimeter (Anton Paar Louis 2000ME), using a capillary (diameter 1.59 mm) and a steel ball (ref 19847023).
The density of the DMSO was fixed at 1.100 (g/cm^3) and the temperature at 20°C on the Microviscosimeter.

Xylan solutions were prepared by dissolving freeze-dried xylan extracted from MFC from birch kraft never dried pulp at different concentration in DMSO at room temperature for 12h.
The solutions were centrifuged 1h at 50 000 g to remove the residual cellulose contamination (less than 2%). The supernatants were gently collected and poured in capped tube at room temperature. The exact xylan concentration was recalculated by dialysis and freeze-drying of a fixed volume of each xylan solutions.
The xylan concentrations in DMSO solutions after the centrifugation step were: 3.7 g/L ; 8.2 g/L ; 11.4 g/L and 13.4 g/L.

The dynamic viscosity was measured on each xylan solutions and the DMSO pure at the three angles of 20°, 50° and 80°. Each measurements corresponds to the average of 20 values with 10 measures at 20°, 50° and 80° and 10 measures at -20°, -50° and -80°.

3.3 SEC- MALS

This analysis was performed in the Paper Science Laboratory, Tokyo University, thanks to Yuko Ono. The existing procedure developed for cellulose DP characterization with DMAC -LiCl was followed in the case of xylan (Ono *et al.* 2016).

Freeze dried xylan (200 mg) was dissolved in 5 mL of DMAC - 8%LiCl for one week at room temperature. Then the solution was injected on SEC columns (KD-806M KD-802M, Shodex, Japan), with 1.0% w/v LiCl/DMAC as solvent and the detection was performed with MALLS detector (DAWN HELEOS-II, λ = 658 nm, Wyatt Technologies, USA), and RI detector (RID-10A, Shimadzu, Japan).

4. MFC films production

Two techniques were employed to produce MFC films: the casting-evaporation method, also simply called casting and the handsheet method.

4.1 MFC films by casting

In order to obtain a homogeneous suspension, the MFC suspension at 2 wt% was preliminary diluted to 0.5 wt% and magnetically stirred for 30 min. Then, the desired amount of suspension was poured into polystyrene petri dishes (Thermo Fisher Scientific) with a diameter of 9 cm (Figure 27).

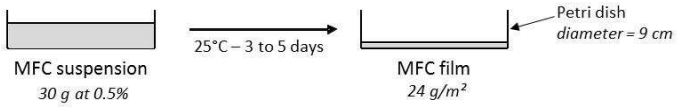

Figure 27: Casting process

MFC films with varied density were obtained after a few days of drying at room temperature.

4.2 Deionized MFC films by casting

To provide ion surface contamination of the film, the MFC suspensions were rinsed by repeated centrifugation and redispersion of the pellet into hydrochloric acid solution at 0.5%. At the end of the third centrifugation, the MFC pellet were rinsed by repeated redispersion in deionized water and centrifugation until the neutral pH is recovered.

The MFC casting films were performed with this deionized MFC suspension with the same procedure described above.

4.3 MFC films by handsheet method

The handsheet method used a semi-automatic sheet former (Rapid-Khöten) to produce MFC films. This device is currently used to produce model paper sheet, called handsheet, at lab scale (Figure 28).

Figure 28: Handsheet formers

4.3.a Classic MFC films

This method for films formation was adapted from the protocol already described in literature (Sehaqui *et al.* 2010) and the main steps were illustrated in Figure 29.

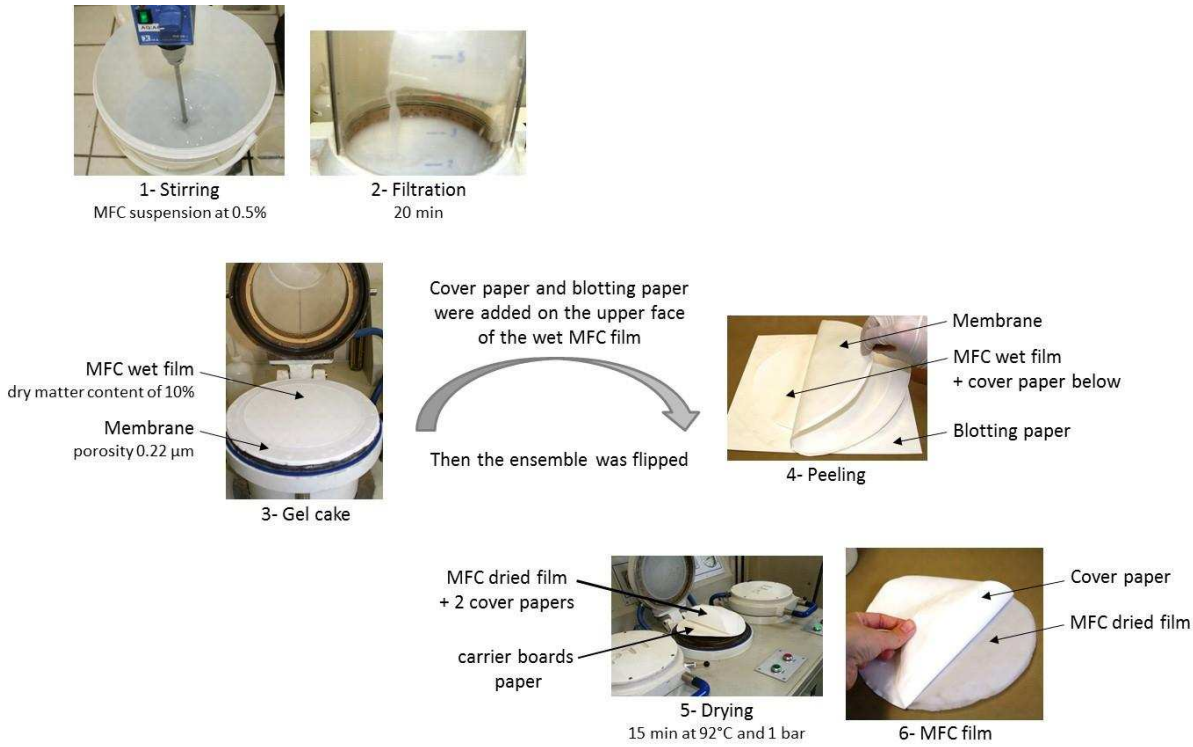

Figure 29: MFC films formation with handsheet formers

The MFC suspension was firstly prepared at 0.5% and stirred using a disperser for 30 min. The MFC suspension at 0.5% was always kept stirring and the desired amount of suspension was sampled and weighted just before the film formation to avoid sedimentation and concentration fluctuation in the suspension (Figure 29 -1).

The sampled MFC suspension was then poured into the bottom of a hollow cylinder (Figure 29 -2) containing a metallic sieve at its bottom covered with a mixed cellulose ester (nitrocellulose, cellulose acetate) membrane with 0.22 µm pore size (Milipore GSWP29325).
The suspension was vacuum sucked for 20 min.

After filtration, the MFC wet film (Figure 29 -3) had a dry matter content closed to 10%. One cover paper was placed at the upper face of the wet MFC film then a blotting paper was used to flip the system including, membrane, MFC wet film and cover paper.

The membrane was gently peeled off from the wet film (Figure 29 -4) after that a pressure was applied with a roller. A second cover paper was then added on the wet MFC film. Then the MFC wet film between the two cover papers was positioned between two carrier boards and dried in a sheet dryer for 15 min at 93°C under 1 bar of vacuum.(Figure 29 -5).

At last, the carrier boards were removed and the dried MFC films were separated from the two cover papers (Figure 29 -6).

The diameter of the films reached 20 cm with this method. Therefore, MFC films with density of 25, 50 and 100 g/m² were respectively obtained by filtration of around 157 g, 314 g and 618 g of the MFC suspension at 0.5%.

Because the smallest elements contained in MFC suspensions might be eliminated during the filtration, the initial filtrated amount of MFC suspension at 0.5% (Mass *i.*) must be reevaluated to achieve the desired film density. The dried MFC film (Mass of dried film *exp.*) was weighted and compared with the desired mass of dried film.

The corrected mass of MFC suspension at 0.5% (Mass corrected) was calculated in Table 12 with:

$$Mass\ corrected = Mass\ i. + \frac{Mass\ of\ dried\ film - Mass\ of\ dried\ film\ exp.}{0.5\%}$$

The mass of dried film corresponded to: $Mass\ of\ dried\ film = film\ density\ x\ film\ surface$

Then the corrected mass was used for the films formation with the corresponding desired density.

In the case of handsheet former, the surface of the MFC film corresponded to 3.14 10^{-2} m² and the expected films density and example of corrected mass are summarized in Table 12.

Table 12: Film density and MFC suspension sampled

Film density desired	**100 g/m²**	**50 g/m²**	**25 g/m²**
Mass *i.* of MFC sampled	618 g	314 g	157 g
Mass of dried film desired	3.14 g	1.57 g	0.79 g
Mass of dried film *exp.*	3.05 g		
Mass corrected	636 g		

4.3.b Reinforced MFC films

MFC films supported with coated calendered paper were produced according to the CTP patent (B248470-D34495FD-2015).

The wet MFC film was obtained with MFC suspension at 0.5% by the same procedure as described above for classic MFC films formation. The upper face of the wet film was covered by the coated calendered paper instead of the cover paper (Figure 29 -3), then same procedures for membrane removing and film drying were used as it was described above.

Finally, the dried MFC film was separated from the only cover paper and the coated calendered paper stayed on the other face of the film as a support (Figure 29 -6).

5. MFC film examinations with SEM-FEG

MFC films were first coated with 2 nm of Au/Pd to prevent spurious charging. MFC films surfaces were then examined with the kind help of Christelle Boucherand and Caroline Duprat (CERMAV using a Scanning Electron Microscope (SEM) equipped with a Field Emission Gun (FEG SEM Ultra55, Zeiss) enabling the visualization of elements at the nanoscale.

Energy dispersive spectroscopy analyses (Silicon Drift Detector, Bruker) on SEM were also performed to identify the origin of inorganic particles at the surface of MFC films.

6. Three layers systems of MFC films and xylan

6.1 Xylan gel formation

The xylan was dissolved in dimethylsulfoxide (DMSO) by stirring at 25°C for 12h. The xylan extracted from birch kraft samples (MFC and pulp) was dissolved at the concentration of 60 g/L (i.e. 5.2 wt%) while the commercial one extracted from oat was dissolved at 80 g/L (i.e. 6.7 wt%).

The xylan solutions were poured into a Teflon hollow rectangle (60 x 40 x 2 mm), put on a dialysis membrane (cut-off of 12000 Da) which was in contact with a bath of water/DMSO mixture (Figure 30).

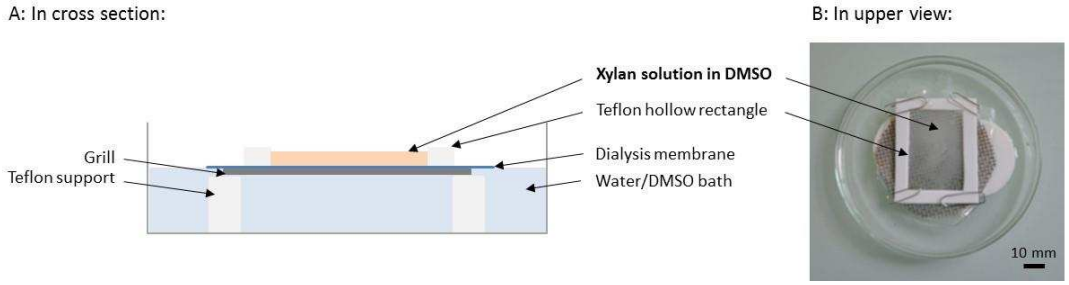

Figure 30: Experimental system for xylan gelation A: illustration B: photograph

In the case of extracted xylan from birch kraft samples, the water/DMSO proportion of the dialysis bath corresponded to 9:1 while with the commercial xylan the proportions were 1:1.

Both xylan gels were formed after 1h of contact with the dialysis bath, then they were transferred to a deionized-water bath to remove the DMSO completely from the gel.
The water bath was changed 3 times for 3h then the dialysis was extended for 12h.

The xylan gels were used directly after their formations.

6.2 Optimized protocol of three layers system formation System 1 (for peeling test)

The MFC dried handsheet films reinforced with coated calendered paper are cut with scissors into rectangles of 6 x 6.5 cm. Then the xylan gel was rolled out on the upper side of the MFC films in order to cover a rectangle of 4.5 x 6 cm (i.e. a surface of 27 cm²).
To improve the rolling out, the gel of commercial xylan is crushed using a double cylinder disperser, Ultra-turrax, prior to its deposition at the MFC film surface.

The xylan covering surface was voluntary smaller than the total surface of the MFC films and a band of 1 x 6 cm of MFC film was let uncovered (Figure 31 A).

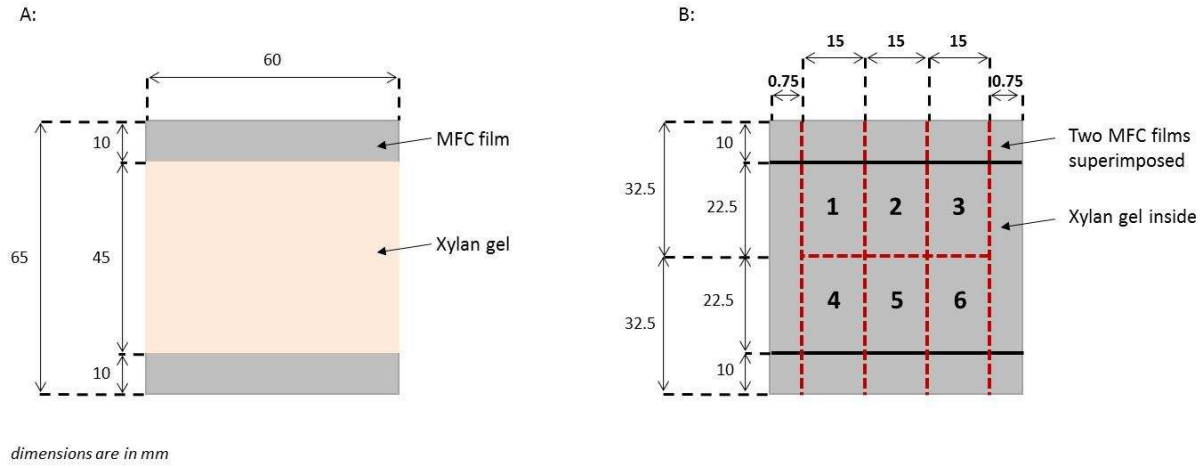

Figure 31: Illustration of the three layers system 1 formation

A second MFC film, with same dimensions than the first one (6 x 6.5 cm), was positioned above the xylan gel layer to form a three layers system. This complex was then dried at room temperature under constrain for 12h.
The three layers dried system was divided into 6 smaller systems of 15 mm width and 22.5 mm length with a razor blade. (Figure 31 B).
The smaller systems were cut from 0.75 mm from the extremity to avoid border disturbances.

A tab cardboard was fixed on the uncovered MFC film surface with Loctite super glue (Figure 32).

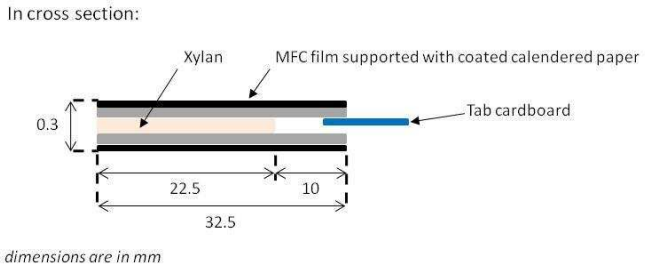

Figure 32: Illustration of the final three layer system 1

The final systems were kept dried in desiccator with silica gel or they were rehydrated at 75%, 85% or 97% relative humidity in desiccators using, respectively saturated sodium chloride solution (Sigma Aldrich ≥ 99%), potassium chloride solution (Sigma Aldrich > 99%) and potassium sulphate aqueous solution (Merck, > 99%).
To reduce the time of humidity equilibration, ventilators were installed inside the desiccator.

6.3 Optimized protocol of three layers system formation System 2 (for shearing test)

The MFC handsheet film without reinforcement was fixed on a flat surface and covered with epoxy glue obtained by mixing resin Araldite AW 106 and Hardener HV 953 U BD (from Huntsman Advanced Materials) in mass ratio 4:5.

The spatula, (Roth, oral spatula - rotilabo- 150 x 18 x 2 mm) with initial length of 150 mm were divided with cutting pliers in two parts of 75 mm. Then they were placed on the epoxy layer and the system was dried at room temperature for 5h (Figure 33 A).
Prior to their deposition at the epoxy layer surface, the spatula were heated at 120° for 40 min with hydraulic press (carver Laboratory Press) at 10 bar then cooled under constraints to avoid deformations during the final heating.

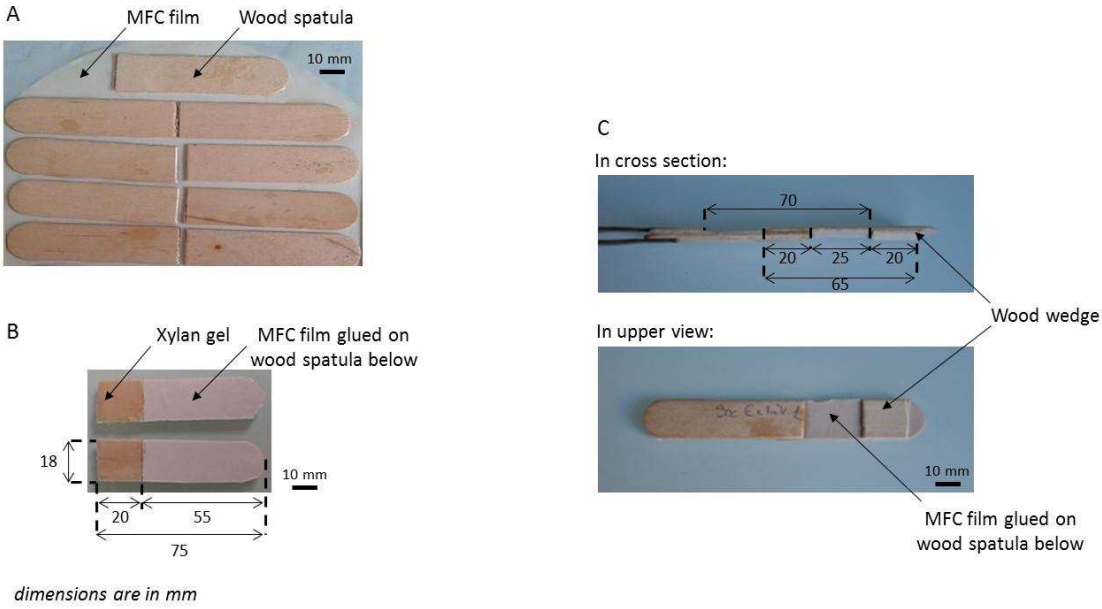

Figure 33: MFC films glued on wood spatula

MFC films glued on spatula, were isolated from the other with razor blade cutting. Then 75 mg of xylan gel at 10 wt % was rolled on each delimited surface (Figure 33 B) on the spatula (18 x 20 mm, i.e 360 mm²). To improve the rolling out, the gel of commercial xylan was crushed using a double cylinder type homogenizer, Ultra-turrax, prior its deposition at the MFC film surface.
The spatula were assembled by pairs with superimposition of the xylan gel to achieve a final amount of xylan gel in the system of 150 mg at 10 wt %. The whole assembly was dried at room temperature under constraints for 4h then heated at 120° for 3h with a hydraulic press at 10 bar then cooled under constraints. Some wedges (18*20*2 mm) were glued with Superglue Loctite at both end of the spatula to avoid any high difference and to provide a good alignment in the pulling jaws (Figure 33 C). The wedges are made off by cutting the wood spatula with cutting pliers.
The final systems were kept dried in desiccator with silica gel (orange from Roth).

6.4 Three layers system formation System 2 (for shearing test) with hot melt glue

The same three layer system with MFC supported on wood spatula was made- of hot melt glue instead of xylan. The hot melt glue (Technomelt cool 120 E3525101 from Henkel) was crushed with a razor blade then 5 mg was deposed on the MFC film prior be assemblinge by pairs. Then the system was placed in a hot press at 130°C for 10 min to melt the glue.
The final systems were kept dried in a desiccator with silica gel (orange from Roth).

6.5 Adhesion on the three layer model

6.5.a Peeling test

The three layer system was fixed on cardboard with paper clip to provide alignment into the pulling clamp and avoid deformation of the system during the peeling test (Figure 34).

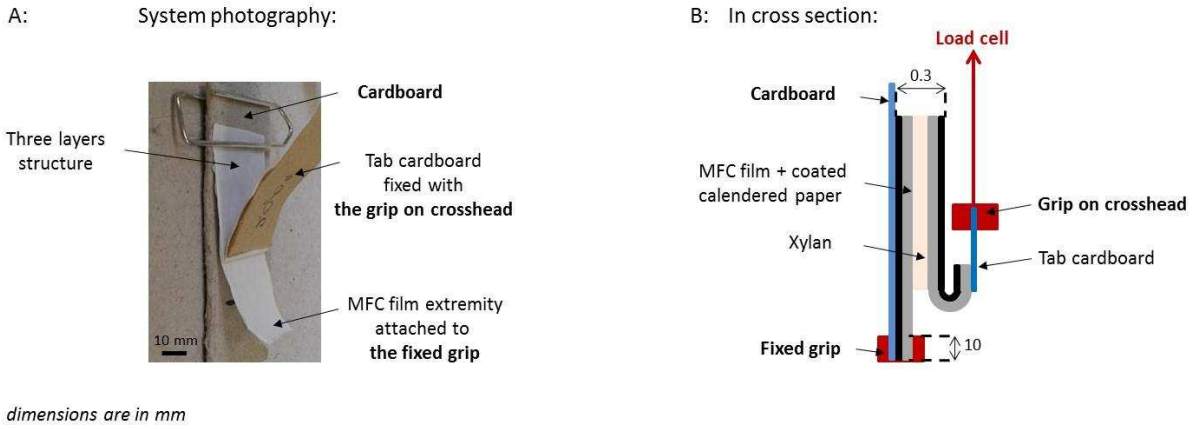

Figure 34: A: Photograph of a three-layer sample for peeling test and B: scheme of the experimental set-up used for the peeling test

The peeling test was performed at room temperature and atmosphere with the tensile testing machine Shimadzu AGS-X with the load cell of 20 N at the speed of 1 mm/min.

6.5.b Shearing test

The sample was placed in the pulling clamp with the Teflon wedges glued at the both extremity of the spatula. The initial displacement between the pulling clamps was 70 mm (Figure 35).

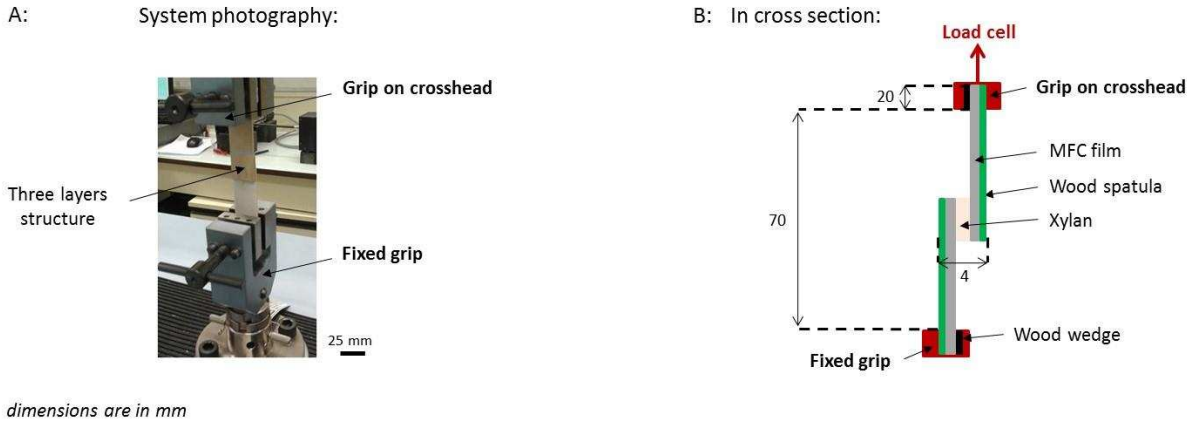

Figure 35: A: Photograph of a three-layer sample for shearing test and B: scheme of the experimental set-up used for the shearing test

The shearing test was performed at room temperature and atmosphere with the tensile testing machine Shimadzu AGS-X with the load cell of 500 N at the speed of 5 mm/min.

Chapter 1

MFC components isolation and characterization

Various bleached chemical pulps, differing in wood species (softwood/hardwood), pulping processes (sulfite/ kraft) and drying history (never dried/dried) were used as raw materials for MFC production.

Both kraft and sulfite pulps (dissolving cellulose) originated from softwood (spruce and pine) and hardwood (birch and eucalyptus) were selected.

Two grades of pine sulfite pulps were used with different cellulose contents, namely 92 and 96 %. Birch kraft pulps were used both never dried and after one drying step (Figure 36).

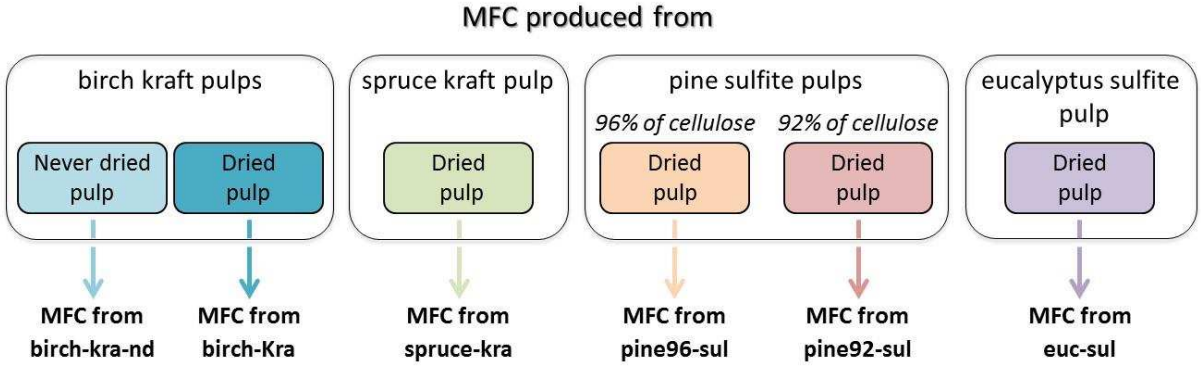

Figure 36: Panel of MFC and abbreviation names

The characteristics of the starting pulps are summarized in Figure 36 along with their abbreviations used in the manuscript. For example, “MFC from birch-kra-nd” corresponds to “MFC produced from never dried birch kraft pulp” and “MFC from birch-kra” means “MFC produced from dried birch kraft pulp”.

1. Initial composition of MFC

1.1 MFC characterization by solid state NMR of dry sample

Solid state NMR spectra of five different types of freeze-dried MFC are shown in Figure 37. The spectra were normalized with respect to the integrated intensities ranging between 55 and 155 ppm. Assignment of the peaks was done according to Kono *et al.* (2002) and Larsson *et al.* (1999).

The peaks with chemical shifts from 57 to 67 ppm correspond to the carbon C6 and the one at 105 ppm to the carbon C1. The peaks of carbons C2, C3 and C5 are overlapping and match the signals appearing between 69 and 79 ppm. The resonances from 80 to 92 ppm correspond to the C4 carbon atom of the glycosyl residue in the cellulose chains constrained in a two-fold helical conformation in the solid state, while the resonance in dissolved state occurred at the higher-magnetic field end, typically at around 81 ppm (Isogai 1997).

Within this broad chemical shift range, the crystalline core and the disordered / surfaces of the cellulose microfibrils were distinguished as lower (86 to 92 ppm) and higher (80 to 86 ppm) magnetic field contributions respectively.

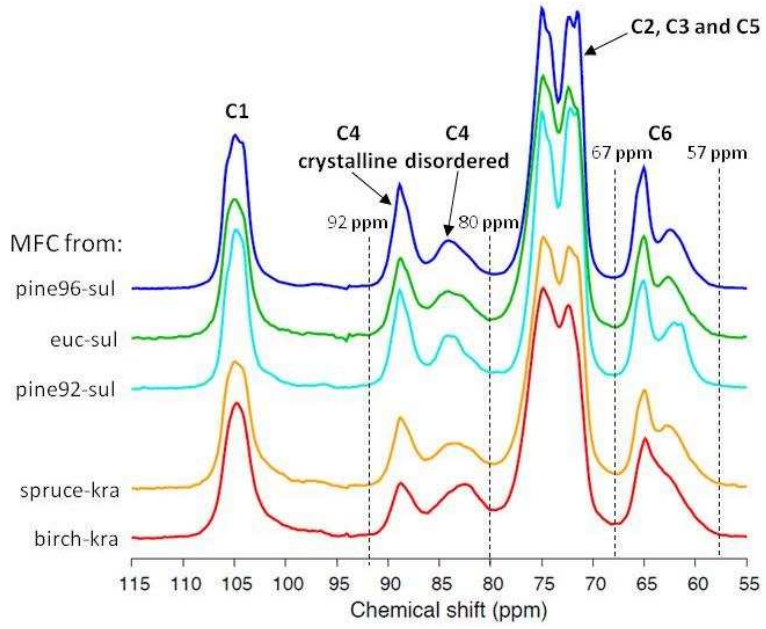

Figure 37: ^{13}C CP-MAS solid state NMR spectra of dry MFC samples from sulfite (pine 96, pine 92 and eucalyptus) and kraft (birch and spruce) pulps

According to Larsson *et al.* (1999), different contributions can be distinguished in this so-called disordered peak regions as follow: two signals from accessible fibril surfaces (at 84.4 ppm and 83.4 ppm), and a broad contribution from the inaccessible fibril surfaces in the same range. An additional contribution from interacting xylan chains is also expected around 82 ppm, as concluded from cotton cellulose/xylan interaction, and further confirmed by alkali extraction of xylan chains (Teleman, Larsson, and Iversen. 2001).

A first visual inspection reveals clear differences between MFC from kraft pulp and MFC from sulfite pulp at around 82 ppm and 62 ppm (Figure 37). Sulfite pulps showed much smaller intensity compared to kraft pulps, but the lack of spectral details hampered a quantitative discussion of the differences.

The initial hemicelluloses/cellulose compositions of the various MFC normalized with the total sugar content is presented in Table 13. The non-normalized compositions together with the hydrolysis yields are also available in Annex 1.

Table 13: Neutral sugar compositions of MFCs

	MFC from birch-kra	**MFC from spruce-kra**	**MFC from pine92-sul**	**MFC from pine96-sul**	**MFC from euc-sul**
Glucose (%)	76.6	84.0	93.8	97.5	96.7
Hemicelluloses (%)	23.4	16.0	6.2	2.5	3.3
Xylose (%)	22.5	8.7	2.5	1.5	2.4
Mannose (%)	0.9	6.5	3.5	1.0	0.9
Arabinose (%)	0.0	0.6	0.1	0.0	0.0
Galactose (%)	0.0	0.2	0.1	0.0	0.0

As expected, MFC from sulfite pulps had the lowest hemicelluloses content, accounting for 2.5 % up to 6.2 % whereas those from kraft pulps contained from 16.0 % to 23.4 % of hemicelluloses.

Birch kraft pulp had the highest amount of hemicellulose (23.4%), in which xylan was dominant representing more than 95 % of hemicellulose. Spruce kraft pulp contained significant amount of glucomannan as suggested by the presence of mannose residues.

Arabinose and galactose were undetected in the MFC from hardwood pulps indicating that the xylan and glucomannan are not branched, contrary to the hemicelluloses extracted from wood. Considering that arabinose and galactose groups are more sensitive to hydrolysis, they were most probably removed during the pulping process by both alkaline (kraft) and acid (sulfite) cooking conditions.

The small hemicellulose content in sulfite pulps corroborates with the reduced NMR resonance peak intensities at 82 ppm when compared to the kraft pulps.

1.2 Influence of drying history and the presence of salts on the solid state NMR spectra

In order to investigate the effect of the physico-chemical conditions on the spectral features, we recorded a series of NMR spectra with different preparation conditions. The preparation included wet or freeze-dried sample and salt removal (Figure 38).
Indeed the MFC production was performed with tap water and the MFC suspensions contain salts. We tried to remove them with dialysis against deionized water or by rinsing with 0.5% HCl solution.

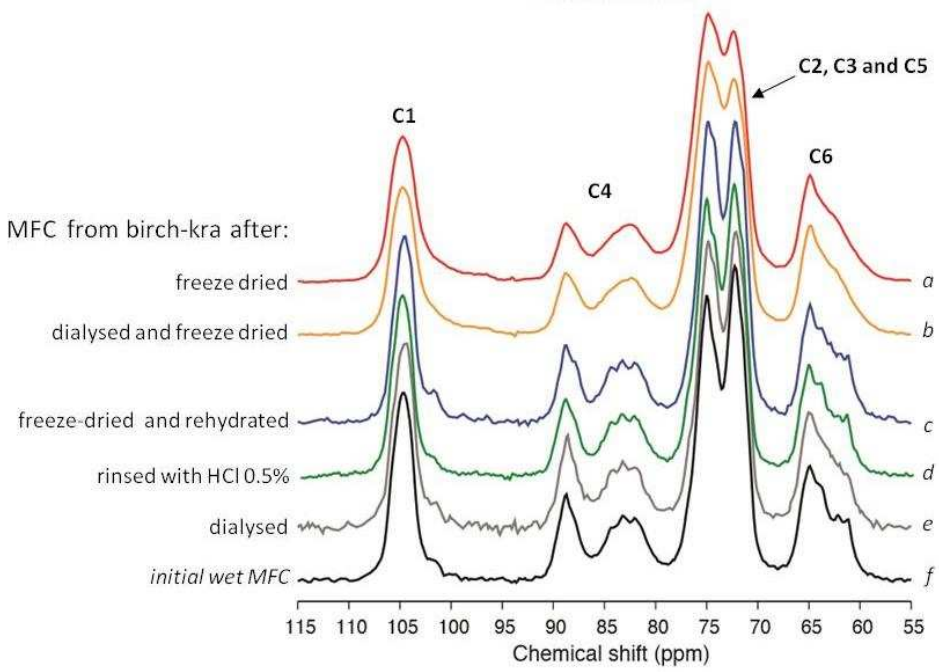

Figure 38: ^{13}C CP-MAS solid state NMR spectra of wet MFC samples from kraft birch pulp in different physic-chemical conditions

The spectra of freeze-dried MFC (Figure 38 *a* and *b*) were identical and did not show any evidence of the effect of dialysis. The spectral details are obviously lost compared to wet samples, probably due the constraints induced by strong cellulose-cellulose interaction upon drying resulting in a broad distribution of chemical shifts (Larsson *et al*. 1999). The effect of drying has been highlighted in the context of study on the hornification phenomena by (Newman 2004) . In this case the peak intensity at 84 and 84.9 ppm was shown to decrease during drying and did not fully recover its intensity after subsequent uptake of humidity, suggesting an occurrence of co-crystallization eliminating part of accessible surface. We didn't observe a similar effect in our samples.

The presence of water revealed spectral details that were previously hidden by the broadening of the peaks. At least three independent contributions could be identified in the so-called disordered contribution of the C4 peak between 80 and 85 ppm. The effect of the initial pulp compositions will be discussed in more details in the next paragraph.
Subtle differences could also be seen on the other contributions among the preparations measured under wet conditions (Figure 3 *c*, *d*, *e*, *f*) such as the line shapes of C1 and its subpeak at 102 ppm and the overall shape of C6. However, the origin and nature of these differences are not clear for the moment and needs further analysis based on relaxation measurements.

1.3 Solid state NMR spectra of wet MFC: effect of the cooking process

Figure 4 displays the spectra obtained in wet conditions on the five samples already analyzed in paragraph 1.1. As previously observed in the case of the birch kraft sample, the presence of water revealed different spectral details depending on the cooking process.

First, the C4 contributions (Figure 4, right) appeared very different for the sulfite and kraft pulps, for which two or three distinct contributions can be observed respectively. The xylan content in the MFC was indeed correlated to the intensity of the C4 peak at 82 ppm (Figure 39 right).

In the case of MFC from sulfite pulp, which contained a maximum of 2.5% xylan, the signal of C4 disordered region contained two peaks at 84.4 and 83.4 ppm. A third peak at 82 ppm was observed on the spectra of MFC from birch-kra and the MFC from spruce-kra containing respectively 22.5% and 8.7% of xylan.
This is in good agreement with Teleman's study (Teleman, Larsson, and Iversen. 2001), in which a decrease in the peak intensity at 82 ppm was observed after removal of xylan from the pulp by sodium hydroxide solution.

The presence of xylan also influenced the intensity of the C6 and C1 carbon contributions. Two additional peaks were observed at 64 ppm and 102 ppm (Figure 39 left). The presence of galactose was not evidenced in this study, as it was not detected in the MFC chemical compositions analyzed in paragraph 1.1.

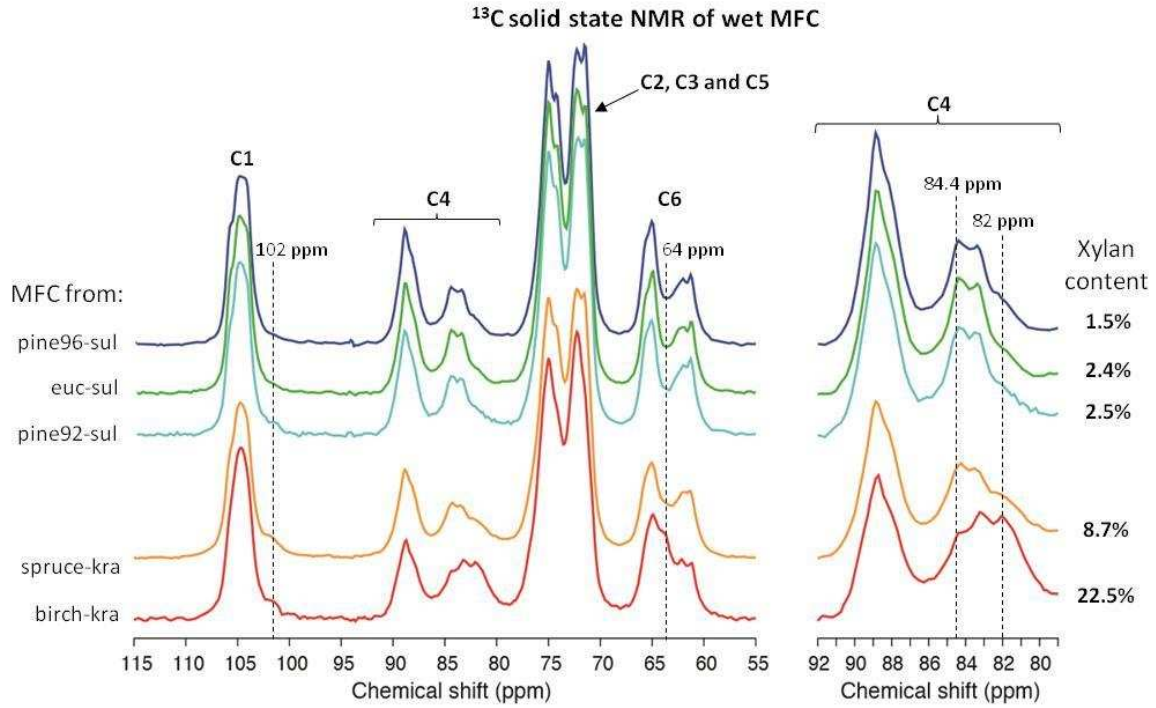

Figure 39: ^{13}C CP-MAS solid state NMR spectra of wet MFC samples from sulfite (pine 96, pine 92 and eucalyptus) and kraft (birch and spruce) pulps

Consequently, solid state NMR can be used to trace the presence of xylan in MFC using the intensity of the peak at 82 ppm. A method for quantitative evaluation of the xylan content will be presented in Chapter 3.

2. Xylan extraction from birch kraft MFC

In order to understand the interaction between the hemicelluloses chains and the microfibrils, we developed and optimized a protocol of xylan extraction from the MFC from kraft pulps, which had the highest xylan content of 22.5% according to sugar analysis. We restricted the study to the pulp from birch as the composition of the remaining hemicelluloses was shown to be almost pure xylose. The presence of xylan was traced by the peak intensity at 82 ppm of the solid-state NMR spectrum and related to the sugar composition.

2.1 Protocol description

The most efficient way to perform the xylan isolation from MFC is to dissolve the xylan chains without dissolving cellulose, then to separate the undissolved cellulose from the xylan solution by centrifugation.

Xylan is commonly extracted from wood by alkali treatments with potassium hydroxide (Timell 1967) or sodium hydroxide (Teleman, Larsson, and Iversen. 2001). However, in the case of this study, the pulp used to produce MFC had already undergone an alkaline cooking which is renowned to degrade hemicelluloses by peeling reactions and alkaline hydrolysis. Thus, we tried dimethylsulfoxide (DMSO), which is a polar aprotic organic solvent, and was previously used to dissolve residual xylan (Hägglund, Lindberg, and McPherson 1956).

First the wet MFC suspension was used in order to keep the open structure and facilitate the xylan extraction. Indeed the drying would irreversibly close the structure and potentially prevent the xylan to be extracted. However, when large amount of DMSO was added to the wet MFC, a viscous gel like substance was formed, and no liquid could be separated even after long centrifugation times.
Therefore we first dried the MFC, then dispersed it in DMSO and finally centrifuged the mixture to separate the xylan solution in DMSO and the MFC (Figure 40 *a* and *b*).

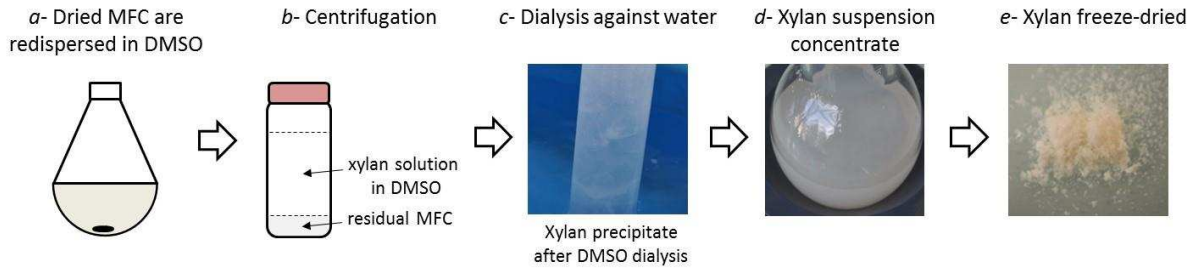

Figure 40: Illustration of the main steps of the protocol of xylan extraction

The xylan solubilized in DMSO was then recovered by replacing DMSO with water by dialysis against deionized water. Xylan extracted with this procedure was not soluble in water contrary to the one extracted from wood chips using sodium hydroxide. Indeed, the xylan chains precipitates in contact with water during dialysis in the form of colloidal particles and a xylan suspension in water was obtained at the end of process (Figure 40 *c*).
Because the volume of the suspension strongly increased during DMSO dialysis, the xylan suspension was first concentrated by water-evaporation then freeze dried (Figure 40 *d* and *e*).

2.2 Optimization of the extraction protocol

The xylan extraction was optimized by considering the influence of three different parameters: the drying step or accessibility (never dried and dried pulps, lyophilized from water or after solvent exchange with tert-buthyl-alcohol), the extraction conditions (solvent, temperature, time), the centrifugation set-up (speed and time) and the presence of aiding salts (LiCl). As the quantitative exploitation was tedious to implement (the recovery of the extracted and remaining part is complicated by the non-volatility of DMSO), only few experiments have been tested.

For calculating the yield of extraction, we considered that the total xylan content was given by the sugar analysis and called Xy. The yield of each xylan extraction was then calculated from the ratio of the mass of extracted xylan (M xylan *ex.*) to the xylan content in the MFC calculated from the sugar analysis (Xy) that gives the equation below:

$$\text{Yield} = \frac{\text{M xylan } ex.}{\text{M MFC x Xy } /100} \text{ x } 100$$

All the different extraction conditions are reported in Table 14 along with the corresponding yield of xylan extraction.

Table 14: Optimization of the protocol xylan extraction

	MFC from	Freeze-drying solvent	Extraction conditions	Centrifugation conditions	M MFC (g)	Xy (%)	M xylan *ex.* (g)	Yield (%)
P1	birch-kra	water	DMSO, 70°C, 2h30	11 200 rpm , 1h	0.25	22.5	0.014	**25**
P2	birch-kra	water	DMSO, 130°C, 2h30	11 200 rpm, 1h	0.28	22.5	0.010	**16**
P3	birch-kra -nd	TBA	DMSO, 25°C, 48h	11 200 rpm, < 14h	0.40	23.7	/*	**/***
P4	birch-kra-nd	TBA	DMSO, 25°C, 48h	11 200 rpm, 14h	3.00	23.7	0.183	**26**
P5	birch-kra -nd	TBA	DMSO - 5% LiCl, 25°C, 48h	11 200 rpm, < 14h	0.84	23.7	/*	**/***
P.Op.	**birch-kra-nd**	**TBA**	**DMSO - 5% LiCl, 25°C, 48h**	**11 200 rpm, 14h**	**2.77**	**23.7**	**0.434**	**66**

*xylan is contaminated with cellulose

The impacts of the different parameters on the xylan extraction yield will be discussed here under.

2.2.a Extraction temperature

In the two first protocols, P1 and P2, MFC were freeze dried in water, then redispersed in DMSO and heated at 70°C (Groendahl and Gatenholm 2005) or 130°C for 2h30. The xylan solution in DMSO was then isolated from the residual MFC by 1h centrifugation at 11 200 rpm.

The yield of extracted xylan was quite low and the temperature increase from 70°C to 130°C further reduced the mass yield from 25% to 16% (Table 14 – P2). Consequently, the temperature increase did not improve the extraction of xylan.

2.2.b Xylan accessibility

We thought that the hornification during the pulp drying or freeze drying might partially hinder the xylan extractability. To minimize the drying effect, we performed the extraction procedure on MFC from never dried pulp (MFC from birch-kra-nd) instead of MFC from dried pulp. Furthermore, a solvent exchange from water to tert-buthyl-alcohol (TBA) was performed to reduce collapse of the cellulose chains during the MFC freeze-drying (Fumagalli *et al.* 2013).

Scanning electron micrographs of the MFC from birch-kra-nd freeze-dried from water and from TBA are shown in Figure 41. As expected, a much open structure was obtained with MFC freeze-dried from TBA (Figure 41 B) compared to the one freeze-dried from water (Figure 41 A).

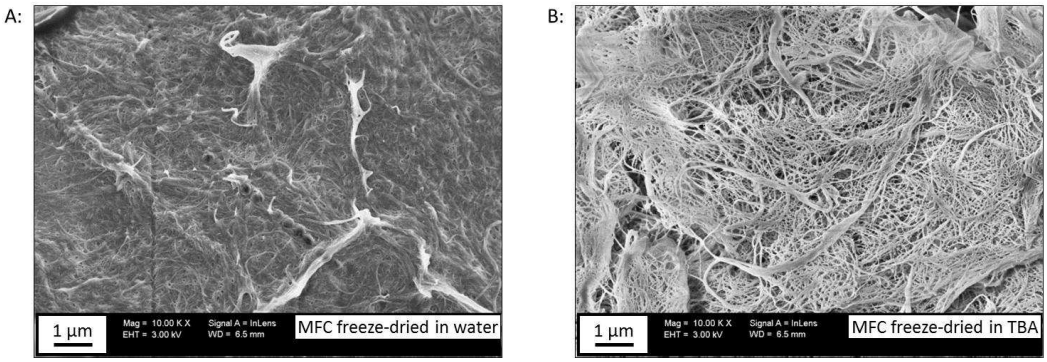

Figure 41: SEM images on MFC freeze-dried in A: water and B: TBA

The solvent-exchanged freeze-dried MFC were easily and well redispersed in DMSO. However, they were also more difficult to sediment by centrifugation. It was necessary to centrifuge at least for 15h at 11 200 rpm to settle all the residual MFC and to avoid cellulose contamination in the xylan solution supernatant as confirmed by 13C NMR spectra (Figure 42).

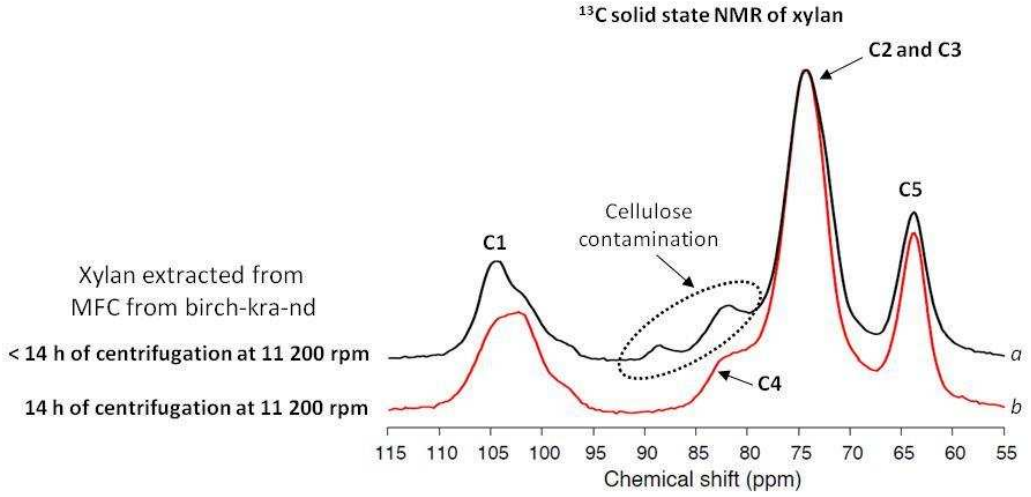

Figure 42: ^{13}C CP-MAS solid state NMR spectra of freeze-dried xylan extracted with centrifugation conditions: (a) bellow 14h at 11 200 rpm and (b) 14h at 11 200 rpm

The three main peaks centered at 102.0, 74.4 and 63.5 ppm are assigned respectively to the C1, C2 and C3 then C5 of the β-(1->4)-linked D-xylose residues (Teleman, Larsson, and Iversen 2001; Habibi *et al.* 2008). The shoulder at 82 ppm of the C2 and C3 peak at 74.4 ppm corresponds to the C4 of dried xylan, which moved to 74.4 ppm when it is hydrated.

When xylan was isolated with a centrifugation time lower than 14 h (Table 14 – P3), the cellulose C4 peak appeared in the 80 to 92 ppm range. In contrast, xylan isolated after 15 h of centrifugation (Table 14 – P4) was free from this kind of contamination and was considered pure (Figure 42 *b*).

The yield of xylan extraction was however not improved by the freeze-drying solvent modification and by the use of never dried MFC (Table 14 – P4). It remains around at the same value of 25% already obtained with the condition P1, using MFC from birch kraft dried pulp, freeze-dried in water.

2.2.c Role of LiCl

Lithium chloride salt (LiCl) is often added to polar aprotic solvent to improve polymer solubility. One example is LiCl/DMAC which is a solvent of cellulose (McCormick and Dawsey 1990). But LiCl/DMSO is also known to dissolve ethylene diamine treated cellulose (Wang, Yokoyama, and Matsumoto 2010).

Based on the previous conditions, the addition of 5% lithium chloride salt (LiCl) increased the yield up to 66% (Table 14 – P.Op.) from 26 %. Two centrifugation conditions were also tested, but as shown previously the xylan isolated with centrifugation time lower than 15h is contaminated with cellulose (Table 14 – P5).

To recover a maximum of dissolved xylan, the MFC were redispersed a second time in DMSO, after the centrifugation step. This optimized conditions illustrated in Figure 43, will be used in the rest of the study.

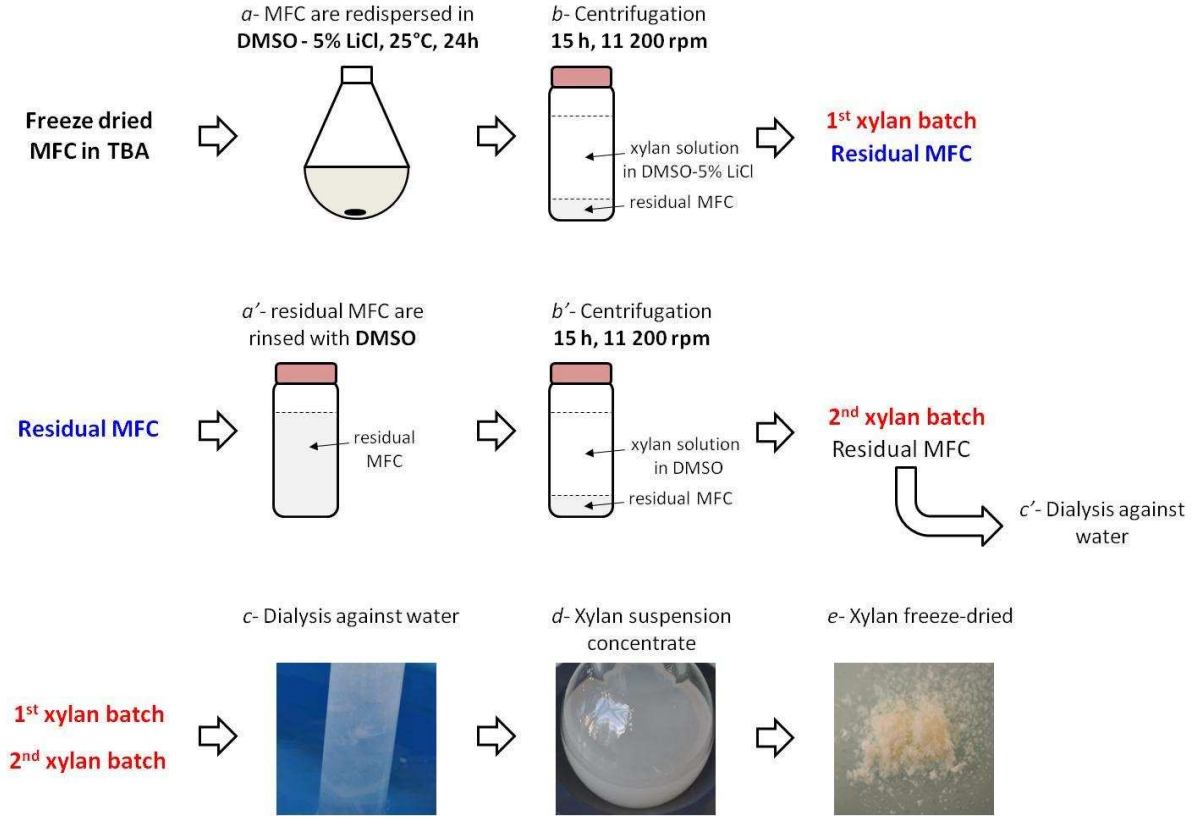

Figure 43: Illustration of the optimized xylan extraction protocol P.Op.

2.3 Extracted MFC characterization

Characterization by solid state NMR of MFC after the xylan extraction under the optimized conditions were performed on dried and wet samples and compared with the initial MFC (Figure 44).

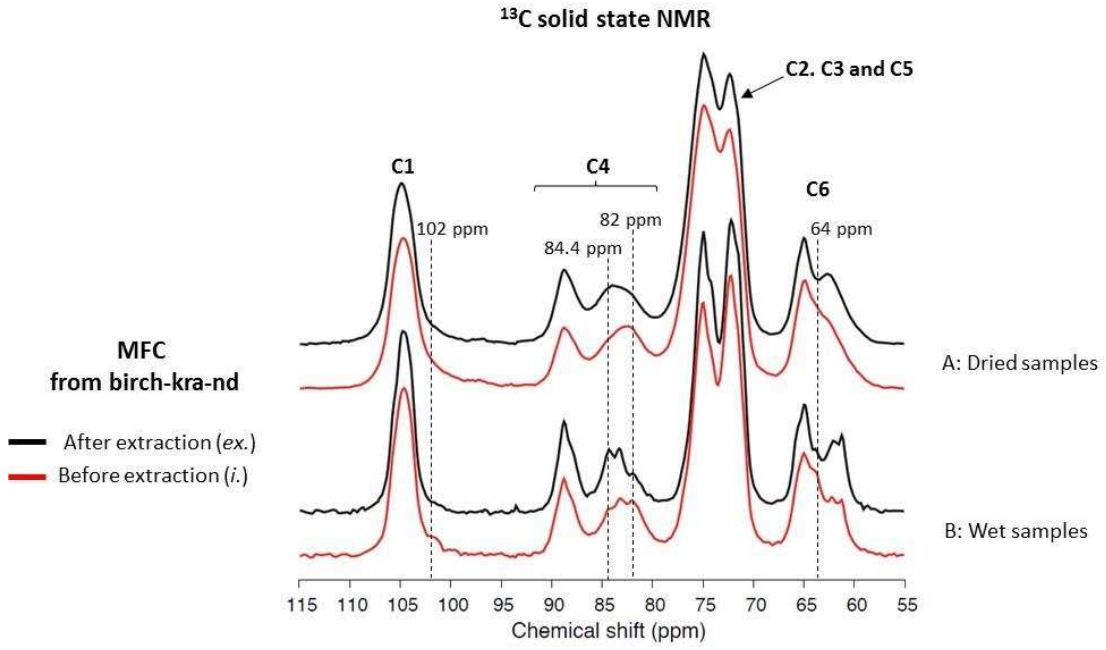

Figure 44: ^{13}C CP-MAS NMR spectra of freeze dried MFC (A) and wet MFC (B) before (red) and after (black) extraction of the MFC with the DMSO/LiCl.

The spectrum modifications due to xylan removal can be readily noticed on hydrated and dried samples even if the intensity changes of C6, C4 and C1 peaks are clearer on the hydrated spectra.

The spectrum of wet MFC after xylan extraction showed a characteristic intensity decrease of the peak at 82 ppm similar to that previously described by Teleman, Larsson, and Iversen (2001) who extracted xylan from pulp using sodium hydroxide.
The extinction of the C1 peak at 102 ppm and the modification of the C6 peak at 64 ppm were also observed on the signal of wet MFC after the xylan extraction.

The signal of C4 disordered at 84.4 ppm corresponding to the accessible fibril surfaces, according to Larsson *et al.* (1999), was also modified; its intensity increased after the xylan extraction. Indeed, the xylan removal from the surface should enhance the number of accessible cellulose chains at the microfibrils surfaces.

The evolution of the signals identified previously for tracing the xylan extraction behaves as expected from the mass yield results: the decreasing of the signal at 82 ppm, revealing the presence of xylan, was moderate for the two non-optimized protocols, whereas the intensity of the signal assigned to the accessible surface was only slightly increasing. Interestingly, in the case of the more open structure (MFC lyophilized from TBA, protocol P4), this signal from accessible surface appeared higher compared to the one obtained with more collapsed structures (MFC lyophilized from water, protocol P1).

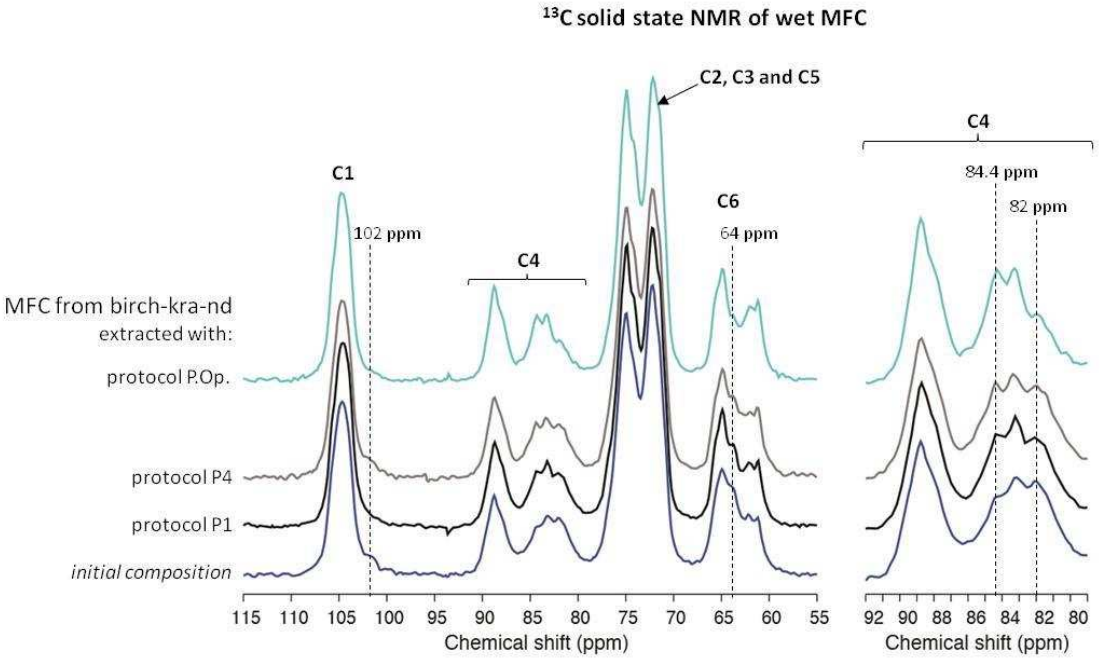

Figure 45: ^{13}C CP-MAS NMR spectra of freeze dried MFC with different xylan extraction protocols

To conclude, xylan could be extracted from MFC from never dried birch kraft pulp with a yield of 66% thanks to an optimized protocol using DMSO with 5% LiCl salt at 25°C for 24h. The solvent exchange from water to TBA had apparently little effect on the extraction yield, but the number of conditions that have been explored was small enough to remain cautious in terms of generalized conclusions.

2.4 Determination of extraction yield

Chemical compositions of the MFC after the xylan extraction were determined by sugar analysis (cf. Annex 2) and were compared with the initial compositions of the MFC before extraction (Table 15).

Assuming that we are dealing with a binary system of cellulose and xylan, and that only xylan is extracted by the process, the yield of xylan extraction was calculated from the initial xylan content in the sample (Xy *i.*) and the xylan content after the xylan extraction (Xy *ex.*) using the following equation:

$$\text{Yield S. A.} = \left(1 - \frac{\text{Xy } ex.}{\text{Xy } i.} \frac{(1 - \text{Xy } i)}{(1 - \text{Xy } ex)}\right) \text{ x } 100$$

This yield estimated from sugar analysis will be noted yield S.A. and it was compared in Table 15 with the yield calculated from the mass of the isolated xylan.

Table 15: Chemical composition of MFC by sugar analysis

	Initial MFC	**MFC after xylan extraction with protocol P4**	**MFC after xylan extraction with optimized protocol P.Op**
Glucose (%)	75.0	83.6	88.7
Xylose (%)	**23.7**	**16.3**	**9.2**
Mannose (%)	1.0	0.1	1.5
Arabinose (%)	0.1	0	0.1
Galactose (%)	0.2	0	0.5
Yield S.A. (%)	**/**	**37**	**67**
Yield (%)	**/**	**26**	**66**

As expected, the xylose content, initially quantified at 23.7% in the MFC from never dried birch kraft pulp decreased to 16.3 **%** after the non-optimized extraction (P4), which corresponds to a yield S.A. of 37 %. The lowest xylose concentration of 9.2% was obtained after the extraction with the optimized protocol P.Op and corresponds to a yield S.A. of 67%. Due to handling problems the weight of xylan extracted was under -estimated, but the overall results were still in the same range.
In order to confirm the complete removal of LiCl salt by dialysis, mineral impurities characterization have been performed on extracted xylan (cf. Annex 3) and revealed that xylan was mainly polluted by LiCl metal impurities or salt coming from MFC production in tap water.

In Teleman's study, (Teleman, Larsson, and Iversen. 2001) xylan has been extracted from birch kraft pulp with 9% of sodium hydroxide with a yield of 80% determined from sugar analysis corresponding to a decrease of the xylose content in the pulp from 26% to 5%. However, this was done at expense of a slight but discernible mercerization of the native microfibrils, whereas our process maintains the native character of the objects.

Whatever the process used to extract xylan from kraft MFC, it seems that a fraction of xylan remained inaccessible to the extraction procedures. Xylan might be irreversible attached to cellulose because of oxidative treatment during pulp bleaching or trapped in inaccessible regions after the collapse of the microfibrils, during freeze-drying.

3. Extension of the extraction protocol

The protocol of extraction, which has been first optimized on MFC from never dried birch kraft pulp, was extended to other substrates to test the possible generalization of the procedure on samples from different origin (birch and spruce) or form (non-refined and refined pulp, MFC suspensions). However, it has been limited to kraft samples due to their high content in hemicelluloses (Figure 46).

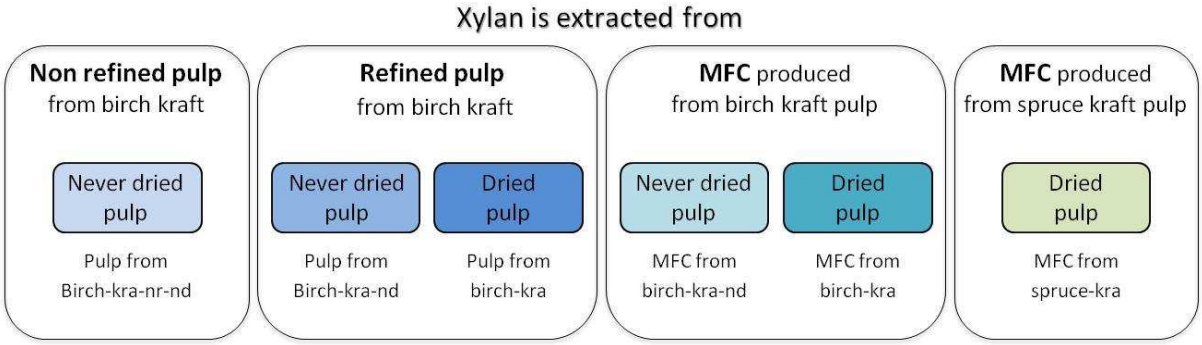

Figure 46: Summary of the different substrates extracted with the optimized protocol

Six xylan fractions were isolated after the extraction from the various kraft samples and the yields of extraction were determined by sugar analysis (Table 16). The non-normalized compositions as well as the hydrolysis yields are also available in Annex 4.

Table 16: Chemical composition before and after xylan extraction

	MFC from birch-kra-nd		**pulp from birch-kra-nd**		**MFC from spruce-kra**		**pulp from birch-kra**		**pulp from birch-kra-nd-nr**	
Glucose (%)	75.0	88.7	75.3	89.8	84.0	90.2	74.1	89.3	72.3	88.5
Xylose (%)	**23.7**	**9.2**	**23.4**	**9.1**	**8.7**	**3.2**	**25.5**	**9.9**	**25.2**	**10.2**
Mannose (%)	1.0	1.5	1.0	1.1	**6.5**	**6.5**	0.3	0.7	1.2	1.2
Arabinose (%)	0.1	0.1	0.1	0.0	0.6	0	0.1	0	0.9	0.1
Galactose (%)	0.2	0.5	0.2	0.0	0.2	0	0.0	0	0.4	0.0
Yield of xylan extraction (%)	**67**		**67**		**65**		**68**		**66**	

i.: initial pulp or MFC composition; *ex.*: pulp and MFC composition after xylan extraction

The xylose contents in birch kraft samples decreased after the xylan extraction and similar extraction yields of 67% are remarkably obtained regardless the samples degree of fineness (non-refined pulp, refined pulp and MFC) and the drying pulp history (never dried and dried). Interestingly, the spruce MFC obtained the same score, without any change in the mannose content, suggesting a mode of interaction of glucomannans with cellulose substantially different from xylan.

Solid state NMR characterization of the samples before and after xylan extraction was performed (Figure 47). As expected, the results confirmed the first observations deduced from the sugar analysis. The diminution of C4 peak intensity at 82 ppm and 84.4 ppm, the modification of C6 peak at 64 ppm and the extinction of C1 peak at 102 ppm were observed on all birch kraft samples spectra after the xylan removal and confirmed the yield of around 2/3 of extracted xylans.

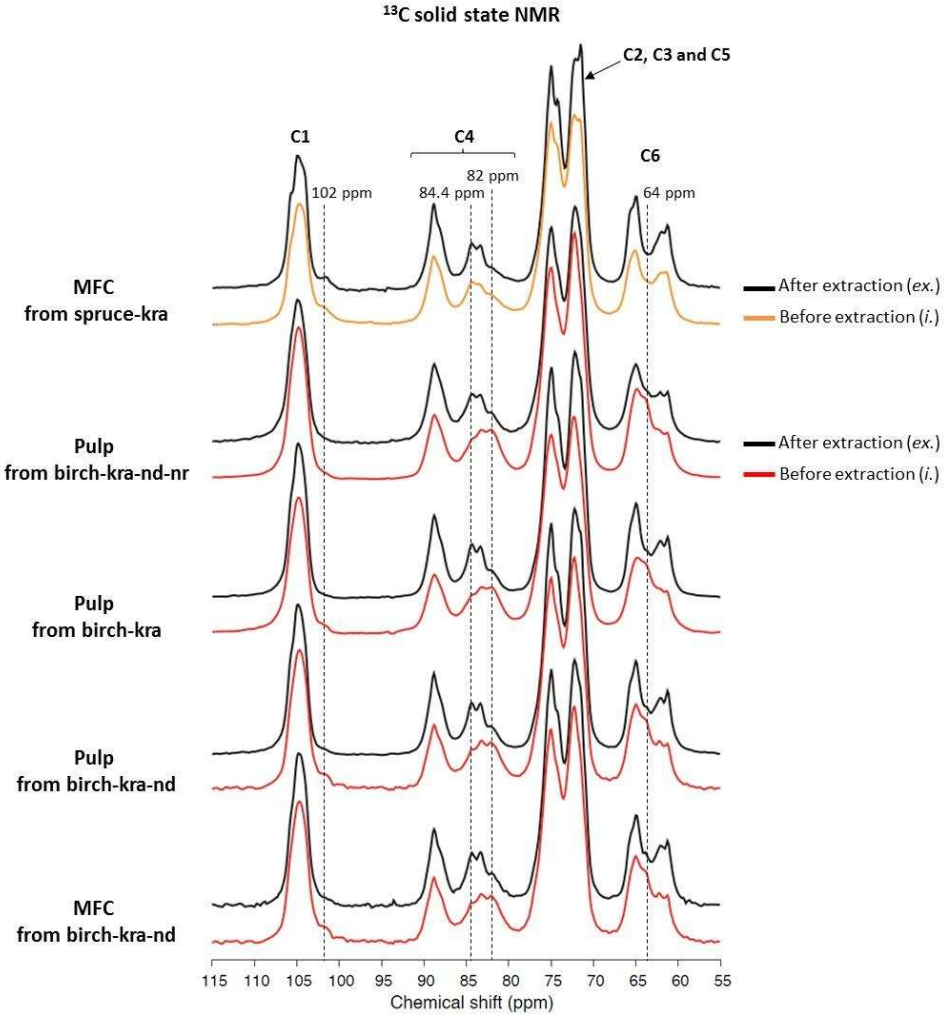

Figure 47: ^{13}C CP-MAS spectra of kraft pulp and MFC before and after xylan extraction

An intriguing result came from the MFC from spruce kraft pulp, containing glucomannan, but leading to similar yield of xylan extraction (67 %) than the birch samples. Indeed, even if small differences persist at 64 ppm, the NMR spectra after xylan extraction were quite similar, regardless of the initial wood species (birch or spruce) and the samples degree of fineness (pulp or MFC).
However the xylan purity extracted from the different samples will be discussed in the following paragraphs.

In conclusion, the protocol of xylan extraction can be extended to different kraft processed products from different physical forms and wood species. The typical extraction yield was around 67%, pointing out the impressing invariability of the extraction procedure. In all cases, the xylan removal resulted in very similar solid-state NMR spectra, with the same modification between 82 and 64 ppm. This last feature is in favor of an intrinsic association of xylan with cellulose.

4. Characterization of the extracted xylans

4.1 Chemical composition of the extracted xylans

The sugar composition of the xylans extracted from pulps and MFC were compared with a xylan extracted from birch wood chips using 5% sodium hydroxide at CTP and with a commercial xylan extracted from oat (Table 17).

Table 17: Chemical composition of the extracted xylans by sugar analysis*

	Xylan extracted from						
	MFC from birch-kra-nd	**pulp from birch-kra-nd**	**pulp from birch-kra**	**pulp from birch-kra-nd-nr**	**MFC from spruce-kra**	**oat (commercial)**	**birch wood chips**
Glucose (%)	5.1	2.5	2.1	5.9	34.2	13.0	**1.6**
Xylose (%)	94.4	97.0	97.6	93.5	54.7	76.5	53.1
Other (%)	**0.5**	**0.5**	**0.3**	**0.6**	**11.1**	**10.5**	**45.3**
Mannose (%)	0.0	0.0	0.0	0.0	4.5	0.0	0.7
Arabinose (%)	0.3	0.3	0.2	0.0	5.5	9.6	2.7
Galactose (%)	0.2	0.2	0.1	0.6	1.1	0.9	6.6
Lignin (%)	/	/	/	/	/	/	35.3

*Details about the non-normalized compositions and the hydrolysis yields are available in Annex 5.

All xylans extracted from birch kraft samples are pure at 93.5 to 97.6%, regardless the size of the substrate (MFC, refined pulp or non-refined pulp) or the pulp drying history (dried or never-dried pulp). Contaminations by cellulose, which accounts for 2.1% to 5.9%, are probably due to handling problems. The xylan extracted from birch wood chips was mixed (35%) with residual lignin because of sodium hydroxide extraction.

As already observed in the preceding paragraphs, the hemicellulose extracted from birch kraft samples did not have any arabinose side groups and can be considered as pure xylan at the sensibility of the experiment. By contrast to the hemicelluloses extracted from birch kraft samples, those extracted from spruce kraft MFC were a mixture of 60.2% of arabino-xylan and 6.7% of galacto-glucomannan, and were also contaminated with 33.1% of cellulose.

The contribution of the galacto-glucomannan in the glucose content is determined with the following equation, where *b* is a correcting factor, that corresponds to the proportion of glucose and mannose in the glucomannan chain fixed at 4.15 in the case of softwood (Genco *et al.* 1990).

$$[Galacto-glucomannan] = [Mannose] \times \left(1 + \frac{1}{b}\right) + [Galactose]$$

$$[Cellulose] = [Glucose] - \frac{[Mannose]}{b}$$

The glucomannan extraction was first not detected by chemical composition performed on MFC (cf. paragraph 3. - Table 16) but it might be negligible as it represented only 1/10 of extracted xylan.

Xylan is often decorated by 4-O-methyl D-glucuronic acid residues and *O*-acetyl groups in hardwood, while L-arabinosyl residues are also found as pendant groups in softwood xylan (Pinto, Evtuguin, and Neto 2005; Ebringerová and Heinze 2000; Timell TE 1964). However, the O-acetyl group is very labile and should be easily removed by the basic conditions during the kraft pulping process (Aurell and Hartler 1965).
The arabinose branches are also affected by the kraft cooking (Hansson and Hartler 1968; Aurell and Hartler 1965) which explain that no arabinose group were found in xylan extracted from birch kraft pulp or MFC, but some 2.7% were found in the xylan extracted from birch wood chips.
Because xylan from softwood is initially more substituted with arabinose residue than the one from hardwood, some residual arabinose branches may be conserved after the kraft cooking and the xylan extracted from MFC from spruce kraft pulp contained 5.5% of arabinose.
To compare, the commercial xylan extracted from oat is the most branched with 9.6% of arabinose residues but it is also less pure with 13.0% of cellulose. Therefore, the xylan extracted from birch kraft samples (pulp or MFC) is the purest in xylose, its maximal cellulose contamination of 5.9% is two times lower than in the commercial xylan extracted from oat.

4.2 Solid state NMR characterization of the extracted xylan

The xylans structure was also analyzed by solid state NMR (Figure 48) and the peak attribution is performed according to the literature (Teleman, Larsson, and Iversen 2001; Habibi *et al*. 2008).

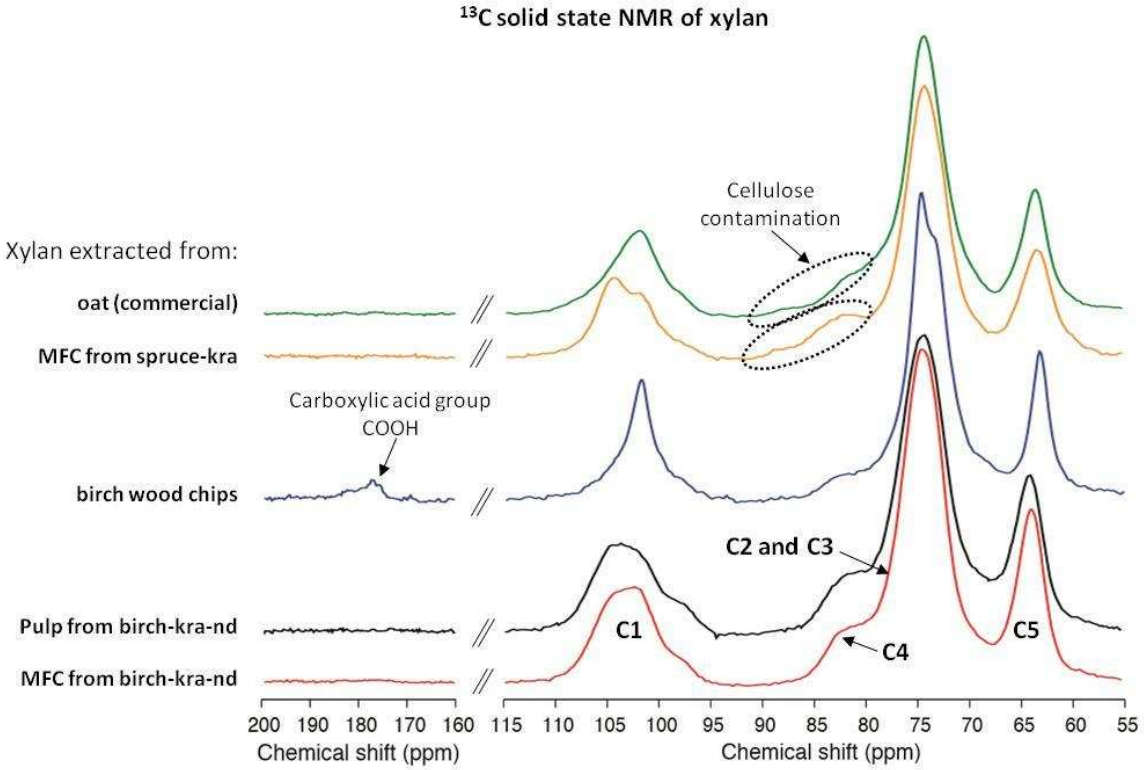

Figure 48: ^{13}C CP-MAS spectra of hemicelluloses extracted by DMSO from MFC from oat, MFC from spruce kraft pulp, MFC and pulp from never dried birch kraft pulp.

The cellulose contamination is apparent on NMR spectra of xylan extracted from MFC from spruce kraft pulp (33.1%) and the commercial one extracted from oat (13.0%) by the signal from 79 ppm to 92 ppm.

The NMR spectra from xylan extracted from birch kraft samples (pulp and MFC) were similar. They differed from the xylan extracted from birch wood chips by the absence of signal at 177 ppm attributed to the carboxylic acids of the 4-O methyl-glucuronic acid branches.

In some preparations (Figure 49), DMSO contaminations due to incomplete dialysis, were visible with a distinct peak at 40 ppm on NMR spectra and were taken into account in the mass calculation for chemical composition determination.

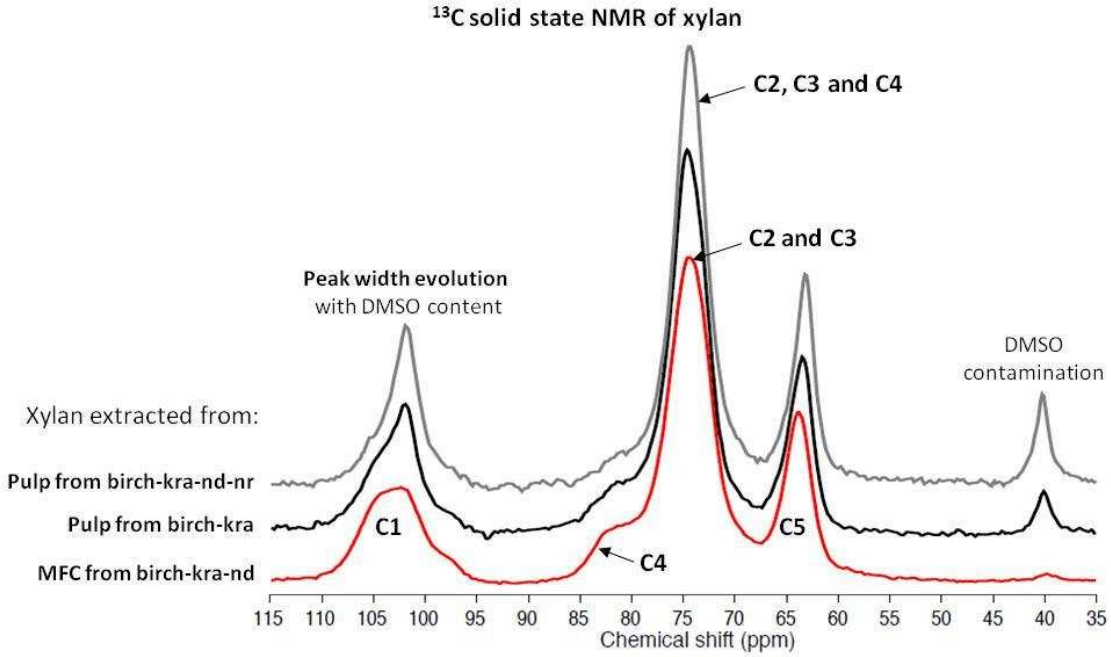

Figure 49: ^{13}C CP-MAS spectra of xylan extracted from non-refined never dried pulp from birch kraft, dried pulp from birch kraft and MFC from birch kraft never dried pulp

The spectral profiles were different depending on the sample preparations, especially on the shape of the C1 peak and C4 shoulder at 83 ppm. The xylan peaks were narrower in presence of DMSO and the xylan conformation might be also modified by the presence of DMSO and water.

Since no arabinose could be detected by sugar analysis (below 0.5%) and no signal of 4-O methyl-glucuronic acid branches was detected by solid state NMR (at 177 ppm), we considered the xylans extracted from birch kraft samples as a homopolymer of xylose.

4.3 Liquid state NMR characterization of the extracted xylan

In order to confirm the absence of branches, further analysis are performed by liquid state NMR (proton ^{1}H and carbon ^{13}C) on the xylan extracted from birch kraft samples (pulp and MFC) and compared with the xylan extracted from birch wood chips and the commercial one extracted from oat.

The xylan extracted from birch wood chips was easily dissolved in heavy water (D_2O) while the one extracted from birch kraft samples (pulp and MFC) was only soluble in DMSO among the solvents tested, including other polar aprotic organic solvents such as dimethylformamide (DMF) or tetrahydrofurane (THF). All the liquid NMR analysis of the extracted xylan from kraft samples were thus performed in deuterated dimethylsulfoxide (DMSO-d_6). The peaks attribution of the liquid NMR spectra proton ^{1}H and carbon ^{13}C, (Figure 50 and Figure 51) have been established according to the xylan already described in the literature (Teleman *et al.* 2000; Habibi and Vignon 2005) and with proton-carbon correlation (HSQC) measurements (cf. Annex 6).

4.3.a Carbon ^{13}C NMR

The carbon (^{13}C) NMR spectrum of xylan extracted from birch kraft samples (pulp or MFC) shows a pure signal of unsubstituted xylose residue (Teleman *et al.* 2000; Habibi and Vignon 2005) and the peaks at 101.4 ; 75.2; 73.7; 72.3 ppm and 62.9 ppm are attributed to C1, C4, C3, C2 and C5.

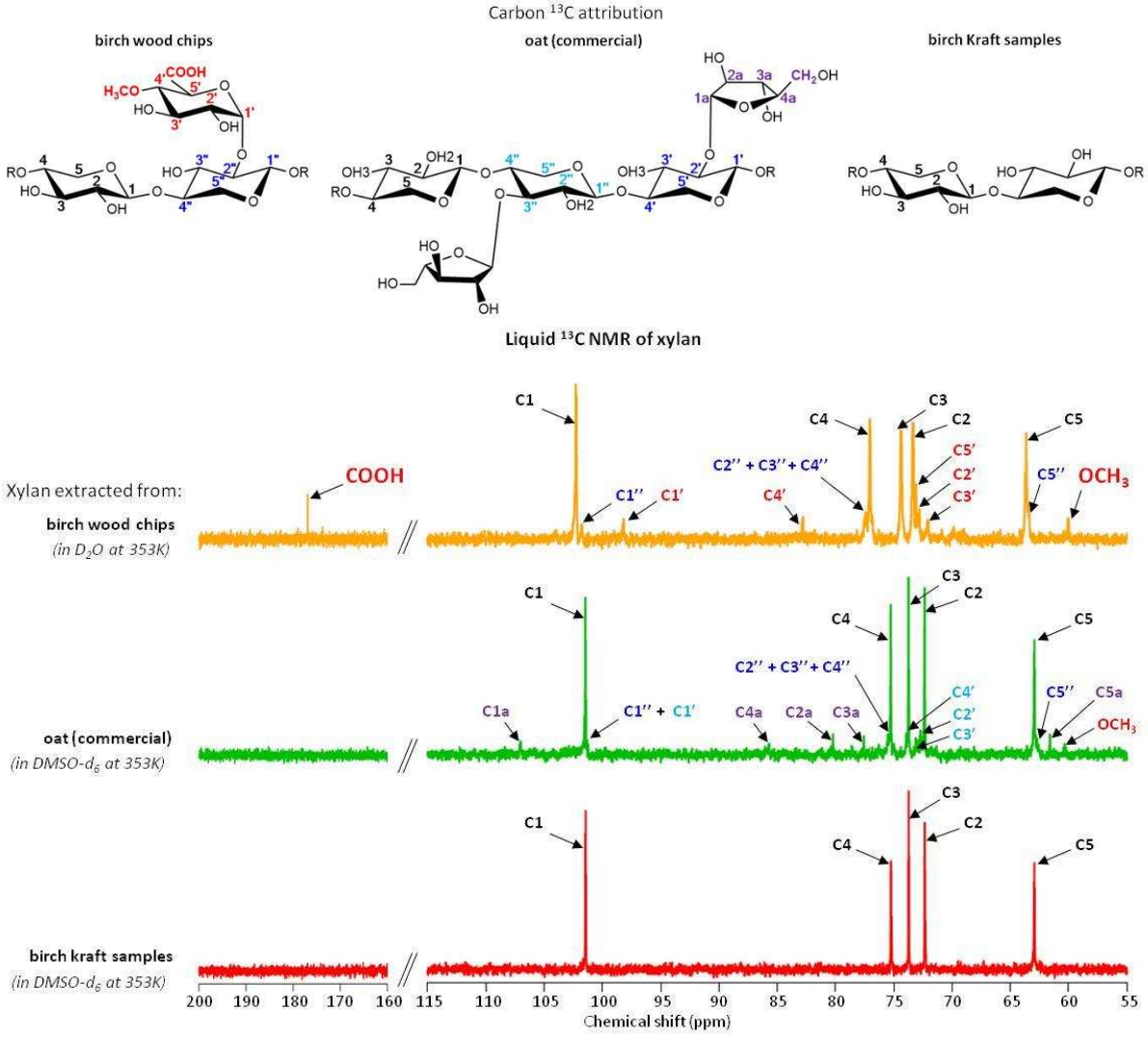

Figure 50: Carbon (^{13}C) liquid NMR of xylan extracted from birch wood chips, oat and birch kraft samples (pulp and MFC)

It is noticed that similar chemical shift was observed between the carbon (^{13}C) NMR liquid spectrum and the one of ^{13}C solid state NMR. The only difference was observed for the signal of C4 which is shifted from 75.2 ppm to 82.0 ppm. The two other NMR spectra of xylan extracted from oat and birch wood chips had in common with the xylan extracted from birch kraft samples, the signal of unsubstituted xylose residue. A shift from 1 to 2 ppm was observed on the spectrum of xylan extracted from birch wood chips, but it must be attributed to the difference in solvent used to perform the NMR analysis from DMSO-d_6 to D_2O. The presence of 4-O methyl glucuronic acid branches in xylan extracted from birch wood chips, already observed on solid state NMR with the carboxylic acid peak at 177 ppm was confirmed by carbon (^{13}C) NMR (Figure 50). The two characteristic peaks of carboxylic acid (COOH) and methoxy group (OCH_3) were detected at 176.9 ppm and 60.0 ppm.

Furthermore, three distinct resonance peaks of C1 at 102.3 ppm, 101.7 ppm and 98.1 ppm can be respectively attributed to the unsubstituted xylose residue, the xylose residue branched in O3 with glucuronic acid and the 4-O methyl-glucuronic acid branches itself (Habibi and Vignon 2005).

For steric reason, no glucuronic acid was branched in the O2 of xylose contrary to the xylan extracted from oat which was substituted with arabinose group in O2 and in O3 position. Four different signals on NMR spectrum corresponding to the unsubstituted xylose residue, the xylose branched in O2, the one branched in O3 and the arabinose branches were observed.

The peaks at 61.6 ppm and 107.0 ppm respectively corresponded to the C5 ethoxyl goup (CH_2OH) and C1 of the arabinose branches. The attribution of the peaks at 77.6 ppm, 80.2 ppm and 85.7 ppm to the C3, C2 and C4 of the arabinose residue may be commutable.

However other carbon signal which were not visible on carbon (^{13}C) NMR were detected by HSQC measurement, further described in Annex 6. Two peak characteristics of 4-O methyl glucuronic acid branches were visible at 60.31 ppm - 3.42 ppm and 99.62 ppm -5.14 ppm and corresponded to the methoxy group (OCH_3) and the (C1,H1) of the 4-O methyl glucuronic acid branches.

Then the small peak at 60.3 ppm visible on carbon (^{13}C) NMR was attributed to the methoxy group (OCH_3) of the 4-O methyl glucuronic acid branches. The other signal at 72.7 ppm, 73.1 ppm and 73.9 ppm may be commutable and corresponded to the C2, C3 and C4 the xylose residue substituted in O3 with arabinose or glucuronic acid.

4.3.b Proton ^{1}H NMR

Similar observations are performed on proton (^{1}H) NMR spectra (Figure 51) where the signal of unsubstituted xylose residue visible on spectrum of xylan extracted from birch kraft samples is common with the two other spectra. As for carbon (^{13}C) NMR spectrum, this signal was shifted in the case of xylan extracted from birch wood chips due to the change of deuterium solvent.

The peaks were attributed according to literature (Habibi and Vignon 2005) and the signal at 4.3 ppm, 3.5 ppm, 3.3 ppm and 3.1 ppm corresponded to the proton H1, H4, H3 and H2. The characteristic signal of non-equivalent CH_2 protons in C5 position were noticed with H5 in equatorial position (H5eq) at 3.9 ppm and H5 in axial position (H5ax) at 3.2 ppm.
The two peaks at 4.8 ppm and 4.6 ppm corresponding to the hydroxyl protons linked to C2 (OH2) and to C3 (OH3) and attribution may be commutable. It is only occurred when spectrum was recorded in DMSO-d_6 solvent because of proton-deuterium exchange in D_2O.

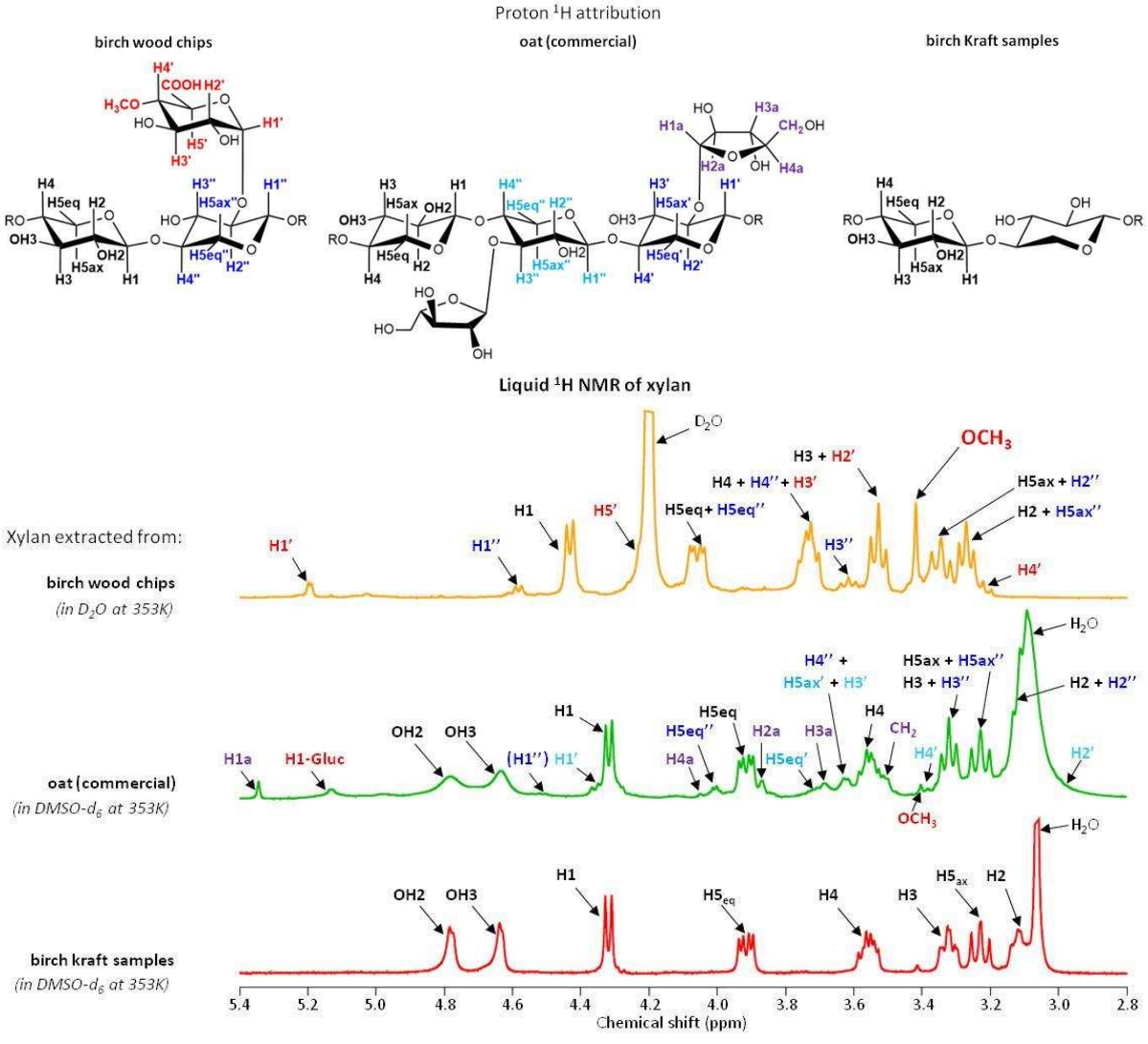

Figure 51: Proton (^{1}H) liquid NMR of xylan extracted from birch wood chips, oat and birch kraft samples (pulp and MFC)

The presence of the 4-O methyl glucuronic acid branches was detected on the proton (^{1}H) NMR spectrum of xylan extracted from birch wood chips with the singlet peak at 3.4 ppm and the three different protons signals H1.

They were attributed to the unsubstituted xylose residue (4.4 ppm), the xylose residue branched in O3 with glucuronic acid (4.6 ppm) and the 4-O methyl-glucuronic acid branches itself (5.2 ppm).

The degree of branching of xylan can be evaluated by peaks integration of the three protons (cf. Annex 6). In that case, the ratio between the 4-O methyl glucuronic acid residue, the xylose branched with glucuronic acid and the unsubstituted xylose was 6.1.1 and corresponded to the previous one determined in the literature (Habibi and Vignon 2005).

In the case of xylan extracted from oat, four different signals of H1 were respectively attributed to the unsubstituted xylose (4.3 ppm), the xylose branched in O3 (4.4 ppm), the glucuronic acid branches (5.1 ppm) and the arabinose branches (5.3ppm). The signal of xylose substituted in O2 was not clearly detected in proton NMR spectrum but was visible on HSCQ at 4.51 ppm -101.42 ppm.

The smaller peaks which cannot be linked with the unsubstituted xylan backbone correspond to the 9.5% of arabinose branches determined by sugar analysis and the 4-O methyl glucuronic acid residue. The signal at 3.4 ppm may be attributed to the methoxy group (OCH_3) and correspond to the one detected on HSQC at 3.42 ppm - 60.31 ppm.

4.3.c Xylan NMR characterization conclusion

To conclude, after sugar analysis and NMR performed in liquid and solid states, the xylan extracted from birch kraft samples (MFC and pulp) showed pure xylose spectra and a chemical structure corresponding to a homopolymer of xylose at the sensibility of the experiment.
The two other xylans were found to be branched with glucuronic acid and arabinose residues. In any case no acetyl group was detected. They have been most probably removed during the pulping chemistry (Aurell and Hartler 1965) for the xylan extracted from birch kraft samples or during the extraction with sodium hydroxide for the other xylans (Ebringerová, Hromádková, and Heinze 2005).

4.4 Conclusion on the xylan extracted from birch kraft samples

A homopolymer of xylose has been extracted with a yield of 60% from various birch kraft samples including non-refined pulp, refined pulp and MFC with or without drying step. To reach this yield of extraction it was necessary to use as solvent the mixture of DMSO with 5% of LiCl salt. The xylan purity was from 93% to 97% based on sugar analysis when cellulose microfibrils were eliminated by centrifugation at 11 200 rpm for 15h.

This homopolymer of xylan was found to be only soluble in DMSO and not at all in water contrary to the xylan with side groups extracted from wood chips with sodium hydroxide.

The unsubstituted xylan extracted from the pulp and MFC may have resisted to the cooking conditions while the one extracted from wood chips would have been eliminated during the cooking process.

There are two possibilities for the origin of non-branched homo-xylan we extracted. (a) Two types of xylan are biosynthesized, a homopolymer resisting to extraction and a branched xylan easier to be extracted, or (b) xylan are all branched in the wood cell wall, but the pulping processes chop all side groups leaving the bare homopolymer backbone.

5. Characterization of the xylose homopolymer

5.1 Crystallinity

The crystallinity of the xylan extracted from birch kraft samples (pulp and MFC) has been characterized by solid-state NMR and X-Ray Diffraction measurements (XRD) on the dried sample and after its rehydration at 97% of relative humidity (Figure 52).

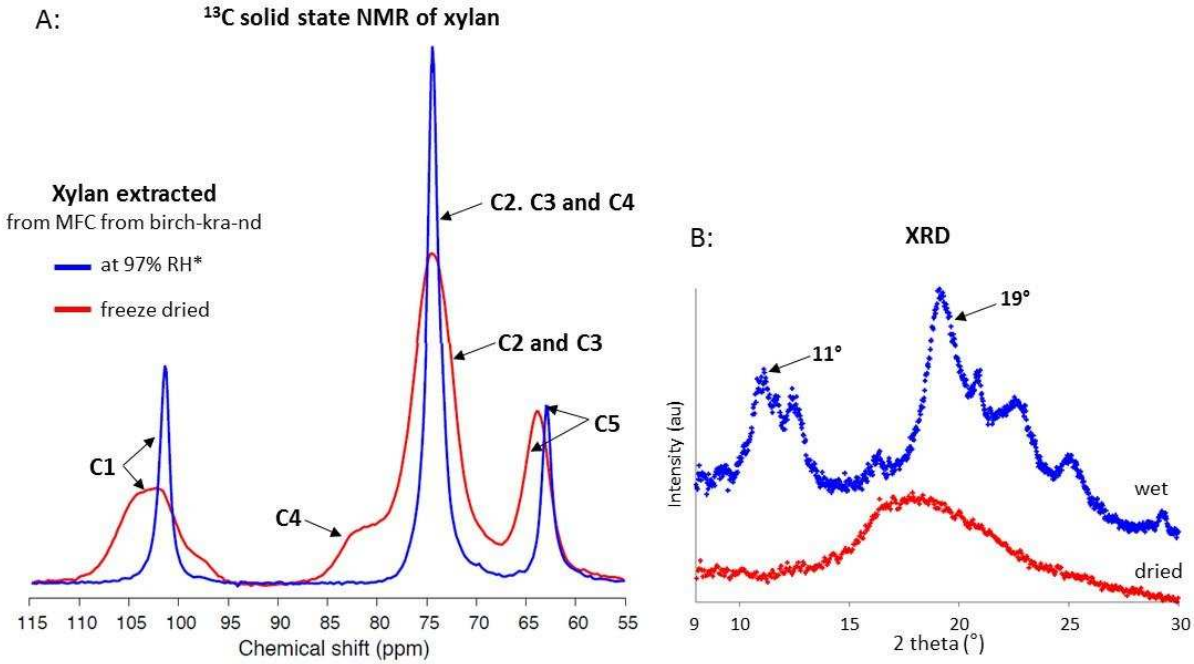

Figure 52: ^{13}C CP-MAS spectra (A) and XRD measurement (B) of freeze-dried and wet (97% of RH) xylan extracted from MFC from birch kraft never dried pulp (*I wet = I real/5)

As previously described by (Teleman, Larsson, and Iversen 2001; Habibi *et al.* 2008), xylan is more organized in the hydrated state than in the dried one as thinner peaks are observed on solid state NMR spectrum of the hydrated sample (Figure 52 A). Compared to the dried sample spectrum, no characteristic peak of C4 at 82 ppm was observed when the sample was rehydrated which may represent a strong conformational change in the xylan structure.

Previously, similar peak evolution was observed on the xylan fractions contaminated with DMSO (Figure 48). It may come from residual water in the DMSO or that the DMSO itself provides some conformational change in the xylan structure.

The corresponding X-ray diffraction spectra were provided for the dried and rehydrated samples (Figure 52 B). No sharp peak can be observed in the dried sample spectrum while a number of diffraction peaks can be seen in the humidified sample. The two strongest peaks at 11° and 19° corresponded to the Miller indices of (1-10, 010) (110, -120) according to (Nieduszynski and Marchessault 1972) the structure in which the xylan forms a three fold helix 3_2.
In conclusion, the extracted xylan is crystalline in presence of water as a three-fold helix 3_2 and its structure is less organized when it is dried.

5.2 Degree of Polymerization

The DP of hardwood xylan in its native state in the wood is estimated in the range of 100 to 200 (Koshijima, Timell, and Zinbo 1965; Westbye, Svanberg, and Gatenholm 2006). The DP of an extracted xylan from birch kraft pulp by sodium hydroxide treatment, was also estimated to 70 by peak integration on liquid NMR spectrum (Teleman, Larsson, and Iversen 2001).

In this study, the DP of the xylan extracted from birch kraft samples (pulp and MFC) was calculated from three different techniques: by peak integration on liquid NMR, by viscosimetry measurement on a range of xylan solution in DMSO and by SEC-MALS analysis with xylan dissolved in DMAC-LiCl.

5.2.a Determination of DP with liquid NMR

The peak integration was performed by integrating the proton of the chain end and comparison with the signal from the main chain. The ratio between the two forms α and β of the chain end in the case of xylan was estimated at 35/65.

The peak of proton α is observed at 5.18 ppm and the one of β at 4.15 ppm (Figure 53).

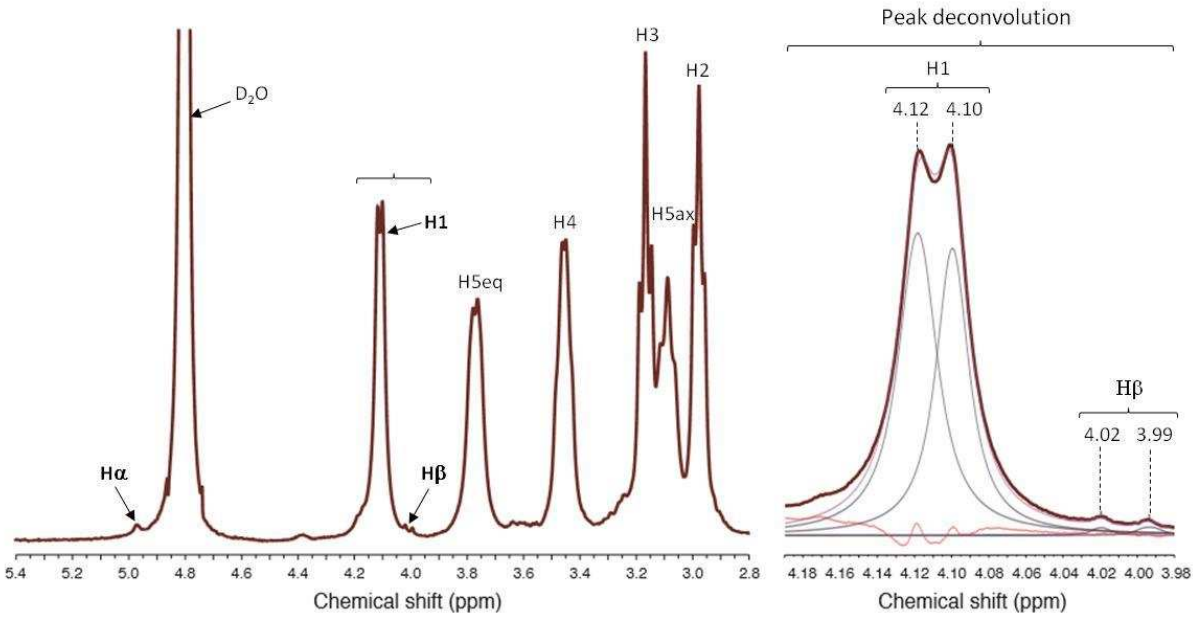

Figure 53: Proton (^{1}H) liquid NMR spectrum of xylan extracted from birch kraft (D_2O + 9% NaOD, 298 K)

Because the peak of the proton α was too close to the signal of D_2O, the deconvolution was performed on the signal of proton β.

Two subdivided peaks were attributed at 4.12ppm and 4.10 ppm for the proton H1 of xylose residue and 4.02 ppm and 3.99 ppm for the proton β. Then the intensity of each peak was adjusted in order to fit the original spectrum with signal resulting from the sum of intensity of the four subdivided peaks.

The area was calculated from the width and the intensity of each subdivided peaks. Then the area for each proton was determined with the sum of the area of each contribution (Table 18).

Table 18: Peak integration of the two protons H1 and Hβ

Proton	Chemical shift (ppm)	Intensity	Width	L/G	Area per peak	Area per proton
H1	4.12	3099	10.1	0.18	784534	1424688
	4.10	2942	8.6	0.10	640154	
Hβ	4.02	78	5.1	0.60	9347	21598
	3.99	84.8	6.6	1.0	12251	

The number of chain ends was calculated with the area of H1 and Hβ and the proportion of chain ends in the β form (65%):

$$Number\ of\ chain\ ends = \frac{area\ H\beta}{area\ H1\ \times\ 0.65}$$

Then a rough estimation of the DP of xylan was calculated from the inverse of the number of the end of the chain. In that case, the DP of xylan extracted from birch kraft samples was around 43, which corresponds to a molar mass of 5600 g/mol. This first DP estimation is smaller than previous determined in Teleman study's (Teleman, Larsson, and Iversen 2001) where xylan DP was around to 70 but it is in the same range of value.

However, one has to emphasize that liquid sate NMR give an average value of the DP, which is not able to discriminate between a mix of oligomers and very long chains, and an average number of middle sized chains.

5.2.b Viscosimetry

The dynamic viscosity was measured for a range of xylan concentration solution at the different angles. Then the average value of dynamic viscosity (Xyl visco) was calculated for each xylan concentration and is presented in Table 19.

Table 19: Dynamic viscosity at different angles

Cxyl (g/dL)	Dynamic viscosity (at 80°)	Dynamic viscosity (at 50°)	Dynamic viscosity (at 20°)	Xyl visco (mPa·s)	Reduced viscosity (dL/g)	Inherent viscosity (dL /g)
0.37	2.696	2.759	2.761	**2.739**	0.506	0.464
0.82	3.239	3.303	3.300	**3.281**	0.512*	0.427*
1.14	4.112	4.231	4.238	**4.194**	0.714	0.522
1.34	4.714	4.851	4.866	**4.810**	0.809	0.548
				DMSO visco (mPa·s)		
DMSO pure	2.273	2.320	2.331	**2.308**	/	/

*Points are removed because there are too different from the others.

The reduced viscosity and the inherent viscosity in Table 19 are calculated from the dynamic viscosity (Xyl visco), the xylan concentration in the solution (Cxyl) and the dynamic viscosity of the DMSO (visco DMSO) with the following equation:

$$Reduced\ viscosity = \frac{(Xyl\ visco - DMSO\ visco)}{DMSO\ visco \times Cxyl} \qquad Inherent\ viscosity = Ln\left(\frac{Xyl\ visco}{DMSO\ visco}\right)/Cxyl$$

The reduced and inherent viscosity are plotted as a function of the xylan concentration (Figure 54) and the intrinsic viscosity corresponded to the average value of the interception at the origin of both curves which is egal to 0.412 dL /g.

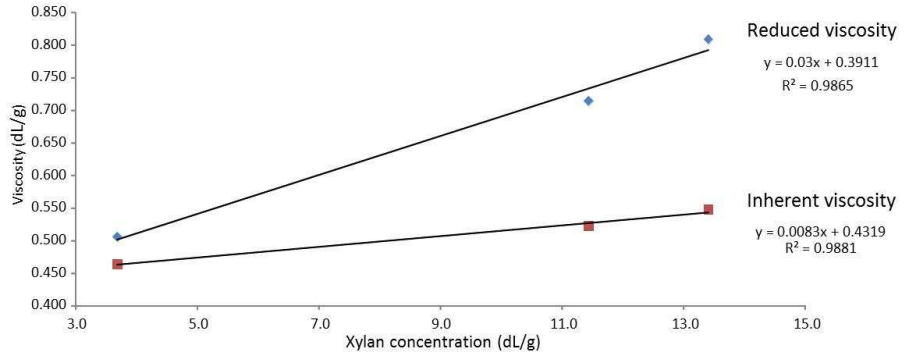

Figure 54: Intrinsic viscosity determination of xylan solution in DMSO

The DP of the xylan was calculated from the equation of Mark–Houwink where the values of α and k, depend on the particular polymer-solvent system.
For most flexible polymers α value is between 0.5 and 0.8 depending on the quality of the solvent $0.5 \leq \alpha \leq 0.8$. For semi-flexible polymers, α is higher than 0.8, ($\alpha \geq 0.8$) and polymers with an absolute rigid rod behavior get α value equal to 2 ($\alpha = 2.0$).

$$DP = \left[\frac{Intrinsic\ viscosity}{\mathrm{k}}\right]^{1/\alpha}$$

The α and k parameters have been determined by Lebel, Goring, and Timell (1963) for xylan and correspond to:

$$\alpha = 0.94 \text{ and } k = 5.9\ 10^{-3}\ g/dL$$

The DP of xylan extracted from birch kraft sample was 91, which corresponded to a molar mass of 12 000 g/mol. The difference in the obtained value of molar mass obtain may be justified by fact that small molecules contribute a lot in the liquid NMR determination which provide only a rough estimation of the DP, but also inherent problems of viscosity measurements, especially with low DP.

Furthermore, the viscosimetry average molar mass (M_v) determined by viscosimetry measurement is not an absolute value because it depends on the quality of the solvent used to perform the measure and will be always higher than the mass average molar mass (M_w).

5.2.c SEC- MALS measurement (Tokyo)

To determine the molecular weight distribution, the xylan sample was dissolved in DMAC – 8%LiCl and measured using Size Exclusion Chromatography with Multiple Angle Light Scattering and refractive index detector (SEC- MALS-RI instruments - Tokyo), with the kind help of Dr. Yuko Ono of the University of Tokyo.

Two peaks are visible with light scattering detectors at retention times of 25.5 min and 31 min (Figure 55). Only the peak at 31 min has reflective index signal, which means that it corresponded to the majority of xylan molecule while the peak at 25.5 min was not associated with an increase in refractive index and represented only negligible amount of xylan, probably in aggregated form.

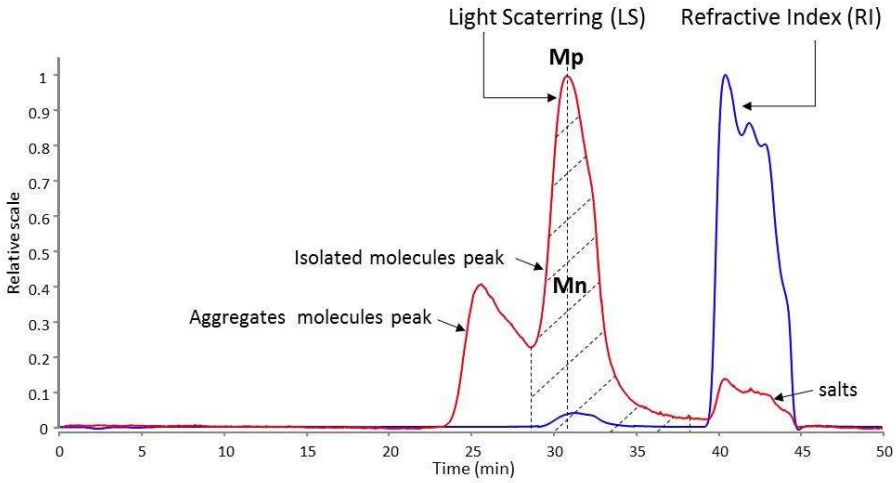

Figure 55 SEC-MALS-RI curve of xylan solution in DMAC-LiCl. Light scattering signal (red) and refractive index (blue)

The number average molecular weight (Mn) is calculated from the peak at 31 min as

$$Mn = \frac{\sum NiMi}{\sum Ni}$$

where Mi is the molecular weight of a chain and Ni is the number of chains

A series of weighted average molecular weights defined as:

$$M = \frac{\sum NiMi^{n+1}}{\sum Ni\,Mi}$$

were also calculated where: n = 1 gives Mw, n = 2 gives Mz and n = 3 gives Mz+1

The molecular weight of the highest peak (Mp) may be quoted for very narrowly distributed polymers and is fixed by the peak intensity at 31 min.

The different weighted molecular weights are listed in (Table 20):

Table 20: Xylan molecular weights

Molar mass moment	**Mn**	**Mp**	**Mw**	**Mz**	**Mz+1**
(x 10^4 g/mol)	1.058	1.133	1.089	1.117	1.143

The polydispersity index of the xylan was:

$$\frac{Mw}{Mn} = 1.03$$

The value is very closed to 1, which means it is quite monodisperse.

The molar mass of the xylan was measured at around 10 000 g/mol and corresponded to a DP of 75 which is in good agreement with DP determined by viscosimetry measurement and it was in the same range as the liquid NMR estimation.

The value of DP 75 for a xylan extracted from birch kraft samples (pulp and MFC) was also in agreement with the DP of the original xylan in the hardwood estimated between 100 and 200 (Koshijima, Timell, and Zinbo 1965, Westbye, Svanberg, and Gatenholm 2006).

Annex 1: MFC chemical composition by sugar analysis

The chemical composition of the five different types of MFC are summarized in the table below.

The composition of sugar residues (glucose, xylose, mannose, arabinose and galactose) and the yield of hydrolysis are presented in the upper table.

Then the normalized sugar content is calculated in the lower table as:

$$[Glucose\ normalized] = \frac{[Glucose]\ \times\ 100}{Yield\ of\ hydrolysis}$$

Table 21: Chemical composition by sugar analysis

	MFC from birch-kra	**MFC from spruce-kra**	**MFC from pine92-sul**	**MFC from pine96-sul**	**MFC from euc-sul**
Glucose (%)	71.7	74.7	78.5	91.6	93.8
Xylose (%)	21.0	7.8	2.1	1.4	2.3
Mannose(%)	0.9	5.8	3.0	0.9	0.9
Arabinose (%)	0.0	0.5	0.1	0.1	0.0
Galactose (%)	0.0	0.2	0.0	0.0	0.0
yield of hydrolysis (%)	93.6	89.0	83.7	94.0	97.0
Normalized					
Glucose (%)	**76.6**	**84.0**	**93.8**	**97.5**	**96.7**
Xylose (%)	**22.5**	**8.7**	**2.5**	**1.5**	**2.4**
Mannose(%)	**0.9**	**6.5**	**3.5**	**1.0**	**0.9**
Arabinose (%)	**0.0**	**0.6**	**0.1**	**0.0**	**0.0**
Galactose (%)	**0.0**	**0.2**	**0.1**	**0.0**	**0.0**

Annex 2: MFC chemical composition by sugar analysis for xylan extraction protocol optimization

The chemical composition of the MFC before and after xylan extraction are summarized in the table below.

The composition of sugar residues (glucose, xylose, mannose, arabinose and galactose) and the yield of hydrolysis are presented in the upper table.

Then the normalized sugar content is calculated in the lower table as:

$$[Glucose\ normalized] = \frac{[Glucose] \times 100}{Yield\ of\ hydrolysis}$$

Table 22: Chemical composition by sugar analysis

	Initial MFC	**MFC after xylan extraction with protocol P4**	**MFC after xylan extraction with optimized protocol P.Op**
Glucose (%)	67.2	**81.8**	78.6
Xylose (%)	**21.3**	**15.9**	**8.2**
Mannose (%)	0.9	0.1	1.4
Arabinose (%)	0.1	0	0.1
Galactose (%)	0.1	0	0.4
yield of hydrolysis (%)	89.6	97.8	88.7
Normalized			
Glucose (%)	75.0	**83.6**	88.6
Xylose (%)	**23.7**	**16.3**	**9.2**
Mannose(%)	1.0	0.1	1.6
Arabinose (%)	0.1	0	0.1
Galactose (%)	0.2	0	0.5

Annex 3: Characterization of xylan mineral impurity

Elementary analysis and ash content (Table 23) are performed on the xylan extracted by using the optimized procedure with LiCl (xylan 1) and compared with the xylan from the procedure (P4) without LiCl (xylan 2).

Chloride anion (Cl^-) and lithium cation (Li^+) content were quantified by elementary analysis in Institut des Sciences Analytiques (ISA-Lyon) to ensure that dialysis eliminates the lithium chloride salt (LiCl). Similarly, concentration of hard water cations such as, calcium (Ca^+), sodium (Na^+) and potassium (K^+) were also analyzed to confirm if they are efficiently removed by dialysis against deionized water or if part of them remained in the xylan samples as in the case for the MFC suspension.

Table 23: Elementary analysis and ash content

	Xylan extracted with LiCl (Xylan 1)	**Xylan extracted without LiCl (Xylan 2)**
Ash content*	7%	0.4%
Lithium cation (Li^+)	<20 ppm**	< 20 ppm
Chloride anion (Cl^-)	1700 ppm	1300 ppm
Calcium cation (Ca^+)	1320 ppm	1074 ppm
Sodium cation (Na^+)	210 ppm	54 ppm
Potassium cation (K^+)	209 ppm	77 ppm

*More details about ash content experiment are available bellow in part 1.
**ppm corresponds to parts per million in this table

The ash content varied from 0.4% to 7% depending on whether or not LiCl salt was used for the extraction. The residual LiCl in xylan 1 cannot explain such difference as elementary analysis shows that the two samples contain less than 20 ppm of lithium (Li^+) anion.

High content of chloride (Cl^-) anion is found in both xylan fractions regardless whether it is extracted with LiCl salt or not. The principal counter ions were calcium (Ca^+), sodium (Na^+) and potassium (K^+) cations in both xylan cases.
The chloride contamination and its counter anions: calcium (Ca^+), sodium (Na^+) and potassium (K^+) may come from hard water which were not completely removed by simple dialysis as it was the case for MFC.

Higher contamination of chlorides and counter anion is observed in xylan extracted with LiCl. It may come from the fluctuation in the hardness of tap water, and also from LiCl salt impurities as its nominal purity was 99% and added in large amount compared to xylan.
The main impurities of the LiCl salt is written to be NaCl salt and KCl salt but also metals traces, which have been noticed on Energy Dispersive X-Ray Analysis (EDXA details bellow in part 2.) on xylan ash

The relatively high ash content and variation implies that the weight yield has to be taken with care and has to be combined with sugar analysis for reliable yield estimation.

1. Ash content of extracted xylan

In order to characterize the influence of mineral impurity on the yield of xylan extraction, three different batches of xylan are analyzed by ash content: Xylan 1a and 1b have been extracted with LiCl salt (protocol P.Op.) while xylan 2 is extracted with the non-optimized protocol P4 using only DMSO.

Table 24: Determination of ash content of xylan

Sample	Initial mass of xylan (mg)	Mass of water (mg)	Dry mass content (%)	Dry mass of xylan (mg)	Mass of ash (mg)	ash content(%)
Xylan 1a	33.92	2.50	92.6	31.42	2.39	**7.6**
Xylan 1b	28.27	2.30	91.9	26.0	1.22	**4.7**
Xylan 2	226.00	28.20	87.5	197.80	0.80	**0.4**

To perform the ash analysis, the wet xylan mass (around 200 mg) was placed in the oven at 105°C for 4h to determine the dry matter content with:

$$Dry\ mass\ content = \frac{Dry\ mass\ of\ xylan}{Initial\ mass\ of\ xylan} \times 100$$

where the dry mass of xylan is correspond to:

$$Dry\ mass\ of\ xylan = Initial\ mass\ of\ xylan - mass\ of\ water$$

Then the sample was replaced in the oven from 0°C to 525°C and kept at 525°C for 4h. The mass of ash is weighted and the percentage of ash is determined with:

$$Ash\ content = \frac{Mass\ of\ ash}{Dry\ mass\ of\ xylan} \times 100$$

Because this methods is quite material consuming compare to the amount of extracted xylan, the ash content is also determine with Thermogravimetric Analysis (TGA) from Setaram-9212 without nitrogen to avoid ash modification (under atmosphere). In this case, around 30 mg of xylan was placed in the TGA basket, then the temperature was increased from 0°C to 780°C with a slop of 1°C/min. The evolution of mass was reported each 4 seconds. The mass diminution may be plotted in function of temperature:

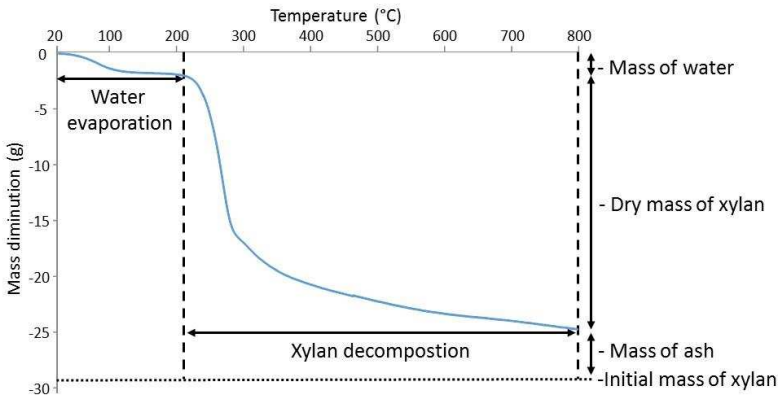

Figure 56: TGA curve example

The mass of water and the mass of ash are deduced from the curve then the dry mass of xylan and the percentage of ash were determined with the same equation than described above.

2. Energy Dispersive X-Ray Analysis of xylan ash

Ash from xylan were analyzed using energy dispersive spectroscopy detector (Silicon Drift Detector, Bruker) mounted in a Scanning Electron Microscope (JEOL 6400).

This technique allowed identifying the elemental composition of ash.

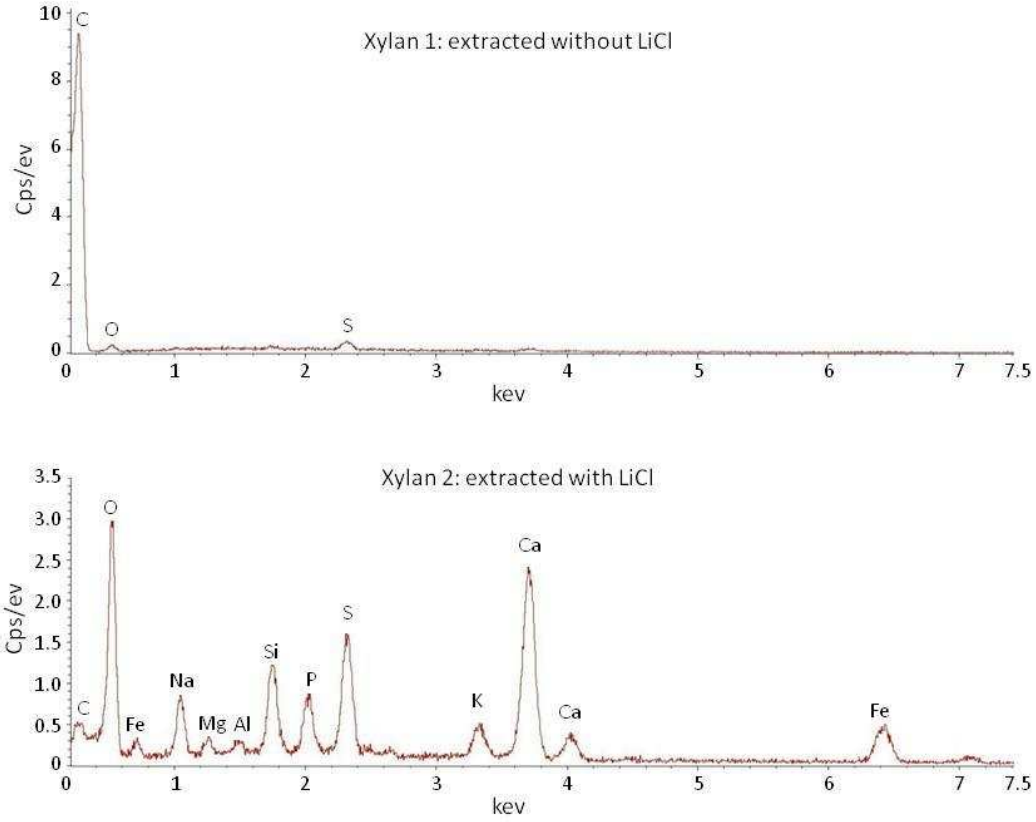

Figure 57: Energetic spectrum of the X-ray photons detected at the surface of xylan ash with xylan extracted without LiCl salt (up) and with LiCl salt (down)

Annex 4: Chemical composition of MFC before and after xylan extraction

The chemical composition of the birch kraft samples is determined by sugar analysis before (*i.*) and after xylan extraction (*ex.*).

The composition in five sugar residues (glucose, xylose, mannose, arabinose and galactose) and the yield of hydrolysis are presented in the upper table. Then the normalized sugar content is calculated in the lower table with: [Glucose normalized] = [Glucose] / (yield of hydrolysis / 100)

The yield of xylan extraction is now determined with the initial xylan content in the sample (Xy *i.*) and the xylan content after the xylan extraction (Xy *ex.*).

$$\text{Yield S. A.} = \left(1 - \frac{\text{Xy } ex.}{\text{Xy } i.} \frac{(1 - \text{Xy } i)}{(1 - \text{Xy } ex)}\right) \times 100$$

Table 25: Chemical composition by sugar analysis

	MFC from birch-kra-nd		**pulp from birch-kra-nd**		**MFC from spruce-kra**		**pulp from birch-kra**		**pulp from birch-kra-nd-nr**	
	i.	***ex.***	***i.***	***ex.***	***i.***	***ex.***	***i.***	***ex.***	***i.***	***ex.***
Glucose (%)	67.2	78.6	67.2	78.6	74.7	88.9	69.8	86.5	62.3	81.3
Xylose (%)	**21.3**	**8.2**	**21.3**	**8.2**	**7.8**	**3.1**	**24.1**	**9.6**	**21.7**	**9.4**
Mannose (%)	0.9	1.4	0.9	1.4	5.8	6.4	0.2	0.7	1.1	1.1
Arabinose (%)	0.1	0.1	0.1	0.1	0.5	0	0.1	0	0.7	0.1
Galactose (%)	0.1	0.4	0.1	0.4	0.2	0.1	0.0	0.1	0.3	0.0
yield of hydrolysis (%)	89.6	88.7	89.6	88.7	94.9	98.5	94.2	96.9	86.1	91.9

i.: initial pulp or MFC composition; *ex.*: pulp and MFC composition after xylan extraction

Normalized:

Glucose (%)	75.0	88.7	75.3	89.8	84.0	90.2	74.1	89.3	72.3	88.5
Xylose (%)	**23.7**	**9.2**	**23.4**	**9.1**	**8.7**	**3.2**	**25.5**	**9.9**	**25.2**	**10.2**
Mannose (%)	1.0	1.5	1.0	1.1	6.5	6.5	0.3	0.7	1.2	1.2
Arabinose (%)	0.1	0.1	0.1	0.0	0.6	0	0.1	0	0.9	0.1
Galactose (%)	0.2	0.5	0.2	0.0	0.2	0.1	0.0	0.1	0.4	0.0

Yield of xylan extraction (%)	**67**	**67**	**68**	**68**	**66**

Annex 5: Extracted xylan chemical composition by sugar analysis

The chemical composition of the xylan extracted from the birch kraft samples is determined by sugar analysis. The mineral impurities as well as DMSO contamination are taken in account in the mass of xylan weight to perform the sugar analysis as:

$$Mass\ of\ xylan\ S.A. = Mass\ of\ xylan - (Mass\ of\ xylan \times\ 0.07) - \ (Mass\ of xylan\ \times\ \%DMSO\ )$$

The composition in five sugar residues (glucose, xylose, mannose, arabinose and galactose) and the yield of hydrolysis are presented in the upper table.

Then the normalized sugar content is calculated in the middle table with:

$$[Glucose\ normalized] = \frac{[Glucose]\ \times\ 100}{Yield\ of\ hydrolysis}$$

Table 26: Chemical composition by sugar analysis

	Xylan extracted from						
	MFC from birch-kra-nd	**pulp from birch-kra-nd**	**pulp from birch-kra**	**pulp from birch-kra-nd-nr**	**MFC from spruce-kra**	**oat (commercial)**	**birch wood chips**
Glucose (%)	4.5	2.3	2.0	5.2	27.2	10.1	1.4
Xylose (%)	**84.0**	**88.4**	**94.8**	**82.0**	**43.6**	**59.6**	**45.2**
Mannose (%)	0.0	0.0	0.0	0.0	3.6	0.0	0.6
Arabinose (%)	0.3	0.3	0.2	0.0	4.4	7.5	2.3
Galactose (%)	0.2	0.2	0.1	0.5	0.9	0.7	5.6
Lignin (%)	/	/	/	/	/	/	30
yield of hydrolysis (%)	89.0	91.2	97.1	87.7	79.7	77.9	85.1

Normalized:

Glucose (%)	5.1	2.5	2.1	5.9	34.2	13.0	1.6
Xylose (%)	**94.4**	**97.0**	**97.6**	**93.5**	**54.7**	**76.5**	**53.1**
Mannose (%)	0.0	0.0	0.0	0.0	4.5	0.0	0.7
Arabinose (%)	0.3	0.3	0.2	0.0	5.5	9.6	2.7
Galactose (%)	0.2	0.2	0.1	0.6	1.1	0.9	6.6
Lignin (%)	/	/	/	/	/	/	35.3

Annex 6: Xylan peaks attribution on NMR liquid spectra

The proton (^{1}H) and carbon (^{13}C) chemical shifts are calibrated with the solvent deuterium peak with temperature dependence taken into account (Fulmer *et al.* 2010).

In the ^{13}C NMR analysis, an equivalent carbon atom of the sample always gives a single resonance peak, while with ^{1}H NMR analysis, the signal of each proton of the sample differs with the number of non-equivalent proton. On ^{1}H NMR spectrum, the number of peaks per signal of proton, corresponded to the number of the non-equivalent protons plus one (n+1).
A proton without a non-equivalent proton, such as a hydroxyl group, gives a single resonance peak on the ^{1}H NMR spectrum and is called a singlet (*s*). A proton with one non-equivalent proton emits a signal with two peaks and is called a doublet (*d*) and a proton with two non-equivalent protons emits a signal of three peaks and is called a triplet (*t*).

Due to the ring nature of xylose residue, it is very common to have different types of non-equivalent proton, as it can correspond to the proton bond to the next carbon but also to the proton spatially closed in the ring.

In that case of two different kind of non-equivalent proton, the signal is doubled and the peak number of each signal corresponds to the number of the respective non-equivalent proton plus one (n+1). When there is only one proton per type of non-equivalent proton, the signal emits have four peaks and is called a doublet of doublet (*dd*).

Finally, the signal may be too noisy to distinguish the number of the peak and is called a massif (*m*) when the number of the non-equivalent proton is too high, when there is too many quid of non-equivalent proton or when different proton signals are superimposed.

One of the xylose residue particularity is to have a CH_2 in position five of the ring. This two protons H5 are not equivalent in ^{1}H NMR analysis, as one is in axial position (H5 ax) and the other one in equatorial position (H5 eq).

Due to this, each proton H5 will have its own signal in ^{1}H NMR spectrum.

1. Xylan extracted from MFC from birch kra-nd

All the spectra are calibrated with DMSO-d_6 peak at 2.50 ppm for proton and 39.52 ppm for carbon.

Proton ^{1}H attribution

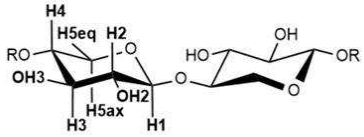

Carbon ^{13}C attribution

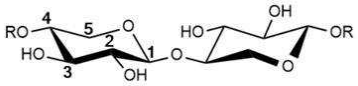

Table 27: Proton NMR analysis

Residues	Chemical shift (ppm)	Peak	Integral	Coulping constante J (Hz)	Attribution
Xy	3.11	*m*	/	/	**H2**
	3.20; 3.23; 3.25	*t*	1H	J (H5 axial -H5 equatorial) = 12 J (H5 axial -H1) = 12	**H5 axial**
	3.33	*m*	1H	/	**H3**
	3.55	*m*	1H	/	**H4**
	3.89; 3.91; 3.92; 3.94	*dd*	1H	J (H5 equatorial -H5 axial) = 12 J (H5 equatorial - H4) = 8	**H5 equatorial**
	4.31; 4.33	d	1H	J (H1 - H5 axial) = 12	**H1**
	4.64	*m*	1H	/	**OH2**
	4.79	*m*	1H	/	**OH3**

Xy : 1,4 β-D-Xylose; J = chemical shift difference x 400 Hz

Table 28: Proton, Carbon and HSQC NMR analysis

Residues	Chemical shift (ppm)	Attribution HSQC	Chemical shift (ppm)	Attribution carbon	Chemical shift (ppm)	Attribution proton
Xy	3.11 ; 72.03	**H2 ; C2**	72.34	**C2**	3.11	**H2**
	3.23 ; 62.63	**H5 ax ; C5**	62.95	**C5**	3.23	**H5 ax**
	3.32 ; 73.44	**H3 ; C3**	73.72	**C3**	3.33	**H3**
	3.55 ; 74.96	**H4 ; C4**	75.24	**C4**	3.55	**H4**
	3.91 ; 62.63	**H5 eq ; C5**	/	**/**	3.91	**H5 eq**
	4.32 ; 101.13	**H1 ; C1**	101.43	**C1**	4.31	**H1**
					4.64	**OH2**
					4.79	**OH3**

Xy : 1,4 β-D-Xylose

2. Xylan extracted from birch wood chips

All the spectra are calibrated with the D_2O peak at 4.20 ppm for proton (353K)

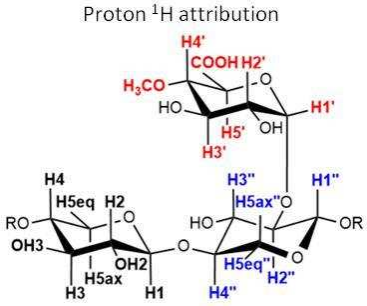

Table 29: Proton NMR analysis:

Residues	Chemical shift (ppm)	Peak	Integral	Attribution proton
Xy	3.27	*m*	/	**H2**
	3.35	*m*	/	**H5 axial**
	3.53	*m*	/	**H3**
	3.73	*m*		**H4**
	4.07	*m*	/	**H5 equatorial**
	4.42 ; 4.44	***d***	**1 H**	**H1**
Xy - 2-*O* Glc	3.27	*m*	/	**H5" axial**
	3.35	*m*	/	**H2"**
	3.59; 3.62; 3.64	*t*	/	**H3"**
	3.73	*m*		**H4"**
	4.07	*m*	/	**H5" equatorial**
	4.57 ; 4.59	***d***	**0.16 H**	**H1"**
4-*O* Glc	3.20; 3.22	*d*	/	**H4'**
	3.41	***s***	**/**	**OCH_3**
	3.53	*m*	/	**H2'**
	3.73	*m*		**H3'**
	4.25	*m*	**/**	**H5'**
	5.19	**massif**	**0.16 H**	**H1'**

Xy : 1,4 β-D-Xylose

Xy - 2-*O*-Glc : 1,4 β-D-Xylose branched in O2 with 4-*O*-methyl-glucuronic acid

4-*O* Glc: 4-*O*-methylglucuronic acid

Proton ^{1}H attribution

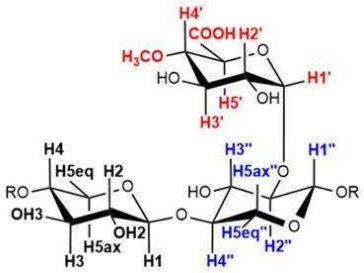

Carbon ^{13}C attribution

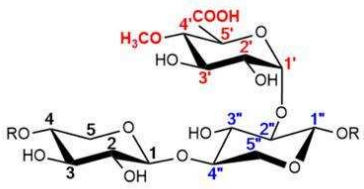

Table 30: Proton, Carbon and HSQC NMR analysis

Residues	Chemical shift (ppm)	Attribution HSQC	Chemical shift (ppm)	Attribution carbon	Chemical shift (ppm)	Attribution proton
Xy	3.28 ; 73.42	**H2 ; C2**	73.32	**C2**	3.27	**H2**
	3.36 ; 63.62	**H5 ax ; C5**	63.64	**C5**	3.35	**H5 ax**
	3.54 ; 74.40	**H3 ; C3**	74.40	**C3**	3.53	**H3**
	3.74 ; 77.08	**H4 ; C4**	77.05	**C4**	3.73	**H4**
	4.06 ; 63.64	**H5 eq; C5**	63.64	**C5**	4.07	**H5 eq**
	4.44 ; 102.28	**H1 ; C1**	**102.27**	**C1**	**4.43**	**H1**
Xy - 2-*O* Glc	3.44 ; 63.51	**H5”ax ; C5”ax**	63.45	**C5"**	3.35	**H5”ax**
	3.44 ; 77.61	**H2” ; C2”**	77.48	**C2"**	3.35	**H2”**
	3.55 ; 77.03	**H3” ; C3”**	76.86	**C3"**	3.62	**H3”**
	3.65 ; 77.22	**H4” ; C4”**	77.42	**C4"**	3.73	**H4”**
	4.12 ; 63.54	**H5”eq ; C5”**	63.45	**C5"**	4.07	**H5”eq**
	4.59 ; 101.63	**H1” ; C1”**	**101.74**	**C1"**	**4.58**	**H1”**
4-*O* Glc	3.25 ; 82.79	**H4’ ; C4’**	82.78	**C4'**	3.21	**H4'**
	3.43 ; 59.98	**OCH_3**	60.00	**OCH_3**	3.41	**OCH_3**
	3.54 ; 72.18	**H2’ ; C2’**	72.02	**C2'**	3.53	**H2’**
	3.74 ; 72.96	**H3’ ; C3’**	72.79	**C3'**	3.73	**H3’**
	4.21 ; 73.28	**H5’ ; C5’**	73.08	**C5'**	4.25	**H5’**
	5.18 ; 98.29	**H1’ ; C1’**	**98.17**	**C1'**	**5.19**	**H1’**
	/	**/**	**176.90**	**COOH**	**/**	**COOH**

Xy : 1,4 β-D-Xylose

Xy - 2-*O*-Glc : 1,4 β-D-Xylose branched in O2 with 4-*O*-methyl-glucuronic acid

4-*O* Glc: 4-*O*-methylglucuronic acid

3. Commercial xylan extracted from oat

All the spectra are calibrated with DMSO-d_6 peak at 2.50 ppm for proton and 39.52 ppm for carbon.

Proton ^{1}H attribution

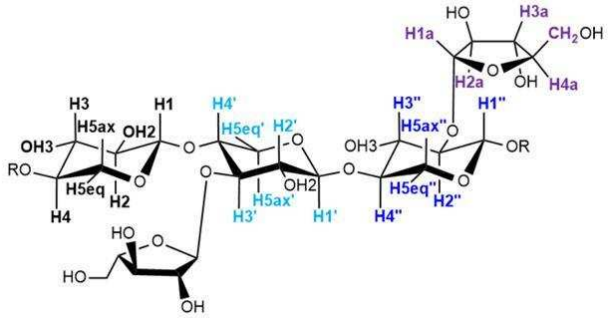

Table 31: Proton NMR analysis

Residues	Chemical shift (ppm)	Peak	Integral	Attribution proton
Xy	3.13	*m*	/	**H2**
	3.23	*m*	/	**H5 axial**
	3.32	*m*	/	**H3**
	3.55	*m*		**H4**
	3.91	*m*	/	**H5 equatorial**
	4.33 ; 4.31	***d***	**1 H**	**H1**
Xy - 2-*O* Ar	3.13	*m*	/	**H2”**
	3.23	*m*	/	**H5”ax**
	3.32	*t*	/	**H3”**
	3.62	*m*		**H4”**
	4.01	*m*	/	**H5”eq**
	4.35 ; 4.37	***d***	**H**	**H1”**
Xy - 3-*O* Ar	3.62	*m*	/	**H5'ax**
	3.04	*m*	/	**H2'**
	3.70	*m*		**H5'eq**
	3.40	*m*	**/**	**H4'**
	3.64			**H3'**
	5.13	*m*	**H**	**H1'**
Ar	**3.50**	*d*	/	**CH_2**
	3.69	*m*	/	**H3a**
	3.87	***m***		**H2a**
	4.05	*m*	**/**	**H4a**
	5.34	***m***	**H**	**H1a**

Xy : 1,4 β-D-Xylose ; **Xy - 2-*O* Ar**: 1,4 β-D-Xylose branched in O2 with arabinose;
Xy - 3-*O* Ar: 1,4 β-D-Xylose branched in O3 with arabinose**; Ar:** arabinose

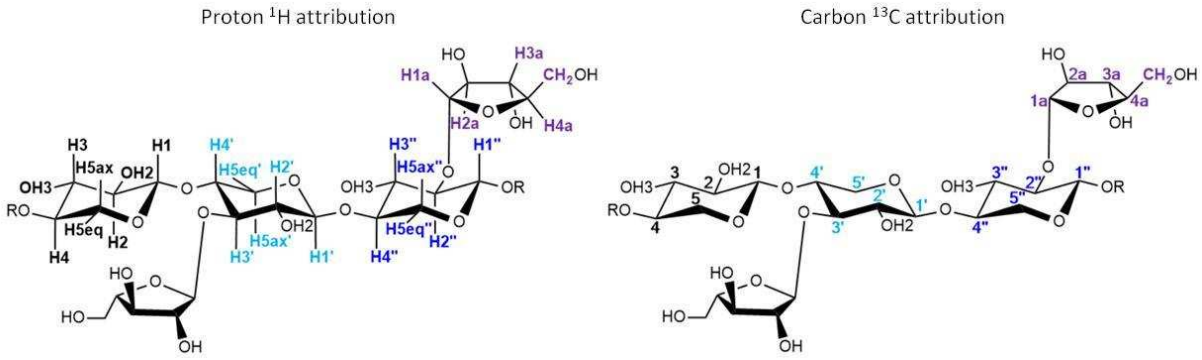

Table 32: Proton, Carbon and HSQC NMR analysis

Residues	Chemical shift (ppm)	Attribution HSQC	Chemical shift (ppm)	Attribution carbon	Chemical shift (ppm)	Attribution proton
Xy	3.13 ; 73.39	**H2 ; C2**	73.35	**C2**	3.13	**H2**
	3.24 ; 62.93	**H5 ax ; C5**	62.95	**C5**	3.23	**H5 ax**
	3.36 ; 73.72	**H3 ; C3**	73.73	**C3**	3.32	**H3**
	3.57 ; 75.26	**H4 ; C4**	75.26	**C4**	3.55	**H4**
	3.94 ; 62.95	**H5 eq; C5**	62.95	**C5**	3.91	**H5 eq**
	4.33 ; 101.42	**H1 ; C1**	**101.45**	**C1**	**4.32**	**H1**
					4.64	**OH2**
					4.79	**OH3**
Xy - 2-*O* Ar:	3.16 ; 76.11	**H2" ; C2"**	(76.30)	**C2"**	3.13	**H2"**
	3.27 ; 62.90	**H5"ax ; C5"ax**	62.72	**C5"**	3.23	**H5"ax**
	3.34 ; 75.84	**H3" ; C3"**	(76.30)	**C3"**	3.32	**H3"**
	3.63 ; 75.43	**H4" ; C4"**	75.51	**C4"**	3.62	**H4"**
	4.01 ; 62.81	**H5"eq ; C5"**	62.72	**C5"**	4.01	**H5"eq**
	4.51 ; 101.36	**H1" ; C1"**	**101.32**	**C1"**	**4.51**	**H1"**
Xy - 3-*O* Ar	3.62 ; 60.31	**H5'ax ; C5'ax**	60.35	**C5'**	3.62	**H5'ax**
	3.04 ; 72.66	**H2' ; C2'**	72.72	**C2'**	3.04	**H2'**
	3.71 ; 60.36	**H5'eq ; C5'**	(60.35)	**C5'**	3.70	**H5'eq**
	3.34 ; 73.72	**H4' ; C4'**	73.93	**C4'**	3.37	**H4'**
	3.64 ; 73.11	**H3' ; C3'**	73.13	**C3'**	3.64	**H3'**
	4.38; 101.42	**H1' ; C1'**	/	**C1'**	**4.37**	**H1'**
Ar	**3.52 ; 61.58**	**CH_2 ; C5a**	**61.61**	**C5a**	**3.50**	**CH_2**
	3.70 ; 77.57	**H3a ; C3a**	77.57	**C3a**	3.69	**H3a**
	3.88 ; 80.29	**H2a ; C2a**	80.21	**C2a**	3.87	**H2a**
	4.03 ; 85.63	**H4a ; C4a**	85.69	**C4a**	4.05	**H4a**
	5.35 ; 107.11	**H1a ; C1a**	**106.98**	**C1a**	**5.34**	**H1a**

4-*O* Glc	3.42; 60.31	**OCH_3**	/	**OCH_3**	3.40	**OCH_3**
	5.15; 99.62	**H1 ; C1**	/	**C1**	5.13	**H1**

Xy : 1,4 β-D-Xylose ; **Xy - 2-*O* Ar**: 1,4 β-D-Xylose branched in O2 with arabinose;
Xy - 3-*O* Ar: 1,4 β-D-Xylose branched in O3 with arabinose; **Ar:** arabinose

Chapter 2

Characterization of MFC dispersion in suspension and dried forms

The CTP recently carried out a study on different pulps as raw materials for MFC production and compared parameters such as the number of residual fibers and fines in the suspension as well as the physical properties of handsheets when MFC are added to unrefined fibers (Tapin-Lingua, Meyer, and Petit-Conil 2013). In this study, the hemicellulose content in the pulp was spotted as an important factor of the properties of MFC suspension and handsheets. As a general rule, the studies revealed that pulps with higher hemicelluloses content led to more homogeneous MFC suspensions with less residual coarse elements and higher strength enhancement of handsheets.

In order to have a better understanding of these different MFC potentials we sought for robust and rapid measurement to qualify the MFC suspensions that correlates well with existing methods and investigated different characterization approaches for evaluating the dispersion characteristics of the different MFC suspensions.

The first one is an optical measurement of the turbidity of MFC suspensions. It is empirically known that when cellulose is dispersed at the microfibrils level, the suspension becomes translucent/transparent (Saito and Isogai 2006), while heterogeneous suspensions appeared opaque.

However the optical properties have not been used for qualitative analysis of microfibrillated cellulose. Only recently Shimizu *et al.* (2016) demonstrated that nanocellulose width can be obtained from turbidity measurement, applying a method on fibrin gel, first by Carr and Hermans (1978) then recently developed by Ferri *et al.* (2015). In collaboration with Dr. Y. Nishiyama, we have taken advantage of this new formalism to revisit the Carr and Hermans method accounting for porosity in the case of MFC suspensions.

The second one is based on the measurements of the specific surface of aerogels of MFC obtained after freeze-drying of tert-Butyl Alcohol solvent exchanged suspensions, reported to preserve the overall shape of nanocelluloses suspensions (Fumagalli *et al.* 2013). The specific surface of the different grades of suspensions has been evaluated and compared to the results obtained by scattering techniques.

Both characteristics will be related to the performance of MFC in handsheets reinforcement and to their morphological analysis (MorFi) already studied at CTP.

1. Light scattering of fibrillar objects

In the first part, we will present the major trends that can be expected from the scattering on a heterogeneous suspension made of a dispersion of elongated objects of very different sizes and shapes.

The light scattering by a very small object compared to the wavelength of the light, λ, is inversely proportional to λ^4. A rough physical explanation can be given as the bound electron oscillation induced by the electric field of light. When the angular frequency of the light ω is much smaller than the natural frequency of the system, the oscillation amplitude is governed by polarizability and the emitting electromagnetic radiation will be proportional to ω^2 (second derivative).

This is the typical case of visible light scattered by a molecule. The intensity of the light is proportional to the square of amplitude, and since the angular frequency is corresponding to $\omega = 2\pi c/\lambda$, where c is the speed of light, we get the scattering cross-section inversely proportional to λ^4 with ω^2 (second derivative).

For fibrillar objects, the segments inside the fibrils are correlated and we need to consider the structure factor.

In the case of infinitely long thin rod, the scattering intensity becomes inversely proportional to the amplitude of scattering vector *q* which corresponds to:

$$q = 4\pi \sin(\theta/2)/\lambda \qquad (1)$$

and the scattering intensity is proportional to the weight per length.

The form factor of infinitely long cylinder in the plane perpendicular to the cylinder can be expressed as:

$$F(q) = 2\,\mathrm{J}_1(q\,R)/q\,R \qquad (2)$$

The structure factor of suspension with random orientation can be obtained by integration over all orientations

$$P(q) = \int_0^{\pi} \frac{F(q)^2}{q}\,\mathrm{d}\gamma = \frac{\mathrm{F(q)}^2\,\pi}{q} \qquad (3)$$

As the fibril diameter *R* approaches zero, *F* approaches 1 and thus *P* approaches π/q.

2. Wave-length dependence of the turbidity with the size of the objects

The turbidity, τ, is a measure of attenuation of transmitted light due to elastic light scattering coming from the heterogeneous character of the suspension. The light going through a suspension through a path length of *w*, attenuates as

$$I = I_o \exp(-\tau\, w) \qquad (4)$$

For an unpolarized beam, the scattering power as a function of scattering angle $S(\theta)$ is

$$S(\theta) = (1 + \cos^2\theta)\, KP\, c\, \mu/n \qquad (5)$$

where the term $(1 + \cos^2\theta)$ is the polarization factor, c and μ are the concentration and the mass per volume length respectively and K is the constant of Rayleigh scattering.

$$K = 2\pi^2 n^2 \left(\frac{dn}{dc}\right)^2 \lambda^{-4} \qquad (6)$$

where λ is the wavelength, n the refractive index of the medium and dn/dc the refractive index increment

The MFC suspensions contain three classes of elements (1) microfibrils aggregates that have nanometric width, (2) fines with thicknesses in the micrometer length scale, and (3) residual fibers that have diameter of the order of tens of micrometers and wall thickness in microns, i.e. much larger than the wavelength, and the turbidity would reflect the relative amount of the elements as well as their size distributions.

2.1 Very thin fibrils

For very thin fibrils with R<<λ, the fibrils radius R may be negligible and the structure factor of the suspension P *(3)* approaches π/q which after combination with the scattering vectors expression *q (1)* lead to *P*:

$$P \sim \frac{\lambda}{4\sin(\theta/2)} \qquad (7)$$

After replacing this expression of *P* in *(5),* the turbidity may be expressed as a function of K and λ by replacing *(6)* in *(5)*. In the case of very thin fibrils, the turbidity τ is proportional to $K\lambda$. As K is proportional to λ^{-4} *(6)*, the turbidity is proportional to λ^{-3} *(A).*

$$\boldsymbol{\tau = \left(\frac{88}{15}\right)\pi^2\, n\, \left(\frac{dn}{dc}\right)^2 c\lambda^{-3}\mu} \qquad \textbf{(A)}$$

2.2 Thin fibrils

When the fibril radius *R* is small but is no more negligible in the structure factor of suspension *P* equation *(3)*, the Bessel function J_1 *(2)* can be approximated as:

$$2(J_1(qR)/qR)^2 \sim 1 - (qR/2)^2$$

which leads to a second expression of the turbidity:

$$\tau = \left(\frac{88}{15}\right)\pi^3 n \left(\frac{dn}{dc}\right)^2 c\lambda^{-3}\mu\left[1 - \frac{92}{77}\pi^2 n^2 R^2 \lambda^{-2}\right] \qquad \textit{(B)}$$

In this case, the turbidity deviates at shorter wavelength from the $\propto \lambda^{-3}$ tendency towards smaller values.

2.3 Thick fibrils

For a fibril diameter much thicker than the wavelength, there is no analytical solution but Ferri *et al.* (2015) reports a numerical integration of somehow arbitrary scattering behavior at low *q* leading to:

$$\tau = 4\pi\,(8.41)\,n\,(\frac{dn}{dc})^2 c\rho R\,\lambda^{-2} \qquad \textit{(C)}$$

where ρ is the density of the particle.

Thus, depending of the dispersion state of the suspension and the relative amount of each category of different elements, referred to as fibers, fines and microfibrils, a complex behavior of the scattered light is expected. The wavelength dependency will depend on the diameter of the objects, and thus will give statistical information on the aggregation state of the dispersion.

3. MFC suspension analysis with turbidity measurements

In order to explore different aggregation situations, we measured the turbidity (Table 33) of a series of MFC selected from different wood sources, pulping process, drying history and with different hemicellulose contents (cf. Chapter 1).

Table 33: abbreviation used for MFC and pulp

MFC from	Wood species	Pulping process	Pulp drying history	Hemicellulose content
birch-kra-nd	birch	kraft	never dried pulp	24%
birch-kra	birch	kraft	dried pulp	24%
spruce-kra	spruce	kraft	dried pulp	16%
pine96-sul-nd	pine (96% of cellulose)	sulfite	never dried pulp	2.5%
pine96-sul	pine (96% of cellulose)	sulfite	dried pulp	2.5%
pine92-sul-nd	pine (92% of cellulose)	sulfite	never dried pulp	6%
pine92-sul	pine (92% of cellulose)	sulfite	dried pulp	6%
euc-sul	eucalyptus	sulfite	dried pulp	3%

For all samples, the turbidity τ monotonically decreased as a function of wavelength λ as expected from the Rayleigh scattering cross-section, but did not follow a λ^{-3} or even λ^{-2} tendency as expected from cylinder scattered of diameters small compared to their lengths (cf. paragraphs 2.2 thin fibrils and 2.3 and thick fibrils).

Thus to enhance the contrast among different samples and get rid of the overall decrease with λ, we defined a reduced turbidity λτ/c, normalized against solid content c as a function of λ in order to discriminate different behaviors and dispersions states. We do not have a descriptive dedicated model that explains the type of λ dependency we observe, but it allowed us to discriminate different types of MFC suspension in the first place. At least, we expected that the suspension containing the largest quantity of objects close to the infinite long rods approximation will have a behavior closer to λ^{-2}, whereas more aggregated samples will more or less deviate from this behavior.

Figure 58 presents the evolution of this reduced turbidity against λ for different types of wood species and pulping process.

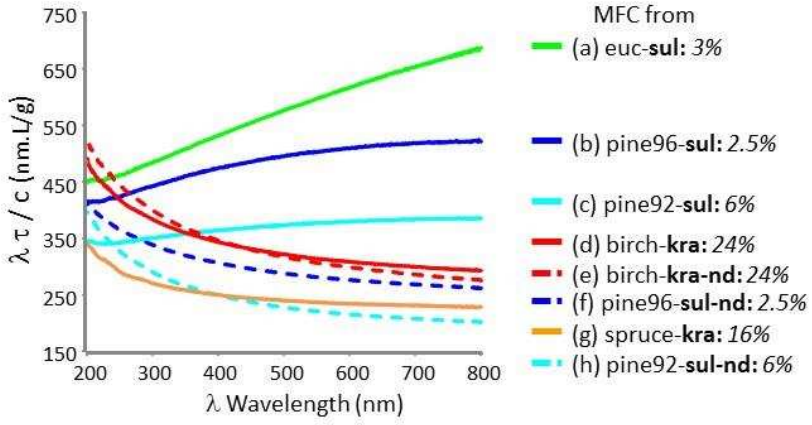

Figure 58: Reduced turbidity as a function of λ for MFC from: kraft pulps from birch (*d* and *e*), spruce (*g*), sulfite pulps from pine (*b* and *f*; and *c* and *h*) and eucalyptus (*a*).

The curves we measured can be roughly separated in two categories: (i) concave monotonically increasing curves and (ii) convex monotonically decreasing curves. All MFC suspensions from dried sulfite pulps were in the (i) type whereas MFC suspensions from kraft pulps and never dried sulfite pulps were in type (ii). Although less drastic, the effect of drying history could be seen on MFC from kraft pulps where the never-dried pulps show steeper decrease in the plot.

Thus both drying history and hemicellulose content had a strong influence on the turbidity of MFC suspension. A low hemicellulose content is enhanced the drying history impact and leads to less dispersed MFC suspensions.

These results may be compared with the ones obtained at CTP with morphological analysis where the number of fines and fibers was counted by MorFi for each MFC sources (Table 34). It's worth to note that with this optical technique, the finest elements at a submicronic size are not detected.

Table 34: Fine and fibers content according to MorFi analysis

MFC from	Fiber content (millions/g of MFC)	Fines content (x 10^2 millions/g of MFC)
birch-kra-nd	5.0	2.2
birch-kra	9.1	4.9
spruce-kra	9.4	6.2
pine96-sul-nd	4.8	5.7
pine96-sul	16.7	11.0
pine92-sul-nd	5.5	4.6
pine92-sul	11.9	11.3
euc-sul	49.5	14.3

Concerning the drying history, the number of bigger elements (fibers and fines) systematically increases when MFC are processed from dried pulp. Similarly, the sulfite process appeared to favor the presence of coarse elements compared to the kraft one and the presence of hemicelluloses seems to be in favor of a better dispersion. However, when combining both parameters, the influence of the drying history on the fibers and fines content in the MFC suspensions is stronger in the case of sulfite pulps, i.e. with low hemicellulose content. Indeed the MFC from sulfite dried pulp shows the highest number of big elements while the corresponding MFC from sulfite never dried pulp is in the same range of value than the MFC from kraft pulp.

A similar trend can be extracted from the turbidity measurements: the MFC containing the higher number of fibers and fines showed higher turbidity at longer wavelength.

4. Specific surface area and dispersion of MFC

As mentioned above, previous works have shown that the overall shape of MFC can be preserved in aerogels when freeze-drying them from tert-butyl alcohol (TBA) suspensions after solvent exchange (Fumagalli *et al.* 2013). We thus processed aerogels from MFC suspensions and compared their specific surface areas with the turbidimetry.

The specific surface area (S_{spe}) was determined by nitrogen adsorption for the MFC with different parameters: pulp drying history, solvent exchange process and hemicelluloses content (Table 35).

Table 35: Specific surface area of MFC

MFC from	Solvent exchange conditions	Specific surface area (m^2/g)	Hemicelluloses content (%)
pine96-sul-nd	TBA-harsh	**156.3**	2.5
pine96-sul	TBA-harsh	**119.4**	2.5
pine92-sul-nd	TBA-harsh	**141.8**	6
pine92-sul	TBA-harsh	**100.9**	6
pine92-sul-nd	TBA-soft	**159.6**	6
spruce-kra	TBA-harsh	**168.5**	16
birch-kra-nd	TBA-harsh	**158.0**	24

TBA-harsh: 13500 tr/min, 3 times TBA; *TBA-soft*: 2000 tr/min, 3 times EtOH, 3 times TBA

The S_{spe} of MFC aerogels seems to be correlated with the presence of hemicelluloses and drying history. It appears that the sulfite pulps from pine (i.e. the lowest hemicelluloses content) exhibited the lowest surface area when coming from dried pulps, whereas never dried pulps lead to aerogels with higher specific surface. It has to be noticed that a smoother exchange process gave an aerogel with a slightly higher specific surface, pointed out the complex interplay between the behavior in suspension and the exposed surface in the dry form (cf. Annex 7).

Although the series is not complete, it appeared also that the aerogels obtained from pulps with high hemicelluloses content resulted in the aerogels with the highest specific surface, whatever the drying history. Those results can be compared to the turbidity curves of the suspension (Figure 59).

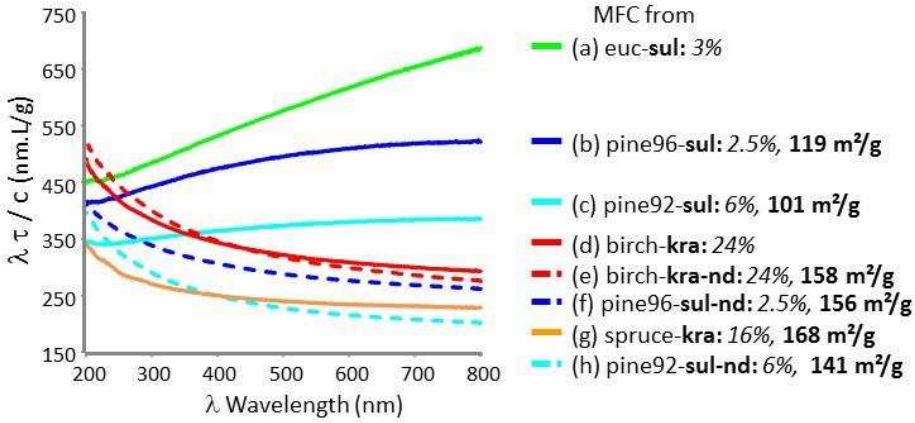

Figure 59: Reduced turbidity as a function of λ for the various MFC and corresponding specific surface area (m^2/g)

Two groups of MFC can be clearly distinguished among the different samples under study. The more opaque suspensions, such as MFC from sulfite dried pulp with a concave monotonically increasing turbidity, resulted in aerogels with specific surface around 100 to 120 m^2/g. The less turbid suspensions from kraft pulp and never-dried sulfite pulp with decreasing convex turbidity gave specific surface values of the resulting aerogels in the range of 140 to 170 m^2/g. Thus the two types of MFC suspensions, distinguishable by the turbidimetry have different specific surface area range. Both characteristics seems to be strongly related to the dispersion state of the MFC, which depends on drying history and hemicelluloses content.

5. Correlation of MFC dispersion with reinforcement capacity

As aforementioned in the introduction, a recent study at CTP pointed out the role of pulping chemistry and drying history on the mechanical properties of handsheets made of unrefined fibers supplemented with MFC suspensions as a mechanical reinforcing additive. In this study, both tear and tensile indexes were measured and correlated with the hemicelluloses content and drying history.

In the light of the preceding observations on the MFC dispersion behavior, we compared the mechanical performance with the aerogels specific surface and turbidity behavior (Table 36).

Table 36: Hemicellulose content, specific surface of aerogels of different MFC and mechanical performance of supplemented handsheets

MFC from	Hemicelluloses content (%)	Specific surface area (m^2/g)	Tear index ($mN.m^2/g$)	Tensile index (N.m/g)
pine96-sul-nd	2.5	156.3	9.2	60.8
pine96-sul	2.5	119.4	7.1	43.8
euc-sul	3	/	7.5	45.3
pine92-sul-nd	6	141.8	8.6	60.4
pine92-sul	6	100.9	8.0	52.0
spruce-kra	16	168.5	8.5	55.0
birch-kra-nd	24	158.0	/	/
birch-kra	24	/	8.7	60.9

The tear and tensile indexes of handsheets supplemented with MFC are well correlated with the specific surface measured on the aerogels. Indeed, MFC suspensions that resulted in aerogels with the highest specific surfaces (> 120 m^2/g) led to handsheets with tear index higher than 8 $mN.m^2/g$ and tensile index higher than 50 N.m/g, whereas the reverse trend was observed for the MFC suspensions with corresponding aerogels of lower specific surfaces.

As this series was incomplete for practical reasons, we proceeded to the comparison with the turbidity measurements for which the complete set of values was available (Figure 60 B). Because the difference in turbidity among different samples was most pronounced at higher wavelength, the values of the reduced turbidities at 800 nm were plotted against the tensile index of the supplemented handsheets, as an indicator of the degree of dispersion (Figure 60 A).

From the general inspection of both graphs, it appears that two groups of MFC suspensions can be clearly distinguished: the more heterogeneous suspensions with the concave shape exhibited obviously the highest reduced turbidity at 800 nm, and the poorest tensile index, whereas well dispersed suspension with the convex turbidity curves resulted in lower reduced turbidity at 800 nm and better mechanical properties.

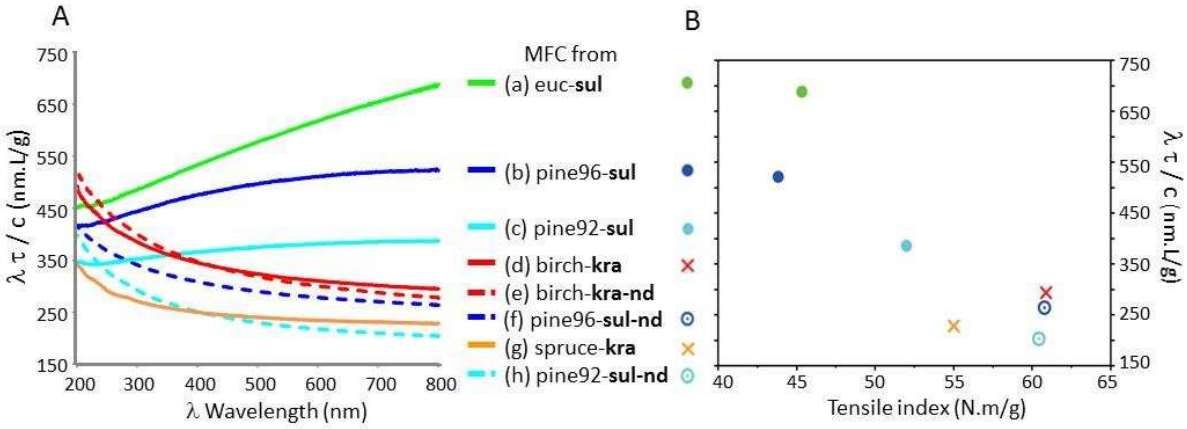

Figure 60: A: Reduced turbidity as a function of λ for the various MFC, B: Correlation between tensile index and MFC aggregation for τ at 800 nm

We propose that the key point for the reinforcing effect of the MFC suspensions is their dispersion state, which in turn depends on the hemicelluloses content and drying history. Indeed a suspension of MFC resulting from never dried sulfite pulp has the same effect on the mechanical properties as the one from dried birch kraft pulp or spruce kraft pulp and they share the same aggregation behavior as observed from the reduced turbidity curves. They also exhibit very similar surface area of the corresponding aerogel, illustrating the impact of the dispersion behavior of the suspensions on the final material properties.

Our first intuitive guess was that the nature of the surface of the cellulose microfibrils be the key parameter governing the reinforcing effect of MFC added to handsheets. However, it appears from this analysis that the mechanical properties are dominated by the dispersion state of the suspensions, for which the nature of surfaces would play a role, but not as the only factor, explaining the relative dispersion of the results.

6. Conclusion

In this chapter, we have shown that the dispersion behavior of the suspensions can be followed by turbidity measurements that accounts for the presence of elements of different sizes. Distinct behavior can be observed depending on the quality of the suspensions, particularly enhanced by the representation of the reduced turbidity ($\lambda\tau/c$) as a function of the wavelength. Concave behavior with monotonically increasing values has been observed for the more suspensions containing fibers and fines, whereas convex decreasing curves have been observed for dispersion of better quality.

These behaviors correlate well with the pulping and drying history of the initial pulps from which the microfibrils originate: hemicellulose-rich pulps and/or never dried pulps gave rise to more homogeneous suspensions whereas pulps poor in hemicelluloses that had been dried resulted in highly opaque suspensions.

The quality of the suspensions has consequences on the physical properties of materials made thereof. We showed that the aerogels made with procedures that roughly preserve their aggregation state exhibited the highest specific surface when originating from more homogenous suspensions.

Concomitantly, the complex role of the MFC as a reinforcing agent in handsheets of unrefined fibers can be rationalized with regard to their dispersion behavior. We also proposed to use the value of the reduced turbidity at 800 nm as a marker of the quality of the suspension that correlates well with the mechanical properties of the reinforced handsheets. We believe that this turbidity measure represents a robust and simple way of testing the quality of the suspensions, and hence their ability to exhibit better performance in a wide range of physical properties that requires the largest exposed surface, as in the case of the aerogels or the interaction with unrefined fibers.

Annex 7: Influence of solvent exchange by turbidimetry

The influence of the solvent exchange on the different MFC suspension in TBA was analyzed with turbidimetry. Two solvent exchange conditions were tested:

1. Harsh exchange:

Water contained in the MFC suspensions (2% solid content) was replaced with tert-butyl alcohol (TBA) by repeated centrifugation (11 200 rpm, 2 h, 25°C) and redispersion of the pellet in TBA using a double cylinder type disperser, Ultra-turrax.
After the third centrifugation, the MFC were suspended in TBA at 1.25wt% (Fumagalli *et al.* 2013) and frozen with liquid nitrogen and freeze-dried at 100 mili-torr for two days.

2. Soft exchange:

To avoid interface tension between water and TBA which might induce irreversible aggregation among cellulose fibrils, the water of the MFC suspensions (2% solid content) was replaced with ethanol (3 times) prior to TBA (3 times) and the centrifugation speed was decreased at 2000 tr/min. The rest of the procedure was identical to the harsh exchange.

When aqueous MFC suspensions were solvent exchanged into TBA using harsh centrifugation all samples showed almost constant λτ (the turbidity inversely proportional to λ) after this solvent exchange (Figure 61), while only the MFC suspensions coming from the never dried birch kraft pulp showed a behavior close to the initial features. In this situation, the low polarity of the solvent most probably promotes the flocculation of the suspensions.

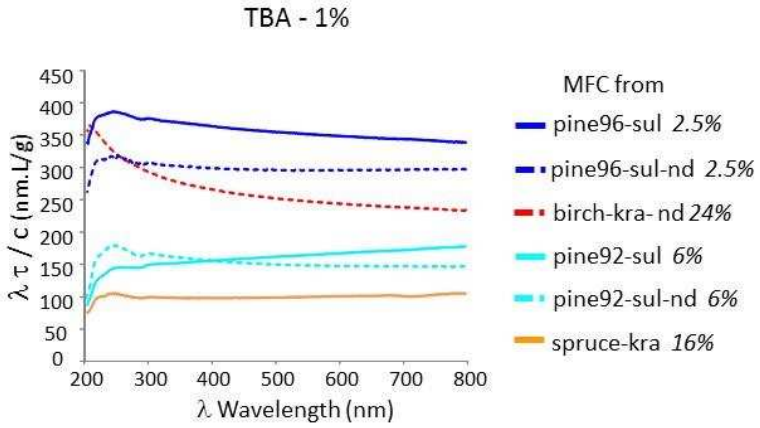

Figure 61: Reduced turbidity of TBA exchanged MFC suspensions as a function of λ.

The strong centrifugal force and/or the interface tension between water and TBA might have induced some associations among cellulose fibrils, modifying their overall structure in the suspension. The high hemicelluloses content (25%) of the MFC from birch-kra-nd seems to prevent this effect.

To reduce the centrifugal force and interface tension, we used the soft centrifugation condition (2000 tr/min - 40 times reduction in force) and added an intermediate solvent exchange with ethanol before TBA to reduce the interfacial tension.
These conditions were tested on MFC from pine92-sul-nd, which have low hemicelluloses content (6%). Figure 62 shows the reduced optical density after solvent exchange compared with the one obtained in water after reflective index correction.

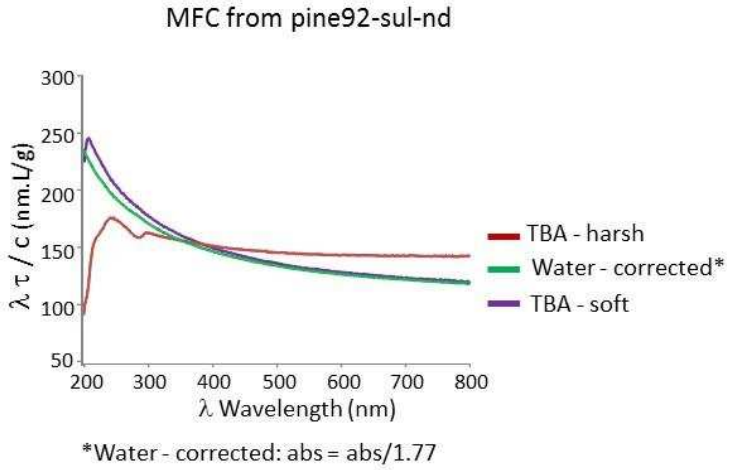

Figure 62: Influence of solvent exchange condition on the reduced turbidity of MFC from pine 92-sul-nd as a function of λ.

The correction for reflective index was considered as follows. The refractive index of TBA is 1.385, (O'Neil and Chemistry 2013), while water is 1.33 and cellulose 1.55 (Krishna, Neelakantan, and Radhakrishnan 1968). Taking the crystal density of cellulose Iβ, 1.63 g/cm^3, the theoretical dn/dc for cellulose in TBA and cellulose in water is 0.135 and 0.101 respectively. As the scattering is proportional to (dn/dc)^2, the turbidity profile should match with a scaling of 1.77 if the spatial arrangement of the suspension is identical.

This is indeed the case as shown in Figure 62, where a step-wise solvent exchange and slow centrifugation is enough to preserve the structure of the initial MFC suspensions and to prevent the flocculation of the suspensions.

Annex 8: Influence of xylan extraction

The turbidity of suspensions of birch kraft pulps and MFC with different drying history and their corresponding MFC were measured using UV-vis spectrometer, before and after xylan extraction, (cf. Chapter 1) to evaluate the influence of hemicelluloses on the suspensions' dispersion state.

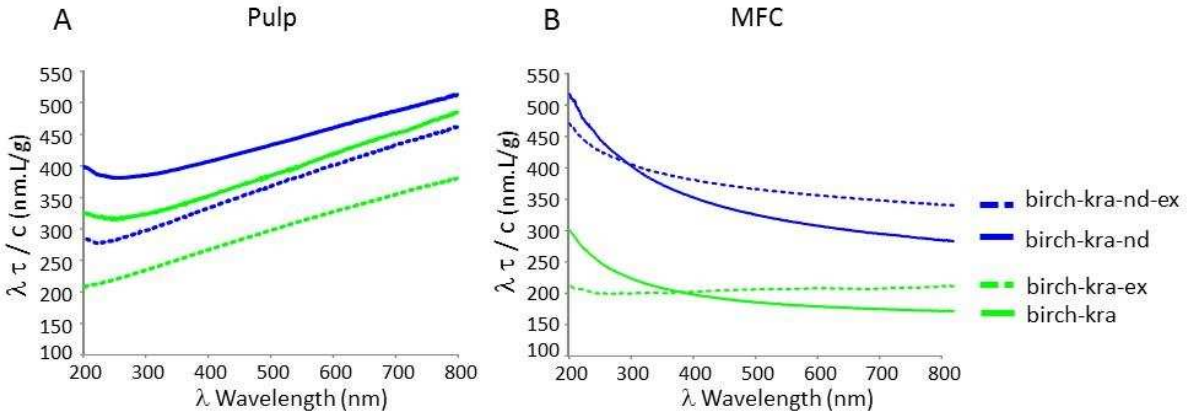

Figure 63: Reduced turbidity as a function of λ for the various samples in water showing the influence of xylan extraction on: A: pulp and B: MFC

The optical density of pulps generally decreased by the xylan extraction while the general shape of wavelength dependency was maintained, regardless of the pulp origin and drying history (Figure 63 A). The decrease can be explained by swelling leading to decrease in average of the pulp refractive index, while maintaining the overall morphology.

When xylan was extracted from MFC by DMSO, the general aspects of the turbidity curve were modified and resulted in flattened curve (Figure 63 B). This effect can happen during the centrifugation in DMSO as in the case of TBA exchange.

The corresponding specific surface area of MFC and birch kraft never dried pulp before and after xylan extraction estimated by nitrogen adsorption isotherm are presented in Table 37.

Table 37: Specific surface area before and after xylan extraction of MFC and pulp from birch kraft never dried

Sample	Solvent exchange condition	Xylan extraction	Hemicelluloses content (%)	Specific surface area (m^2/g)
pulp from birch-kra-nd	TBA-harsh	before	24	96.7
		after	9	70.2
MFC from birch-kra-nd	TBA-harsh	before	24	158.0
		after	9	134.6

TBA-harsh: 13500 tr/min, 3 times TBA; *TBA-soft*: 2000 tr/min, 3 times EtOH, 3 times TBA

The xylan extraction resulted in decrease of specific surface area of MFC and pulp. The decrease was accompanied by increase in turbidity at longer wavelength for MFC, but pulp suspension decreased in turbidity although the specific surface area decreased (Figure 64).

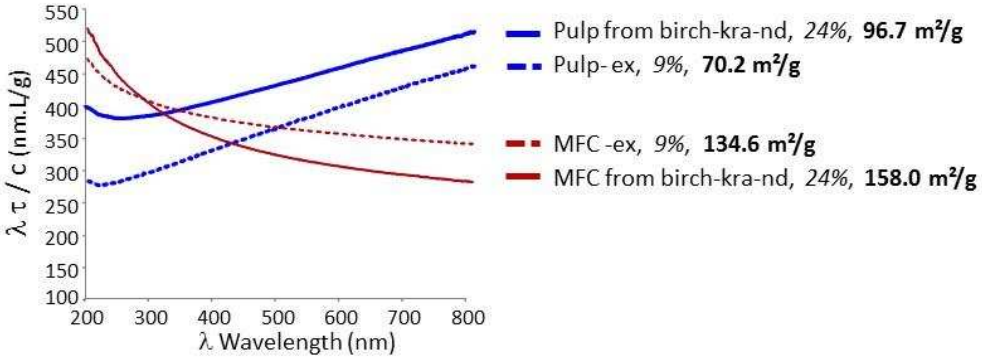

Figure 64: Reduced turbidity as a function of λ for pulps and MFC showing the correlation between water optical density and specific surface area (m^2/g) and hemicelluloses content

Chapter 3

We have previously shown that the MFC differ by their proportions of hemicelluloses. The MFC resulting from kraft pulp have the highest content of hemicellulose while that from sulfite pulp, also called dissolving pulp have the lowest.

Thanks to the extraction and characterization performed in chapter 1, it was found that the main hemicellulose of MFC from birch kraft pulp is a pure homopolymer of xylan with DP 75.
In chapter 2, we found good correlation between the mechanical properties, the turbidity and the specific surface area measurements.
Indeed, the most influent factor responsible for the decrease of the mechanical properties is the pulp drying in the case of low hemicellulose content. The MFC from sulfite dried pulp, which have the lowest hemicellulose have the lowest specific surface and lowest tear index resistance compared to the MFC from kraft pulps, which are less sensitive to the drying process.

Because hemicelluloses seem to have a strong influence on the MFC mechanical resistance to provide fibers aggregation during pulp drying, it is the topic of the next chapter.
The xylan influence on the MFC structure studied by solid state NMR then the xylan adsorption at the cellulose surface and its conformational adaptation performed by atomistic simulation is presented bellow as a publication.

Conformational Adaptation of *β*-(1→4) Xylan at the Cellulose Surface in Nature and Biomimetic Reconstruction

By

Léa Falcoz-Vigne,[1,2,3] Yu Ogawa,[1,2*] Sonia Molina-Boisseau, [1,2] Yoshiharu Nishiyama,[1,2] Valérie Meyer,[3] Michel Petit-Conil,[3] Karim Mazeau,[1,2] Laurent Heux[1,2*]

[1]*CNRS, Cermav, F-38000 Grenoble France*

[2]*Univ. Grenoble Alpes, Cermav F-38000 Grenoble France*

[3] *Centre Technique du Papier 38044, Grenoble Cedex France*

* Corresponding authors

Table of contents graphics

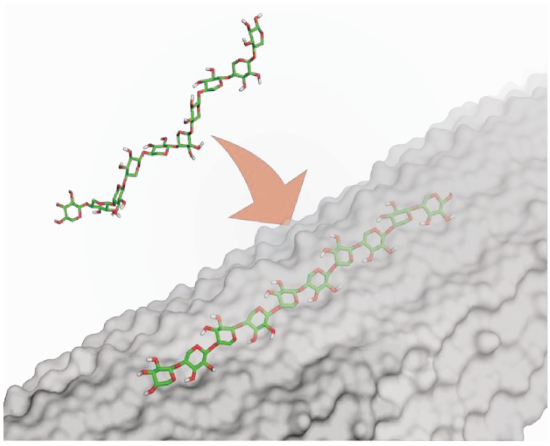

ABSTRACT

The conformational adaptation of a linear β-(1→4) xylan extracted from microfibrillated birch pulp to crystalline cellulose surfaces, was investigated using solid-state CP/MAS ^{13}C NMR spectroscopy, specific surface area measurements and atomistic molecular dynamics (MD) simulations. The NMR spectra confirmed that when in contact with cellulose, in newly formed biomimetic nanocomposites, the xylan molecules altered their conformation from the classical bulk left-handed three-fold to a different conformation, presumably a cellulose-like two-fold one. Combining these data with specific surface area measurements, this conformational adaptation was observed only when the xylan amount was limited to the first adsorbed layer in direct interaction with the cellulose surface. It is only when an excess xylan was present and after full cellulose surface coverage, that the subsequent deposited layers took the classical three-fold organization. The MD simulations confirmed that xylan in three-fold conformation had a weaker affinity for the cellulose surface than its two-fold counterpart, thus supporting the hypothesis of the two-fold conformation for xylan at the cellulose surface. When adsorbed on the hydrophobic surface of crystalline cellulose, the MD simulation showed that xylan maximized its hydrophobic interaction with cellulose by superposing its xylosyl rings on those of the glucosyl of cellulose. The MD simulations also showed that in contact with cellulose, the adsorbed xylan was mainly organized as extended molecular chain aligned parallel to the cellulose chain direction.

INTRODUCTION

In lignocellulosic plants, the cell wall is composed of two distinguishable layers, namely an external extensible thin primary wall surrounding a rigid and thick secondary wall.[1,2] The secondary wall confers mechanical strength, robustness and durability to the plant body, these properties being essentially derived from the wall structure and ultrastructure.[3] Commonly, the secondary cell wall consists of three major components: cellulose, hemicellulose, and lignin. Hemicelluloses and lignin are covalently and non-covalently linked, while cellulose and hemicelluloses are connected exclusively by non-covalent interactions.[3] With the current goal of finding new uses for plant cell walls, and in particular for wood fibers, it is important to clarify the molecular interactions existing between these wall components, not only for the fundamental understanding of the cell wall architecture and ultrastructure, but also for finding the most cost-effective way for converting them into bio-based advanced materials.

Xylan is the most abundant hemicellulose in plants.[4] This polysaccharide with a degree of polymerization (DP) in the range of 100 to 200 when extracted from hardwood chips,[5,6] is considered as being essentially linear even if short xylan branches attached to its backbone- reported at least in aspen cell wall[7]-are likely to occur in other hardwood samples. The backbone of xylan consists of poly β-(1→4) linked D-xylopyranosyl units, to which are attached a variety of side groups. In hardwood, xylan is often decorated by 4-O-methyl D-glucuronic acid residues and *O*-acetyl groups, while L-arabinosyl residues are also found as pendant groups in softwood xylan.[8,4,9] The crystalline organization of xylan hydrate in the solid state was investigated by fiber diffraction analysis of samples extracted from birch wood.[10] In these, xylan adopts a left handed 3-fold conformation with a periodicity of 1.48 nm. Such a 3-fold helical conformation is also found in the stacking of xylopentaose in the binding cleft of a xylan carbohydrate-binding module (CBM) from *Pseudomonas cellulosa*.[11] Even if the 3-fold helical structure of xylan is well comforted by computational studies,[12,13] several X-ray and electron diffraction diagrams of xylan cannot be resolved with the unit cell and symmetry deduced from the established crystal structure of birch xylan hydrate.[14,15] These different patterns, which have not been fully explained, indicate that other crystalline allomorphs, with probable conformations different from that of the 3-fold one are likely to exist for xylan.

Xylan is renowned to have a strong affinity for cellulose[16-18] and its co-alignment with cellulose has been indicated by polarized infrared spectroscopy.[19,20] The adsorption of xylan on cellulose, which is quite important for the pulp and paper process,[21] can be related to the similarity existing between the chemical structures of these two molecules. It is also this strong adsorption, which is believed to act as the limiting factor in the enzymatic hydrolysis of cellulose.[22] Despite this affinity, the difference between the dominant molecular conformations of xylan into 3-fold helix [10] and that of cellulose in 2-fold helix [23] in the bulk states, likely implies a structural conformational adaptation of xylan to form strong interaction with cellulose. Such possible conformational adaptation has been proposed in several reports. In solid-state ^{13}C NMR studies by Larsson et al. [24] and Teleman et al., [25] it was shown that a specific resonance at 81.7 ppm could be assigned to birch xylan in contact with cellulose, thus suggesting a different conformation for the adsorbed xylan.

In their molecular dynamics (MD) investigation of the adsorption behavior of xylan molecules on the hydrophilic surface of cellulose, Mazeau and Charlier [26] found preferential molecular orientation of a xylopentaose along the cellulose chains at the (110) hydrophilic surface of crystalline cellulose, with possibilities for 2-fold and 3-fold conformations. Busse-Wicher et al. [27] suggested a 2-fold helical conformation of xylan molecules decorated by acetyl and glucuronic acid groups, as a stable structure on both hydrophilic and hydrophobic cellulose surfaces, based on biochemical analysis and molecular dynamics simulations.

As mentioned in these reports a conformational adaptation of xylan molecules to crystalline cellulose surfaces appears feasible, but is not clear whether this adaptation is solely due to physico-chemical interaction or to the biosynthetic mechanisms, including for instance xylan decoration and/or co-crystallization with cellulose during the hemicellulose secretion. In the present study, a solid-state ^{13}C nuclear magnetic resonance (NMR) study on mixtures of un-decorated xylan and cellulose was undertaken to investigate the conformational adaptation of the xylan molecules at the cellulose surface. With this spectroscopic study, the main idea was to mimic by physico-chemical means the interaction of xylan at the cellulose surface and hence propose a biomimetic reconstructed model. By sequential re-depositions coupled with specific surface area measurements, it was possible to see whether this adaption was only limited to the first adsorbed layer or also to the next ones. We have constructed a MD model system based on un-decorated xylan molecule and modelled its interaction with the hydrophilic and hydrophobic surfaces of crystalline cellulose. This allowed us to follow the conformational modifications of the xylan backbone, when adsorbed on cellulose.

EXPERIMENTAL SECTION

Materials

In this study, two types of pulp were used: a bleached never-dried birch kraft pulp, provided by UPM and a dried bleached pine sulfite dissolving pulp from Tembec. These samples were subjected to a mechano-enzymatic treatment, adapted at the Centre Technique du Papier, from the method described by Pääkkö et al. [28] In short, the pulp samples were refined at a 4.5% consistency with a 12" single disk refiner for 25 min for the pine pulp and 45 min for the birch pulp after being incubated for 1h at 50°C with a solution of endoglucanase FiberCare R® from Novozyme, buffered at pH 5.0. The digested samples were further refined with the disk refiner to obtain a pulp suspension of Shopper Riegler (SR) drainability number (ISO 5267-1) greater than 80 and mean fiber length lower than 300 μm when analyzed with an optical MorFi camera, considering as fiber each element longer than 80 μm. The fiber suspensions were then diluted to a 2% concentration and processed with an Ariete homogenizer. This treatment involved one pass at 1000 bar followed by 3 passes at 1500 bar. The resulting suspensions of microfibrillated cellulose (MFC) were solvent exchanged to *t*-BuOH (TBA) by successive centrifugations/ re-dispersions. At the end of the third centrifugation, the MFC were suspended into TBA at a 1.25% concentration and freeze-dried at 100 mil-torr for 2 days.

For the extraction of xylan from the birch kraft pulp, the freeze-dried MFC samples were dispersed, at a 1% concentration, into a solution of 5% LiCl/DMSO and, stirred at room temperature for 20 h. The MFC and dissolved xylan were then separated by ultracentrifugation at 20 000 g for 15 h at 25°C.

The supernatant xylan and the MFC pellet were recovered separately and subjected to a 7 day dialysis against water using a dialysis membrane with a cutoff of 12 000 Da, to remove LiCl and DMSO from the specimens. The xylan in the form of a precipitate was concentrated with a rotary evaporator (Rotavapor, Büchi), freeze-dried and kept over P_2O_5 until further use. The MFC pellet was kept under wet state at the end of the dialysis. From sugar analysis coupled with liquid ^{13}C NMR data, the extracted xylan consisted essentially of xylosyl residues and was devoid of (i) OAc moieties, (ii) arabinosyl and (iii) glucuronic acid substituents.

From the sugar composition (Tables 1 and 2, Supporting Information) it was found that the MFC pellet from birch kraft pulp still contained 9.2% xylan after extraction, down from 24% before extraction. Thus a substantial amount of xylan, likely strongly bound in between the fasciated microfibrils remained unaccessible in this extraction. The MFC from Tembec dissolving pulp initially contained less than 2.5% xylan.

Re-adsorption of Xylan on Extracted MFC

The experiments involved the re-adsorption of xylan on either the MFC from birch kraft pulp after xylan extraction or the MFC from Tembec pulp. Both MFC samples were re-dispersed into DMSO at a concentration of 5 g/L. Various quantities of freeze-dried xylan were then added to the suspensions, which were kept under stirring for 20 h at room temperature. These samples were dialyzed for 7 days followed by concentration with a rotatory evaporator (Rotavapor Büchi) and freeze dried until further use. Each sample was analyzed by solid-state ^{13}C NMR spectroscopy to determine the amount of adsorbed xylan.

Solid-state ^{13}C NMR Spectroscopy

All the solid-state ^{13}C NMR spectra were recorded on wet samples: the initial MFC samples in suspension were concentrated by centrifugation and the water in excess in the pellet was wicked away with a filter paper. The freeze-dried MFC specimens with xylan re-adsorbed were rehydrated with water and the water in excess was wicked away. Wet samples of the extracted xylan were prepared by rehydrating the freeze-dried samples at 97% relative humidity in a desiccator containing saturated potassium sulfate aqueous solution.

All ^{13}C solid-state NMR spectra were recorded with a Bruker Avance II spectrometer (^{13}C frequency of 100 MHz), using the combination of magic angle spinning (MAS) and cross-polarization (CP). For this, the spinning speed was set at 12 kHz, the sweep width at 29761 Hz, the recycle delay at 2 s and the cross-polarization contact at 2 ms. The MFC spectra were averaged over 24 k, whereas the pure xylan spectra were averaged over 2 k scans. The ^{13}C chemical shifts were calibrated with the glycine carboxyl group at 176.03 ppm.

Specific Surface Area

The specific surface areas of freeze-dried MFC samples from birch pulp (before and after xylan extraction) and the original Tembec pine pulp were measured using adsorption-desorption isotherms of nitrogen. For this, 0.07–0.15 g of freeze-dried samples were analyzed, using a Surface Area and Pore Analyzer Nova 1200e from Quantachrome instruments. The samples were first degassed at 105°C for 15 h and the adsorption-desorption isotherms were measured at 77 K in the pressure range of 0.01-0.3 bar. The specific surface areas were calculated using the BET equation as described elsewhere.[29, 30]

Molecular Dynamics (MD) Simulation

MD simulations were achieved with GROMACS tools. The molecular structures were visualized using the VMD and PyMOL softwares. In this MD work, we used the GROMACS 5.0 package[31] using the Gromos $56A_{carbo}$ force field[32] with a modified Lennard-Jones repulsive parameter for the CH1 atom type.[33] In the simulations, the motion equations were solved by a standard leapfrog algorithm with integration step of 1 fs. The length of covalent bonds involving hydrogen atom was constrained by using the LINCS algorithm.[34] All the equilibration and production runs were achieved in the NPT (constant number of particles, pressure, and temperature) ensemble. The velocity-rescaling algorithm[35] was used for temperature control with a coupling time of 0.1 ps. The pressure was regulated to 1 bar using a Berendsen pressure coupling algorithm[36] with a pressure coupling constant of 2.0 ps. The pressure regulation was done semi-isotropically: it was regulated isotropically in lateral (x-y) dimensions, but independently along the longitudinal chain (z) direction, with compressibility of 2.5×10^{-5} and 7.9×10^{-7} bar^{-1}, respectively. The long-range interactions were calculated by using the particle-mesh Ewald summation method[37] with a cut-off distance of 0.9 nm and the long-range dispersion force was corrected for both energy and pressure.

The cellulose model in this study was derived from the experimental structure of cellulose Iβ.[23] Only the dominant hydrogen bond network, namely pattern A, was considered. A cellulose model was constructed with 24 molecular chains having a degree of polymerization (DP) of 12. The chosen model had an approximate hexagonal cross section with exposed hydrophilic (110) and (1-10) surfaces, together with the hydrophobic (100) one (see Fig. S1, Supporting Information). This model, which was selected to study the adsorption behavior of xylan on different cellulose surfaces, may be different from reality since the cross sectional shape of the wood cellulose microfibril is still under debate. Each molecular chain was covalently bonded to its periodic images at its both ends to mimic the infinite length of the molecular chain along the fiber direction. This semi-infinite cellulose model was solvated with SPC water,[36] followed by energy minimization calculation using conjugate gradient algorithm with the convergence criterion for force of 1.0 kJ/mol/nm. The energy-minimized (EM) system was equilibrated by MD for 20 ns at 300 K.

The force field parameters for the β-xylosyl residue are not available in the native Gromos $56A_{carbo}$ force field data bank. Thus, the residue was constructed by removing the hydroxymethyl group from the β-glucosyl unit, transforming the C_5H_2 group into a regular CH_2 moiety. A linear xylan molecule, having 10 β-xylosyl residues (Fig. S1), was solvated in a SPC water box. The hydrated system was energy-minimized and then equilibrated for 10 ns at 300K. The equilibrated xylan molecules took an approximate 3-fold conformation as described below. To simulate the 2-fold helical conformation of the xylan molecule, the two dihedral angles at the glycosidic linkage, ϕ (O5-C1-O1-C4) and ψ (C1-O1-C4-C5) were subjected to harmonic restraints with a force constant of 200 kJ/mol/nm and target values of 90° and 140° for the ϕ and ψ angles, respectively. The molecules were then equilibrated under the dihedral restraints in a SPC water box for 10 ns at 300 K.

The adsorption simulation of the xylan molecule on the cellulose surface was performed using these equilibrated cellulose and xylan models. In this study, we investigated the adsorption behavior of xylan under the influence of (i) different molecular conformations of xylan (System 1), (ii) different cellulose surfaces (System 2), and (iii) different initial orientations of the xylan chain with respect to the cellulose chain direction (System 3).

In all these systems, the simulation box size was approximately 7 × 7 × 6.3 nm^3 and periodic boundary conditions were applied to x, y, and z directions. The resulting semi-infinite cellulose crystal was positioned at the center of the box and the xylan chain was inserted at the position approximately 1 nm away from the cellulose surface of interest. The system was then solvated with SPC water molecules and equilibrated at 300 K for 10 ns, unless otherwise specified.

In System 1 and 2, the xylan molecule was oriented with its chain direction parallel to the longitudinal direction of cellulose. In System 1, the xylan chains with 3_2 and 2_1 conformations were subjected to the adsorption simulation. For the chain in the 2_1 conformation, the initial adsorption was performed with the dihedral constraints for 10 ns. Then the further 10 ns simulation was performed without the constraints at 300 K. In System 2, the xylan chain in the 2_1 conformation was positioned close to the three different surfaces, (100), (110) and (1-10). Then the energy minimization calculation and equilibration simulation with the dihedral constraints were performed as aforementioned. After the adsorption, a 10 ns production run was achieved without the constraints. In System 3, the xylan chain was positioned closed to the (100) cellulose surface with different angles between the xylan and the cellulose chains. Then, the energy minimization and MD simulations were performed with the dihedral constraints for 10 ns, followed by the unconstrained 10 ns production simulation. In terms of interaction energy of the adsorbed state, Coulomb and Lennard-Jones (or electrostatic) values were considered. They were calculated by summing up the corresponding non-bonded interaction energies between the constituting atoms of the molecules in the system.

RESULTS AND DISCUSSION

1. Solid-state ^{13}C NMR Spectral Analysis of Xylan onto Cellulose Surface.

1.1 Conformational Diversity of Xylan

Figure 1 shows the ^{13}C solid-state NMR spectra of the wet extracted xylan (Fig 1A), and MFC samples from birch kraft pulp before (Fig. 1B) and after (Fig. 1C) xylan extraction. For comparison, the spectra of the samples in Figures 1B and 1C were normalized with respect to one another, by equalizing their integral intensities in the range 55 to 115 ppm. The spectrum of xylan (Figure 1A) was normalized with its integral intensity being 13.5% of that of each MFC sample, this percentage corresponding to the amount of xylan extracted (see below).

The spectra of both MFC samples (Figure 1B and 1C) show similar spectral features: well separated C1 peak of cellulose at 106 ppm together with overlapped peaks between 68 and 80 ppm originating from the C2, C3, and C5 of cellulose. Clear differences before and after the extraction are found in the C4 (80-92 ppm) and C6 regions (57-68 ppm) of cellulose, with a relative intensity decrease at 64, and 82 ppm, and a slight increase at 84.2 ppm upon xylan extraction.

Similar spectral modification of wood cellulose upon hemicellulose removal using alkaline solution has been reported by Teleman et al.[25], who suggested that the signal at 82 ppm could be assigned to the C4 of xylan in interaction with the cellulose surface. On the other hand the resonance at 84.2 ppm presumably corresponds to the C4 of the accessible cellulose surface.[24] It is thus logical to observe its increase when some cellulose surface is liberated by the departure of xylan.

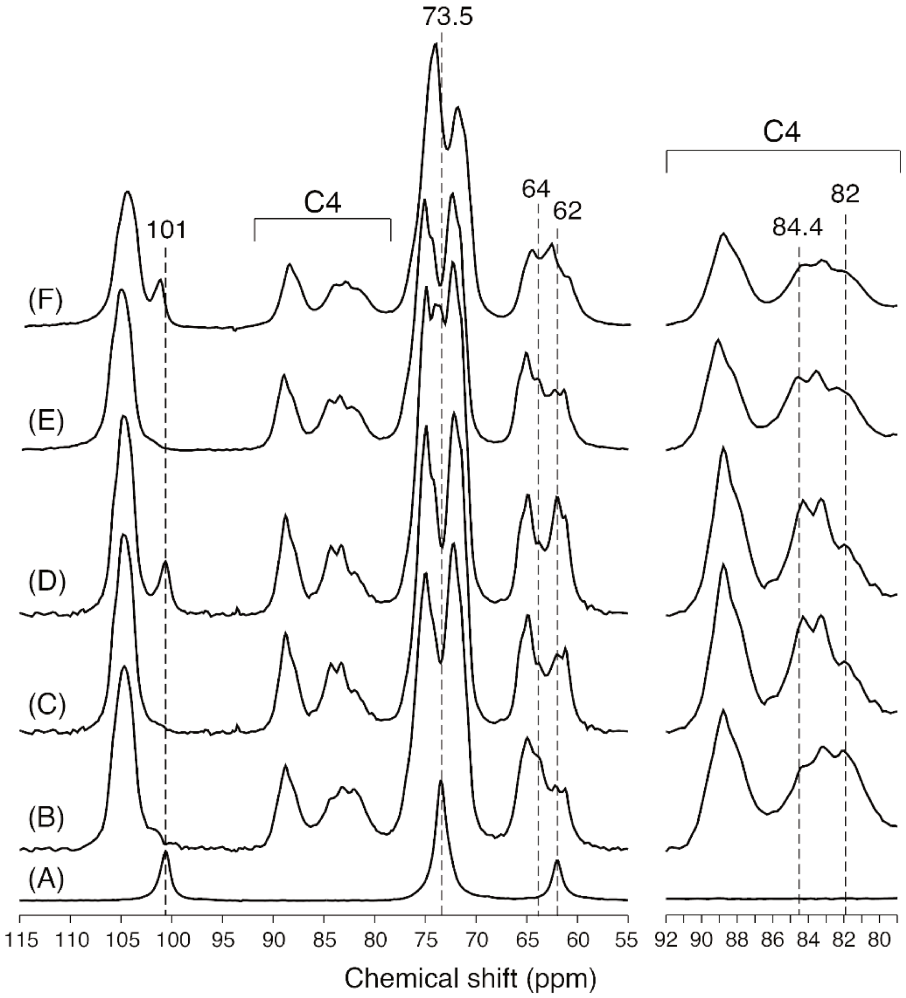

Figure 1. CP/MAS ^{13}CNMR spectra of wet samples: (A) extracted xylan hydrated at 97% relative humidity; (B) MFC from birch kraft pulp before extraction of xylan; (C) as in (B) but after xylan extraction; (D) linear combination of (A) and (C); (E) as in (C) but after re-adsorption of xylan, with xylan/cellulose ratio of 0.28/1. (F) as in (C), but after re-adsorption of of xylan with xylan/cellulose ratio of 0.39/1. Enlargements of the C4 region are presented in the right column.

The spectrum of the extracted bulk xylan (Fig. 1**A**) is typical of that of the hydrated crystalline β-1,4 xylan.[25] Three sharp signals occur at 63, 73.5, and 101 ppm: they are respectively assigned to C5, an overlapped contribution of C2-C3-C4, and C1. Although the molecular structure of xylan is very similar to that of cellulose except for the hydroxymethyl C6 group, its chemical shifts at C1 and C4 are very different from those of cellulose and therefore point to a molecular environment different from that of cellulose at the glycosidic linkage.

Based on the sugar analysis (see Tables S1 and S2, Supporting Information), the MFC from birch kraft pulp contained 24% of xylose and 75% of glucose (w/w) before the extraction and 9% of xylose and 89% of glucose after the extraction. The xylan ratios normalized to the cellulose mass is of 0.31(w/w) before extraction and 0.1 after extraction, this last part being considered as inaccessible xylan. Thus, 68% of the xylosyl residues -*i.e*. more than two third- in the initial MFC sample (1B) was removed as extractible xylan fraction by the DMSO/LiCl treatment. The carbon molar fraction of the removed xylan was therefore 13.5 % of the whole carbon content of the initial MFC. Assuming that the contribution of each component to the signal intensity is proportional to its respective number of carbon atoms and if the mixture of xylan and cellulose did not alter the samples conformation, the NMR spectrum of the mixture should be expressed by a linear combination of the two reference spectra. For a carbon molar fraction of xylan, α in the binary system, the expected signal intensity of the binary system I_{bin} should be:

$$I_{bin} = (1 - \alpha)I_{cel} + \alpha I_{xyl}$$

where I_{cel} and I_{xyl} are signal intensities of cellulose and xylan, respectively.

Thus the spectrum before extraction (1B) should be a linear combination of the spectra of the MFC after extraction (1C) and of xylan (1A). This linear combination is given in Figure 1D, taking the normalized intensity as 0.865×1C, accounting for the respective amount of cellulose and xylan. In comparing the spectrum 1D with the one in 1B, a clear increase of the intensity is observed at 62, 73.5, and 101 ppm, corresponding to the added xylan. Such difference is not observed when comparing the MFC spectra before (1B) and after (1C) xylan extraction, which thus clearly confirms that when adsorbed on cellulose, xylan adopts a conformation different from the one it has in its bulk state.

1.2 Conformational Adaptation of Xylan upon Re-adsorption on MFC

In order to further investigate the conformational change of xylan in the presence of cellulose, we have rebuilt xylan-cellulose complexes by re-adsorption of xylan to the MFC samples where xylan had been initially extracted. In order to do so, the accessible xylan chains were first solubilized in DMSO and then allowed to interact with cellulose surfaces by slowly exchanging DMSO by dialysis against water and thus allowing a conformational freedom. Two different amounts of xylan were used for the re-adsorption experiments (see Table S3 in the Supporting Information). The first complex was constructed to yield an amount of xylan close to what it was in the initial MFCs: a xylan/cellulose mass ratio of 0.28 (22% of total weight). In a second complex, more xylan was added to increase this ratio to 0.39 (28% of total weight). Thus, this second complex contained an excess of xylan/cellulose in mass ratio of 0.11, compared to what it was in the initial MFCs.

The spectrum of the first complex (Fig. 1E) was almost identical to the one of MFC before the extraction (Fig. 1B). The signal intensity increased at 64 and 82 ppm, and no trace of bulk xylan was present in the spectrum unlike in the case of the artificial linear combination of the spectra of the xylan and MFC (Fig. 1D). In Figure 1E, the C1 signal of xylan at 101 ppm is absent upon the adsorption, presumably due to its downfield shift, with the consequence of its merging with the C1 signal of cellulose at 106 ppm. The increase of the signal at 82 ppm is explained as a downfield shift of C4 of the xylan from 73 ppm, as the signal is assigned to the C4 of xylan in interaction with the cellulose surface.[24,25]

These downfield shifts of C1 and C4 signals of the xylan are indicative of a conformational departure from the classical three-fold helical structure observed in the bulk xylan, presumably to adopt a cellulose-like two-fold helical structure. In this respect, our results are in line with to those of Larsson et al [24] who have mixed xylan from bleached birch kraft pulp with disintegrated cotton linters in the presence of water for 48 h at 90°. Despite the dissimilarity between their experimental protocol and ours, the onset of the signal at 82 ppm in their case and its increase in our re-adsorption experiment point toward the same behavior of the adaptation of xylan at fresh cellulose surface.

In the spectrum of the second complex, with the xylan/cellulose ratio of 0.39 (Fig. 1F), an additional signal becomes visible at 101 ppm, and the intensity increased at near 62 ppm. Since the chemical shifts of these signals are very similar to those of the bulk hydrate xylan, the additional intensities likely originate from an excess of xylan in an environment typical of bulk xylan. The amount of this excess xylan in spectrum 1F could be determined by a peak deconvolution of the C1 region (110-95 ppm) using a Gaussian function. The peak at 106 ppm contains the signals of both cellulose and xylan directly adsorbed on cellulose. The ratio between the integral areas of the peaks at 106 and 101 ppm is estimated at 1: 0.13. Thus, the relation between the molar mass of cellulose (m_{cell}), xylan in bulk conformation (m_{bulk}) and xylan in interfacial conformation (m_{inter}) is given as:

$$(m_{cell+}\ m_{inter}) / m_{bulk} = 1/0.13$$

The molar ratio of cellulose and xylan is deduced from their weight ratio 1:0.39 as

$$m_{cell} / (m_{bulk+}\ m_{inter}) = 1/0.39 \times W_{xyl}/W_{cell}$$

Where W_{xyl} and W_{cell} correspond to the molecular weight of xylosyl (132) and glucosyl (162) residues. With respect to cellulose, m_{bulk} and m_{inter} are estimated at 0.17 and 0.31 respectively, which correspond to 0.14 and 0.25 weight of xylan per weight of cellulose (see Table S3 in the Supporting Information).

The conformational adaptation of xylan in the re-adsorption experiments clearly indicates that this specific feature is due to the physical affinity of xylan for cellulose and this is what it likely occurs during the biogenesis of the wood secondary cell wall. The ratio of the bulk state xylan to cellulose: 0.13, calculated from the NMR spectrum is very close to the ratio of excess xylan: 0.11 that was added in the second complex. Since in this experiment, only 66% of xylan was able to conform to cellulose, one can surmise that only the first layer of xylan in contact with cellulose is able to do so, this amount of xylan being enough to saturate the accessible cellulose surface. Following this hypothesis, the remaining 34% will not have any access to the saturated cellulose surface and thus will conform into the classical 3-fold conformation observed in the bulk xylan.

The re-adsorption experiment was also performed with the MFC from pine sulfite pulp as shown in Figure S2 in the Supportding Information. The adsorbed xylan on the MFC from pine sulfite pulp showed a similar conformational change, but only 9% xylan appeared sufficient to saturate the MFC surface.

2. Estimation of the Surface Area of MFC Samples Accessible to Xylan.

In order to quantitatively evaluate the cellulose surface available for xylan interaction, we measured the specific surface area of the DMSO extracted birch kraft and pine sulfite pulps by nitrogen adsorption measurements, using the BET method. The specific surfaces area (S_{spe}) of the freeze-dried MFC samples are given in Table 1. Whereas the MFC from birch pulp presents a S_{spe} value of 158 m^2/g, the MFC from pine pulp has only 119 m^2/g, i.e. a value 30% lower. From these data, an estimation of the maximum coverage of the cellulose surface by a typical xylan monolayer can be calculated attributing a surface of 0.25 nm^2 to each xylosyl residue, as evaluated by MD simulation.[26] This maximum Xyl_m expressed in gram of xylan per gram of cellulose can be deduced from the equation:

$$Xyl_m = 10^{18} (S_{spe} / 0.25) \times (m_{xyl}/N_A)$$

where m_{xyl} (132) is the weight of a xylosyl residue and N_A is the Avogadro's number.

Table1. Xylan amount adsorbable as a monolayer on cellulose, deduced from (i) the specific surface area of the MFC samples after xylan extraction (ii) the percentage xylan in the interfacial conformation, deduced from ^{13}C NMR data following the re-adsorption experiments.

MFC	S_{spe} (m^2/g)	g xylan/g cellulose in a monolayer	g xylan adopting the interfacial conformation/g cellulose in the re-adsorption experiment
Birch pulp	158	0.14	0.15
Pine pulp	119	0.10	0.09

From this equation, we see that a full covering of the MFC from birch pulp by a xylan monolayer will be obtained with 0.14 g xylan per g of cellulose, as opposed to 0.10 for the MFC from pine pulp. Quite remarkably, these values are very close to those deduced from the ^{13}C NMR data about the percentage of xylan, getting organized into the specific interfacial conformation during the re-adsorption experiment: 0.15 g xylan per g cellulose from birch pulp MFCs and 0.09 g xylan per g cellulose for the pine pulp counterpart. The amount of xylan in the interfacial conformation was calculated by omitting the amount of inaccessible xylan that was permanently adsorbed on inaccessible cellulose surface, which therefore was not detected by the specific surface measurements. This concordance strongly substantiates the above hypothesis stating that it was only the first layer of xylan adsorbed at the cellulose surface, which could be converted into this specific interfacial conformation. In the re-adsorption experiment, this is obtained by replenishing the free cellulose surface created by the removal of the accessible xylan from the initial MFCs during the DMSO/LiCl extraction step. When the full cellulose surface is replenished, adsorbed xylan in excess is not influenced any more by this surface and thus is free to adopt the classical 3-fold conformation of the bulk state identified by its specific solid-state ^{13}C NMR signature.

3. Molecular Dynamics (MD) Simulation of Adsorption of Xylan on Cellulose

In order to characterize the interactions of xylan and cellulose at the molecular level, in terms of conformation and interaction energy, we have performed MD simulation to recreate the situation of a xylan chain interacting with surfaces of a cellulose crystal. In the simulation, we have first considered the behavior of a xylan molecule in water, but without cellulose and then in the presence of crystalline cellulose.

3.1 Molecular Conformation of Xylan in Water without Cellulose

The simulated conformation of a xylan molecule in water, defined by the distribution of the two glycosidic dihedral angles, φ (O5-C1-O1-C4') and ψ (C1-O1-C4'-C5'), during a 10 ns run is shown in Figure 2A. This simulation clearly indicates that the molecule of xylan adopts a left-hand three-fold helical (3_2) conformation through almost the entire period of the simulation, and that a two-fold (2_1) conformation does not appear. This observation is consistent with the results of a previous MD study performed by Almond and Sheehan, [12] who used the CHARMM force-field different from ours. To examine the energy difference between the molecular chains of xylan in 3_2 and 2_1 conformations in water, the two glycosidic dihedral angles φ and ψ were constrained to force the molecule to be in the 2_1 conformation. This constrained conformation reverted instantly to the 3_2 structure upon removal of the dihedral constraints (Fig. S3, Supporting Information). Energetically, the 3_2 conformation was much more stable than the 2_1, showing an energy difference of 10 kJ/mol/xylosyl residue, a value significantly large, considering 2.5 kJ/mol for k_bT at 300K.

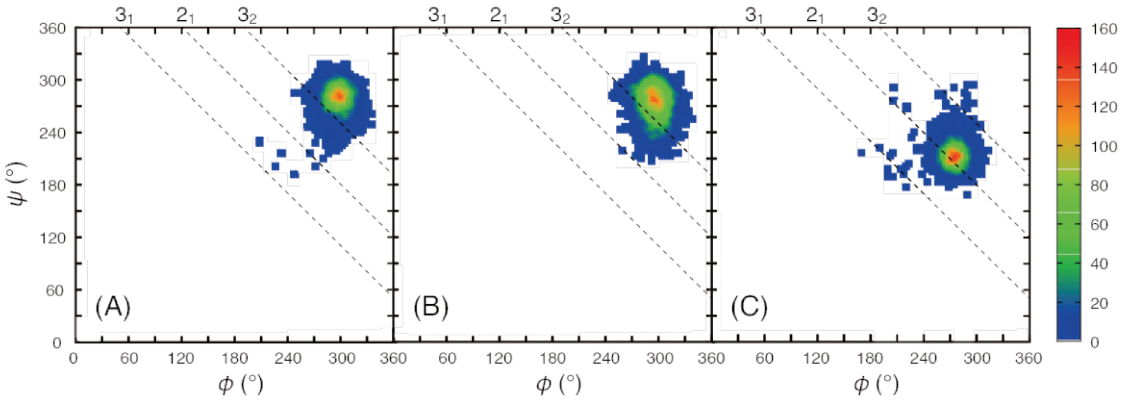

Figure 2. Distribution of the dihedral angles, Φ (O5-C1-O1-C4') and Ψ (C1-O1-C4'-C5') at the glycosidic linkage of xylan: (2A) xylan in water and (2B) xylan adsorbed on the hydrophobic (100) surface, without restraint; (2C) as in 2B, but after first applying a 2_1 dihedral restraint and then removing it. The color code denotes the population at each dihedral pair. The dashed lines correspond to the 2- and 3-fold helicity of the xylan chain: from left to right: $\Phi+\Psi$ = 50° (3_1), 120° (2_1), and 190° (3_2).

3.2 Adsorption Simulation of Xylan on the Cellulose Surfaces

Figure 3 shows some snapshots of xylan molecules on different cellulose surfaces. In all the adsorption simulations a given xylan molecule was immediately adsorbed at the cellulose surface and did not dissociate from the surface during the 10 or 20 ns production runs.

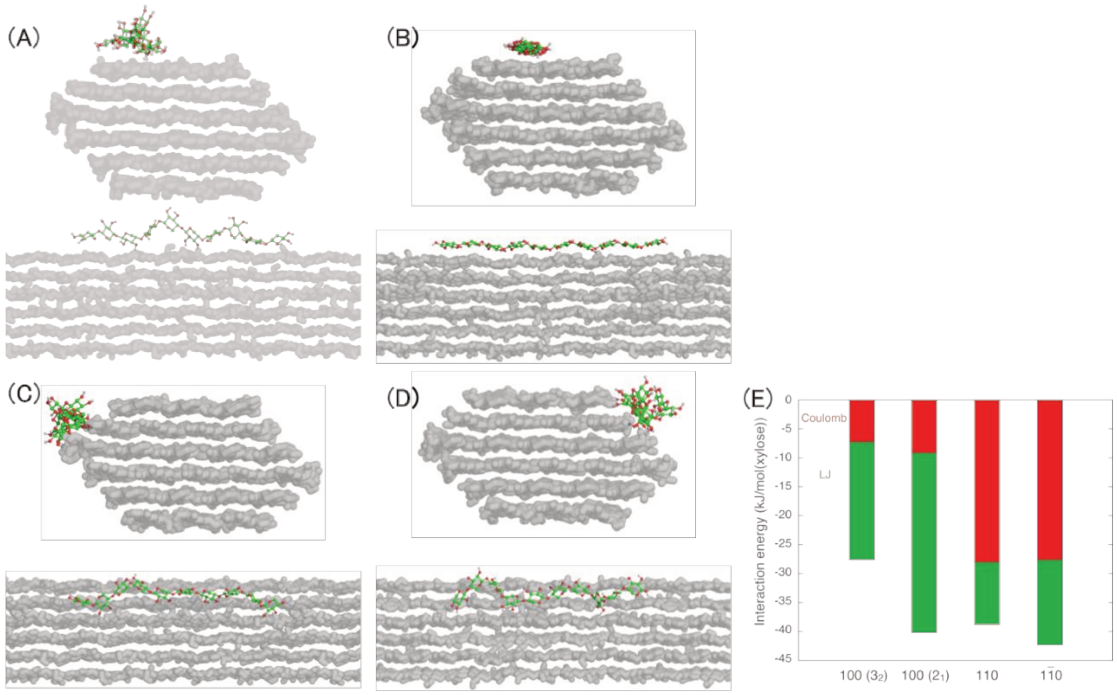

Figure 3. Snapshots of xylan adsorbed on cellulose surfaces in cross-sectional (upper) and side (lower) views. (3A) Adsorbed on the (100) surface without dihedral restraints throughout the simulation. (3B) Same as in (3A) but with restraints at the first adsorption, followed by unconstrained equilibration. (3C) As in 3B, but adsorption on the (110) surface. (3D) As in 3B, but adsorption on the (1-10) surface. (E) Interaction energy between xylan and cellulose: the Lennard-Jones and Coulomb contributions are denoted with green and red colors, respectively.

3.2.a Adsorption of Xylan on the Hydrophobic (100) Surface.

First, we examined the adsorption of xylan with the different molecular conformations, namely 2- and 3-fold conformations on the hydrophobic (100) surface of cellulose: snapshots are given in Figures 3A and 3B. When the restraints were not applied to the glycosidic dihedral angles, the xylan chain remained in its initial 3_2 conformation after the adsorption (Fig. 2B) even if the distribution of the glycosidic dihedral angles became slightly wider on the cellulose surface in comparison to the corresponding distribution in water. With the restraint applied to the glycosidic dihedral angles, the xylan molecule was initially adsorbed in the 2-fold conformation. This conformation was maintained even after the removal of the dihedral restraints over the whole simulation time as shown in the dihedral distribution of xylan (Fig. 2C) and the evolution of $\varphi + \psi$ with simulation time (Fig. S4 C, Supporting Information), unlike in the case of xylan in water without cellulose (Fig. S3, Supporting Information). This indicates that the 2-fold conformation of xylan molecule is stabilized by the presence of the cellulose surface and thus, the interaction between xylan and cellulose is stronger when xylan is in the 2-fold conformation than when it is in the 3-fold one (Fig. 3E).

This stronger hydrophobic interaction may arise from the more compact and close packing of xylan to the cellulose surface, when the interaction between the rings of xylan and those of cellulose are maximized. It is worth also mentioning that the water molecules, which were initially associated with bulk xylan for the stabilization of the 3_2 conformation, become expelled when the 2-fold conformation is reached.

The organization of adsorbed xylan on the cellulose surface was characterized as shown in Figure 4. An end-to-end vector, *r*, of xylan was defined as a vector starting at the C1 of the second residue from the reducing end and ending at the C4 of the ninth residue. The first and last residues were omitted from the analyses as they were occasionally disorganized due to their higher flexibility. The end-to-end distance was defined as amplitude of the end-to-end vector, and the chain orientation angle, ϑ was defined as the angle between the chain direction of cellulose and this vector (Fig. 4A). Considering the length of a xylosyl residue along chain direction to be about 0.5 nm, an *r*-value of 4 nm means that the molecular chain is fully extended. Note that the xylan was initially arranged with ϑ being roughly 0° in the adsorption simulations unless otherwise specified. The planar orientation angle, γ was defined as the angle between the glycosidic mean ring planes of cellulose and xylan (Fig. 4B).

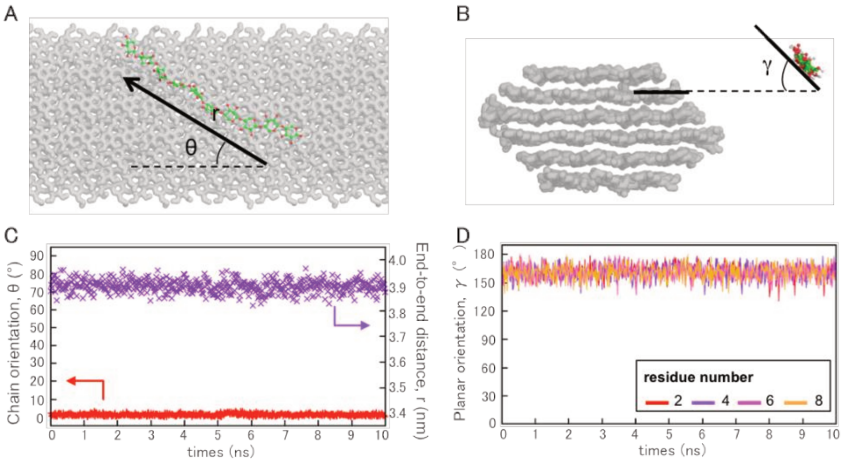

Figure 4. (A) Schematic image of chain orientation angle ϑ, and end-to-end distance, *r*, and (B) planar orientation angle, γ. (C) chain orientation (red) and end-to-end distance (purple) of adsorbed xylan on the (100) cellulose surface as a function of simulation time. (D) Planar orientation angles of selected xylan residues as a function of simulation time.

On the (100) surface of cellulose, the xylan molecule was adsorbed with its chain axis roughly parallel to that of the cellulose surface (Figure 3). This adsorption behavior, which is consistent with data from spectroscopic measurements,[19,20] is similar to the one observed in a previous MD study, where the axes of the xylan molecules were preferably aligned with the cellulose chain direction.[26]

In addition, the adsorbed xylan in 2-fold conformation was also aligned parallel to the chain direction of cellulose with the ϑ value of 0° throughout the simulation, and almost fully extended as the *r*-value was about 3.9 nm (Fig. 4C). No kinking or bending was observed through the simulation. The planar orientation angle γ was close to 180° (Fig 4D), which means that the pyranosyl mean plane of the xylan residues were parallel to those of cellulose yielding hydrophobic stacking as in the native cellulose crystal.

This stacking accounts for the stronger hydrophobic interaction between the cellulose surface and xylan in the 2-fold conformation as opposed to the weaker when xylan was in the 3-fold counterpart (Fig. 3E).

To investigate the preferential chain orientation of xylan on the cellulose surface, we performed a series of adsorption simulations on the (100) cellulose surface using a xylan chain positioned with different initial chain orientation angles, at ϑ = 30, 60, 90°.

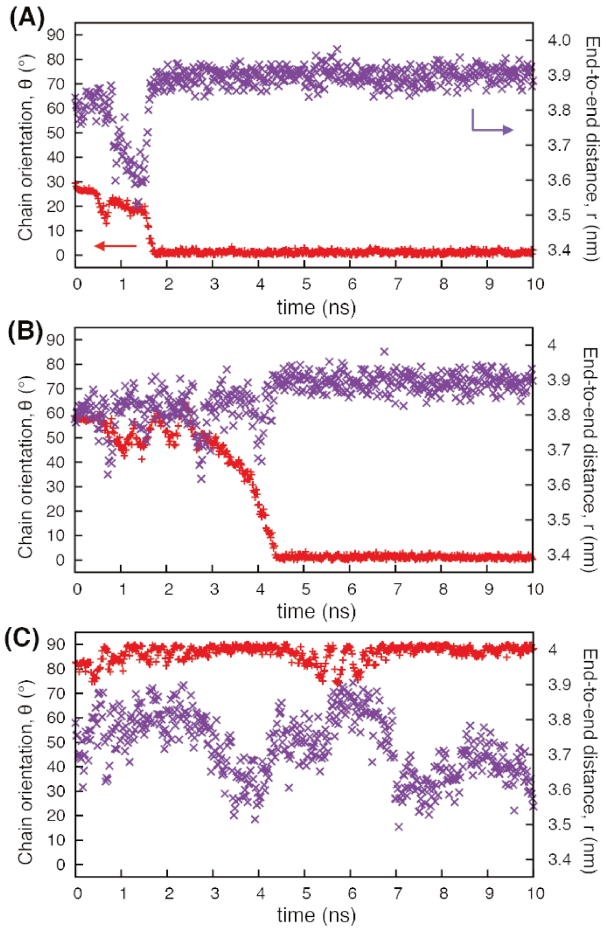

Figure 5. Time evolution of the chain orientation angle, ϑ (in red) and end-to-end distance, *r* (in purple) during the adsorption simulation with starting ϑ values of (A) 30°, (B) 60°, and (C) 90°.

Figure 5 shows the evolution of the chain orientation angles, ϑ and that of the end-to-end distance, *r* of the adsorbed xylan chain as a function of the simulation time. In the initial orientation with ϑ = 30° and 60°, the xylan chain was rotated during the time course of the MD simulation to be aligned along the cellulose chain direction with a ϑ value of 0° (Figures 5A and 5B). After the rotation, the xylan chain was almost fully extended with the *r*-value of about 3.9 nm. On the other hand, the xylan chain remained perpendicular to the microfibrils when the initial orientation was ϑ = 90° (Figure 5C). This simulation was prolonged to 30 ns, but the system kept the same organization during the whole simulation time. The end-to-end distance of the xylan with ϑ = 90° fluctuated more than those where ϑ took the initial value of 30° and 60° (see Fig. 5A-5C).

The xylan was bent at the edge of the cellulose microfibril and temporarily covered the adjacent surfaces, so that the *r*-value changed quite frequently. Thus the parallel alignment of the xylan molecules with those of cellulose and the xylan extended organization seems to be generally favored on the cellulose surface.

3. 2. b. Adsorption of Xylan on the Hydrophilic (110) and (1-10) Surfaces.

Snapshots of the adsorption states on these surfaces are given in Figures 3C and 3D. The sum of the glycosidic dihedral angles $\varphi + \psi$ and the planar orientation angle, γ as a function of simulation time are given in Figures S4A, S4B, S5A, S5B in the Supporting Information. We can observe that the adsorbed xylan molecules were less organized than in the case of the adsorption on the (100) surface, as $\varphi + \psi$ and γ values fluctuated during the simulation. On these surfaces, the xylan molecules became reorganized from the 2- to 3-fold conformations on both chain ends, while the chain middle remained in the initial 2-fold conformation (Figs. S4A and S4B, Supporting Information). This partial reorganization probably arises from high flexibility of the chain ends, so that this type of the adsorption state may be observed particularly with a short xylan chain, and more residues in the 2-fold conformation may be observed for longer xylan chains. The hydrophobic stacking between xylan and cellulose was not clearly formed on these hydrophilic surfaces (Figs. S5A and S5B, Supporting Information), as the glucosidic rings of cellulose were not fully exposed in these hydrophilic surfaces unlike in the case of the hydrophobic (100) surface. Thus, in the case of the adsorption on the two hydrophilic surfaces (110) and (1-10), the interaction energy is controlled essentially by electrostatic forces, which dominate the hydrophobic interaction (Figure 3E). This is the result of the strong hydrogen bonding associating the hydroxyl groups of xylan and cellulose.

Interestingly, the adsorbed xylan chains on these two surfaces tend to be less extended as in the case of the adsorption on the (100) surface (Figure 4C). Indeed a substantial shrinkage of the end-to-end distance occurs on these hydrophilic surfaces during the simulation time. This is clearly exemplified in Figures S6 A and S6B when the xylan chains with an initial *r*-value of 3.9 nm shrank by 0.2 [on the (110) surface] and 0.4 nm [on the (1-10) surface] after a simulation time of 10 ns. Such shrinkage is consistent with the scheme of xylan adsorption, which on these two surfaces depends less on a hydrophobic stacking and more on a hydrophilic one. Also the presence of few xylosyl residues in the 3_2 conformation is likely to locally lift the xylan chains from the surface and thus favor their shrinkage. Nevertheless, a global rearrangement of the whole xylan chains into a 3-fold conformation was not observed on these surfaces, justifying the absence of the 3_2 xylan signal in the ^{13}C CP/ MAS NMR spectra (1B and 1E) of the initial and reconstructed samples.

CONCLUSION

The conformational adaptation of undecorated linear β-(1→4) xylan upon its adsorption on the surface of microfibrillated cellulose was investigated by means of solid-state ^{13}C NMR spectroscopy, specific surface area measurement, and atomistic MD simulations. The solid-state NMR data confirmed that xylan was able to adapt its molecular conformation in presence of cellulose surface, from a bulk-like 3-fold conformation to a presumed cellulose-like 2-fold one. By sequential re-depositions, coupled with specific area measurements, it was possible to see that in these biomimetic reconstructed models, this adaption was only limited to the first adsorbed layer, where xylan was in direct contact with the cellulose surface. With atomistic MD simulations, we followed the adsorption behavior of xylan molecule on various cellulose surfaces and found that the presence of cellulose could stabilize the 2-fold conformation of the xylan molecules in aqueous environment on the hydrophobic surfaces of cellulose. In that case, the adsorbed xylan was preferentially arranged with its chain axis parallel to that of cellulose and formed hydrophobic stacking structure with the xylosyl mean planes stacked parallel to the glucosyl units of the cellulose crystal surfaces. Our study shows that this structural adaptation from 3-fold to the presumable 2-fold conformation was solely due to physicochemical interactions and corresponds to what is observed during the biosynthesis of the plant cell walls.

ACKNOWLEDGEMENTS

We acknowledge the help of Dr M. Schelcher from CTP and Ms. A Guillemain from FCBA for the sugar analysis and Ms. M-F. Metral from CERMAV for technical assistance. The PhD program of L. F-V. was financially supported by the Institut Carnot PolyNat and the Agence Nationale pour la Recherche et la Technologie. We thank the companies sponsoring the Curtain II research project from CTP for their support and enriching exchanges. We also acknowledge the help of Dr. H. Chanzy for fruitful discussions during the writing of this work.

REFERENCES

(1) Albersheim, P.; Darvill, A.; Roberts, K.; Sederoff, R.; Staehlin. A in "Plant Cell Walls" Garland Science, Taylor and Francis Group, LLC, New York 2011.

(2) Varner, J. E.; Lin, L-S. *Cell* **1989**, *56*, 231.

(3) Cosgrove, D. J.; Jarvis, M. C. *Front. Plant. Sci.* **2012**, *3*, 204.

(4) Ebringerova, A.; Heinze, T. *Macromol. Rapid Commun.* **2000**, *21*, 542.

(5) Koshijima, T.; Timell, T.E. *J. Polym Part C* **1965**, *11*, 265.

(6) Westtbye, P.; Köhnke, T.; Gatenholm, P. *Holzforschung* **2008**, *62*, 31.

(7) Zinbo, M.; Timell T. E. *Sven. Papperstidn.* **1965**, *68*, 647.

(8) Timell, T. E. *Adv. Carbohydr. Chem.* **1964**, *19*, 247.

(9) Pinto, P. C.; Evtuguin, D. V.; Neto, C. P. *Carbohydr. Polym.* **2005**, *60*, 489.

(10) Nieduszynski, A.; Marchessault R. H. *Biopolymers* **1972**, *11*, 1335.

(11) Szabo, L.; Jamal, S.; Xie, H.; Charnok, S. J.; Bolam, D. N.; Gilbert, H. J.; Davies G. J. *J. Biol. Chem.* **2001**, *276*, 49061.

(12) Almond, A.; Sheehan, J. K. *Glycobiology* **2003**, *13,* 255.

(13) Mazeau, K.; Moine, C.; Krausz, P.; Gloaguen, V. *Carbohydr. Res.* **2005**, *340*, 2752.

(14) Roelofsen, P. A. *Biochem. Biophys. Acta* **1954**, *13*, 592.

(15) Chanzy, H.; Dubé, M.; Marchessault, R. H. *Polymer* **1979**, *20*, 1037.

(16) Mora, F.; Ruel, K.; Comtat, J.; Joseleau, J-P. *Holzforschung* **1986**, *40*, 85.

(17) Henriksson, B. Å.; Gatenholm, P. *Holzforschung* **2001**, *55*, 494.

(18) Köhnke, T.; Öslund, Å.; Brelid, H. *Biomacromolecules* **2011**, *12*, 2633.

(19) Marchessault, R. H.; Liang, C. Y. *J. Polym. Sci.* **1962**, *59*, 367.

(20) Stevanic, J. S.; Salmén, L. *Holzforschung* **2009**, *63*, 497.

(21) Yllner, S.; Enström, B. *Sven. Papperstidn*. **1956**, *59*, 229.

(22) Penttilä, P. A.; Varnai, A.; Pere, J.; Tammelin, T.; Salmén, L.; Siika-aho. M.; Viikari, L.; Serimaa, R. *Biores. Techn.* **2013**, *129*, 135.

(23) Nishiyama, Y.; Langan, P.; Chanzy, H. *J. Am. Chem. Soc.* **2002**, *124*, 9074.

(24) Larsson, P. T.; Hult, H-L.; Wickholm, K.; Pettersson, E.; Iversen, E.; Iversen, T. *Solid State Nucl. Mag.* **1999**, *15*, 31

(25) Teleman, A.; Larsson, P.T.; Iversen, T. *Cellulose* **2001**, *8*, 209.

(26) Mazeau, K.; Charlier, L. *Cellulose* **2012**, *19*, 337.

(27) Busse-Wicher, M.; Gomes, T. C. F.; Tryfona, T.; Nikolovski, N.; Stott, K.; Grantham, N. J.; Bolam, D. N.; Skaf, M. S.; Dupree, P. *Plant J.* **2014**, *79,* 492.

(28) Pääkkö, M. M.; Ankerfors, M.; Kosonen, H.; Nykänen, A.; Ahola, S.; Österberg, M.; Ruokolainen, J.; Laine, J.; Larsson, P. T.; Ikkala, O.; Lindström, T. B*iomacromolecules* **2007**, *8*, 1934.

(29) Brunauer, S.; Emmett, P. H.; Teller, E. *J. Am. Chem. Soc.* **1938**, *60*, 309.

(30) Fumagalli, M.; Ouhab, D.; Molina-Boisseau, S.; Heux, L. *Biomacromolecules* **2013**, *14*, 3246.

(31) Hess, B.; Kutzner, C.; van der Spoel, D.; Lindhal, E. *J. Chem. Theory Comput.* **2008**, *4*, 435.

(32) Hansen, H.; Hünenberger, P. A. J Comput. Chem. **2011**, *32*, 998.

(33) Chen, P.; Nishiyama, Y.; Mazeau, K. *Cellulose* **2014**, *21*, 2207.

(34) Hess, B.; Bekker, H.; Berendsen, H. J. C.; Fraaije, J. G. E. M. *J. Comput. Chem.* **1997**, *18*, 1463.

(35) Bussi, G.; Donadio, D.; Parrinello, M. *J. Chem. Phys.* **2007**, *126*, 014101.

(36) Berendsen, H. J. C.; Postma, J. P. M.; van Gunsteren, W. F.; DiNola, A.; Haak, J. R. *J. Chem. Phys.* **1984**, *81*, 1463.

(37) Darden, T.; Perera, L.; Li, L.; Pedersen, L. *Structure* **1999**, *7*, R55.

SUPPORTING INFORMATION

Chemical Composition of the MFC

The sugar composition of the MFC from birch kraft pulp before (*i*) and after xylan extraction (*ex*) and one from pine dissolving pulp was determined by classical sugar analysis, using high-pressure liquid chromatography (HPLC) with a Dionex DX500 apparatus, equipped with a Carbopac PA10 column, with water/NaOH 150 mM gradient as eluent. Prior to the analysis, the MFC samples were freeze-dried and then dissolved/hydrolyzed in/by sulphuric acid. Fucose (Sigma Aldrich) was used as internal standard.

The composition in five sugar residues namely: glucose, xylose, mannose, arabinose and galactose and the yield of hydrolysis are presented in Table S1. The normalized sugar content is calculated in Table S2 as [Glucose normalized] = [Glucose] / (yield of hydrolysis / 100)

The yield of xylan extraction (Table S2) is determined from the initial xylan content in the sample (Xy *i.*) and the xylan content after the xylan extraction (Xy *ex.*).

$$\text{Yield (\%)} = (\text{Xy } i. - \text{Xy } ex.)/ \text{Xy } i. \times 100$$

Table S1. Sugar composition of the various samples used in this work

	MFC from birch kraft pulp		MFC from pine sulfite pulp
(w/w %)	*i*	*ex*	*i*
Glucose %	67.2	78.6	91.6
Xylose %	21.3	8.2	1.4
Mannose %	0.9	1.4	0.9
Arabinose %	0.1	0.1	0.1
Galactose %	0.0	0.1	0.1
Hydrolysis yield %	89.6	88.7	94

Table S2. Normalized sugar composition of the various samples used in this work

	MFC from birch kraft pulp		MFC from pine sulfite pulp
(w/w %)	*i*	*ex*	*i*
Glucose %	75	88.7	97.5
Xylose %	23.7	9.2	1.5
Mannose %	1.0	1.5	1
Arabinose %	0.1	0.1	0.0
Galactose %	0.2	0.5	0.1
Yield of xylan extraction %		61	

Table S3. Correspondence between the xylosyl/xylan and glucosyl/cellulose contents in the different birch pulp samples used in this study

	Xylosyl/glucosyl (w/w) from sugar analysis	Xylan ratio normalized to cellulose (w/w)	Xylan in interfacial conformation normalized to cellulose (NMR)
Initial sample	24% / 75%	0.31	0.31
After DMSO/LiCl extraction	9% / 89%	0.1	0.1
Readsorption system I	21% / 79%	0.28	0.28
Readsorption system II	28% / 72%	0.39	0.25

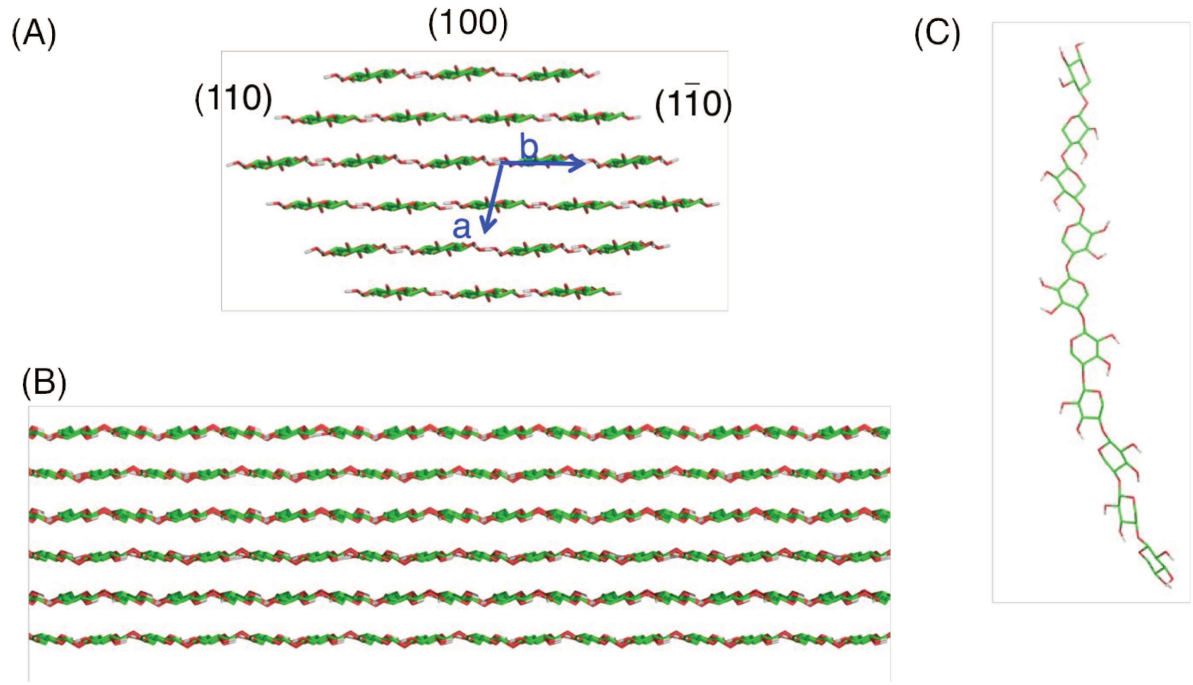

Figure S1. Models of xylan and cellulose microfibrils used in this study. 24-chain cellulose Iβ model in (A) lateral view and (B) side view. (C) Molecule of xylan with DP of 10.

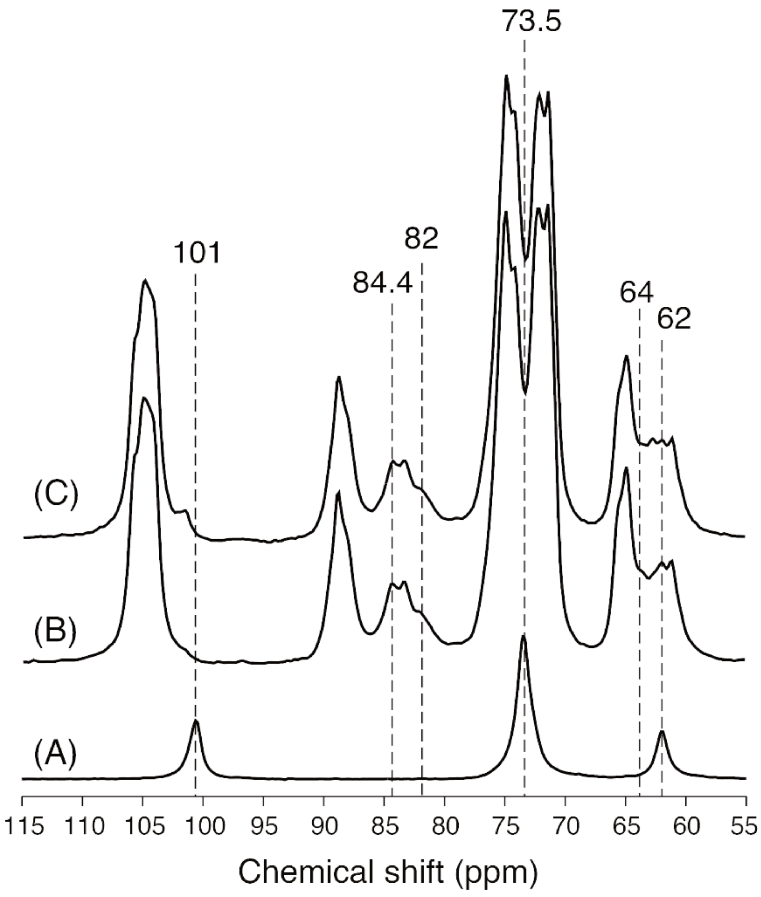

Figure S2. CP/MAS ^{13}C NMR spectra of wet samples. (A): extracted xylan hydrated at 97% relative humidity. (B): MFC from pine sulphite dissolving pulp after re-adsorption of 9% of xylan. (C): MFC from pine sulphite dissolving pulp after re-adsorption of 13.5% of xylan.

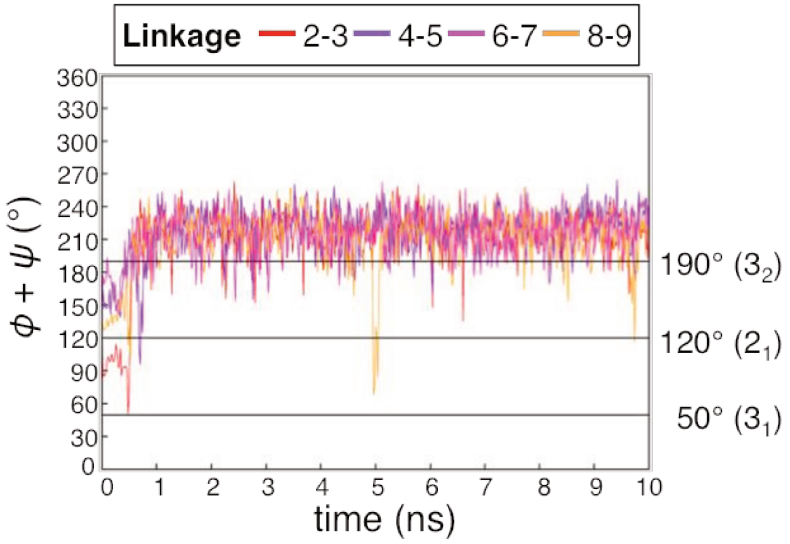

Figure S3. Change in sum of glycosidic dihedral angles (ϕ+ψ) of a xylan molecule during 10-ns equilibration run in water. At t = 0 ns, the dihedral constraints which forced the xylan to the 2_1 conformation was removed. The color code for the linkages corresponds to the succession of the xylosyl residues along the xylodecaose chain, starting from the non-reducing end.

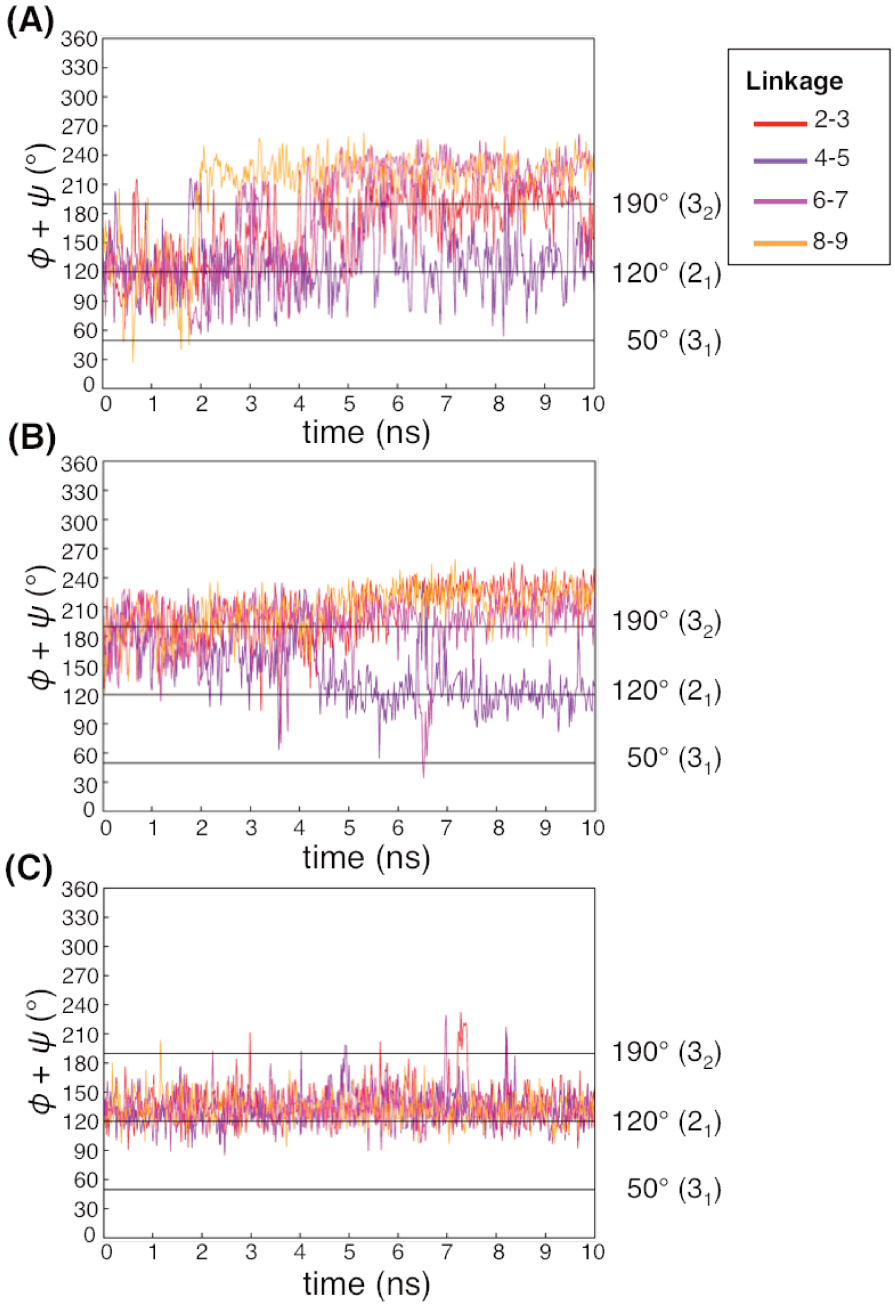

Figure S4. Changes in the sum of the glycosidic dihedral angles (ϕ + ψ) of adsorbed xylan on different cellulose surfaces as a function of simulation time. A: (110) surface. B: (1-10) surface. C: (100) surface. The color code for the linkages corresponds to the succession of the xylosyl residues along the xylodecaose chain, starting from the non-reducing end.

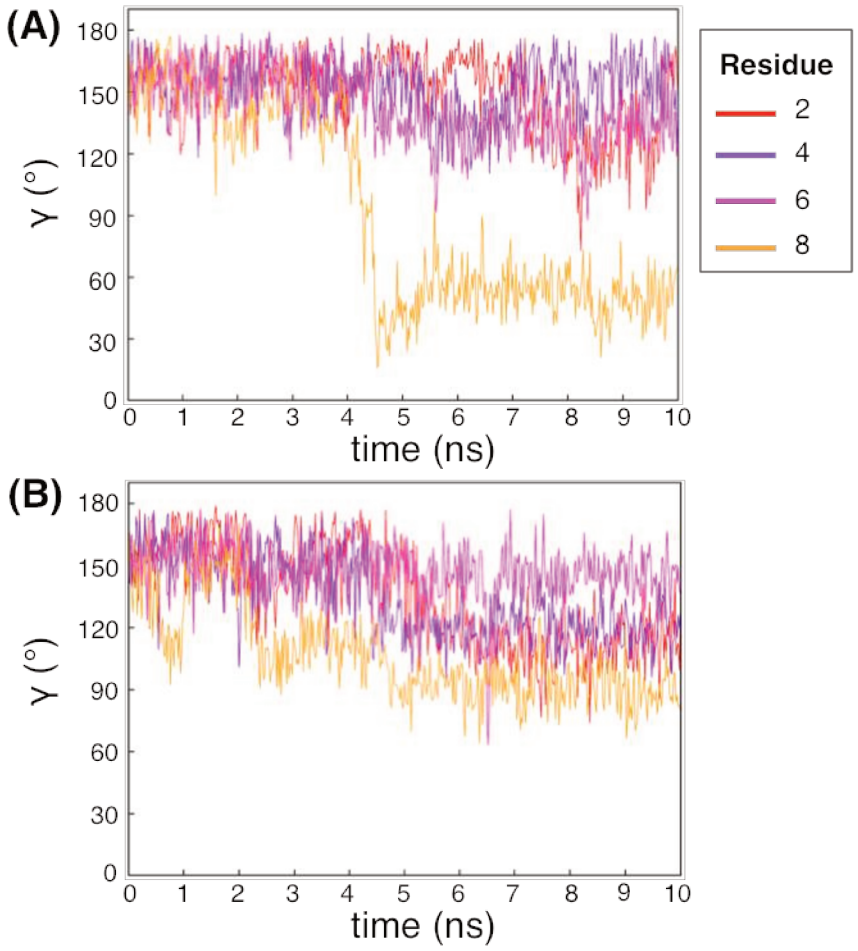

Figure S5. Changes in the planar orientation angle, *γ* between adsorbed xylan and cellulose as a function of simulation time. A: (110) surface. B: (1-10) surface. The color code of the residues corresponds to the succession of the xylosyl residues along the xylodecaose chain, starting from the non-reducing end.

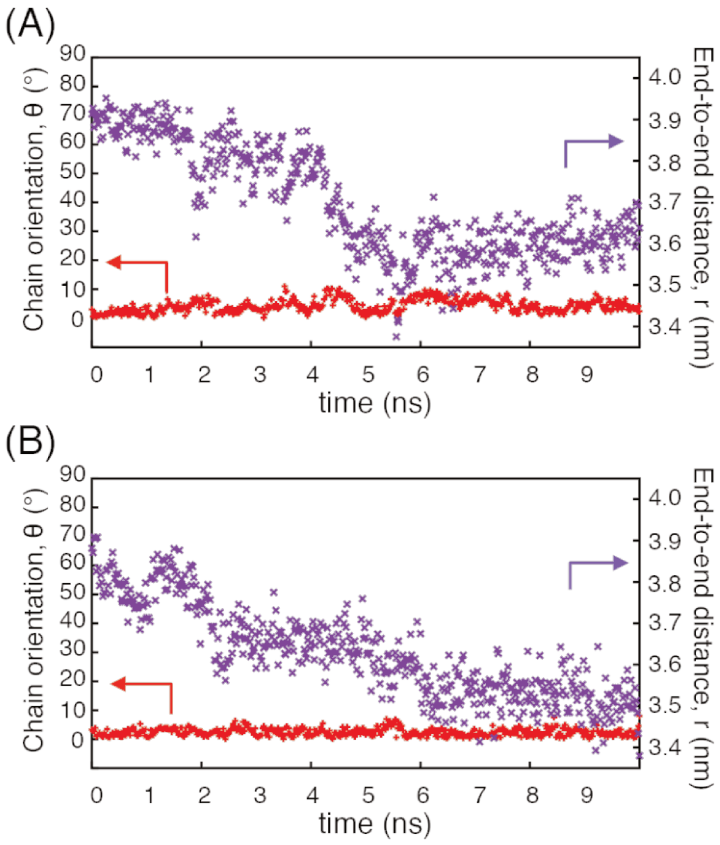

Figure S6. Chain orientation, θ (red) and end-to-end distance, r (purple) of adsorbed xylan on the cellulose surface as a function of simulation time. A: (110) surface. B: (1-10) surface.

Annex 9: Xylan-cellulose adsorption energy

The binding energy between adsorbed xylan and cellulose, ΔG_{bind} was calculated by pulling simulations using the pull code in GROMACS.

The starting coordinates were the last frame of each adsorption simulation of xylan adsorbed on 100 surface in 3_1 conformations (System 1) and xylan adsorbed in 2_1 conformation on 100, 110 and 1-10 surface (System 2).
The reaction coordinate was set as a direction orthogonal to the pyranoside plane of cellulose then the xylan residue at the reducing end was pulled off with a harmonic force constant of 200 kJ/mol/nm^2 and a displacement rate of 0.01 nm/ps (Figure 65).
Umbrella sampling simulations were then performed for 1-2 ns at each configuration with every 0.2 nm displacement intervals.
The potential of mean force (PMF) represented in Figure 66 shows the dissociation energy of xylan and cellulose crystal from each different adsorption state.

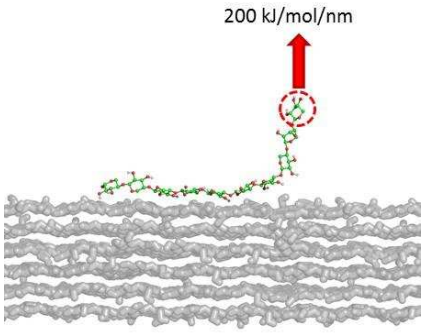

Figure 65: Snap shot of pulling simulation

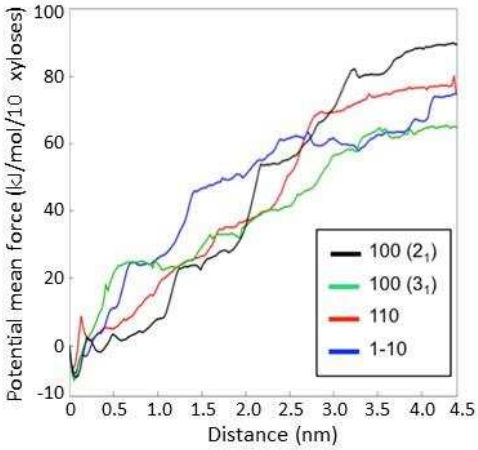

Figure 66: Potential of mean force of xylan dissociated from different cellulose surfaces.

The adsorption system between the xylan in 2_1 conformation and the 100 surface gave the highest value of ΔG_{bind}, 9 kJ/mol/xylose residue, while the lowest value, 6.2 kJ/mol/xylose residue was found in the xylan in 3_1 conformation on the 100 surface. Thus the xylan in 2_1 conformation has stronger interaction and affinity to the cellulose surface in comparison to that in 3_1 conformation.

The stronger affinity found in the adsorption with 2_1 conformation may come from the stronger hydrophobic interaction between the glycosidic rings. Owing to this strong interaction the xylan was packed tightly and water molecules were excluded between xylan and cellulose.
On the other hand, the adsorbed xylan in 3_1 conformation showed more bulky nature and interacted with surrounding water molecules, which consequently reduced the effective interaction between xylan and cellulose.
The ΔG_{bind} values for the adsorption on 110 and 1-10 surfaces were nearly the same, at 7.5 kJ/mol/xylose residue, and smaller than xylan in 2_1 conformation at the 100 surface. This weaker interaction was presumably due to the partial disorganization of the adsorption state at the chain ends.

Annex 10: Re-adsorption after TBA freeze-drying

In the above publication, we found that xylan adsorbed amount is correlated with the specific surface of MFC and only the first layer of xylan adsorbed on cellulose adapt its conformation. The xylan in excess kept its preferred 3_1 conformation.

Note that the xylan readsorption shown in the publication was only performed with MFC freeze-dried in water and redispersed in DMSO in presence of xylan. Then the DMSO is removed by dialysis and the sample is freeze-dried and rehydrated prior the NMR analysis.
We also performed the same experiment with MFC freeze-dried in TBA prior its redispersion in DMSO with xylan to see if the amount of reabsorbed xylan may be increased as the specific surface of MFC freeze-dried in TBA is higher than the one in water.
This experiment has been performed on MFC from pine sulfite dissolving pulp. Figure 67 shows the comparison of NMR solid state spectra of: (A) the initial MFC (2.5% of xylan), (B) MFC with 16% of xylan, MFC freeze-dried in water prior the readsorption, (C) MFC with 16% of xylan, MFC freeze- dried in TBA prior the readsorption.

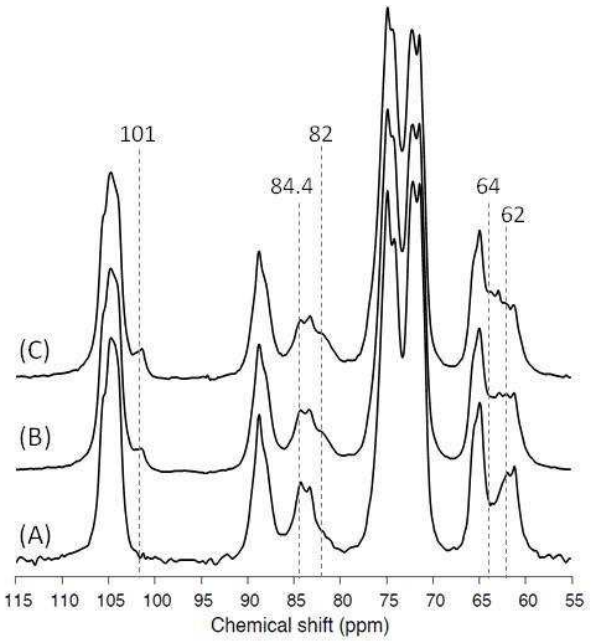

Figure 67: CP/MAS ^{13}C NMR spectra of wet samples. (A): MFC from pine sulfite dissolving pulp. MFC from pine sulfite dissolving pulp after re-adsorption of 13.5% of xylan (B) with classic protocol. (C) with MFC freeze-dried in TBA

According to our previous observations, the freeze-drying in TBA prior the xylan readsorption in DMSO did not improve the amount of xylan in interaction with cellulose. The peak at 101 ppm which represent the xylan in excess have similar intensity in both spectrum B and C. Furthermore, the same amount of xylan is adsorbed at the cellulose surface according to the peaks intensity at 84.4, 82 and 64 ppm. Thus, redispersion of freeze-dried MFC in DMSO is the limiting factor, regardless of the solvent used for MFC freeze-drying. The amount of reabsorbed xylan might be linked to the specific surface of MFC in DMSO suspension, which is so far unknown, as specific surfaces were measured on solids.

Annex 11: Arabino-xylan re-adsorption

It was previously shown by solid-state NMR experiments that the xylan adapted its conformation from 3_1 to 2_1 in presence of cellulose. However this modification is only observed for the first layer of xylan which is directly in contact with cellulose surface.
Indeed the amount of readsorbed xylan in 2_1 conformation is correlated with the MFC specific surface. The readsorption of xylan on MFC from birch-kra-nd after extraction was performed with a maximum cellulose/xylan ratio at 0.28/1 while it is limited at 0.12/1 in the case of MFC from pine96-sulf.

In order to study the influence of the xylan origin on the readsorbed amount, the xylan extracted from MFC from birch -kra-nd was replaced by commercial arabino-xylan extracted from oat.
The main difference between these two xylans is the presence of 9.6% of arabinose group in the xylan extracted from oat while no branches has been characterized on xylan extracted from MFC from birch-kra-nd as described in chapter 1 (NMR and sugar analysis).

The procedure for xylan readsorption is the one described in the publication. Different amounts of arabino-xylan (extracted from oat) were dissolved in DMSO in presence of MFC from birch-kra-nd after xylan extraction (i.e.MFC with 9% of residual xylan content). Then this system was dialysed to remove DMSO and freeze-dried in water.
Solid state NMR was performed on rehydrated samples (Figure 68).

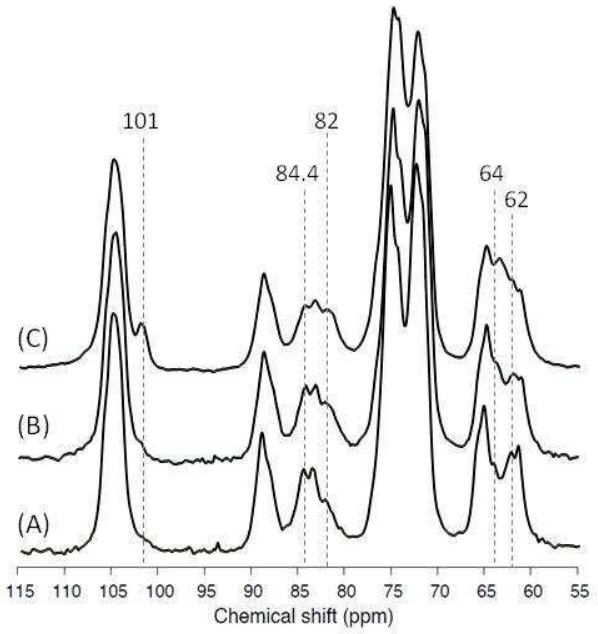

Figure 68: CP/MAS ^{13}C NMR spectra of wet samples. (A): MFC from birch-kra-nd after xylan extraction. (B) as in (A) but after re-adsorption of xylan with xylan/cellulose ratio of 0.28/1. (13.5%) (C) as in (A) but after re-adsorption of xylan with xylan/cellulose ratio 0.53/1 (30%)

No difference in xylan readsorbed amount are observed. According to NMR spectra, the arabinose branches did not increase or decrease the xylan adsorption. When arabino-xylan is added at 0.53/1 (i.e. 22% of excess compared to the initial xylose MFC content before xylan extraction of 0.31/1), the xylan that does not interact with cellulose is clearly visible with the peaks at 62, 73.5 and 101 ppm.
The limit of xylan conformational change from 3_1 to 2_1 is still at 0.28/1 even with arabinose branches.

It seems that xylan readsorption in this case, is more controlled by the specific surface area of the MFC than the xylan branches.

It is also possible that 9.6% of arabinose branches is not sufficient to create a significant difference with the unsubstituted xylan.

Furthermore the initial xylan present in wood chips is renowned to be one of the less substituted and the MFC from birch-kra might be not the most suitable choice to study the influence of branches on xylan adsorption.

Chapter 4

Adhesion between cellulose and xylan

This chapter is devoted to an explorative study of the adhesive properties of xylan onto cellulose surfaces. Part of the work was the subject of the Master Thesis of Louis Gbodossou from Grenoble-INP between March and August 2016.

In order to evaluate the interaction between cellulose and xylan at a macroscopic scale, we intended to design experiments aimed to measure the adhesion between cellulose and xylan by mechanical measurements. One of the greatest difficulties was to build a system that allows the evaluation of the adhesion forces by mechanical measurements. This chapter begins with a rapid description of the adhesion mechanisms and adhesion tests. We will first present the experimental set-ups that has been developed in the particular case of cellulose/xylan interaction, and then the two types of experiments that have been investigated to acquire experimental data.

1. Adhesion mechanisms

The adhesion of polymers onto paper is a broad topic that has been largely studied since it concerns a large set of application in paper and cellulose materials (Zhao and Kwon 2011). The adhesion may be defined as the ensemble of physico-chemical phenomena that prevent the separation of two surfaces. The work of adhesion or failure energy is often given by a symbol G (J/m^2) and corresponds to the work required to separate two surfaces in contact. As the Joule corresponds to N.m, the work of adhesion G may be also express in N/m.

The adhesion results from three main factors: the non-covalent bonds, the covalent bonds and entanglement. The non-covalent bonds are due to electrostatic attraction such as ionic linkages or hydrogen bonds, π - π interactions and London dispersion interactions collectively called Van der Waals (VdW) interactions. In the case of the three layers system made of cellulose and xylan, the main weak interactions are the hydrogen bonds and London dispersion interactions. Beyond the molecular interactions, the physical properties of the substrates (roughness, micro-asperities or mechanical anchoring) will bring an additional contribution to the measured energies. Details of the different theories of adhesion mechanisms can be found in classical textbooks such as that by Kinloch (1987).

The mode of failure is very informative to characterize the adhesion between two materials (Figure 69). The adhesive failure corresponds to a failure at the material interface and is due to the low adhesion between the two materials. The cohesive failure appears when the interface is stronger than the interlayer material itself. In this last case, the energy that is measured depends on the viscoelastic properties of the material itself and its mode of failure, as recently reviewed by Creton and Ciccotti (2016).

Figure 69: Scheme of adhesive and cohesive failures

There are also several types of experimental set-ups for adhesion measurements (Figure 70). To choose among the different types of tests, the adhesive properties and the substrate properties have to be taken into consideration. Figure 70 gives the three main types of adhesion tests that are commonly used in the field of paper adhesives.

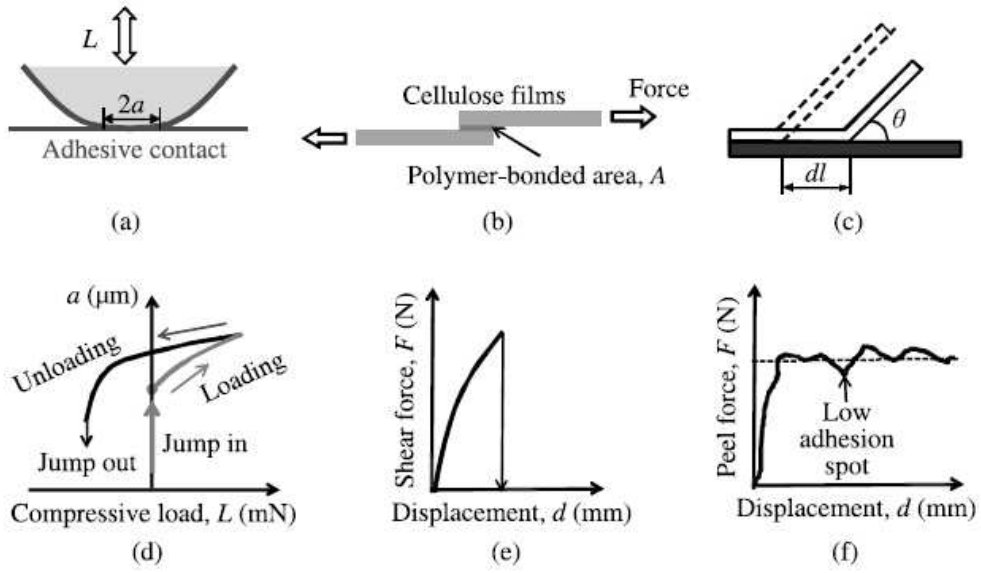

Figure 70: Three typical adhesion tests: (a) JKR-adhesion testing, (b) single-lap shear testing and (c) peel adhesion testing, and their force curves: (d) JKR-type plot of contact radius a vs load L, (e) shear force vs displacement curve and (f) peel force vs displacement (or peel distance) curve. (Adapted from Zhao *et al*, 2011)

We selected the peel and tensile shear test for our three-layer systems, as they can be adapted on tensile machine and flexible films.

2. Three layer system formation

We chose a three layered system with a xylan film in between two cellulose films (Sulfite MFC) to evaluate adhesion forces through different classical mechanical tests, i.e. peeling and shear tests. Model cellulosic surface has been extensively used to study the interaction of polymers with cellulose, that were obtained from the hydrolysis of cellulose derivatives like trimethysillyl cellulose (Holmberg *et al.* 1997; Rehfeldt and Tanaka 2003) or from spin coated CNC (Edgar and Gray 2003) or NFC (Olszewska *et al.* 2013), but those surfaces, well adapted for adsorption studies by AFM or QCMD techniques, are too thin to allow the elaboration of self-standing films. We then chose to process films from our own MFC suspensions. The first difficulty was to process MFC films able to bear the loads of the adhesion tests and dense enough to avoid the diffusion of xylan into the MFC sheets. Another problem arose from the generation of a contact between cellulose and xylan, since few solvents are available for xylan.
We thus first tried to characterize and optimize the surface roughness of MFC films.

2.1 MFC films

We chose MFC from pine96 sulfite pulp because of their high purity in cellulose (97.5% cf. chapter 1). The MFC films were produced by handsheet formers according to the procedure adapted at CTP (Sehaqui *et al.* 2010). The MFC suspensions were diluted to 0.5 wt%, and filtrated through handsheet formers with a 0.22 µm mesh membrane to limit the loss of the smallest elements. The wet MFC film with 10% solid content was covered with two carrier board paper and dried in a sheet dryer.
The films thickness (grammage) was varied by changing the initial volume of MFC suspension to be filtrated. We prepared MFC films of 25, 50 and 100 g/m². It was difficult to further reduce the thickness below 25 g/m² by this method because the MFC suspension started to form flocks below 0.5 wt% and a reduction in MFC suspension volume led to inhomogeneous coverage of the filtration membrane, as already described in the literature by Rodionova *et al.* (2012).

We also used casting technique to make thin MFC films without loss in elements. A 0.5% MFC suspension was poured in a polystyrene Petri dish and left at ambient conditions (23°C, for 72 hours) until complete water evaporation.
Visual aspects of the resulting MFC films were very different depending on the process (Figure 71).

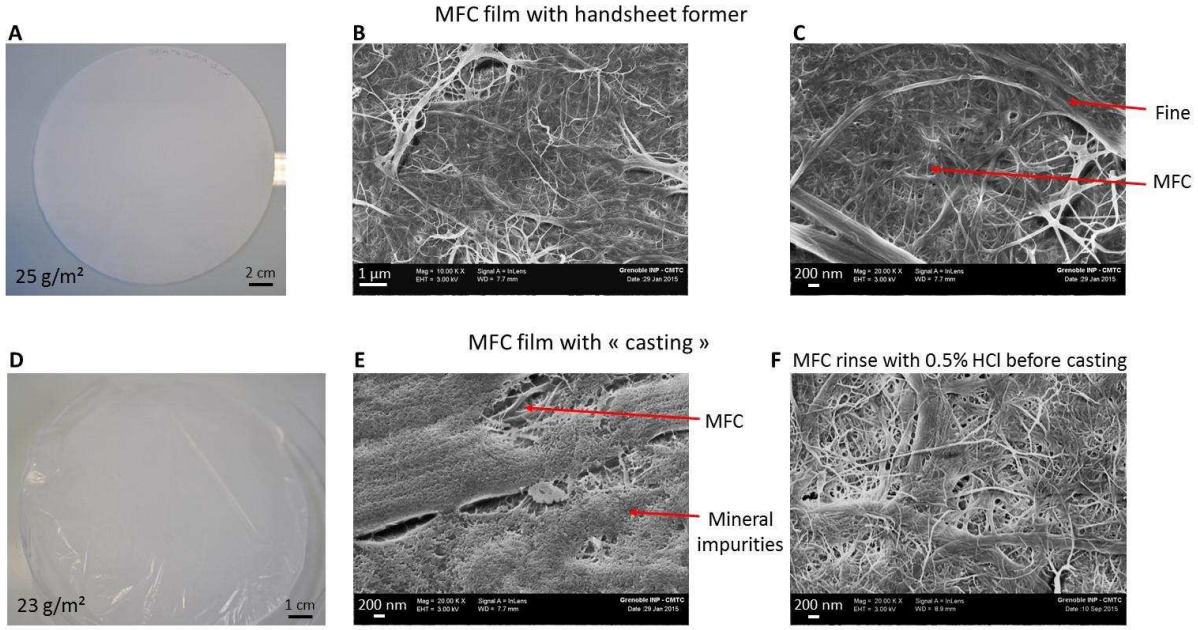

Figure 71: MFC films observations: (A) and (D) at macroscopic scale (B), (C) (E) and (F) with SEM

The handsheet films (Figure 71 A) had more matt appearance than the casted films which were glossier (Figure 71 B). In the casted films, the roughness of the cover paper was "printed" on the surface of the MFC film during the drying, while the Petri dish surface was smooth.

On the SEM images (Figure 71 B and C), the influence of the heterogeneity of the MFC suspension was clearly visible and the presence of larger elements, called fines, confirmed the incomplete microfibrillation during the homogenization. The SEM images of casted films (Figure 71 E) showed coverage by granular objects. These objects were mainly constituted of calcium according to the energy dispersive X-ray analysis (cf. Annex 12). Indeed, the MFC were produced in hard water and any mineral water impurities were kept in the casting process, while filtration by handsheet formers would eliminate most of them.

To remove the mineral salts, the MFC suspensions were washed prior casting by repeated centrifugation and redispersion in a solution of 0.5 wt% HCl then in deionized water until neutral pH.

The SEM image of casting film after this procedure (Figure 71 F) confirmed the absence of salt and the fine details reflecting the heterogeneity of the MFC suspension were also observed.

2.2 Xylan deposition

Xylan previously extracted (cf. Chapter 1) from MFC from birch kraft never never-dried pulp and the commercial arabino-xylan extracted from oat were used to make the internal layer of the system. The methods used for MFC films formation were not applicable to xylan, which is not soluble in water, and then precipitates, and will not have the suitable conformation for interacting with cellulose (cf. Chapter 3).

As the extracted xylan is only soluble in DMSO, which is nonvolatile, the casting method was not adapted to produce films of xylan. However, we occasionally observed that concentrated solution of xylan in DMSO led to thick gels with high viscosity when dialyzed against water.

Thus we tried to deposit the xylan gel in water between the two MFC films and let it dry. To restrain the swelling by osmotic pressure the solution was placed in a hollow rectangle. Different xylan concentrations were tested and the best gelation was observed at 60 g/L and 80 g/L for the xylan extracted from MFC from birch kraft and the commercial one extracted from oat, respectively.

To characterize the three-layers structure formation, we observed the cross section of the assembly made of fluorescent-labeled xylan using fluorescence microscopy (cf. Annex 13).

3. Peeling test results

3.1 Peeling test principle

The peeling test consists of pulling out the adhesive from its substrate at 90° or 180° (Figure 72). The adhesion G (N.m) may be determined from force of peeling according to the relation (1) where *b* is the adhesive width (m), θ is the peeling angle (°) and F_p the requested pulling force for the system delamination. During the test, the pulling force (F_p) reaches a plateau and this value is reported in *(1)* for the adhesion calculation.

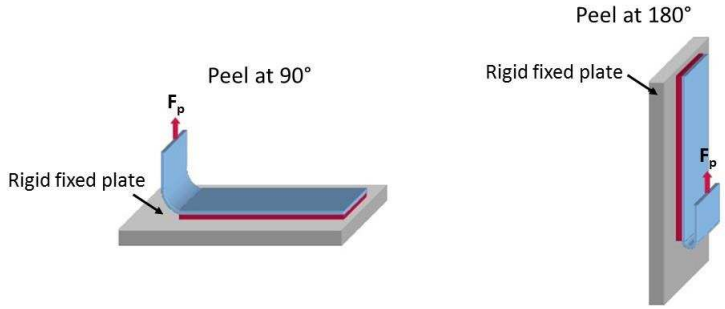

$$G = \frac{Fp}{b}(1 - \cos\theta) - \left(\frac{Fp^2}{2\,b\,t\,E}\right) \quad (1)$$

Figure 72: Different configuration of peeling tests

The second term of the equation *(1)* refers to the elastic deformation of the substrate during the peeling test. Indeed, the work required to pull out the adhesive from its substrate corresponds to the sum of the adhesion and the plastic deformation work of the substrate (Satas 1989). In the case of MFC films, this second term will be negligible as the plastic deformation of MFC is negligible. As the pulling force (F_p) changes with peeling angle (the peeling at 90° requires a pulling force two times larger than the peeling at 180°), the peeling angle must be stabilized during the measurement.
We chose the peeling at 180° which was easy to achieve on a tensile testing instrument. A cardboard was placed to maintain the system and a cardboard tab was glued at the end of MFC film supported with coated calendered paper (50 g.cm² of grammage) to be fixed to the clamp (Figure 73).

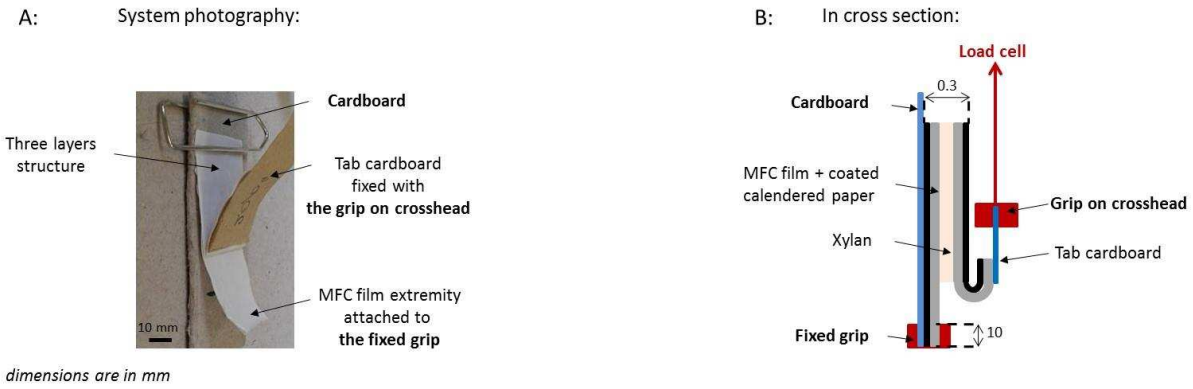

Figure 73: A: Photograph of a three-layer sample and B: scheme of the experimental set-up used for the peeling test

The speed of the peeling has also a strong influence on the adhesion measurement. The pulling force increased with the speed as a function of the viscoelasticity of the adhesive. Indeed, at low speed from 10 to 150 mm/min, the adhesive is deformed plastically, which increases the pulling force required for system delamination.

For higher speed, the constraint applied on the system is too fast and the plastic deformation of the adhesive layer may be limited. At this stage, the pulling force measured is independent of the speed.

3.2 Preliminary study

Peeling test measurements were performed at 180° (Figure 74) with adhesive tape (Advance AT206 PVC color coding Gaffa Tape) on steel plate (90 x 90 mm) at different speed of peeling (1, 10, 50, 100 and 200 mm/min). Then the adhesion values (G) were calculated from the measured pulling force (F_p) using equation *(1)* and were compared with the data sheet of the manufacturer (cf. Annex 14).

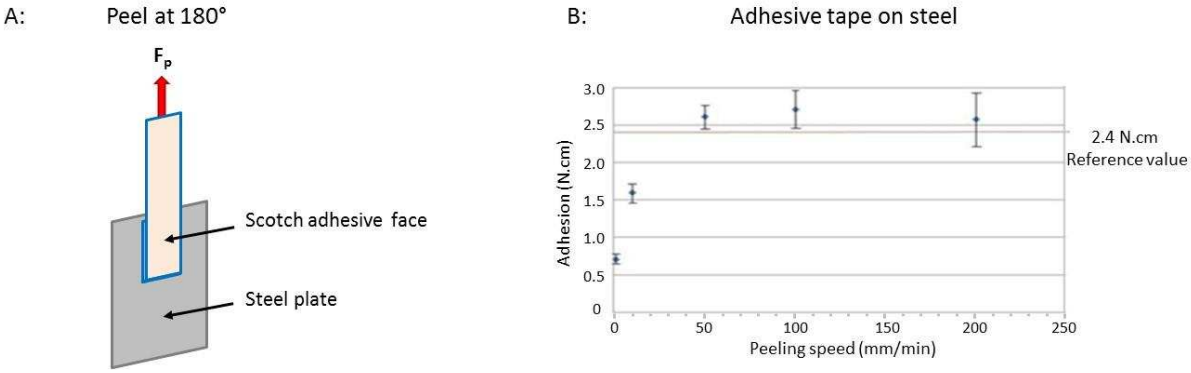

Figure 74: A: Illustration of the peeling test at 180° with adhesive tape. B: Adhesive tape adhesion as a function of peeling speed

As expected, the adhesion increased for the lowest peeling speeds from 1 to 50 mm/min and remained constant for higher speed from 50 to 200 mm/min. The adhesion measured was 2.65 N.cm, which is close to the data sheet value of 2.4 N.cm.

This experiment revealed the instability of the test for the highest speeds, which induced higher standard deviation on the adhesion measurement and confirmed the adhesion variation with the peeling speed (Figure 75).

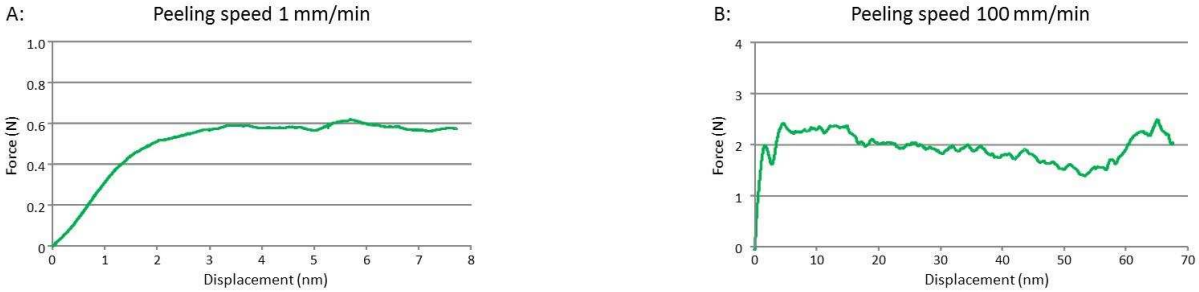

Figure 75: Peeling test curves at the peeling speed of A: 1mm/min and B: 100 mm/min

The best adhesion value estimation and the lowest standard deviation was found with a speed of 50 mm/min, this condition will be used for the peeling at 180° of the three layer systems even though the characteristics of the adhesive tape are very different from those of xylan.

3.3 Peeling test on three layer system

Two types of xylan were used as adhesive layer of the three-layer system: the arabino-xylan extracted from oat (commercial) and the homopolymer of xylan extracted from MFC from birch kraft pulp. The film MFC supported with coated calendered paper was fixed at 50 g/cm² of grammage. The three-layer systems were conditioned at different relative humidities prior to testing (Table 38).

Table 38: Peeling test conditions

Xylan sources	Relative Humidity	Failure types
Arabino-xylan (form oat)	95%	No-adhesion
	85%	Failure inside the MFC film + adhesive failure
	70%	Failure inside the MFC film
	room (46%)	Failure inside the MFC film
Xylan from birch kraft	95%	No-adhesion
	85%	Failure inside the MFC film + adhesive failure
	70%	Failure inside the MFC film

The peeling test performed at relative humidities below 70%, induced a failure inside the MFC film regardless the xylan source (Figure 76 A). This means that xylan adhesion on the cellulose film was stronger than the cohesion of the film itself. It was not possible to evaluate the adhesion between xylan and cellulose from these experiments as the measured pulling force corresponded to the intrinsic resistance of the MFC film (Figure 76 B).

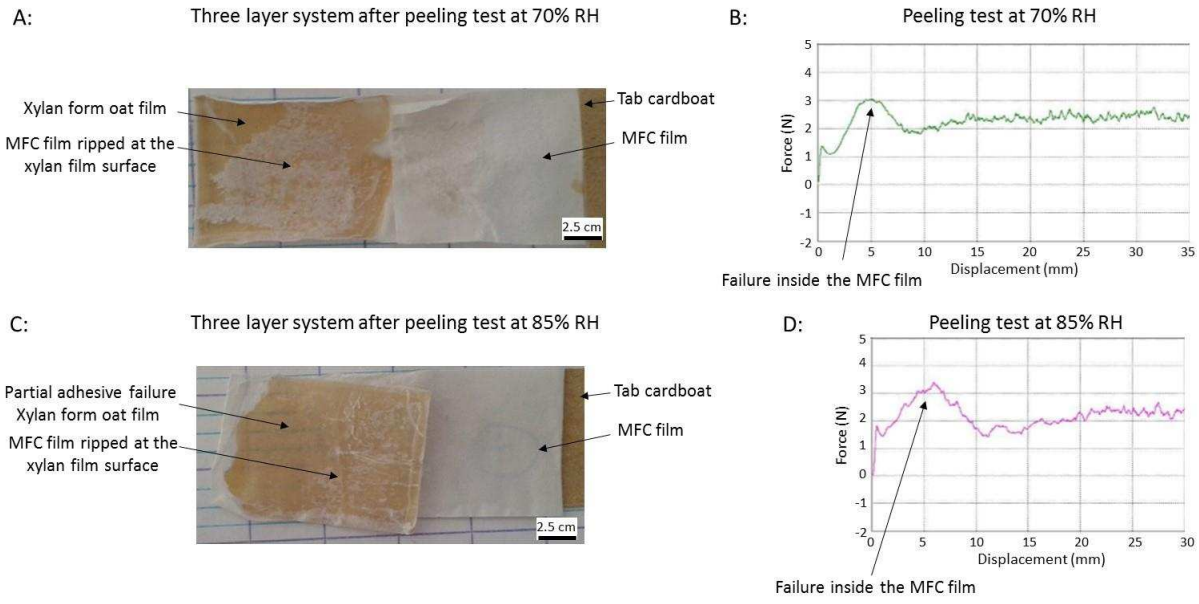

Figure 76: Photograph of three layer systems after peeling test at A: 70% of RH, C: 85%; Adhesion curve of peeling test at B: 70% of RH, D: 85% of RH

However, the maximum pulling force obtained in this test is around 3N (the peak force), which corresponds to a value of 4.5 N.cm (i.e. 45mJ/m²) that can be considered as a lowest limit of the adhesion value, so higher than the common adhesive that was tested in the preliminary study.

Comparison with values obtained in the literature is problematic as very few studies report quantitative measurement from adhesion tests. One has to mention Gustafsson *et al.* (2012) who measured directly from a JKR test the interaction between a model surface made of NFC multilayers on PDMS caps and model surface deposited on silica and found work of adhesion of around 50 mJ/m² for cellulose/glucomannan interaction, that is in good agreement with our own finding.
Double cantilever beam (DCB) method has been also used to evaluate adhesion in NFC–PLA laminates (Siro *et al.* 2013), but the author argued a discrepancy between their experimental values and commonly measured adhesion energies that comes from the interpenetration of PLA and NFC films.

Delamination between the xylan layer and the cellulose film has been observed with both xylan sources at 85% of relative humidity. However this adhesive failure was always mixed with failure inside the MFC film (Figure 76 C). It seems that in some part of the sample the adhesion between xylan and cellulose was still stronger than the cellulose film itself. The resulting pulling force (Figure 76 D) showed too high fluctuation to give a reliable value of adhesion.

At the relative humidity of 95%, the opposite situation was observed and the force was not detectable, as the xylan film detached almost spontaneously from the cellulosic substrate.

3.4 Conclusion on peeling test

The peeling test did not provide adhesion values between the xylan and cellulose film in the three-layer system as no pure adhesive failure was achieved. Nevertheless the following conclusions can be drawn:

1. The adhesion between xylan and cellulose was unexpectedly high at relative humidity below 85% RH. It was not possible to delaminate the system without any failure inside the cellulose film, but a minimal value of 4.5 N.cm was derived from the tests.
2. The humidity of the system dramatically reduces the adhesion. When equilibrated at 95% relative humidity, the peeling tests were unable to measure any adhesion between the layers.

The main limitation of the peeling test on the tensile instrument is the fixed angle at 180°. In this geometry the MFC film is more subjected to tear stress, to which MFC films are very sensitive. It was tried to limit this fragility by decreasing the thickness of the adhesive layer in order to decrease the dissipation within the xylan layer. The peeling tests were also performed on three layer system made of films of 25 g/cm² of grammage, to reduce the deformation of the MFC films. However, no improvement was observed and the failure still occurred inside the cellulosic film.

Casted films were also used to further reduce the film thickness in the three-layer system but the film was deteriorated when the xylan gel was deposited on it, due to its high water content. As the tensile strength of MFC film is higher than their shear strength, we implemented an experiment in which the solicitation of the cellulose films was more adapted to their properties. This was the shearing test as will be explained in the following section. Moreover, shearing is probably more representative of the forces exerted on the microfibrils during the homogenization process.

4. Shear test

4.1 Shear test principle

Shear test is a common method to compare adhesive resistance by applying deformation in the longitudinal direction and measuring the maximum force before failure *(F_m)* (Zhao and Kwon 2011). However, it is not possible to calculate an adhesion value from shearing test. Shear strength *(σ_{shear})* can be determined as:

$$\sigma\ shear = \frac{Fm}{L \times W} \qquad (2)$$

where (L x W) corresponds to the adhesion surface.

In this experiment, rigid supports are required to exert the shearing force on the substrate. The three-layer system was modified to avoid any deformation of the supports during test. First, the MFC films were glued on wood spatula, then xylan layer was deposited on surface of 18 x 20 mm (i.e 360 mm²). Wood spatulas were assembled by pairs with xylan layer inside and some wood wedges were added at both wood spatula ends to provide sample alignment in the clamp (Figure 77).

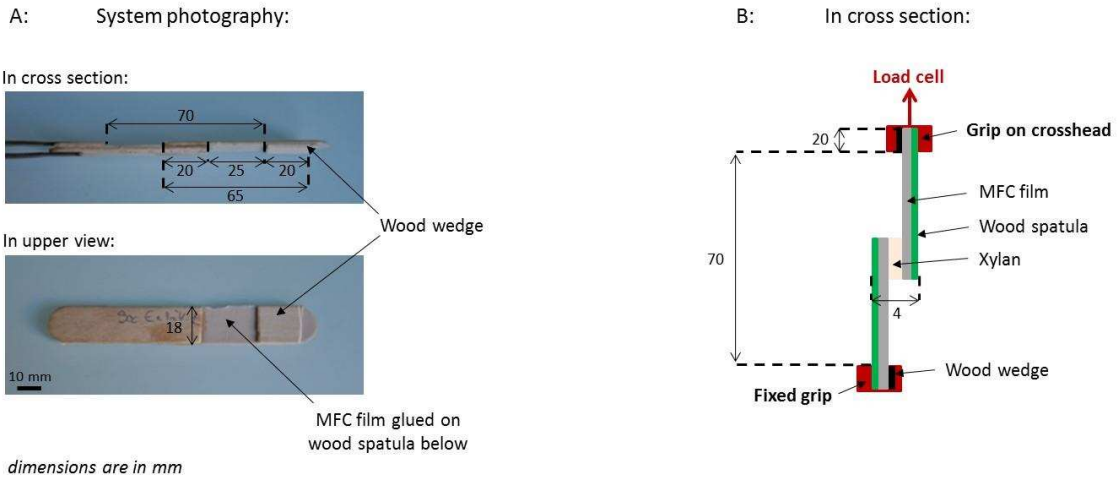

Figure 77: A: Photograph of a three-layer sample for shearing test and B: scheme of the experimental set-up used for the shearing test

To limit the influence of the roughness on the shear test result, MFC film with grammage of 100 g/m² was used to avoid transfer of roughness from the wood spatula to the film upper surface. The MFC films were fixed with epoxy resin on the wood spatula. Direct casting of MFC films on the spatula or wet film MFC (handsheet formers) deposited on wood spatula prior drying were also tried.

1. Casting:

The MFC suspension (at 0.5%) was poured on the wood spatula deposited at the bottom of a beaker. Then the water was able to evaporate at room temperature until the film formation on the upper layer of the spatula.

2. Handsheet formers:

The wet MFC mat obtained after filtration on handsheet formers was covered with wood spatula then placed in the sheet dryer.

The MFC films obtained by casting were highly heterogeneous (Figure 78 A). In the case of film formation in Petri dish, the adhesion of the cellulose film to the polystyrene surface was strong enough to compensate the retraction forces generated during water evaporation due to the capillary forces. The adhesion on wood spatula was probably lower due to its high surface roughness compared to the Petri dish surface.
When the wet film was dried in the sheet dryer with wood spatula at the surface, the MFC film was partially take- off from the spatula after the drying (Figure 78 B). Again, the roughness of wood spatula might lead to the reduced adhesion. Only the epoxy glue provided a homogenous, flat MFC film surface (Figure 78 C).

Figure 78: Illustration of MFC film fixed on wood spatula with A : casting, B : handsheet formers, C : epoxy glue

It is postulated that no contamination of the upper surface of the MFC film happened as MFC films are known to have high barrier properties with very low permeability even against oxygen permeation.

To perform a complete drying of the system prior the shearing test, the three layer systems were placed on the hot press at 120°C, 10 bars for 40 min then they were kept in desiccator with controlled relative humidity for further conditioning. Because the wood spatula were deformed during the first drying, they were pre-dried at 120°C for 40 min on the hot press prior the three layer system formation.

The glass transition temperature (Tg) of xylan was evaluated using modulated Differential Scanning Calorimetry (DSC) by Dr. Augstin Rios des ANDA. A Tg at 140°C was detected in the case of xylan extracted from MFC from birch kraft pulp (cf. Annex 15).

4.2 Shear test results

The hot melt glue (Technomelt cool 120 E3525101 from Henkel) with melting temperature of 130°C and viscosity (1050 mPa.s at 130°C) was chosen as a control sample. The results of the shearing test performed on the three layer system made with hot melt were compared with those obtained with the systems made with the two xylan types. The influence of the relative humidity on the shear strength was also studied.

Cohesive failure in xylan layer and hot melt layer was observed in all shearing test measurements at any humidity conditions (Table 39).

Table 39: Shearing test conditions

Intern layer	Relative Humidity	Failure types	Shear strength (σ_{shear})
Arabino-xylan (form oat)	15%	Cohesive failure	760 ± 50 MPa
	45%		540 ± 60 MPa
	95%		0-5 MPa
Xylan from birch kraft	15%	Cohesive failure	910 ± 10 MPa
	45%		650 ± 15 MPa
	95%		40 ± 5 MPa
Hot melt	15%	Cohesive failure	2200 MPa
	45%		1800 MPa
	95%		1400 MPa

The maximum force before failure was measured (Figure 79) and the shear strength was calculated with the equation *(2)*.

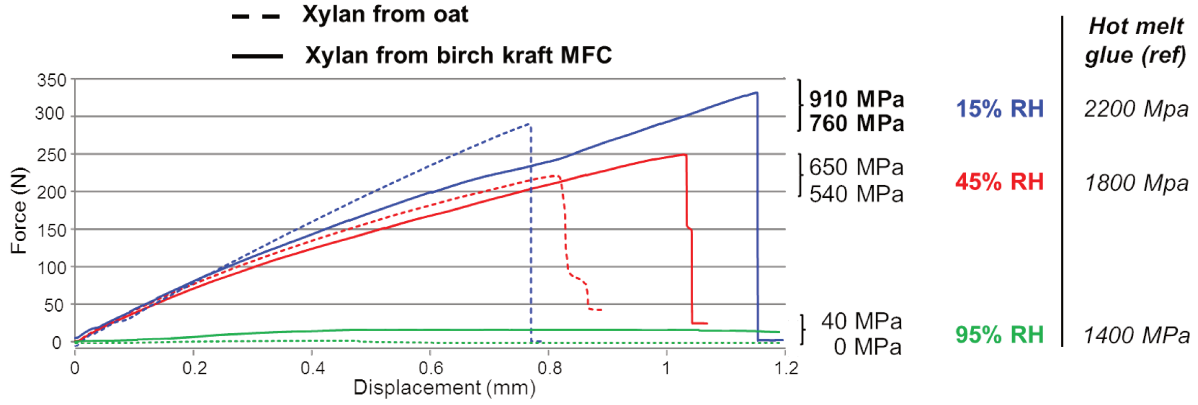

Figure 79: Shear curves at 15%, 45% and 95% of relative humidity (RH) with the three layer system made-of xylan from oat and xylan extracted from MFC from birch kraft pulp

For the xylan extracted from birch Kraft pulps, the measured shear strength values were found between 910 MPa and 650 MPa at 95% and 45 % RH respectively, a little more than twice as low as the commercial hot-melt glue.
Slightly lower shear strengths were observed for xylan, which contains arabinose side groups. Further studies are needed to check whether the presence of the side groups can reduce the shear strength.

However, for both substrates, the shear strength strongly fell down to very low values (for extracted xylan) or even closed to zero (for the commercial one) at 95% RH. This result is in agreement with the observations made for the peeling test, for which a strong transition in the behavior was observed between moderate and high relative humidity.

5. Conclusion on peeling and shear tests

The peeling test did not lead to an adhesion value between xylan and cellulose layer as the failure always occurred inside the MFC film and not at the interface between xylan and cellulose film. This is mainly because the peeling at 180° leads to high shear stress inside MFC, but is a clear sign of the high level of interaction between xylan and cellulose surfaces.

The shear test performed on the adapted three-layer system allowed us to compare xylan with hot melt glue, as the MFC films were much more resistant to this mode of solicitation. The values obtained with xylan were in the same range as the hot melt resin on dried systems. However the humidity has a strong influence on the systems and the shear strength was close to 0 at high humidity.

The results obtained in this chapter are too preliminary to draw any firm conclusions on the interaction of cellulose and xylan at the macroscopic level. The macroscopic model of xylan-cellulose interaction demonstrated the high affinity of xylan to cellulose in dry condition as the interfaces never failed even at high stress. However, major drawbacks come from the geometry of the solicitation. In the case of peeling test, the MFC films were solicited by tear forces, for which they were found to be very sensitive, while in the case of shearing tests it was the xylan cohesion that was the limiting factor. At high humidity, both substrates are highly plasticized and failed to support the deformation imposed during the test. It is an indirect sign that the adhesion between xylan and cellulose is very strong.

In order to be closer to the interaction of xylan with cellulose at the molecular level, nanocomposite film were formed with redispersed MFC and different xylan fractions. Tensile test experiments were performed on these composite films but the results still suffered from statistical fluctuations due to the heterogeneity of the film and to the low dispersibility of the MFC (cf. Annex 16).

Annex 12: Energy dispersive X-ray analysis (EDXA) on MFC film casting

Observation and surface analysis were performed on MFC films produced by casting with Scanning Electron Microscopy (SEM) and the EDXA.

The surface chemical composition of the film made of MFC rinsed with HCl 0.5 wt % solution then deionized water was compared with the one made of MFC in hard water.

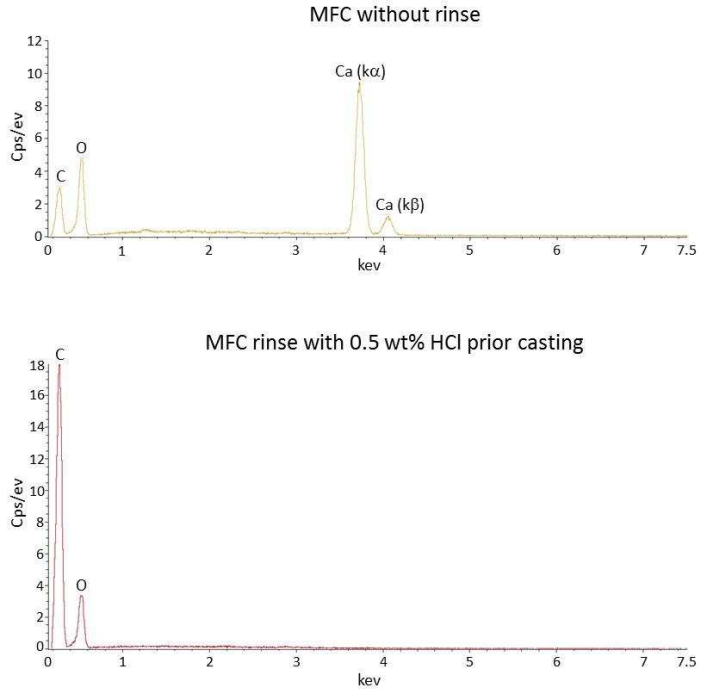

Figure 80: Energetic spectrum of the X-ray photons detected at the surface of the MFC films

The presence of calcium anion was detected on the film when the MFC was not rinsed with HCl solution. This explains the pollution, which is visible in SEM on the film surface.

Annex 13: Xylan non penetration control

1. Xylan grafting with fluorescein isothiocyanate isomer I

The fluorescein isothiocyanate isomer 1 (FITC) is a fluorescent label with different isomer according to the pH (Figure 81). For pH below 4.3 or above 6.6, the FITC exists under the carboxylic acid and the lactone isomer respectively while for pH between 4.3 and 6.6 both of isomers co-exist. The di-anionic lactone isomer which exists for pH ≥ 11, have been described in literature (Dong and Roman 2007; Nielsen *et al.* 2010) to provide good correlation between the FITC fluorescence and UV spectroscopy absorbance measurement.

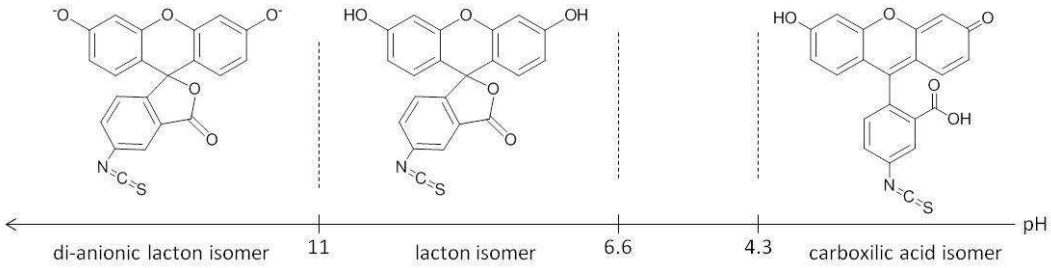

Figure 81: FITC isomers form with pH

Because xylan was not soluble in water, the freeze-dried xylan (550 mg, i.e. 3.7 10^{-3} mol of xylose) was dissolved in 150 mL of DMSO (i.e. concentration of 4 g/L) at room temperature in presence of 0.55 mL (i.e. 0.55 eq [Et_3N]/[OH]) of triethylamine (Et_3N, from Sigma Aldrich >99%) added in excess for full hydroxyl deprotonation (Figure 82). Then FITC was added with different concentrations: 0.3%, 1.25% and 5%.

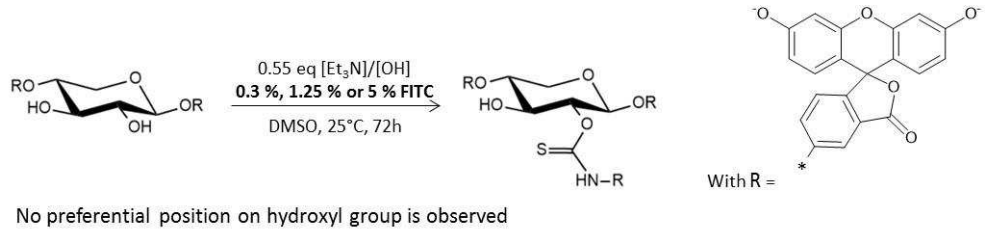

Figure 82: Reaction of xylan labelling with FITC

After keeping 72h at room temperature, the DMSO, Et_3N and the non-reacted FITC were removed by dialysis against water. A slightly yellow-orange solid was recovered after freeze-drying of the xylan precipitate in water.

2. Xylan substitution degree measurement with UV-vis spectroscopy

2.1 Calibration curve

Four FITC solutions (0.25 mg/L ; 0.5 mg/L ; 1.25 mg/L and 2.5 mg/L) were prepared by dilution of the initial FITC solution at 1.00 g/L in DMSO (10.0 mg in 10.0 mL with volumetric flask). Then 4 mL of each diluted FITC solutions were basified with triethylamine (4 µL) to provide the di-anionic FITC form.

A straight calibration curve (Figure 83) could be obtained by using the value at the maximum of absorbance of the FITC (λ= 521 nm).

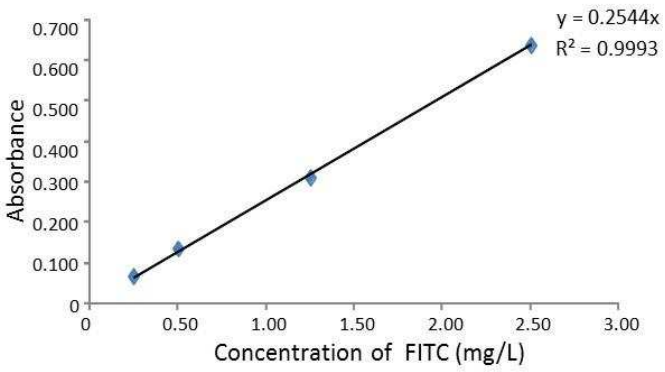

Figure 83: Calibration curve of FITC in DMSO

The data were performed by using a UV quartz cell with cover (dimension of 44.5 x 12.5 x 13.5 mm and layer thickness of 1 cm) and UV - visible spectrometer (Varian Carry-50 Bio). They were collected at the scan speed of 600 nm/min and a resolution of 1 nm. The blank was performed with a solution of 4 mL of DMSO with 4 µL of Et_3N.

2.2 Xylan substitution degree

The labeled xylan was dissolved in DMSO and the solution was basified with triethylamine to provide the di-anionic form of the FITC. Then the FITC contents measured by UV-vis absorbance were converted to percentage of FITC and degrees of substitution per hydroxyl group (i.e [FITC]/ [OH]) thanks to the following equations:

$$Percentage\ of\ FITC = \frac{Mass\ of\ FITC}{Mass\ of\ xylan} \times 100$$

$$[\mathrm{FITC}]/[\mathrm{OH}] = \frac{2 \times Mass\ of\ FITC / M\ FITC}{Mass\ of\ xylan\ /\ M\ xylose} \times 100$$

where the mass of FITC is deduced from the concentration of FITC determined with the calibration curve (Figure 83). Because, the FITC should not interfere with the cellulose - xylan interaction in the three layers systems, the xylan extracted from MFC from birch-kra-nd was grafted in presence with 0.3% of FITC. It was previously established with xylan from oat (commercial) that 0.3 % of FITC corresponded to the lowest substitution degree (Table 40).

Table 40: Degree of substitution of FITC per hydroxyl group on xylan

Xylan extracted from	Percentage of FITC introduced	Absorbance measure	Concentration of FITC grafted	Percentage of FITC grafted	Degree of substitution [FITC]/[OH]
oat	0.3 %	0.309	1.22 mg/L	0.07 %	0.05 %
oat	1.25 %	0.456	1.79 mg/L	0.18 %	0.14 %
oat	5.0 %	0.587	2.31 mg/L	0.54 %	0.42 %
MFC from birch kra-nd	0.3 %	0.071	0.28 mg/L	0.01 %	0.01 %

The DS of xylan extracted from MFC from birch-kra-nd was lower than the one of xylan from oat. The FITC might be also grafted on arabinose branches that are only present on xylan extracted from oat.

3. Fluorescence microscopy observation of three layers structure

Three layer structures were built with FITC labeled xylan according to the same protocol described for System 1 formation (section 6.2 in materials and methods). In order to obtain the fluorescence form of the FITC fixed on xylan, some sodium hydroxide (from VWR Chemical-analysis grade) solution at 1 g/L is added until pH 10 in the final water bath of xylan gel formation.

The three-layer system was then included in a matrix of resin (resin epoxy LR White) and semi-thin cross sections (1µm) were cut with ultra-microtome (Leica EM UC6) at CTP thanks to Christelle Boucherand and Caroline Duprat.
The cross sections were then examined with fluorescence microscopy (ZEISS- AXIO green A1) with FITC channel.

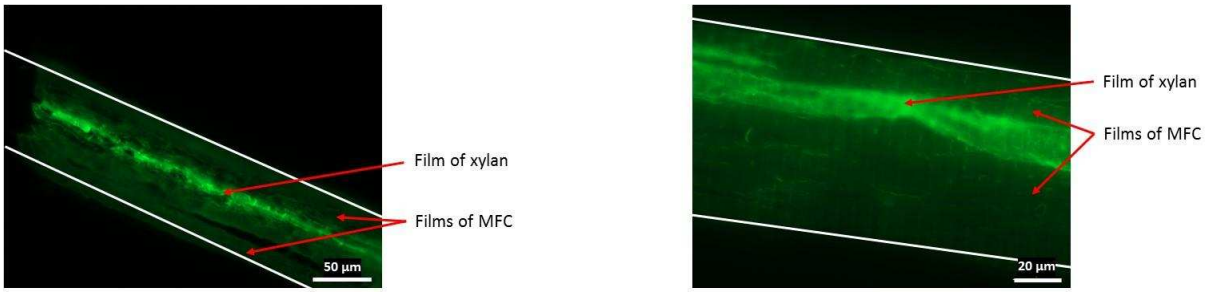

Figure 84: Cross section (1µm) of three-layer system labeled with FITC

The micrographs in Figure 84 show relatively well-defined three layers and with limited penetration of xylan into the MFC layers.

Annex 14: Technical informations on Tape AT-206

TECHNICAL DATA

Version 3

AT206 PVC Colour Coding Gaffa® Tape

General Description
A PVC Electrical Insulation Tape coated with pressure sensitive adhesive.

- Flame retardant
- Self-extinguishing
- Easy unwind
- Easy tear
- Conformable to awkward shapes
- Good abrasion resistance
- Water resistant in situ
- UV resistant
- Non-corrosive adhesive
- Wide colour range in stick packaging

Specification
Certification* to the following standards may be available on request.
BS EN 60454-3-1/Type 2.

Technical Details
Typical Values

Thickness	0.13mm
Breaking Load	26 N/cm
Elongation	180%
Adhesion	
Steel	2.4 N/cm
Self	2.1 N/cm
Water Extract	
pH	6.8
Conductivity Max	2mS/m
Electrical Properties	
B/down Voltage	8.0 kV
1 Min Proof Test	6.0 kV
Insulation Resist	10_{11} ohms
Cu Corrosion	No Staining
Flame Retardancy	Self extinguishing
RoHS compliant	Yes
Service Temperature	-5℃ to +70℃
Application Temperature	0℃ to +40℃
Storage Temperature	+12℃ to +25℃

*Standard charge for certificate: £25.00.

ADVANCE®

Afera

AFERA
Association des Fabricants Européens de Rubans Auto-Adhésifs.

Annex 15: DSC measurement on xylan

Differential Scanning Calorimetry (DSC) analysis was performed on freeze dried xylan extracted from MFC from birch kraft pulp. Samples (between 7 and 15 mg) were introduced in non-hermetic aluminum pans then temperature was increased from -80°C to 200°C with a slop of 10°C/min with the DSC from TA instruments Q 200.

Thanks to Agustin Rios de Anda, temperature-modulated mode was also used on xylan samples (freeze-dried and gel) with the DSC from TA instrument Q2000 in the Laboratoire des Polymères et Matériaux Avancés (LPMA Lyon).
The samples were heated from 0°C to 140°C with a heating rate of 3°C/min and temperature modulation of ±2°C every 60 s.

The glass transition (Tg) at 140°C was only observed with the DSC modulated mode.

A: DSC

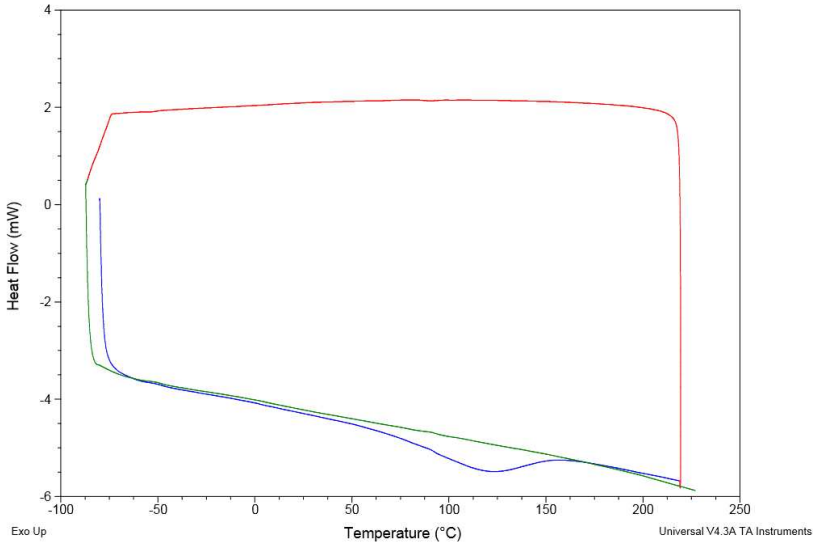

B: DSC modulated

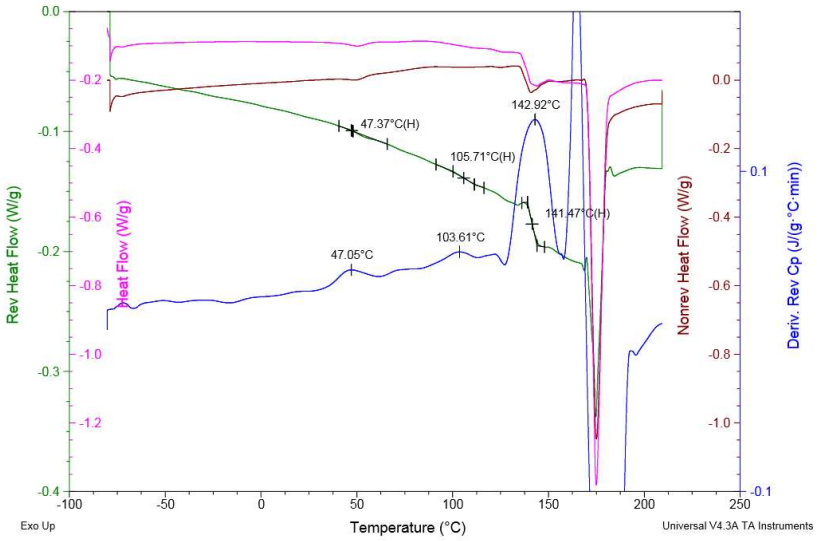

Figure 85: A : DSC and B: DSC modulated of xylan

Annex 16: Composite films and tensile test

MFC films were produced by casting with additional amount of xylan (extracted from birch kraft samples or commercial) to the MFC from birch kraft pulp after xylan extraction.

As it was described for the xylan re-adsorption experiment, the freeze-dried MFC samples were suspended in DMSO at the concentration of 5 g/L (i.e. 0.45 wt%) with varied amount of dried xylan and stirred for 20 h at room temperature then stirred with a double cylinder type disperser, Ultra-Turrax. The gel of MFC - xylan recomposed system was obtained with the same procedure than xylan gel formation detailed above. The suspension of MFC - xylan system was first placed 1h in contact of water bath thanks to the dialysis membrane. Then the DMSO was completely removed from the system by dialysis against deionized-water as it was described above.

The system was gently transferred from the Teflon hollow rectangle to the Petri dish surface and dried for 12h days under constraint (Figure 86).

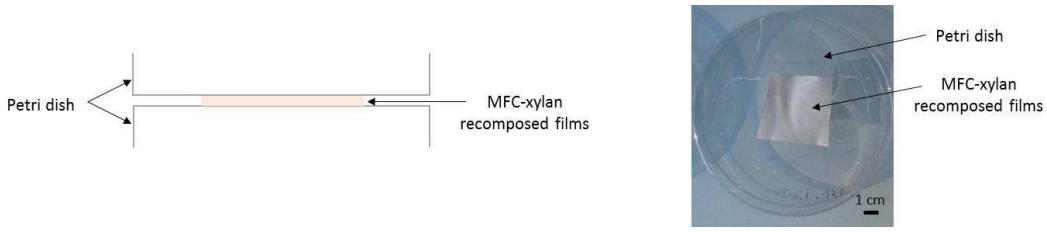

Figure 86: Illustration of recomposed film drying

The proportions of xylan added into the MFC suspension corresponded to the cellulose /xylan ratio where the xylan is in excess (0.39/1) or is fully adsorbed on cellulose surface (0.28/1) as established in Chapter 3.

General Conclusion and Perspectives

This project was at first devoted to bring some knowledge on the interactions between cellulose microfibrils and hemicelluloses, in order to better understand the key parameters on which one can play to help the microfibrillation process. For that, we designed an approach at different levels, including a classical characterization of the individual components and their interaction at the molecular level, mainly by solid state NMR, their simulation by molecular modeling at an atomistic level and the evaluation of their properties at the macroscopic level (General Introduction), in order to guide operating conditions on the pilot installation. Meanwhile, we discovered that a pure homopolymer of xylan can be extracted from the MFC produced from kraft pulps (Chapter 1). Models could be reconstructed and the role of the conformational change of xylan chains was studied by solid state NMR and atomistic simulations (Chapter 3), whereas macroscopic models were experimentally difficult to implement and the results dominated by the dissipation in the reconstructed system (Chapter 4). Incidentally, careful turbidity measurements of different MFC suspensions allowed us to point out the relationships between the quality of the dispersions and the properties of handsheets supplemented with MFC (Chapter 2). At the end of the work, the main results can be described as follow.

In Chapter 1, the hemicelluloses/cellulose compositions of the different MFC, in terms of wood species and pulping processes, were determined by sugar analysis. We observed that the main hemicellulose present in MFC from hardwoods is xylan and a mixture of xylan and glucomamans in the case of softwoods MFC. The hemicellulose/cellulose ratio is mainly affected by the pulping process and the MFC from kraft pulp have the highest hemicellulose content, close to 25%, while the hemicellulose content of MFC produced from sulfite pulp (dissolving pulp) is below 5%.
The MFC suspensions were also characterized by solid state NMR spectroscopy in wet and dry conditions. As already observed by Larsson *et al.* (1999) and Teleman, Larsson, and Iversen (2001), the xylan has a specific signature and the xylan content in MFC may be quantified by the peak intensity at 82 ppm on the NMR signal with wet MFC.

A protocol of xylan extraction, including a freeze-drying step in tert-buthyl alcohol and a redispersion in DMSO-LiCl 5 wt % was established from the MFC produced from never dried birch kraft pulp. The yield of extraction of 65% determined with the xylan mass isolated and sugar analysis performed on MFC after xylan extraction was confirmed by solid state NMR. Indeed a peak intensity diminution in the signal of MFC was observed at 82 ppm after xylan extraction and the change was in good agreement with the yield of 65% of xylan extracted.
The protocol was extended to MFC from spruce kraft and to pulp from birch kraft: refined and non-refined, dried and never dried. As the yield of 65% of extracted xylan is conserved, the particle size, the wood species and the drying history did not influence the xylan extraction.

The chemical composition of extracted xylan was determined from sugar analysis and liquid and solid state NMR. The extracted xylan contained in MFC and bleached pulp is a highly pure homopolymer of β-1,4 linked xylan, at the opposite of the xylan extracted from birch wood chips and xylan from oat (commercial) which contain 4-O-methylglucuronic acids and arabinose substitutions, respectively.
One of the hypotheses, explaining these results, is that the most accessible xylan substituted with arabinose and 4-O-methylglucuronic acids is eliminated from the wood pulp during the pulping process and the less accessible xylan is unsubstituted and could be only extracted using DMSO.

The polymerization degree of this extracted xylan was estimated by liquid NMR then was determined by viscosimetry and SEC-MALS measurement. The three methods converged to a DP of 75 corresponding to a molar mass of 10 000 g/mol which is in good correlation with the established DP of xylan in wood of 100 to 200 (Koshijima, Timell, and Zinbo 1965).

To complete the MFC characterization, the quality of the dispersion was evaluated in Chapter 2 by turbidity measurement performed with UV visible spectrometer. The turbidity of MFC suspensions had high correlation with their residual content in coarse elements, their paper reinforcement potential and the specific surface area measured with nitrogen adsorption on resulting aerogels.
The pulp drying history is the most impacting factors on the dispersion state in the case of low hemicellulose content. Indeed the highest turbidity level was observed for the MFC from sulfite dried pulp while the MFC from sulfite never dried pulp exhibit the lowest turbidity level whereas the MFC from kraft pulp (higher hemicellulose content) were not influenced by the pulp drying. Furthermore good correlations were found between the dispersion level evaluated with turbidity and the specific surface area of MFC. The lowest turbidity corresponded to the highest specific surface.

These results were compared with fibers and fines content in MFC suspensions and with MFC potential as a strengthening agent in handsheets of unrefined fibers. This comparison revealed a strong correlation between the aggregation level of MFC, represented by the turbidity and the specific area measurement, and the mechanical resistance. The better tear and tensile indexes of handsheets were provided by the addition of the most dispersed MFC with lowest fines and fibers content.

The turbidity measurement and the specific surface area are global methods that require little preparation to characterize the dispersion level of MFC and predict their impact as additive on paper mechanical properties. They might be used as standard methods for the MFC characterization in complement of MorFi analysis and mechanical tests.

In Chapter 3, the cellulose-xylan interactions were first studied by combination of solid state NMR, specific surface area measurement and atomistic simulation.

The isolated xylan, in the wet state, exhibited a typical solid-state NMR spectrum of three-fold helix with a C4 contribution at 75 ppm whereas the MFC before xylan extraction had a supplementary component at 82 ppm.
The putative conformational adaptation of xylan in presence of cellulose from a bulk-like 3-fold conformation to a presumed cellulose-like 2-fold one was confirmed by solid-state NMR spectroscopy on biomimetic models made of xylan readsorbed on MFC with varied proportions. By sequential xylan re-depositions, coupled with MFC specific area measurements, it was possible to show that the conformational adaptation was only limited to the first adsorbed layer, where xylan was in direct contact with the cellulose surface.
With atomistic MD simulation, we followed the adsorption behavior of xylan molecules of DP 10 on various cellulose surfaces and found that the presence of the surface could stabilize the 2-fold conformation of the xylan molecules in aqueous environment. The adsorbed xylan was preferentially arranged with its chain axis parallel to that of cellulose and formed hydrophobic stacking structure with the xylan pyranosyl mean planes stacked parallel to those of the cellulose crystal surfaces.

A pulling test was proposed further in this work and consisted of pulling out the xylan chain from the cellulose surface where it was adsorbed. The energy of adhesion between the two parts may be followed during the pulling tests and varied with the cellulose surface.

The highest adhesion force was observed for xylan in 2_1 conformation on hydrophobic cellulose surface (100) and corresponded to 9 kJ /xylose residue. Because we still do not understand the thermodynamics behind the pull code used in this simulation, further study is needed to confirm these first results. It might be a powerful technique to study interaction between xylan and cellulose and it might be also extended to study the influence of xylan branches on the adsorption on cellulose and other hemicellulose adsorption such as glucomannan.

A third model was designed in Chapter 4 to study the cellulose xylan interaction and adhesion using mechanical test.

A three layer system was built with two cellulose films and one of xylan inserted between them. The cellulose films were obtained by filtration of MFC from pine sulfite pulp with handsheet formers and drying with sheet dryer. Then a xylan gel in water previously obtained from the dialysis against water of a DMSO-xylan solution, was deposited at the cellulose film surface. The ensemble was covered with a second cellulose film then dried.

Peeling tests at 180° were performed on the three-layer structure after conditioning at various relative humidities. Failure inside the MFC film were always obtained for relative humidity (RH) ≤ 85% and complete loss of adhesion between the system layer were observed for RH equal of 95%.
Because the peeling test at 180° was testing the MFC film along its tear resistance which is lower compared to its shear one, the three layer system was modified and adapted to a shearing test. The MFC was supported on wood spatula and two of them were assembled with xylan film in the middle. The shearing test did not provide adhesion measurement but it was used to compare the resistance of the three-layer system with a hot melt glue at different relative humidity.
At moderate relative humidity, the shear strength of the hot melt glue system is twice time higher than the three layer system made with xylans in the same range. However the humidity condition highly affected the resistance of the three-layer system. The shear strength is close to zero at 95% which revealed the intrinsic plasticization of xylan with water.

This model might not be the most accurate as the main factors governing the adhesion were shown to come from the resistance of the bulk. However it provided some comparison with standard glue on a macroscopic model with established mechanical test, at least in the shearing configuration.
The interaction of xylan with cellulose at the microfibrils level has been contemplated but was hampered by the insolubility of xylan in water, which hampers a classical film casting experiments. Indeed the spectacular adaptation of the conformation of the xylan chain on the cellulose surface, and its intrinsic resistance to water is appealing in terms of material design, to obtain strong and water resistant nanomaterials, as wood can be, but difficult to implement experimentally.

In order to stick to the initial objective of facilitating and enhancing the microfibrillation process and in view of the above results, we intended to explore the potentiality of the use of xylanase that could weaken this strong hemicellulose glue thus facilitating the liberation of microfibrills. The results of these attempts have been gathered in the following section, as a conclusive chapter.

Conclusion Chapter

Xylanase pre-treatment before MFC production

Regarding the results on the interaction between hemicelluloses and cellulose in the fiber wall, it was underlined that presence of xylan in the initial pulp had a strong influence on the resulting MFC quality (Meyer *et al.* 2016; Tapin-Lingua, Meyer, Petit-Conil 2013). According to correlations found between mechanical resistance of MFC, turbidimetry and specific surface measurements, the presence of xylan clearly helps in the separation of cellulose microfibrils by protecting them against the irreversible hornification occurring during pulp drying.
Besides, xylan extracted from kraft pulp-based MFC was a particular homopolymer of xylose which strongly interact with cellulose surface according to experiments carried out on three layer models and atomistic simulation. When xylan is in presence of cellulose, it adopts a particular conformation of 2-fold helix.

Thanks to these observations, a never dried birch kraft pulp was selected (rich in xylan) and xylanase reaction was proposed as pulp pretreatment prior to homogenization to weaken xylan structure and facilitate the liberation of microfibrils from the fiber wall.
This new pretreatment was tested and compared with the common endoglucanase pre-treatment. The synergistic effect of both enzymes was also evaluated.
The characterization methods developed during the previous parts of this work as solid state NMR and turbidimetry analyzes will be applied on this MFC production.

1. MFC production

MFCs were produced from a never-dried birch Kraft pulp provided by Stora Enso according to conventional methods adapted by the Centre Technique du Papier, from the method described by Pääkko *et al*. (2007).
Endoglucanase treatment was performed with FiberCareR® from Novozymes and xylanase treatment with Xylanase2##SPW from Metgen:

1. Mechano-enzymatic treatment

For each treatment, 5 kg of o.d. pulp was rehydrated in a pulper at 4.5% consistency for 10 minutes. Then four different treatments were carried out before refining: water, endoglucanase 2.5 L/t, xylanase 10 L/t and a mix of both previous enzymes. The enzymatic treatments were applied for 1h at pH 5 and 50°C. At the end of the reaction time, a 12” single disk refining was performed to reach the targeted fiber length of 300 µm of the pre-treated suspension before homogenization. The refined pulp was then boiled for 10 minutes to inactivate the residual enzymes.

2. Homogenization

The four different pre-treated fiber suspensions were then diluted to 2% consistency and processed with a high pressure homogenizer (NS006 apparatus from GEA Niro Soavi). This treatment was performed in one pass at 1000 bar followed by 4 passes at 1500 bar.

2. Chemical composition of MFC

2.1 Sugar analysis

The composition in five sugar residues namely: glucose, xylose, mannose, arabinose and galactose and the yield of hydrolysis of the MFC from birch bleached kraft pulp pretreated with the different enzymatic pre-treatments are presented in Table 41.

The normalized sugars content is calculated as:

$$[Glucose\ normalized] = \frac{[Glucose] \times 100}{Yield\ of\ hydrolysis}$$

Table 41: Sugar composition of the MFC from birch kraft pulp.

	MFC from birch kraft pulp			
Pre-treatment	***Without enzyme***	***Endoglucanase***	***Endoxylanase***	***Endoxylanase and Endoglucanase***
Glucose (%)	73.2	72.0	73.1	70.5
Xylose (%)	20.6	21.8	20.8	21.6
Mannose (%)	0.0	0.0	0.0	0.0
Arabinose (%)	0.0	0.0	0.0	0.0
Galactose (%)	0.0	0.0	0.0	0.0
Yield of hydrolysis (%)	93.8	93.8	93.9	92.1
Normalized:				
Glucose (%)	78.0	76.8	77.8	76.5
Xylose (%)	**22.0**	**23.2**	**22.2**	**23.5**
Mannose (%)	0.0	0.0	0.0	0.0
Arabinose (%)	0.0	0.0	0.0	0.0
Galactose (%)	0.0	0.0	0.0	0.0

Regardless the type of enzyme used before refining, the xylose content is around 23%. It is in good correlation with MFC produced form never-dried birch bleached kraft pulp where the xylose content was 23.7% (cf. Chapter 1). Applied xylanase and endoglucanase charges did not lead to more sugar hydrolysis.

2.2 Solid State NMR analysis

Solid state NMR analysis was performed on the four wet MFC samples (Figure 87). As the chemical composition of MFCs are not impacted by the pre-treatment used for the pulp refining, the spectra of the different MFCs are quite identical.

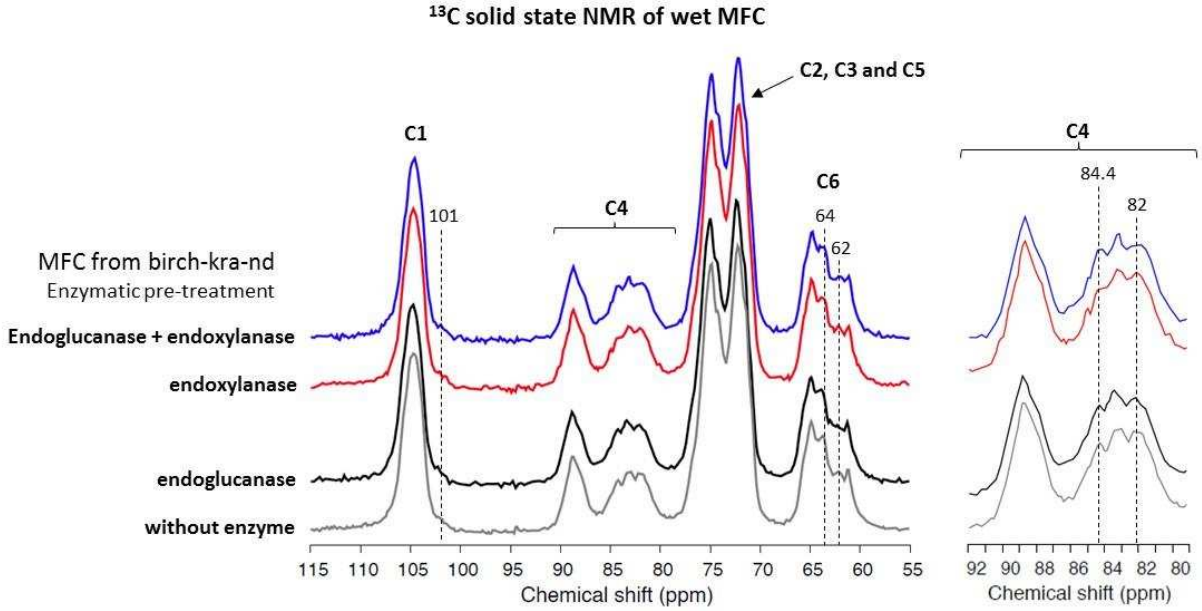

Figure 87: MFC morphology and structure linked to enzymatic pre-treatment.

The conformation and crystallinity of the MFCs are not modified by the enzymatic pre-treatment regardless of the enzyme chosen.

3. Energy consumption

The impact of the enzymatic pretreatments was first evaluated on the energy consumed during refining (Figure 88 A) and in total (refining + homogenization) (Figure 88 B).

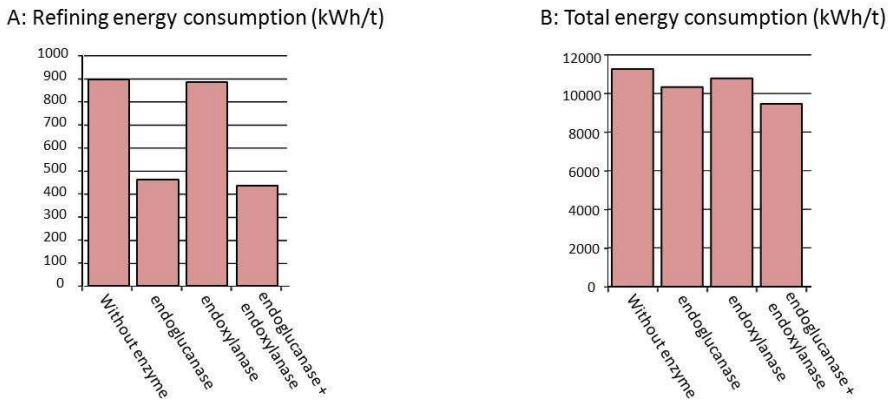

Figure 88: A: Energy consumption after refining of the different pre-treated pulps, B: Total energy consumption after refining and MFC production from the different pre-treated pulps.

As it was already demonstrated, endoglucanase led to a drastic energy savings during refining. Half of the electricity was saved after endoglucanase treatment compared to the reference pulp. On the contrary, xylanase treatment alone showed no effect on the behavior of the fibers into the refiner and the final energy was not impacted by this enzyme. When a combination of both enzymes was applied, refining energy was close to endoglucanase alone.

Concerning the total energy consumption after refining and homogenization at 2% consistency, a clear synergistic effect of both enzymes was noticed. It represented 870 kWh/t (8%) of energy saved compared to endoglucanase treatment alone and even twice compared to the reference pulp with a reduction of 1800 kWh/t (17%). This additional benefit of xylanase treatment was mainly due to a higher flow rate into the homogenizer due to less viscous suspension. An increase in initial pulp consistency could be envisaged to enhance again some energy savings.

4. MorFi analysis and optical microscopy

To evaluate the impact of the enzymatic pretreatments on MFCs quality, an indirect measurement consists in quantifying the residual coarse elements (residual fines and fibers) into the homogenized suspensions thanks to morphological analysis (Figure 89).

Because the MFC sizes are too small to be detected by the optical camera of the MorFi analyzer, it was not possible to directly count the number of MFCs after the homogenization. However, it is possible to determine the residual number of fibers (elements with a length > 80 µm) and fines (elements with a length< 80 µm) into the MFC suspensions.

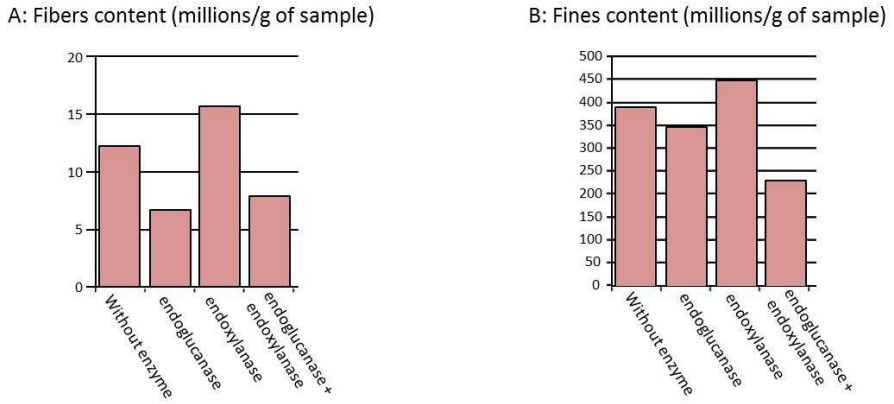

Figure 89: Residual fibers (A) and fines content (B) into MFC suspensions produced from different pre-treated pulps.

The residual fibers content into MFC suspensions (Figure 89 A) was directly impacted by the endoglucanase action through the fiber wall. Compares to the MFCs produced from pulp refined without enzymatic pre-treatment, the fibers content was divided by two when endoglucanase was used before pulp refining (from 12 to 5 million/g). Some cuttings occurred into the cellulose chains, leading to an easier separation of the microfibrils from the fiber wall into the homogenizer. This residual fibers content was very low and an additional xylanase treatment did not affect this value. It was interesting to note that the xylanase pretreatment alone was not sufficient efficient for decreasing the fibers content, indicating that a cellulase pretreatment was needed for MFC production.

On the contrary, xylanase treatment combined with endoglucanase one has a positive effect on the residual fines content. The final MFC suspension contained 30% fewer fines than the endoglucanase treatment alone, traducing a better homogeneity of the suspensions and a higher content of nanoscale elements.

Xylanase pretreatment may facilitate the endoglucanase penetration into the fiber walls by cutting the xylan chain around the fibers. As the endoxylanase had no effect towards the cellulose structure, it was expected to see no improvement in the microfibrillation efficiency when it was used as pretreatment alone.

Figure 90 presents some light microscopy examinations of the different elements observed into the MFC suspensions after 5 passes into the homogenizer. Images were in line with MorFi analyzes highlighting the presence of long fibrillary fines when no enzymatic pretreatment (A) or with a xylanase one alone (C) was carried out. On the contrary, endoglucanase pre-treatment or endoglucanase + xylanase pretreatments led to more homogeneous suspensions, richer in nanoscale elements with smaller fines elements.

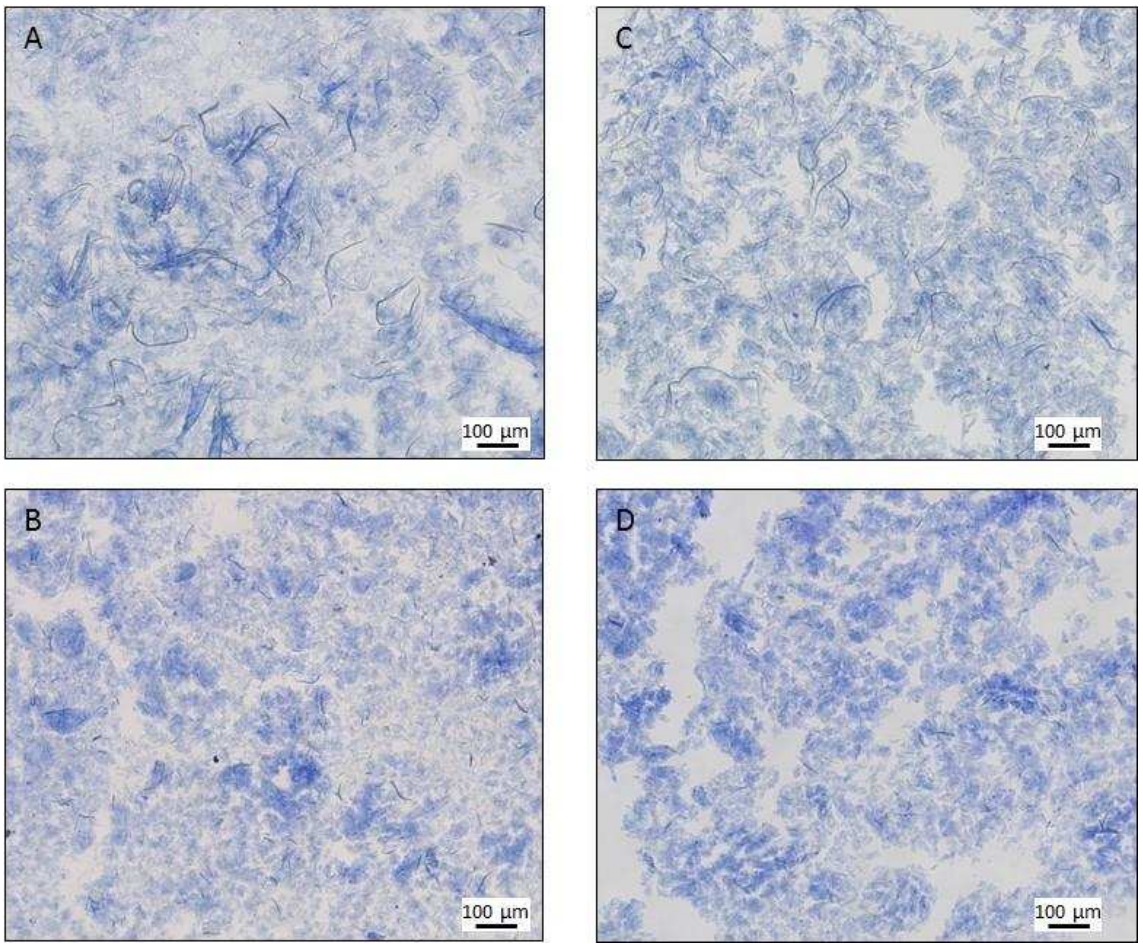

Figure 90: Microphotographs of the MFC suspensions from different pulp pretreatments after the fifth homogenizing pass at 1500 bar A: without enzyme, B: endoglucanase, C: xylanase, D: endoglucanase + xylanase.

5. Turbidity analysis

It was previously visualized that pulp drying history and hemicelluloses content in MFC had a strong influence on the turbidity of MFC suspension. When the hemicelluloses content is low, the drying history has a strong impact. For the reduced turbidity (λτ/c), normalized against solid content (c) as a function of the wavelength (λ), MFC from sulfite dried pulps showed concave increasing curve while all others showed convex decreasing curves and the value at 800 nm was identified as a good number of the quality of the dispersions (Figure 58).

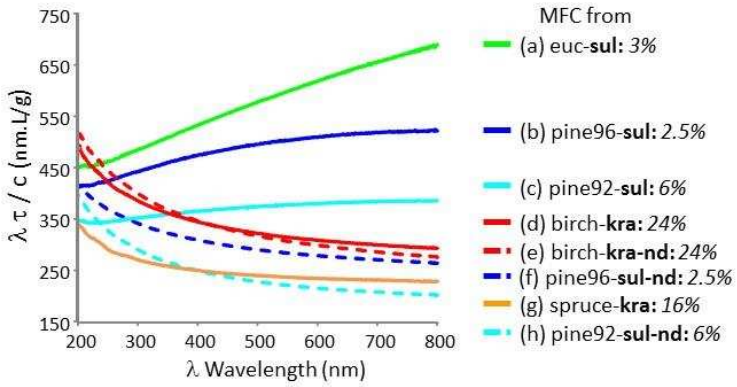

Figure 91: Reduced turbidity as a function of λ for the various MFC and corresponding hemicelluloses' content (%) cf Chapter 2.

In the case of this experiment, the MFCs were produce from never-dried birch bleached kraft pulp with highest hemicelluloses content (24%) and the endoxylanase pre-treatment may decrease the xylan content and influence the MFC aggregation level.

Figure 92 shows that no concave curves were obtained and all MFC curves were convex regardless the pre-treatments.

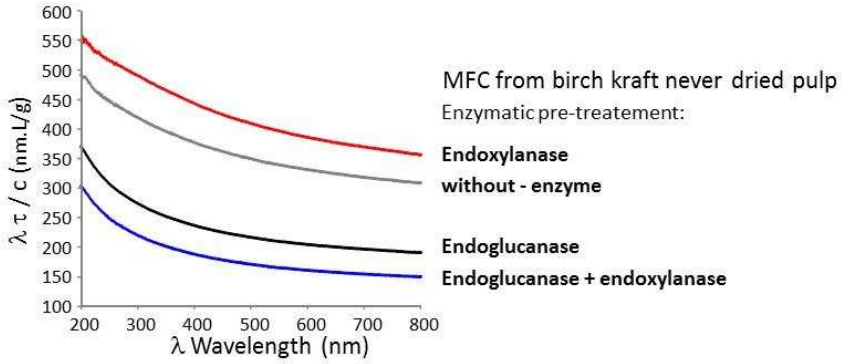

Figure 92: MFC pulp aggregation linked to enzymatic pre-treatments.

However, the turbidity level of the MFC suspension was in good correlation with the fibers and fines contents. Indeed, the MFCs produced from pulp refined without enzyme or with endoxylanase showed the highest turbidity and the MorFi analyzes observed the highest fibers and fines contents. On the opposite, the MFCs produced from pulp refined with endoglucanase alone or mixed with endoxylanase had the lowest turbidity and the lowest fibers content.

The diminution of the fines content, observed by MorFi analysis in the MFCs resulting from the pulp refined with endoxylanase and endoglucanase together, was in good correlation with the lowest reduced turbidity.

6. Conclusion

The chemical composition of the MFCs, according to solid state NMR and sugars analysis, were not influenced by the enzymatic pre-treatment of the pulp.

Different residual fibers and fines contents were observed with MorFi analyzes and influenced the MFC suspension turbidity. The endoxylanase pre-treatment alone did not improve the microfibrillation process as the fibers content and the turbidity level were higher than those produced without enzymes. However, the lowest fines content and the lowest turbidity level were observed when the endoglucanase was mixed with endoxylanase.

Consequently, this new pre-treatment seemed promising as this better MFC quality was obtained with a reduction of 8% of the energy compared to the conventional endoglucanase treatment. Deeper investigations should be done to characterize the MFCs produced in terms of mechanical resistance for example and to understand the right role of each enzyme. Based on these results, a sequential pre-treatment could be envisaged to reveal the best potential of each enzyme that was not optimized so far.

References

Ahola, S., M. Österberg, and J. Laine. 2008. “Cellulose Nanofibrils - Adsorption with Poly(amideamine) Epichlorohydrin Studied by QCM-D and Application as a Paper Strength Additive.” *Cellulose* 15 (2): 303–14.

Ahola, S., J. Salmi, L. S. Johansson, J. Laine, and M. Österberg. 2008. “Model Films from Native Cellulose Nanofibrils. Preparation, Swelling, and Surface Interactions.” *Biomacromolecules* 9 (4): 1273–82.

Åkerholm, M., and L. Salmén. 2001. “Interactions between Wood Polymers Studied by Dynamic FT-IR Spectroscopy.” *Polymer* 42 (3): 963–69.

Alemdar, A., and M. Sain. 2008. “Isolation and Characterization of Nanofibers from Agricultural Residues – Wheat Straw and Soy Hulls.” *Bioresource Technology* 99 (6): 1664–71.

Ankerfors, M., T. Lindström, H. Miroslav, and S. Hainong. 2009. “Composition for Coating of Printing Paper." WO 2009123560 A1.

Ankerfors, M. 2015. “Microfibrillated Cellulose: Energy-Efficient Preparation Techniques and Applications in Paper.” Stockholm, Sweden: PhD, KTH Royal Institute of Technology.

Aulin, C, M. Gällstedt, and T. Lindström. 2010. “Oxygen and Oil Barrier Properties of Microfibrillated Cellulose Films and Coatings.” *Cellulose* 17 (3): 559–74.

Aurell, R. 1965. “Increasing Kraft Pulp Yield by Redeposition of Hemicelluloses.” *TAPPI Journal* 48 (2): 80-84.

Aurell, R., and N. Hartler. 1965. “Kraft Pulping of Pine Part 1. The Changes in the Composition of the Wood Residue during the Cooking Process.” *Svensk Papperstidning* 67: 43-49.

Bendahou, A., H. Kaddami, and A. Dufresne. 2010. “Investigation on the Effect of Cellulosic Nanoparticles ’ Morphology on the Properties of Natural Rubber Based Nanocomposites.” *European Polymer Journal* 46 (4): 609–20.

Beneventi, D., D. Chaussy, D. Curtil, L. Zolin, C. Gerbaldi, and N. Penazzi. 2014. “Highly Porous Paper Loading with Microfibrillated Cellulose by Spray Coating on Wet Substrates.” *Industrial and Engineering Chemistry Research* 53 (27): 10982–89.

Bergnor-Gidnert, E., P. E. Tomani, and O. Dahlman. 1998. “Influence on Pulp Quality of Conditions during the Removal of Hexenuronic Acids.” *Nordic Pulp and Paper Research Journal* 13(4): 310-16.

Bhattacharya, D., L. T. Germinario, and W. T. Winter. 2008. “Isolation, Preparation and Characterization of Cellulose Microfibers Obtained from Bagasse.” *Carbohydrate Polymers* 73 (3): 371–77.

Bosmans T. J., A. M. Stepan, G. Toriz, S. Renneckar, E. Karabulut, L. Wågberg, and P. Gatenholm. 2014. “Assembly of Debranched Xylan from Solution and on Nanocellulosic Surfaces.” *Biomacromolecules* 15 (3): 924–30.

Braunauer, S., P.H. Emmett, and E. Teller. 1938. “_Adsorption of Gases in Multimolecular Layers.” *Journal of the American Chemical Society* 60 (2): 309–19.

Bromley J. R., M. Busse-Wicher, T. Tryfona, J. C. Mortimer, Z. Zhang, D. M. Brown, and P. Dupree. 2013. "GUX1 and GUX2 Glucuronyltransferases Decorate Distinct Domains of Glucuronoxylan with Different Substitution Patterns." *Plant Journal* 74 (3): 423–34.

Buchert, J., A. Teleman, V. Harjunpää, M. Tenkanen, L. Viikari, and T. Vuorinen. 1995. "Effect of Cooking and Bleaching on the Structure of Xylan in Conventional Pine Kraft Pulp." *TAPPI Journal* 78 (11): 130-52.

Busse-Wicher, M., N. J. Grantham, J. J. Lyczakowski, N. Nikolovski, and P. Dupree. 2016. "Xylan Decoration Patterns and the Plant Secondary Cell Wall Molecular Architecture." *Biochemical Society Transactions* 44 (1): 74–78.

Carr, M. E, and J. Hermans. 1978. "Size and Density of Fibrin Fibers from Turbidity." *Macromolecules* 11 (1): 46–50.

Carrilho E., A. W. Martinez, and G. M. Whitesides. 2009. "Understanding Wax Printing: A Simple Micropatterning Process for Paper-Based Microfluidics." *Analytical Chemistry* 81 (16): 7091–95.

Chen P. 2013. PhD thesis "Simulation des Cristaux de Cellulose par Dynamique Moléculaire." Joseph Fourier Université, Grenoble, France.

Chinga-Carrasco, G. 2011. "Cellulose Fibres, Nanofibrils and Microfibrils: The Morphological Sequence of MFC Components from a Plant Physiology and Fibre Technology Point of View." *Nanoscale Research Letters* 6 (417): 1-7.

Chinga-Carrasco, G., N. Kuznetsova, M. Garaeva, I. Leirset, G. Galiullina, A. Kostochko, and K. Syverud. 2012. "Bleached and Unbleached MFC Nanobarriers: Properties and Hydrophobisation with Hexamethyldisilazane." *Journal of Nanoparticle Research* 14 (12): 1–10.

Creton, C., and M. Ciccotti, 2016. ''Fracture and Adhesion of Soft Materials: A Review,'' *Reports on Progress in Physics* 79, (4): 046601

CTP. 2015. Procédé et dispositif de fabrication d'un matériaux stratifié comprenant une couche de cellulose fibrillée, issued 2015.B248470-D34495FD

Dahlman O., J. Sjöberg, U. B. Jansson, and P. O. Larsson. 2003. "Effects of Surface Hardwood Xylan on the Quality of Softwood Pulps." 18 (3):310-15.

Danielsson S., and M. E. Lindström. 2005. "Influence of Birch Xylan Adsorption during Kraft Cooking on Softwood Pulp Strength." *Nordic Pulp and Paper Research Journal* 20 (4): 436–41.

Deepa, B., E. Abraham, B. M. Cherian, A. Bismarck, J. J. Blaker, L. A. Pothan, A. L. Leao, S. F. de Souza, and M. Kottaisamy. 2011. "Structure, Morphology and Thermal Characteristics of Banana Nano Fibers Obtained by Steam Explosion." *Bioresource Technology* 102 (2): 1988–97.

Del Nobile, M. A., P. Fava, and L. Piergiovanni. 2002. "Water Transport Properties of Cellophane Flexible Films Intended for Food Packaging Applications." *Journal of Food Engineering* 53 (4): 295–300.

Dinand, E., H. Chanzy, and M. R. Vignon. 1999. "Suspensions of Cellulose Microfibrils from Sugar Beet Pulp." *Food Hydrocolloids* 13 (3): 275–83.

Doblin, M. S., I. Kurek, D. Jacob-Wilk, and D. P. Delmer. 2002. "Cellulose Biosynthesis in Plants: From Genes to Rosettes." *Plant and Cell Physiology* 43 (12): 1407–20.

Dong, S., and M. Roman. 2007. “Fluorescently Labeled Cellulose Nanocrystals for Bioimaging Applications.” *Journal of the American Chemical Society* 129 (45): 13810–11.

Dupree, R., T. J. Simmons, J. Mortimer, D. Patel, D. Luga, S. P. Brown, and P. Dupree. 2015. “Probing the Molecular Architecture of *Arabidopsis thaliana* Secondary Cell Walls Using Two- and Three-Dimensional ^{13}C Solid-State NMR Spectroscopy.” *Biochemistry* 54 (14): 2335-45.

Ebringerová, A., and T. Heinze. 2000. “Xylan and Xylan Derivatives - Biopolymers with Valuable Properties, 1: Naturally Occurring Xylans Structures, Isolation Procedures and Properties.” *Macromolecular Rapid Communications* 21 (9): 542–56.

Ebringerová, A., Z. Hromádková, and T. Heinze. 2005. “Hemicellulose.” *Advances in Polymer Science* 186: 1–67.

Edgar, C.D. and D. G. Gray. 2003 “Smooth model cellulose I surfaces from nanocrystal suspensions.” *Cellulose*, 10 (4): 299- 306

Eronen, P., M. Österberg, S. Heikkinen, M. Tenkanen, J. Laine. 2011, “Iteractions of structurallly diferent hemicelluloses with nanofibrillar cellulose.” *Carbohydrate Polymers* 86 (3): 1281-90

Esser, A. 2012. “Method for Producing Paper, Paperboard and Carboard Having High Dry Strength" US 20120205065 A1.”

Ferri, F., G. Re Calegari, M. Molteni, B. Cardinali, D. Magatti, M. Rocco, and Dipartimento. 2015. “Size and Density of Fibers in Fibrin and Other Filamentous Networks from Turbidimetry: Beyond a Revisited Carr−Hermans Method, Accounting for Fractality and Porosity.” *Macromolecules* 48: 5423–32.

Fulmer, G. R, A. J. M. Miller, N. H. Sherden, H. E. Gottlieb, A. Nudelman, B. M. Stoltz, J. E. Bercaw, and K. I. Goldberg. 2010. “NMR Chemical Shifts of Trace Impurities: Common Laboratory Solvents, Organics, and Gases in Deuterated Solvents Relevant to the Organometallic Chemist.” *Organometallics* 29 (9): 2176–79.

Fumagalli, M., D. Ouhab, S. Molina Boisseau, and L. Heux. 2013. “Versatile Gas-Phase Reactions for Surface to Bulk Esterification of Cellulose Micro Fi Brils Aerogels.” *Biomacromolecules* 14 (9): 3246−55.

Future Markets 2015. “The Global Market for Nanocellulose,” no. March: 22. www.futuremarketsinc.com

Gane, P. A. C., and K. Koivunen. 2010. “Relating Liquid Location as a Function of Contact Time Within a Porous Coating Structure to Optical Reflectance.” *Transport in Porous Media* 84 (3): 587–603.

Gane, P. A. C., J. P. Kettle, G. Matthews, and C. J. Ridgway. 1996. “Void Space Structure of Compressible Polymer Spheres and Consolidated Calcium Carbonate Paper-Coating Formulations.” *Industrial and Engineering Chemistry Research* 35 (5): 1753–64.

Gellerstedt, G. 2007a. “Chemistry of Bleaching of Chemical Pulp.” In *Pulp and Paper Chemistry and Technology Volume 2, Edited by Ek, M. G. Gellerstedt, and G. Henriksson*, de Gruyter GmbH, Berlin, pp.202–37.

Gellerstedt, G. 2007b. “Chemisty of Chemical Pulping.” In *Pulp and Paper Chemistry and Technology Volume 2, Edited by Ek, M. G. Gellerstedt, and G. Henriksson*, de Gruyter GmbH, Berlin, pp. 92–120.

Genco, J.M., N. Busayasakul, H.K. Medhora, and W. Robbins. 1990. “Hemicellulose Retention during Kraft Pulping.” *TAPPI Journal* 73 (4): 223–33.

Groendahl, M., and P. Gatenholm. 2005. “Role of Acetyl Substitution in Hardwood Xylan.” In *Polysaccharides: Structural Diversity and Functional Versatility, Second Edition*, Edited by Severian Dumitriu, Marcel Dekker publisher, New-York pp 509–14.

Gustafsson, E., E. Johansson, L. Wågberg, T. Pettersson, 2012. “Direct adhesive measurements between wood biopolymer model surfaces.” *Biomacromolecules* 13 (10): 3046-53.

Habibi, Y., L. Heux, M. Mahrouz, and M. R. Vignon. 2008. “Morphological and Structural Study of Seed Pericarp of Opuntia Ficus-Indica Prickly Pear Fruits.” *Carbohydrate Polymers* 72 (1): 102–12.

Habibi, Y., and M. R. Vignon. 2005. “Isolation and Characterization of Xylans from Seed Pericarp of Argania Spinosa Fruit.” *Carbohydrate Research* 340 (7): 1431–36.

Hägglund, E., Bengt Lindberg, and J McPherson. 1956. “Dimethylsulfoxide, a Solvent for Hemicelluloses.” *Acta Chemica Scandinavica* 10: 1160–64.

Hansson, J-A., and N. Hartler. 1968. “Alkaline Degradation of Xylans from Birch and Pine.” *Svensk Papperstidning* 71 (9): 358-65.

Hansson, J-A., and N. Hartler. 1969. “Sorption of Hemicelluloses on Cellulose Fibres Part 1. Sorption of Xylan.” *Svensk Papperstidning* 72 (17): 521-29.

Hayashi, T. 1989. “Xyloglucans in the Primary Cell Wall.” *Annual Review of Cell and Developmental Biology* 40 (1): 139–68.

Henriksson, M., and L. A. Berglund. 2007. “Structure and Properties of Cellulose Nanocomposite Films Containing Melanine Formaldehyde.” *Journal of Applied Physics* 106 (4): 2817–24.

Henriksson, M., G. Henriksson, L. A. Berglund, and T. Lindström. 2007. “An Environmentally Friendly Method for Enzyme-Assisted Preparation of Microfibrillated Cellulose (MFC) Nanofibers.” *European Polymer Journal* 43 (8): 3434–41.

Herrick, F.W., R. L. Casebier, J. K. Hamilton, and K. R. Sandberg. 1983. “Microfibrillated Cellulose: Morphology and Accessibility.” *Journal of Applied Polymer Science: Applied Polymer Symposia* 37: 797–813.

Herth, W. 1983. “Arrays of Plasma-Memebrane ‘Rosettes’ Involved in Cellulose Microfibril Formation of *Spirogyra*.” *Planta* 159 (4): 347–56.

Hilder, M., B. Winther-Jensen, and N. B. Clark. 2009. “Paper-Based, Printed Zinc-Air Battery.” *Journal of Power Sources* 194 (2): 1135–41.

Ho, T. T. T., K. Abe, T. Zimmermann, and H. Yano. 2015. “Nanofibrillation of Pulp Fibers by Twin-Screw Extrusion.” *Cellulose* 22 (1): 421–33.

Holmberg, M., J. Berg, S. Stemme, L. Oedberg, J. Ramusson and P. Calesson, 1997. “Surface Force Studies of Langmuir–Blodgett Cellulose Films.” *Journal of Colloid and Interface Science.* 186 (2): 369-81

Isogai, A. 1997. “NMR analysis of cellulose dissolved in aqueous NaOH solutions.” *Cellulose* 4 (2): 99-107.

Itoh, T., and R. M. Brown Jr. 1984. "The Assembly of Cellulose Microfibrils in *Valonia macrophysa* Kütz," Planta 160: 372–81.

Jacobs, A., and O. Dahlman. 2001. "Characterization of the Molar Masses of Hemicelluloses from Wood and Pulps Employing Size Exclusion Chromatography and Matrix-Assisted Laser Desorption Lonization Time-of-Flight Mass Spectrometry." *Biomacromolecules* 2 (3): 894–905.

Jin, Z., K. Katsumata, T. Lam, and K. Iiyama. 2006. "Covalent Linkages between Cellulose and Lignin in Cell Walls of Coniferous and Nonconiferous Woods." *Biopolymers* 83: 103–10.

Johansson, M. H., and O. Samuelson. 1977. "Alkaline Destruction of Birch Xylan in the Light of Recent Investigations of its Structure." *Svensk Papperstidning* 80 (16): 519-24.

Joseleau, J-P., and C. Gancet. 1981. "Selective Degradations of the Lignin-Carbohydrate Complex from Aspen Wood." *Svensk Papperstidning* 15 (84): 123–27.

Joseleau, J-P., and R. Kesraoui. 1986. "Glycosidic Bonds between Lignin and Carbohydrates." *Holzforschung* 40: 163–68.

Kaboorani, A., B. Riedl, and P. Blanchet. 2013. "Ultrasonication Technique: A Method for Dispersing Nanoclay in Wood Adhesives" *Journal of Nanomaterials* 2013: 1-9.

Kinloch, A.J, 1987. "Mechanism of Adhesion" In *Adhesion and Adhesives: Science and Technology Edited by Chapman and Hall, Springer Netherlands,* pp. 56-100.

Klemm, D., F. Kramer, S. Moritz, T; Lindström, M. Ankerfors, D. Gray, and A. Dorris. 2011. "Nanocelluloses: A New Family of Nature-Based Materials." *Angewandte Chemie - International Edition* 50 (24): 5438–66.

Krishna I., K. R., P. Neelakantan, and T. Radhakrishnan. 1968. "Birefringence of Native Cellulosic Fibers. I. Untreated Cotton and Ramie." *Journal of Polymer Science Part A-2* 6: 1747–58.

Kono, H., S. Yunoki, T. Shikano, M. Fujiwara, T. Erata, and M. Takai. 2002 "CP/MAS 13C NMR Study of Cellulose and Cellulose Derivatives. 1. Complete Assignment of the CP/MAS 13C NMR Spectrum of the Native Cellulose." *Journal of the American Chemical Society* 124 (25): 7506-11

Koshijima, T., T. E. Timell, and M. Zinbo. 1965. "The Number-Average Molecular Weight of Native Hardwood Xylans." *Journal of Polymer Science: Part C* 11 (11): 265–79.

Larsson, P. T., E-L. Hult, K. Wickholm, E. Pettersson, and T. Iversen. 1999. "CP/MAS -NMR Spectroscopy Applied to Structure and Interaction Studies on Cellulose I." *Solid State Nuclear Magnetic Resonance* 15 (1): 31–40.

Lavoine, N., and I. Desloges. 2014. "Controlled Release and Long-Term Antibacterial Activity of Chlorhexidine Digluconate through the Nanoporous Network of Microfibrillated Cellulose." *Cellulose* 21 (6): 4429–42.

Lavoine, N., I. Desloges, A. Dufresne, and J. Bras. 2012. "Microfibrillated Cellulose – Its Barrier Properties and Applications in Cellulosic Materials : A Review." *Carbohydrate Polymers* 90 (2): 735–64.

Lavoine, N., C. Givord, N. Tabary, I. Desloges, B. Martel, and J. Bras. 2014. "Elaboration of a New Antibacterial Bio-Nano-Material for Food-Packaging by Synergistic Action of Cyclodextrin and Microfibrillated Cellulose." *Innovative Food Science and Emerging Technologies* 26: 330–40.

Lennholm, H., T. Larsson, and T. Iversen. 1994. “Determination of Cellulose I-Alpha and I-Beta in Lignocellulosic Materials.” *Carbohydrate Research* 261 (1): 119–31.

Lerouxel, O., D. M. Cavalier, A. H Liepman, and K. Keegstra. 2006. “Biosynthesis of Plant Cell Wall Polysaccharides - a Complex Process.” *Current Opinion in Plant Biology* 9 (6): 621–30.

Lewis, N., and E. Yamamoto. 1990. “Lignin: Occurrence, Biogenesis and Biodegradation.” *Annual Review of Plant Physiology and Plant Molecular Biology* 41: 455-96.

Li, J., and G. Gellerstedt. 1996. “An HPLC Method for the Quantitative Determination of Hexenuronic Acid Groups in Chemical Pulps.” *Carbohydrate Research.* 294 : 41–51.

Lindström, T., M. Ankerfors, and G. Henriksson. 2007. "Method for the manufacturing of microfibrillated celllulose" WO 2007/091942.

Littunen, K., P. Kilpeläinen, K. Junka, M. Sipponen, E. R. Master, and J. Seppälä. 2015. “Effect of Xylan Structure on Reactivity in Graft Copolymerization and Subsequent Binding to Cellulose.” *Biomacromolecules* 16 (4): 1102–11.

Martinez-Sanz, M., P. Lopez-Sanchez, M. J. Gidley, and E. P. Gilbert. 2015. “Evidence for Differential Interaction Mechanism of Plant Cell Wall Matrix Polysaccharides in Hierarchically-Structured Bacterial Cellulose.” *Cellulose* 22 (3): 1541–63.

Mazeau, K. 2011. “On the External Morphology of Native Cellulose Microfibrils.” *Carbohydrate Polymers* 84 (1): 524–32.

Mazeau, K., C. Moine, P. Krausz, and V. Gloaguen. 2005. “Conformational Analysis of Xylan Chains.” *Carbohydrate Research* 340 (18): 2752–60.

McCormick, C L, and Timothy R Dawsey. 1990. “Preparation of Cellulose Derivatives via Ring-Opening Reactions with Cyclic Reagents in Lithium Chloride/N,N-Dimethylacetamide.” *Macromolecules* 23: 3606–10.

Meier, H. 1962. “Chemical and Morphological Aspectsof the Fine Structure of Wood.” *Pure and Applied Chemistry* 5 (1-2): 37–52.

Meier, H. 1985. “Localization of Polysaccharides in Wood Cell Walls.” In *Biosynthesis and Biodegradation of Wood Components*", edited by Higuchi T. Academic Press, Inc. Orlando, 43–50.

Merewether, J. W. T., L. A. M. Samsuzzaman, and R. G. Cooke. 1972. “Studies on a Lignin-Carbohydrate Complex.” *Holtzforschung* 26 (6): 193–97.

Meshitsuka, G., Z. Z. Lee, J. Nakano, and S. Eda. 1982. “Studies on the Nature of Lignin - Carbohydrate Bonding.” *Journal of Wood Chemistry and Technology* 2 (3): 251–67.

Meyer-Pinson V. 2001. PhD Thesis “Utilisation de l’Oxalate et de Systèmes Biomimétiques du Type Manganèse IV-Oxalate dans le Procédé de Fabrication des Pâtes à Haut Rendement.” in Institut National Agronomique Paris Grignon

Meyer, V., Cottin, F., Boucherand, C., Petit-Conil, M., “Ozone, an efficient chemical for microfibrils separation by homogenization”, TAPPI International Conference on Nanotechnology for renewable materials, Proceedings, Oral presentation, Grenoble, France, 13-16 June 2016 (Doc CTP n°2910).

Mikkelsen, D., B. M. Flanagan, S. M. Wilson, A. Bacic, and M. J. Gidley. 2015. “Interactions of Arabinoxylan and (1,3)(1,4)-b-Glucan with Cellulose Networks.” *Biomacromolecules* 16 (4): 1232–39.

Miletzky, A., W. J. Fischer, C. Czibula, C. Teichert, W. Bauer, and R. Schennach. 2015. “How Xylan Effects the Breaking Load of Individual Fiber-fiber Joints and the Single Fiber Tensile Strength.” *Cellulose* 22 (1): 849–59.

Miletzky, A., M. Punz, A. Zankel, S. Schlader, C. Czibula, C. Ganser, C. Teichert, S. Spirk, S. Zöhrer,W. Bauer, and R. Schennach. 2015. “Modifying Cellulose Fibers by Adsorption/precipitation of Xylan.” *Cellulose* 22 (1): 189–201.

Morgan, J. L. W., J. T. MacNamara, M. Fischer, J. Rich, H-M. Chen, S. G. Withers, J. Zimmer. 2016 "Observing Cellulose Biosynthesis and Membrane Translocation *in Crystallo*" *Nature* 531 : 329-34.

Nakagaito, A. N., and H. Yano. 2004. “The Effect of Morphological Changes from Pulp Fiber towards Nano-Scale Fibrillated Cellulose on the Mechanical Properties of High-Strength Plant Fiber Based Composites.” *Applied Physics A: Materials Science and Processing* 78 (4): 547–52.

Nechyporchuk, O., and M. N. Belgacem. 2015. “Morphological Properties of Nanofibrillated Cellulose Produced Using Wet Grinding as an Ultimate Fibrillation Process.” *Journal of Materials Science* 50 (2) 531–41.

Nechyporchuk, O., M. N. Belgacem, and J. Bras. 2016. “Production of Cellulose Nanofibrils: A Review of Recent Advances.” *Industrial Crops and Products* 93: 2-25.

Newman, R. H. 2004. “Carbon-13 NMR Evidence for Cocrystallization of Cellulose as a Mechanism for Hornification of Bleached Kraft Pulp.” *Cellulose* 11 (1): 45–52.

Nieduszynski, A., and R. H. Marchessault. 1972. “Structure of b,D (1-4) Xylan Hydrate.” *Biopolymers* 11: 1335–44.

Nielsen, L. Junker, S. Eyley, W. Thielemans, and J. W. Aylott. 2010. “Dual Fluorescent Labelling of Cellulose Nanocrystals for pH Sensing.” *Chemical Communications (Cambridge, England)* 46 (47): 8929–31.

Nishiyama, Y., J. Sugiyama, H. Chanzy, and P. Langan 2002. “Crystal Structure and Hydrogen Bonding System in Cellulose I(beta) from Synchrotron X-Ray and Neutron Fiber Diffraction.” *Journal of the American Chemical Society* 124 (21): 9074–82.

Nishiyama, Y., J. Sugiyama, H. Chanzy, and P. Langan. 2003. “Crystal Structure and Hydrogen Bonding System in Cellulose I(alpha) from Synchrotron X-Ray and Neutron Fiber Diffraction.” *Journal of the American Chemical Society* 125 (47): 14300–06.

Norell, M., K. Johansson, and M. Persson. 2009. “Chapter 3; Retention and Drainage.” In *Papermaking Science and Technology, Book 4. Papermaking Chemistry.* Edited by Neimo. L, Stryker L. J. Published by Fapet Oy, Helsinki, pp.1–27.

Nyström, G., A. Razaq, M. Strømme, L. Nyholm, and A. Mihranyan. 2009. “Ultrafast All-Polymer Paper-Based Batteries.” *Nano Letters* 9 (10): 3635–39.

Olszewska, A., J.J. Valle-Delgado, M. Nikinmaa, J. Laine, M. Osterberg. 2013. “Direct measurements of non-ionic attraction and nanoscaled lubrication in biomimetic composites from nanofibrillated cellulose and modified carboxymethylated cellulose.” *Nanoscale* 5 (23): 11837-44.

O'Neil, M.J. (Ed.), and UK: Royal Society of Chemistry. 2013. *The Merck Index - An Encyclopedia of Chemicals, Drugs, and Biologicals. Cambridge*.

Ono, Y., T. Ishida, H. Soeta, T. Saito, and A. Isogai. 2016. "Reliable Dn/dc Values of Cellulose, Chitin, and Cellulose Triacetate Dissolved in LiCl/N,N-Dimethylacetamide for Molecular Mass Analysis." *Biomacromolecules* 17 (1): 192–99.

Österberg, M., J. Laine, P. Stenius, A. Kumpulainen, and P. M. Claesson. 2001. "Forces between Xylan-Coated Surfaces: Effect of Polymer Charge Density and Background Electrolyte." *Journal Of Colloid and Interface Science* 242: 59–66.

Paananen, A., Österberg, M., Ruthland, M., Tammelin, T., Saarinen T., Tappura K., Stenius, P., 2003."Chapter 18; Interaction between Cellulose and Xylan: An Atomic Force Microscope and Quartz Crystal Microbalance Study." In *Hemicellulose: Science and Technology, Volume 864.* Edited by Gatenholm P., Tenkanen M., Published by American Chemical Society, pp.269-90.

Pääkko, M., M. Ankerfors, H. Kosonen, A .Nykänen, S. Ahola, M. Österberg, J. Ruokolainen, J. Laine, P. T. Larsson, O. Ikkala, and T. Lindström. 2007. "Enzymatic Hydrolysis Combined with Mechanical Shearing and High-Pressure Homogenization for Nanoscale Cellulose Fibrils and Strong Gels." *Biomacromolecules* 8 (6): 1934–41.

Pear, J. R., Y. Kawagoe, W. E. Schreckengost, D. P. Delmer, and D. M. Stalker. 1996. "Higher Plants Contain Homologs of the Bacterial celA Genes Encoding the Catalytic Subunit of Cellulose Synthase." *Proceedings of the National Academy of Sciences of the United States of America* 93 (22): 12637–42.

Pereira, L., D. Gaspar, D. Guerin, A. Delattre, E. Fortunato, and R. Martins. 2014. "The Influence of Fibril Composition and Dimension on the Performance of Paper Gated Oxide Transistors." *Nanotechnology* 25 (9): 1–11.

Pinto, P. C., D. V. Evtuguin, and C. Pascoal Neto. 2005. "Structure of Hardwood Glucuronoxylans: Modifications and Impact on Pulp Retention during Wood Kraft Pulping." *Carbohydrate Polymers* 60 (4): 489–97.

Plomion, C., G. Leprovost, and A. Stokes. 2001. "Wood Formation in Trees." *Plant Physiology* 127: 1513–23.

Pushparaj, V. L., M. M. Shaijumon, A. Kumar, S. Murugesan, L. Ci, R. Vajtai, R. J. Linhardt, O. Nalamasu, and P. M. Ajayan. 2007. "Flexible Energy Storage Devices Based on Nanocomposite Paper." *Proceedings Of The National Academy of Sciences of the United States of America* 104 (34): 13574–77.

Rehfeldt, F. and M. Tanaka, 2003. "Hydration forces in ultrathin films of cellulose", *Langmuir*, 19 (5): 1467-73

Reis, D., and B. Vian. 2004. "Helicoidal Pattern in Secondary Cell Walls and Possible Role of Xylans in Their Construction." *Comptes Rendus - Biologies* 327 (9-10): 785–90.

Ridgway, C. J., and P. A. C. Gane. 2013. "Size-Selective Absorption and Adsorption in Anionic Pigmented Porous Coating Structures: Case Study Cationic Starch Polymer versus Nanofibrillated Cellulose." *Cellulose* 20 (2): 933–51.

Rodionova G., S. Roudot, O. Eriksen, F. Mannle, O. Gregersen, 2012. "The Formation and Characterization of Sustainable Layered Films Incorporating Microfibrillated Cellulose (MFC)." *Bioresources*, 7 (3): 3690-3700.

Saito, T., and A. Isogai. 2006. "Introduction of Aldehyde Groups on Surfaces of Native Cellulose Fibers by TEMPO-Mediated Oxidation" *Colloids and Surfaces A: Physicochemical and Engineering Aspects* 289: 219 –25.

Saito, T., R. Kuramae, J. Wohlert, L. A .Berglund, and A. Isogai. 2013. "An Ultrastrong Nano Fibrillar Biomaterial: the Strength of Single Cellulose Nano Fibrils Revealed via Sonication-Induced Fragmentation." *Biomacromolecules* 14: 248–53.

Saito, T., Y; Nishiyama, J-L. Putaux, M. R. Vignon, and A. Isogai. 2006. "Homogeneous Suspensions of Individualized Microfibrils from TEMPO-Catalyzed Oxidation of Native Cellulose." *Biomacromolecules* 7 (6): 1687–91.

Satas, D. 1989 In: *Handbook of Pressure Sensitive Adhesive Technology*, Edited by D. Satas, Van Nostrand Rheinhold, New-York, NY. pp. 61-96.

Saxena, I. M., and R. M. Brown Jr. 2005. "Cellulose Biosynthesis: Current Views and Evolving Concepts." *Annals of Botany* 96 (1): 9–21.

Scheible, W. R., R. Eshed, T. Richmond, D. Delmer, and C. Somerville. 2001. "Modifications of Cellulose Synthase Confer Resistance to Isoxaben and Thiazolidinone Herbicides in *Arabidopsis* Ixr1 Mutants." *Proceedings of the National Academy of Sciences of the United States of America* 98 (18): 10079–84.

Sehaqui, H., A. Liu, Q .Zhou, and L. A. Berglund. 2010. "Fast Preparation Procedure for Large, Flat Cellulose and Cellulose/inorganic Nanopaper Structures." *Biomacromolecules* 11 (9): 2195-98

Shahril M., A. Bistamam, H. Takagi, and A. N. Nakagaito. 2015. "Development of Green Nanocomposites Reinforced by Cellulose Nanofibers from Waste Newspaper." *Modern Physics Letters B* 29 (6-7): 1-5.

Siegel, A. C., S. T. Phillips, M. D. Dickey, N. Lu, Z. Suo, and G. M. Whitesides. 2010. "Foldable Printed Circuit Boards on Paper Substrates." *Advanced Functional Materials* 20 (1): 28–35.

Shimizu, M., T. Saito, Y. Nishiyama, S. Iwamoto, H. Yano, A.Isogai, and T. Endo. 2016. "Fast and Robust Nanocellulose Width Estimation Using Turbidimetry." *Macromolecular Rapid Communications*. in press: DOI: 10.1002/marc.201600357

Siro, I., Y. Kusano, K. Norrman, S. Goutianos, D. Plackett 2013. "Surface modification of nanofibrillated cellulose films by atmospheric pressure dielectric barrier discharge." *Journal of Adhesion Science and Technology* 27 (3): 294-308.

Smook, G. A. 2002. "Chapter 4: Overview of Pulping Methodology." In *Handbook for Pulp and Paper Technologists*, (3rd Edition), Angus Wilde Publications Inc. , pp: 37–46.

Somerville, C. 2006. "Cellulose Synthesis in Higher Plants." *Annual Review of Cell and Developmental Biology* 22: 53–78.

Spence, K. L., R. A. Venditti, O. J. Rojas, J. J. Pawlak, and M. A. Hubbe. 2011. "Water Vapor Barrier Properties of Coated and Filled Microfibrillated Cellulose Composite Films." *BioResources* 6 (4): 4370–88.

Sugiyama, J., R. Vuong, and H. Chanzy. 1991. “Electron-Diffraction Study on the Two Crystalline Phases Occurring in Native Cellulose From an Algal Cell-Wall.” *Macromolecules* 24 (14): 4168–75.

Sugiyama, J., J. Persson, and H. Chanzy. 1991. “Combined Infrared and Electron Diffraction Study of the Polymorphism of Native Celluloses.” *Macromolecules* 24 (9): 2461–66.

Syverud, K., and P. Stenius. 2009. “Strength and Barrier Properties of MFC Films.” *Cellulose* 16 (1): 75–85.

Taipale, T., M. Österberg, A. Nykänen, J. Ruokolainen, and J. Laine. 2010. “Effect of Microfibrillated Cellulose and Fines on the Drainage of Kraft Pulp Suspension and Paper Strength.” *Cellulose* 17 (5): 1005–20.

Tammelin, T., A. Paananen, and M. Österberg. 2009. “Chapter 6: Hemicelluloses at Interfaces: Some Aspects of the Interactions.” In *The Nanoscience and Technology of Renewable Biomaterials*, Edited by Lucia and Rojas, Blackwell publishing, pp149–72.

Tapin-Lingua, S., Meyer, V., Petit-Conil, M., “Correlations between pulp composition and efficiency of M/NFC production “, Tappi International conference on nanotechnology on renewable materials, Oral presentation, Stokholm, Sweden, 24-27 June 2013 (Doc CTP n° 2774).

Teeäär, R., R. Serimaa, and T. Paakkari. 1987. “Crystallinity of Cellulose, as Determined by CP/MAS NMR and XRD Methods.” *Polymer Bulletin* 17 (3): 231–37.

Teleman, A., P. T. Larsson, and T. Iversen. 2001. “On the Accessibility and Structure of Xylan in Birch Kraft Pulp.” *Cellulose* 8 (3): 209–15.

Teleman, A., J. Lundqvist, F. Tjerneld, H. Stålbrand, and O. Dahlman. 2000. “Characterization of Acetylated 4-O-Methylglucuronoxylan Isolated from Aspen Employing 1H and 13C NMR Spectroscopy.” *Carbohydrate Research* 329 (4): 807-15

Teleman, A., V. Harjunpää, M. Tenkanen, J. Buchert, T. Hausalo, T. Drakenberg, and T. Vuorinen. 1995. “Characterisation of 4-Deoxy-β-L-Threo-Hex-4-Enopyranosyluronic Acid Attached to Xylan in Pine Kraft Pulp and Pulping Liquor by ^{1}H and ^{13}C NMR Spectroscopy.” *Carbohydrate Research* 272 (1): 55–71.

Tenhunen, T. M., M. S. Peresin, P. A. Penttilä, J. Pere, R. Serimaa, and T. Tammelin. 2014. “Significance of Xylan on the Stability and Water Interactions of Cellulosic Nanofibrils.” *Reactive and Functional Polymers* 85 : 157-66.

Thomas, R. J. 1976. “Wood - Structure and Chemical Composition.” *Abstracts of Papers of the American Chemical Society* 172 (3): 1-23.

Timell, T. E. 1967. “Recent Progress in the Chemistry of Wood Hemicelluloses.” *Wood Science and Technology* 1: 45–70.

Timell, T.E. 1964. “Wood Hemicellulose: Part 1.” *Adv Carbohydr Chem* 19: 247–302.

Tokoh, C., K. Takabe, J. Sugiyama, and M. Fujita. 2002. “CP/MAS ^{13} C NMR and Electron Diffraction Study of Bacterial Cellulose Structure Affected by Cell Wall Polysaccharides.” *Cellulose* 9: 351–60.

Turbak, A. F., F. W. Snyder, and K. R. Sandberg. 1983. “Microfibrillated Cellulose, a New Cellulose Product: Properties, Uses and Commercial Potential.” *Journal of Applied Polymer Science: Applied Polymer Symposia* 37: 815–27.

Wada, M., T. Okano, and J. Sugiyama. 2001. "Allomorphs of Native Crystalline Cellulose I Evaluated by Two Equatorial *d*-Spacings." *Journal of Wood Science* 47 (2): 124–28.

Wågberg, L., G. Decher, M. Norgren, T. Lindström, M. Ankerfors, and K. Axna. 2008. "The Build-Up of Polyelectrolyte Multilayers of Microfibrillated Cellulose and Cationic Polyelectrolytes," Langmuir 24 (3) 784–95.

Wang, T., A. Salazar, O. A. Zabotina, and M. Hong. 2014. "Structure and Dynamics of *Brachypodium* Primary Cell Wall Polysaccharides from Two-Dimensional ^{13}C Solid-State Nuclear Magnetic Resonance Spectroscopy." *Biochemistry* 53 (17): 2840–54.

Wang, Z., T. Yokoyama, Y. Matsumoto. 2010. "Dissolution of ethylenediamine pretreated pulp with high lignin content in LiCl/DMSO without milling." *Journal of Wood Chemistry and Technol*ogy 30 (3):219–29

Westbye, P., C. Svanberg, and P. Gatenholm. 2006. "The Effect of Molecular Composition of Xylan Extracted from Birch on Its Assembly onto Bleached Softwood Kraft Pulp." *Holzforschung* 60 (2): 143–48.

Wigell, A., H. Brelid, and H. Theliander. 2007. "Degradation/dissolution of Softwood Hemicellulose during Alkaline Cooking at Different Temperatures and Alkali Concentrations." *Nordic Pulp and Paper Research Journal* 22 (4): 488–94.

Yang, L., A. Rida, R. Vyas, and M. M. Tentzeris. 2007. "RFID Tag and RF Structures on a Paper Substrate Using Inkjet-Printing Technology." *IEEE Transactions on Microwave Theory and Techniques* 55 (12): 2894–2901.

Yllner, S., and B. F. Enström. 1957. "Studies of the Adsorption of Xylan on Cellulose Fibres during the Sulfate Cook Part 2." *Svensk Papperstidning* 60 (15): 549–54.

Zhao, B., and H.J. Kwon, 2011. "Adhesion of Polymers in Paper Products from the Macroscopic to Molecular Level — An Overview."*Journal of Adhesion Science and Technology* 25 (6-7) 577- 79

Zhang, L., T. Tsuzuki, and X. Wang. 2015. "Preparation of Cellulose Nanofiber from Softwood Pulp by Ball Milling." *Cellulose* 22 (3):1729–41.

Zimmermann, T., N. Bordeanu, and E. Strub. 2010. "Properties of Nanofibrillated Cellulose from Different Raw Materials and Its Reinforcement Potential." *Carbohydrate Polymers* 79 (4): 1086–93.

Zinbo, M, and T E Timell. 1965. "The Degree of Branching of Hardwood Xylans." *Svensk Papperstidning* 68 (19): 647-62

Résumé Etendu

Le cadre de cette étude est le coût énergétique lié à la production des Microfibrilles de Cellulose (MFC) qui est aujourd'hui un facteur limitant à son développement à l'échelle industrielle. Le but de cette étude est de caractériser les interactions cellulose/hémicellulose au sein de ces systèmes.

Des MFC provenant de différentes pâtes à papier chimiques ont été caractérisées par RMN du solide afin d'obtenir des informations à l'échelle moléculaire. Suite à l'optimisation d'un protocole expérimental, les hémicelluloses contenues dans les MFC issues de pâte kraft de bouleau ont ensuite été extraites avec un rendement de 67% et sont composés uniquement d'un homopolymère de xylane de DP 75. La turbidimétrie a été utilisée pour qualifier la qualité des suspensions, dont il a été montré qu'elle dépend fortement du procédé de mise en pâte et du séchage. Des corrélations positives ont été établies entre l'état de dispersion des MFC et les propriétés mécaniques de feuilles de papier renfermant ces microfibrilles. L'analyse RMN de modèles biomimétiques reconstitués a confirmé le changement de conformation du xylane lorsqu'il est adsorbé sur la cellulose et les mesures de surface spécifique ont montré que seule la couche de xylane en contact avec la cellulose était concernée par ce changement.

Les interactions cellulose/xylane ont été étudiées par RMN du solide et par dynamique moléculaire atomistique (MD). Les simulations MD ont montré que le xylane s'adsorbe parallèlement aux chaines de cellulose. Des mesures d'interaction sur ce système ont conduit à une mesure d'énergie de 9kJ/résidu de xylose. Des tests de mesure d'adhésion ont également été réalisés à partir d'un modèle trois couches constitué de xylane entre deux films de cellulose et une forte adhésion a pu être observée. Enfin, l'utilisation de xylanase dans le prétraitement des fibres semble une voie prometteuse pour diminuer la consommation d'énergie et améliorer la qualité des MFC.

Caractérisation des MFC et isolement des principaux composants

1. Préparation des suspensions de MFC

Les suspensions de MFC sont préparées à partir de pâtes chimiques blanchies commerciales selon le procédé breveté par STFI/Innventia et optimisé au CTP consistant à réaliser un prétraitement mécano-enzymatique de la pâte (Endoglucanase 1h puis raffinage poussé) suivie d'une homogénéisation à haute pression (1 passage à 1000 bar + 4 passages à 1500 bar).

Dans le cadre de ce projet, 8 suspensions de MFC ont été utilisées. Elles proviennent de 4 essences de bois, de 2 procédés de cuisson kraft/sulfite et de pâtes séchées ou jamais séchées (Tableau 1).

Tableau 1: Panel des suspensions de MFC

MFC de	Essence de bois	Procédé de mise en pâte	Séchage de la pâte
bouleau-kra-js	bouleau	kraft	pâte jamais séchée
bouleau-kra	bouleau	kraft	pâte séchée
épicéa-kra	épicéa	kraft	pâte séchée
pin96-sul-js	pin (96% of cellulose)	sulfite	pâte jamais séchée
pin96-sul	pin (96% of cellulose)	sulfite	pâte séchée
pin92-sul-js	pin (92% of cellulose)	sulfite	pâte jamais séchée
pin92-sul	pin (92% of cellulose)	sulfite	pâte séchée
euc-sul	eucalyptus	sulfite	pâte séchée

2. Caractérisation des suspensions de MFC

La composition chimique (teneur en hémicellulose) de cinq suspensions de MFC a été déterminée et reliée aux spectres obtenus en RMN du solide (Figure 1). Les spectres ont été normalisés par rapport à la somme de l'intensité du signal entre 55 et 155 ppm et l'attribution des pics a été réalisée selon Kono *et al.* (2002) et Larsson *et al.* (1999).

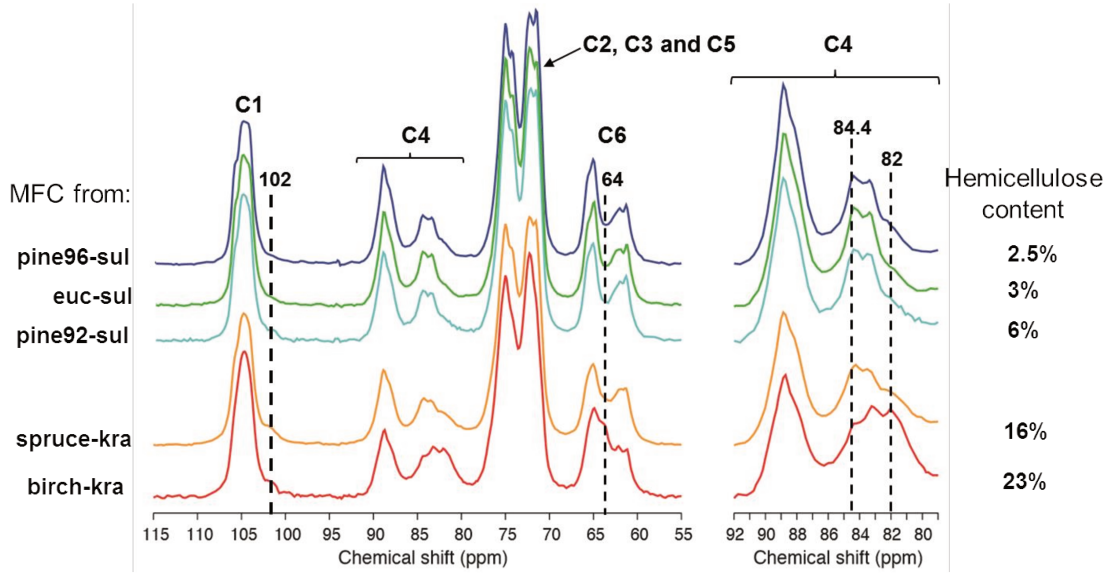

Figure 1: Spectre RMN 13C CP-MAS d'échantillons humides de MFC issus de pâte sulfite (pin96, pin92 et eucalyptus) et de pâte kraft (bouleau et épicéa)

Le signal RMN au niveau du carbone C4 est très différent suivant l'origine de la pâte (kraft ou sulfite) utilisée pour produire les MFC (Figure 1, droite). L'intensité du pic à 82 ppm est directement corrélée à la teneur en xylane des MFC. En effet les spectres RMN des MFC de pâtes sulfites, qui contiennent un maximum de 2,5% de xylane, n'ont que deux pics à 84.4 et 83.4 ppm alors que les MFC de pâtes kraft, qui contiennent entre 8,7% et 22,5% de xylane, en ont un troisième à 82 ppm.

La présence de xylane influence aussi les signaux des carbones C6 et C1 où deux pics supplémentaires sont observés à 64 et 102 ppm (Figure 391 gauche) dans le cas des MFC de pâte kraft. En conclusion, la RMN du solide peut être utilisée pour suivre la teneur en xylane au sein des MFC en utilisant l'intensité du pic à 82 ppm.

3. Protocole optimisé d'extraction du xylane

Dans le but de comprendre les interactions entre les chaines de cellulose et celles d'hémicelluloses, un protocole d'extraction de xylane a été développé à partir des MFC issues de pâte kraft de bouleau jamais séché (22,5% de xylane). La teneur en xylane est suivit par analyses de sucres et RMN du solide.

L'échantillon de MFC kraft de bouleau a été lyophilisé après un échange de solvant eau-ter-butanol (TBA). Il a été redispersé dans un mélange DMSO-5% LiCl (dimethylsulfoxide, sel de chlorure de lithium) à la concentration de 8 g/L et agité pendant 20h à température ambiante. Le mélange est ensuite centrifugé (20 000 g, 15 h, 25°C) pour séparer le xylane en solution dans le DMSO-5% LiCl des MFC insolubles. Le DMSO est éliminé du xylane extrait (surnageant) et des MFC (culot) par dialyse contre l'eau (membrane 12 000 Da) pendant 7 jours. La suspension de MFC est gardée à l'état humide. Le xylane au contact de l'eau pendant la dialyse forme un précipité, qui à l'issu des 7 jours, est concentré (évaporateur rotatif, 30°C, 7 mbar) et lyophilisé.

4. Caractérisation du xylane extrait

La pureté du xylane est caractérisée par analyse de sucres et RMN du liquide. Le xylane extrait à partir de MFC de bouleau kraft est comparé à un xylane commercial extrait d'avoine (Figure 2).

Le xylane extrait de MFC de bouleau kraft est dépourvu de ramification arabinose, contrairement au xylane extrait d'avoine qui en contient 9,6% mais aussi 13,0% de contamination de cellulose.
Les pics sont attribués en accord avec la littérature (Habibi et Vignon 2005) et les signaux à 4,3 ppm, 3,5 ppm, 3,3 ppm et 3,1 ppm sont attribués aux protons H1, H4, H3 et H2. Les signaux caractéristiques des protons CH_2 (carbone C5) sont observés à 3,9 ppm et 3,2 ppm pour le proton équatorial (H5eq) et l'axial (H5ax) respectivement. Les deux pics à 4,8 ppm et 4,6 ppm correspondent aux deux groupes hydroxyles (OH2) et (OH3). Ils sont seulement observés lorsque le solvant utilisé est le DMSO-d_6 à cause de l'échange de proton-deutérium dans D_2O.

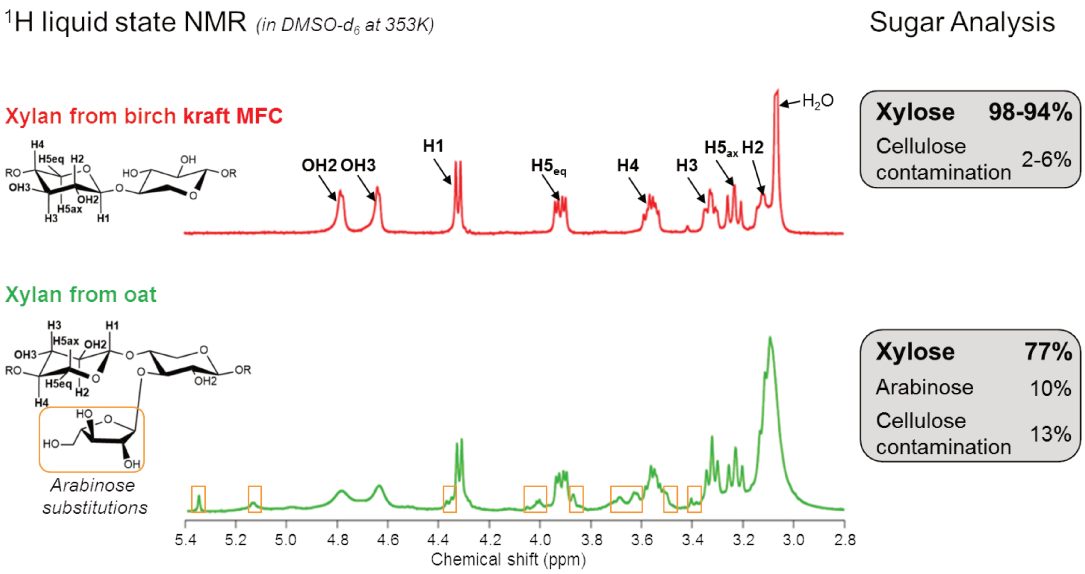

Figure 2: Spectre RMN liquide proton (1H) de xylane extrait à partir copeaux de bouleau d'avoine (commercial) et de MFC de pâte kraft de bouleau

Dans le cas du xylane extrait d'avoine, quatre signaux de protons H1 peuvent être attribués au résidu de xylose seul (4,3 ppm), au xylose branché en O3 (4,4 ppm) par une ramification arabinose et par un acide glucuronique (5,1 ppm) et au xylose branché en O2 par un arabinose (4,5 ppm –HSQC). L'influence de cette différence de structure du xylane sur les propriétés d'adhésion cellulose-xylane sera étudiée dans le paragraphe suivant.

Interactions cellulose-xylane

L'adsorption du xylane à la surface de la cellulose et son adaptation conformationnelle a été étudiée par RMN du solide et simulation atomistique (dynamique moléculaire MD). Le xylane a tout d'abord été ajouté aux MFC extraites en quantité égale à ce qui a été extrait soit 14% puis en excès (20%).

Afin d'évaluer les forces d'adhésion entre la cellulose et le xylane à l'échelle macroscopique, un système trois couches (cellulose-xylane-cellulose) a été développé. Deux types de tests mécaniques, par pelage ou cisaillement, ont été mis en œuvre. Seul le test de cisaillement a permis d'obtenir des valeurs d'énergie d'adhésion.

1. RMN du solide et simulation atomistique

Les spectres de RMN ont confirmé que le xylane adaptait sa conformation lorsqu'il était en présence de cellulose (Figure 3). Initialement en conformation d'hélice à trois résidus par tour (hélice 3), il semblerait qu'il adopte une conformation d'hélice à deux résidus par tour (hélice 2), identique à la conformation des chaines de cellulose. La combinaison de ces données avec les mesures de surface spécifique, a montré que cette adaptation conformationnelle était limitée à la première couche de xylane adsorbée, en interaction directe, avec la surface de la cellulose. L'excès de xylane conserve la conformation initiale d'hélice 3.

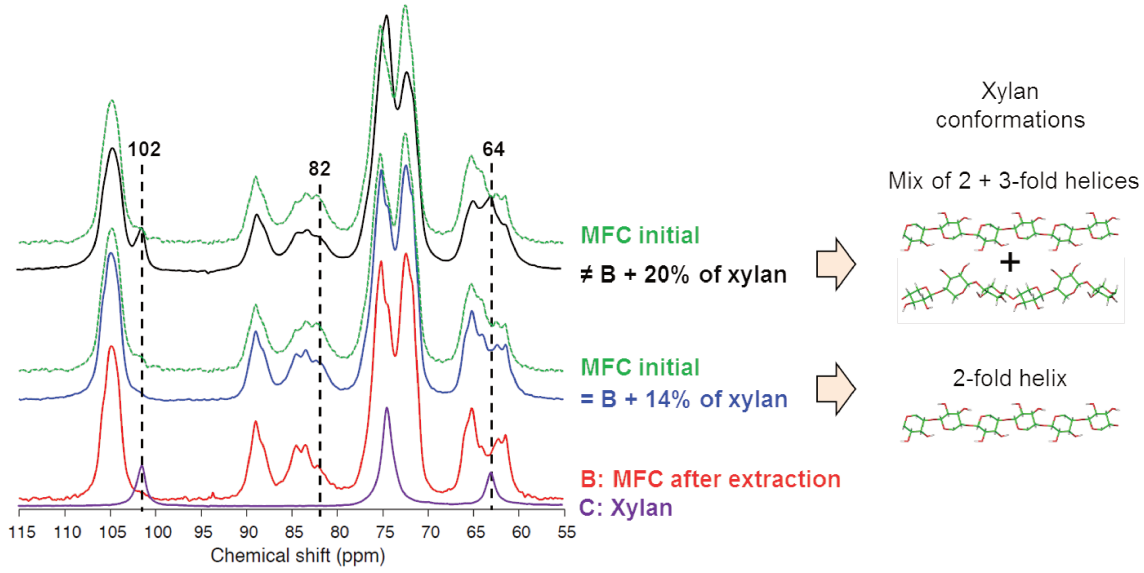

Figure 3: Spectre RMN 13C CP-MAS d'échantillon humide : de MFC initial comparé au MFC extraite (B), au xylane humide seul (C) et aux spectres de MFC après réabsorption de 14 et 20% de xylane

Les simulations MD ont confirmées que le xylane en hélice 3 avait une plus faible affinité pour la surface de la cellulose que son homologue en hélice 2, soutenant ainsi l'hypothèse de la conformation d'hélice 2 du xylane lorsqu'il est adsorbé à la surface de la cellulose.

Les simulations ont aussi montré que seul le xylane en hélice 2 s'adsorbé à la surface de cellulose. Il est parfaitement étendu, aligné parallèlement à la direction de la chaîne de cellulose et dans un plan parallèle à celui de la cellulose. Adsorbé sur les surfaces hydrophobes de la cellulose, il maximise ses interactions avec la cellulose en superposant ces cycles xylosyl sur les cycles glucosyl de la cellulose.

2. Test d'adhésion macroscopique

Formation du modèle trois couches pour le test de cisaillement

Les films de MFC à 50 g/m² réalisés par filtration et séchage sur l'appareil à formette Rapid-Khöten sont fixés à l'aide de colle époxy sur des spatules en bois coupées en leur milieu (75 mm). L'ensemble est séché à température ambiante pendant 5h.

Le gel de xylane (75 mg à 10%) extrait des MFC (kraft bouleau) ou commercial (avoine) est ensuite déposé sur une surface délimitée du film de MFC (18 x 20 mm, soit 360 mm²). Pour améliorer, le dépôt du gel de xylane, il est préalablement broyé à l'ultra-turrax. Les spatules sont ensuite assemblées par paires et la quantité finale de xylane dans le système correspond à 150 mg à 10%. Le système trois couches est séché à température ambiante 4h puis à la presse chauffante (120°C, 3h, 10bar) et refroidit à température ambiante sous contrainte.

Des calles en bois (18*20*2 mm) sont collées à la super glue Loctite à chaque extrémité des spatules pour assurer l'alignement du système dans les mors de la machine de traction (Figure 4 A). Les systèmes sont ensuite conservés dans des dessiccateurs à différentes humidités.
Les même systèmes trois couches sont réalisées avec de la colle hotmelt à la place du xylane pour servir de référence.

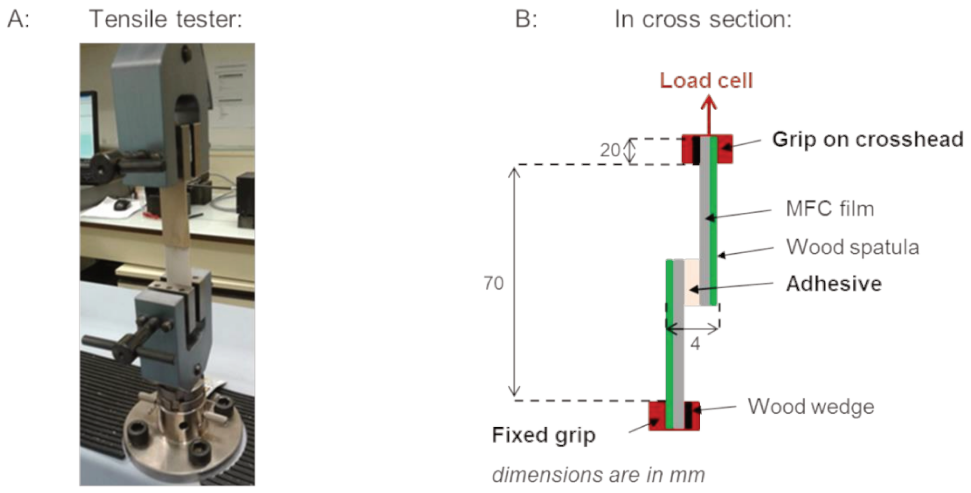

Figure 4: Schéma du test de cisaillement

Le système trois couches est placé avec les calles en bois fixées dans les mors de la machine de traction (Shimadzu AGS-X). L'écart initial entre les mors est fixé à 70 mm (Figure 4 B). Le test de cisaillement est réalisé à température ambiante avec les cellules de mesures de 500 N à la vitesse de 5 mm/min.

La force maximale (*Fm*) avant la rupture est mesurée puis la contrainte de cisaillement est calculée à partir de l'équation suivante, où (l x L) correspond à la surface de gel de xylane déposé sur le film de MFC soit 3,6 cm².

$$\sigma\ cisaillement = \frac{Fm}{l \times L}$$

Les modes de ruptures observés sur tous les systèmes sont uniquement cohésifs (dans la couche de xylane ou de colle hot melt). Les valeurs de cisaillement (Figure 5) obtenues avec les systèmes contenant du xylane sont inférieures à celles de la colle hot melt mais reste dans le même ordre de grandeur dans le cas des essais réalisés à 15% d'humidité.

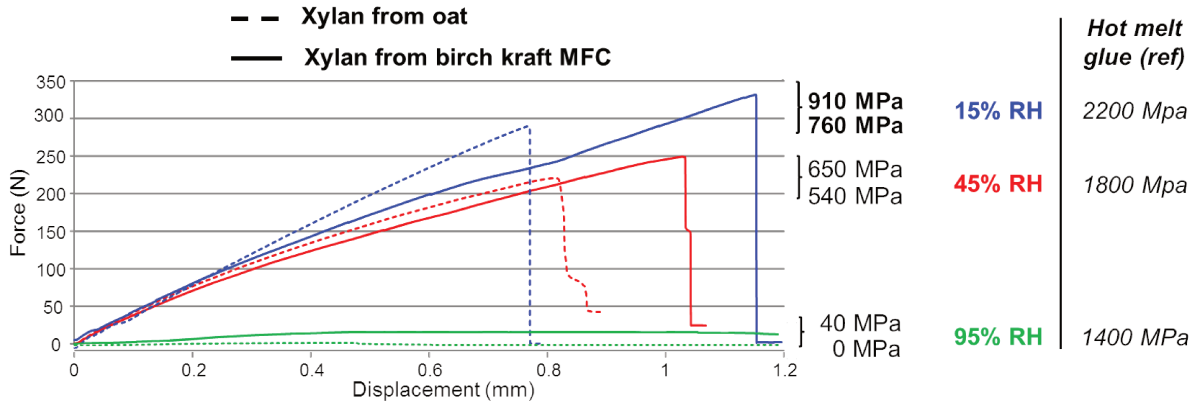

Figure 5: Courbes de cisaillement des modèles 3 couches (xylane extrait ou commercial) à 15%, 45% et 95% d'humidités relatives (RH) et les valeurs d'énergie pour la référence avec la colle

En revanche pour les taux d'humidité supérieurs, une forte diminution du cisaillement est observée, jusqu'à une perte complète d'adhérence à 95% d'humidité. Néanmoins, l'augmentation d'humidité mets en évidence un phénomène de plastification, visible par la diminution de l'élongation, sur les systèmes constitués de xylanes.

Le type de xylane utilisé dans la couche adhésive du système semble influencer le cisaillement : des valeurs légèrement inférieures sont observées avec les systèmes composés de xylane d'avoine. Cette différence peut être expliquée par la présence de branchements arabinoses sur ce type de xylane mais nécessite des études supplémentaires pour confirmer l'influence des groupements arabinoses sur l'adhésion cellulose-xylane.

Etat de dispersion des MFC

L'influence de l'essence de bois et du procédé de mise en pâte sur le nombre d'éléments grossiers résiduels dans les suspensions de MFC et sur les propriétés mécaniques des papiers renforcés avec des MFC, a récemment été étudiée au CTP (Tapin-Lingua, Meyer, et Petit-Conil 2013).
Au cours de cette étude, il est apparu que les hémicelluloses avaient un rôle important dans l'homogénéité des suspensions de MFC et ainsi dans la résistance des papiers renforcées par MFC.

Dans le but de mieux comprendre le rôle de ces hémicelluloses dans les suspensions de MFC, des méthodes de caractérisation de la dispersion de suspensions de MFC contenant plus ou moins d'hémicelluloses ont été développées.
La première est basée sur la mesure de turbidité par spectroscopie UV - visible des suspensions initialement développée par Carr et Hermans (1978) puis adapté récemment sur des gel par Ferri *et al.* (2015). Cette méthode repose sur le principe qu'une suspension est d'autant plus transparente qu'elle est homogène. Inversement une solution est d'autant plus opaque qu'elle est hétérogène (Saito et Isogai 2006).
La deuxième méthode s'appuie sur la mesure de surfaces spécifique d'aérogel de MFC, obtenu après lyophilisation dans le ter-butanol, récemment décrite comme préservant la structure des suspensions de cellulose à l'état sec (Fumagalli *et al.* 2013).

1. Préparation des aérogels et des suspensions de MFC

Les aérogels de MFC sont préparés par échange de solvant eau-ter butanol par centrifugations (11 200 rpm, 2 h, 25°C) et redispersions successives dans le ter-butanol. Après la troisième centrifugations, les MFC sont redispersées à 1,25% en masse dans le ter-butanol, puis congelées à l'azote liquide et lyophilisées 100 mili-torr pendant deux jours (Fumagalli *et al.* 2013).
Les mesures de surface spécifique ont été réalisées par mesure d'adsorption-désorption d'azote en utilisant l'équation BET (Braunauer, Emmett, and Teller 1938). Les échantillons lyophilisés dans le ter-butanol (0,07 – 0,15 g) sont dégazés à 105°C pendant 5h puis l'isotherme d'adsorption-désorption est mesuré à 77K à la pression de 0,01-0,3 bar.

Pour la mesure de turbidité, les suspensions de MFC sont diluées à 1% : en dessous de 0.5% la sédimentation est trop importante et perturbe la mesure ; au-dessus de 1% la suspension est trop opaque et l'atténuation du rayon lumineux est trop importante.
Les mesures de turbidité sont réalisées avec des cuves UV en quartz sur un spectromètre UV visible sur la gamme de longueur d'onde de 200 à 800 nm. Les mesures sont collectées à la vitesse de 600 nm/min avec une résolution de 1 nm.

2. Corrélation entre la surface spécifique et la turbidité des MFC

Les suspensions de MFC étudiées, peuvent être séparées en deux groupes selon leurs courbes de turbidité (Figure 6): (1) les suspensions les moins bien dispersées avec des courbes de turbidité concave qui augmente avec la longueur d'onde ; (2) les suspensions les mieux dispersées, ayant des courbes de turbidité convexe qui diminuent avec la longueur d'onde.

Tous les suspensions des MFC issues de pâtes sulfites séchées font partie du groupe (1) alors que les MFC produites à partir de pâtes krafts et de pâtes sulfites jamais séchées correspondent au groupe (2). Même si l'effet est bien moins important que sur les pâtes sulfites, une faible variation dans l'allure de la courbe est visible pour les MFC de pâtes kraft séchées.

Il semble donc que l'état de dispersion des MFC soit aussi lié au séchage de la pâte. L'effet du séchage sur la dispersion des MFC est d'autant plus marquant que la teneur en hémicellulose est faible.

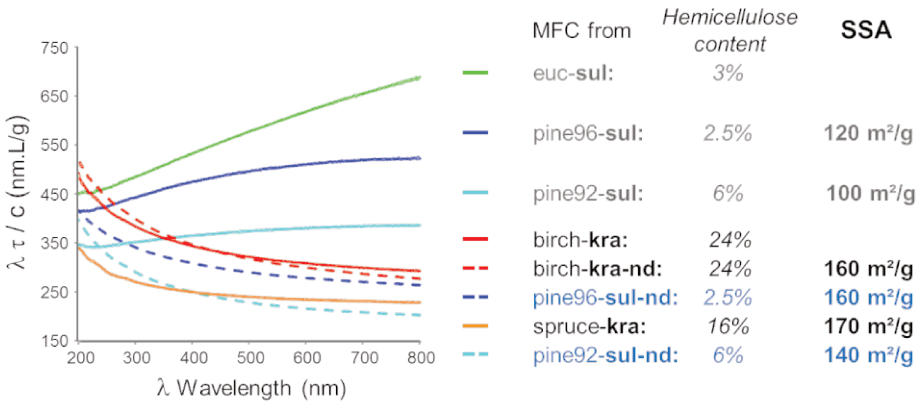

Figure 6: Turbidité des MFC en fonction de la longueur d'onde (λ) corrélé à leurs surfaces spécifiques (m^2/g)

Ce premier résultat est confirmé par les analyses de surfaces spécifiques. Les suspensions les moins bien dispersées (MFC de pâtes sulfites séchées) avec des courbes de turbidité concave (1) ont des surfaces spécifiques comprises entre 100 et 120 m^2/g.
Au contraire, les MFC les mieux dispersées, ayant des courbes de turbidité convexe (2) ont des surfaces spécifiques plus élevées, comprises entre 140 et 170 m^2/g.

3. Corrélation entre la turbidité des MFC et leur potentiel de renfort des papiers

Pour faciliter la comparaison, la turbidité des MFC à la longueur d'onde de 800 nm est tracée en fonction de la valeur d'élongation des films renforcés (Figure 7).

Il semble que l'effet de renfort mécanique des papiers par des suspensions de MFC soit directement lié à leur état de dispersion, qui à son tour dépend de la teneur en hémicelluloses et du séchage de la pâte. En effet, une suspension de MFC résultant de la pâte sulfite jamais séchée a le même effet sur les propriétés mécaniques que celles issues de pâte kraft séchée de bouleau ou d'épicéa et elles partagent le même comportement d'agrégation (courbes de turbidité).
Les aérogels correspondant présentent également des surfaces spécifiques très proches, illustrant l'impact positif de la dispersion des suspensions sur les propriétés du matériau final.

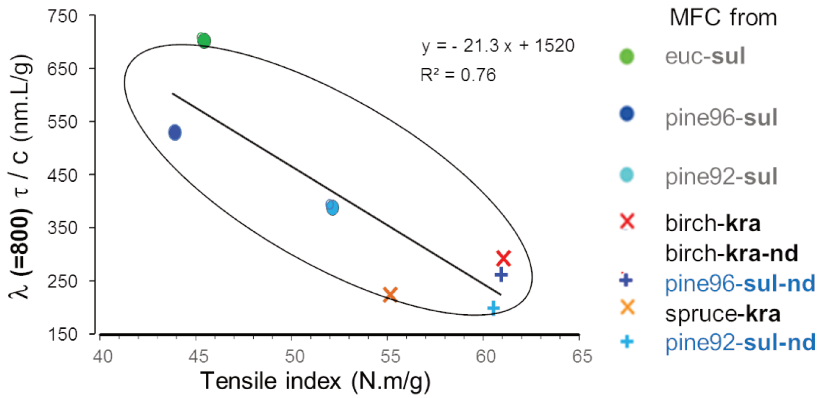

Figure 7: Corrélation entre l'indice de rupture des formettes et la turbidité des suspensions de MFC à 800 nm

Nouveau prétraitement avant production de MFC

La pâte kraft de bouleau jamais séchée a été utilisée pour évaluer l'impact d'un traitement par la xylanase sur le potentiel de séparation des microfibrilles de cellulose dans l'homogénéiseur. Ce nouveau prétraitement a été testé seul ou en combinaison avec le prétraitement conventionnel par une endoglucanase et comparé à une pâte non prétraitée ou prétraitée par l'endoglucanase seule. La pâte prétraitée enzymatiquement a été raffinée avant production de MFC en 5 passages dans l'homogénéiseur haute pression (GEA NS3006) selon la séquence suivante : 1 passage à 1000 bar puis 4 passages à 1500 bar. Les suspensions de MFC ainsi produites ont été caractérisées en termes de teneur résiduelle en éléments grossiers (analyse MorFi), turbidité et composition en sucres.

1. Caractérisation des MFC

Quel que soit le prétraitement utilisé, aucune variation de la teneur en xylane n'est observée (Figure 8). Les charges en enzymes utilisées ici sont volontairement faibles afin de rester compétitif par rapport au coût du raffinage seul. De plus l'utilisation d'enzyme ne vise pas l'extraction complète du xylane mais seulement sa fragilisation afin de préserver les propriétés des MFC en présence d'hémicelluloses.

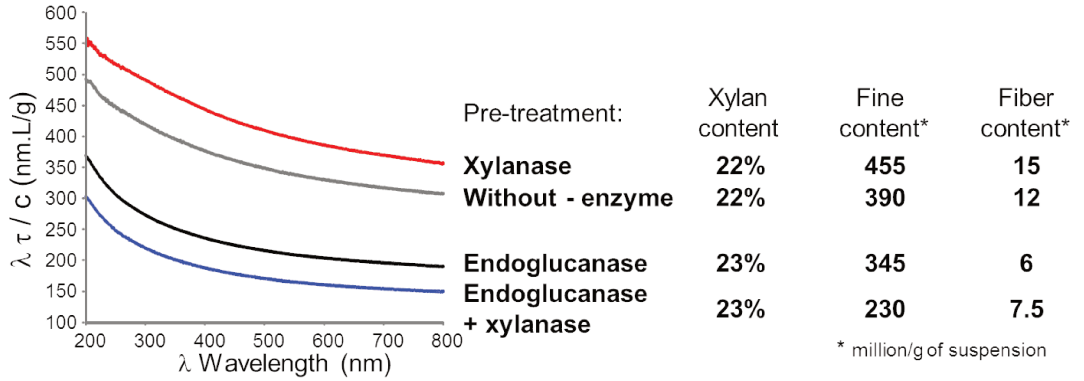

Figure 8 : Impact des différents prétraitements sur la turbidité, la teneur en xylane et la quantité résiduelle des fibres et de fines dans les suspensions de MFC.

Les courbes de turbidité sont convexes et correspondent à des suspensions bien dispersées. Il apparait toutefois une turbidité plus élevée et donc une dispersion un peu inférieure pour les MFC sans enzyme ou les MFC issues de pâte prétraitée par la xylanase seule. Ce résultat est corrélé avec une teneur en fibres (longueur>80 µm) et fines (longueur<80 µm) résiduelles supérieures. La combinaison d'un prétraitement endoglucanase + xylanase conduit à la meillleure qualité de MFC : cette suspension est la mieux dispersée et contient un maximum de microfibrilles.

La xylanase semble faciliter l'action de l'endoglucanase. Elle pourrait fragiliser la structure du xylane et ainsi en permettant une meilleure accessibilité de la cellulose pour l'endoglucanase.

2. Impact sur la consommation d'énergie

Au niveau de l'étape de raffinage, seule l'endoglucanase a un effet majeur en réduisant de 50% la consommation d'énergie par rapport à la référence sans enzyme (Figure 9). Par contre, si l'on considère l'énergie totale incluant l'homogénéisation, le mélange endoglucanase/xylanase conduit à la plus forte économie d'énergie : 1800 kWh/t (soit 17%) par rapport à la référence sans enzyme et 870 kWh/t (soit 8%) par rapport à un traitement endoglucanase seul. Un traitement endoglucanase/xylanase facilité donc la libération des microfibrilles dans l'homogénéiseur ce qui se traduit par un gain énergétique et une qualité de MFC supérieure.

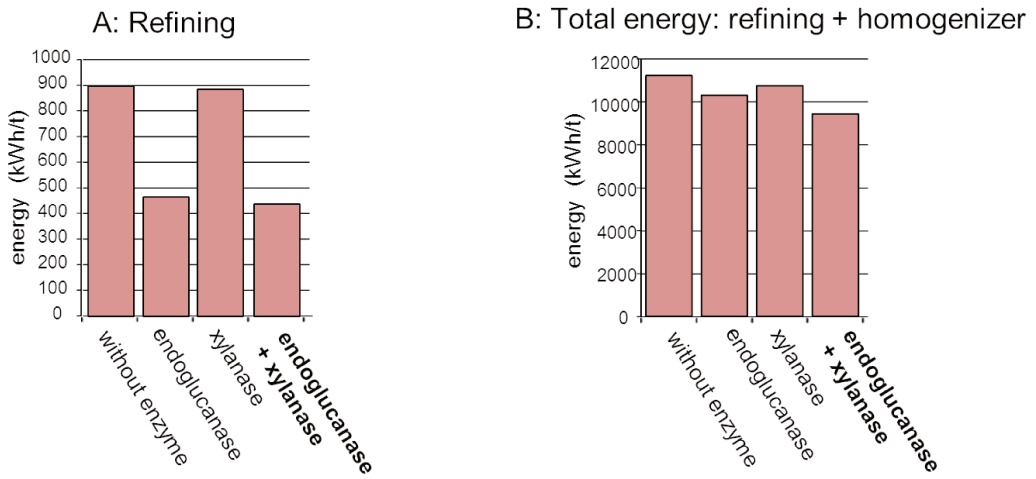

Figure 9 : Impact des différents prétraitements sur la consommation d'énergie après raffinage seul et après raffinage et homogénéisation

Conclusion générale

Ce projet avait pour but de développer les connaissances sur les interactions entre les microfibrilles de cellulose et des hémicelluloses, dans le but de mieux cibler les paramètres pour améliorer le processus de microfibrillation.

Pour cela, une approche à différents niveaux a été envisagée, comprenant une caractérisation classique des composants individuels et de leurs interactions au niveau moléculaire, principalement par RMN du solide, leurs simulations par modélisation moléculaire à un niveau atomistique et l'évaluation de leurs propriétés à l'échelle macroscopique. Sur la base des résultats obtenus un nouveau prétraitement des fibres avec une xylanase a été proposé.

- **Le xylane extrait des MFC est différent du xylane natif du bois**

L'optimisation du protocole d'extration du xylane des MFC a permis d'atteindre un rendement d'extraction de 67%. La pureté du xylane obtenu est très élevée, entre 93% et 97%. Ce xylane est soluble uniquement dans le DMSO et il est cristallin en présence d'eau.

Après caractérisation, il est apparu que ce xylane était dépourvu de branchement arabinose contrairement à son état natif dans le bois. Deux hypothèses sont alors envisagées pour expliquer cette absence de ramifications : (a) Il y a deux types de xylanes synthétisés dans le bois : un homopolymère de xylane dépourvu de ramification et un xylane branché plus facile à extraire. (b) Tous les xylanes sont branchés à l'état natif dans le bois mais les procédés de mise en pâte modifient ces ramifications sans toutefois éliminer le xylane.

- **Le xylane interagit très fortement avec la cellulose**

La caractérisation des MFC après extraction et les modèles de ré-adsorption de xylane suggèrent une modification de conformation du xylane lorsqu'il s'adsorbe à la surface de la cellulose. Initiallement, sous forme d'hélice à trois résidus par tour, il change sa conformation pour adopter celle de la cellulose en hélice à deux résidus par tour

Les résultats des simulations atomistiques montrent que le xylane s'adsorbe en conformation d'hélice 2, (similaire à la cellulose) parallèlement à la direction de la chaîne de cellulose et dans un plan parallèle

- **L'état de dispersion des MFC est un paramètre clé**

Cet état de dispersion des MFC peut être suivi par turbidimétrie qui reflète de manière qualitative l'homogénéité de la suspension. Les allures de courbes de turbidité ont pu être mises en relations avec des mesures de surface spécifiques d'aérogel et de propriétés mécaniques de papiers renforcés par des MFC. Il est apparu que les MFC les mieux dispersées, provenaient de pâtes krafts ou sulfites jamais séchées. Leurs turbidités sont les plus faibles et leurs surfaces spécifiques les plus élevées. La valeur de turbidité des MFC à 800 nm est donc un bon indicateur pour estimer les propriétés mécaniques des films renforcés.

- **La xylanase permet d'améliorer la microfibrillation**

Le pré-traitement des fibres par un mélange endoglucanase et xylanase permet d'obtenir des MFC plus homogènes refermant moins d'éléments grossiers résiduels et montrant un état de dispersion plus élevé. De plus, des économies d'énergie de l'ordre de 17% par rapport à une pâte non traitée et de 8% par rapport à une pâte traitée seulement par l'endoglucanase ont été mesurées lors de la production des MFC.

Résumé court anglais :

The Micro-Fibrillated Cellulose (MFC) are a derivated product from the wood paper industry with nanoscale dimensions, mainly composed of cellulose and hemicelluloses. They found interesting applications as they can enhance materials properties, like the paper strength for example, but their development at industrial scale is still challenging because of the cost of the production. Indeed the MFC are resulting from the wood pulp deconstruction which consume a lot of energy due to the interaction between the cellulose and the hemicelluloses. In this project, hemicelluloses were first isolated by an optimized process from the MFC and analyzed separately. We investigated the hemicelluloses/cellulose interactions by spectroscopy and molecular modeling. Systems made of cellulose and hemicelluloses were then developed at macroscopic scales to evaluate the adhesion between hemicelluloses and cellulose. A solution with enzymatic treatment has been proposed.

Résumé court français :

Les Micro-fibrilles de cellulose (MFC) sont un produit dérivé de l'industrie papetière de dimensions nanométriques et principalement composées de cellulose et d'hémicelluloses. Elles ont des applications dans le renfort de matériaux, comme celles du papier par exemple, mais leur développement à l'échelle industrielle est encore limitée par leurs coûts de production. Les MFC sont issues de la déconstruction de pâte à papier par un procédé limité par les interactions cellulose/hémicelluloses. Dans ce projet, les hémicelluloses ont d'abord été isolées des MFC par un procédé optimisé puis caractérisées séparément. Nous avons ensuite étudié les interactions cellulose/hémicelluloses par des techniques de spectroscopie et de modélisation moléculaire. Des modèles reconstitués ont ensuite été étudiés à l'échelle macroscopique pour évaluer l'adhésion entre les hémicelluloses et la cellulose. Une solution de traitement par des enzymes a été proposée.

Résumé anglais :
The study was motivated by the necessity to reduce the high energy costs of Micro-Fibrillated Cellulose (MFC) production, which is a limiting factor for its industrial development and aimed at understanding the cellulose/hemicelluloses interaction within this system. MFC resulting from different chemical pulps were characterized by solid-state NMR spectroscopy to get information on the hemicelluloses content and molecular conformation. By optimizing an extraction protocol, more than 60% of the residual hemicelluloses were extracted from birch kraft MFC and characterized as a high purity homopolymer of β-1,4 linked xylan of DP 75.
Turbidimetry was used to qualify the quality of the suspensions, which strongly depended on the pulping and drying history. Positive correlations between the state of dispersion, specific surface and mechanical properties of MFC-reinforced handsheets were evidenced.
Cellulose/xylan interactions were investigated using solid-state NMR and atomistic molecular dynamics (MD) simulation. NMR spectra confirmed that xylan in contact with cellulose altered its conformation, from the three-fold helix to a presumable cellulose-like two-fold one. In combination with specific surface area measurements, the conformational change was shown to happen only for the first layer of xylan adsorbed in direct interaction with the cellulose surface. MD simulations showed that adsorbed xylan tends to align parallel to the cellulose chain direction fully extended. Interaction energy between xylan chain and cellulose surface estimated with MD was 9kJ/xylose. Then a three-layers system made of xylan between two cellulose films were built to perform adhesion tests that showed strong adhesion between xylan and cellulose surfaces. Xylanase was proposed as a pulp pretreatment for MFC production.

Résumé français :
Le cadre de cette étude est le coût énergétique lié à la production des Microfibrilles de Cellulose (MFC) qui est aujourd'hui un facteur limitant à son développement à l'échelle industrielle. Le but de cette étude est de caractériser les interactions cellulose/hémicellulose au sein de ces systèmes. Des MFC provenant de différentes pâtes à papier chimiques ont été caractérisées par RMN du solide afin d'obtenir des informations à l'échelle moléculaire. Suite à l'optimisation d'un protocole expérimental, les hémicelluloses contenues dans les MFC issues de pâte kraft de bouleau ont ensuite été extraites avec un rendement de 60% et sont composés uniquement d'un homopolymère de xylane de DP 75.
La turbidimétrie a été utilisée pour qualifier la qualité des suspensions, dont il a été montré qu'elle dépend fortement du procédé de mise en pâte et du séchage. Des corrélations positives ont été établies entre l'état de dispersion et les propriétés mécaniques de feuilles de papier additionnées de microfibrilles. L'analyse RMN de modèles biomimétiques reconstitués a confirmé le changement de conformation du xylane lorsqu'il est adsorbé sur la cellulose et les mesures de surface spécifique ont montré que seule la couche de xylane en contact avec la cellulose était concernée par ce changement. Les interactions cellulose/xylane ont été étudiées par RMN du solide et par dynamique moléculaire atomistique (MD). Les simulations MD ont montré que le xylane s'adsorbe parallèlement aux chaines de cellulose. Des mesures d'interaction sur ce système ont conduit à une mesure d'énergie de 9kJ/résidu de xylose.Des tests de mesure d'adhésion ont également été réalisés à partir d'un modèle trois couches constitué de xylane entre deux films de cellulose et une forte adhésion a pu être observée.
L'utilisation de xylanase comme prétraitement est proposé pour améliorer la production des MFC.